A Three-Dimensional Photoelastic Investigation of the Stress Distribution in the Anchorage Zones of Post-Tensioned Beams

by

Saadoun Saad Al-Saadoun

A Thesis Presented to the

FACULTY OF THE COLLEGE OF GRADUATE STUDIES

KING FAHD UNIVERSITY OF PETROLEUM & MINERALS

DHAHRAN, SAUDI ARABIA

In Partial Fulfillment of the
Requirements for the Degree of

MASTER OF SCIENCE

In

CIVIL ENGINEERING

October, 1980

INFORMATION TO USERS

This manuscript has been reproduced from the microfilm master. UMI films the text directly from the original or copy submitted. Thus, some thesis and dissertation copies are in typewriter face, while others may be from any type of computer printer.

The quality of this reproduction is dependent upon the quality of the copy submitted. Broken or indistinct print, colored or poor quality illustrations and photographs, print bleedthrough, substandard margins, and improper alignment can adversely affect reproduction.

In the unlikely event that the author did not send UMI a complete manuscript and there are missing pages, these will be noted. Also, if unauthorized copyright material had to be removed, a note will indicate the deletion.

Oversize materials (e.g., maps, drawings, charts) are reproduced by sectioning the original, beginning at the upper left-hand corner and continuing from left to right in equal sections with small overlaps. Each original is also photographed in one exposure and is included in reduced form at the back of the book.

Photographs included in the original manuscript have been reproduced xerographically in this copy. Higher quality 6" x 9" black and white photographic prints are available for any photographs or illustrations appearing in this copy for an additional charge. Contact UMI directly to order.

UMI

A Bell & Howell Information Company
300 North Zeeb Road, Ann Arbor MI 48106-1346 USA
313/761-4700 800/521-0600

A THREE-DIMENSIONAL PHOTOELASTIC INVESTIGATION OF THE STRESS DISTRIBUTION IN THE ANCHORAGE ZONES OF POST-TENSIONED BEAMS

by

SAADOUN SAAD AL-SAADOUN

THESIS

Presented to

THE COLLEGE OF GRADUATE STUDIES

University of Petroleum & Minerals
Dhahran, Saudi Arabia

In Partial Fulfillment of the
Requirements for the Degree of

MASTER OF SCIENCE IN CIVIL ENGINEERING

OCTOBER 1980

UNIVERSITY OF PETROLEUM & MINERALS
Dhahran, Saudi Arabia

COLLEGE OF GRADUATE STUDIES

This thesis, written by Saadoun Saad Al-Saadoun under the direction of his Thesis Committee, and approved by all its members, has been presented to and accepted by the Dean of the College of Graduate Studies, in partial fulfillment of the requirements for the degree of MASTER OF SCIENCE IN CIVIL ENGINEERING.

Dean
College of Graduate Studies

Date : 21-1/1/1

Department Chairman

Thesis Committee

Chairman

Member

Member

ACKNOWLEDGMENTS

Acknowledgement is due to the University of Petroleum and Minerals for support of this research.

I wish to express my appreciation to Dr. Rasheeduzzafar who served as my major advisor. I also wish to thank the other members of my Thesis Committee, Dr. Fahd H. Dakhil, and Dr. Zamil A. Mokrin, for their suggestions during this investigation.

My sincere thanks are due to Mr.Rowland Anthony for assisting me in cutting the slices. To Mr. Ismail Ahmed Wangde I am grateful for typing this thesis.

CONTENTS

List of Tables

List of Figures

NOTATIONS

xx, yy, zz	=	Normal stresses in x,y and z directions respectively.
xy, yz, zx	=	Shear stresses in xy, yz and zx planes.
P,Q,R	=	Principal stresses
yy_o	=	Mean compression at the base of the end block
α	=	Angle of indication of the principal stress signs and reference axes defined in Figure 4.3
$2a_1$	=	Width of the anchorage unit (Figure 5.3)
2a	=	Width of the end block (Figure 5.3)
A	=	Area of the end block
A_1	=	Loaded area
2ap	=	Depth of the symmetrical prism
F	=	Prestressing force
b	=	Width of the beam
T	=	Transverse tensile force
k_f	=	$\frac{\text{Maximum transverse stress}}{\text{Mean compression at the base}}$

k_T = $\frac{\text{Transverse tensile force}}{\text{Prestressing force}}$

k = $\frac{\text{Apparent tensile strength}}{\text{Splitting tensile strength}}$

r = Tensile splitting strength of concrete

r_s = Reduced tensile splitting strength of concrete

T_r = Tensile force for which reinforcement is to be provided

A_s = Area of steel reinforcement

f_s = Permissible value of steel stress

f_t = Permissible tensile stress for concrete

f_y = Yield value of stress reinforcement

β = Reduction factor $\frac{r_s}{r}$

cu = Cube crushing strength of concrete

Abstract

Three-dimensional photoelastic investigations were carried out on eight photoelastic models to study the behaviour of end blocks by establishing the magnitude and distribution of stresses on critical planes. The effect of area concentration ratio, cable duct, position of the anchorage unit and interactive effect of multiple anchorages has been investigated. Stress concentrations under the anchorage unit were studied and the role and magnitude of critical sub-surface shears established.

Recommendations have been made for the design of the anchorage block. Concrete blocks were carried out to study the failure mechanism of end blocks.

chapter 1

INTRODUCTION

1.1 THE ANCHORAGE ZONE PROBLEM

One of the most important factors in the design of post-tensioned prestressed concrete members is the magnitude and distribution of the stresses associated with the diffusion of highly localized and discontinuous prestressing loads applied by anchoring the stressed cables at the end of the anchorage blocks. The creation of large prestressing forces through cables or bars gives rise to a high concentration of stresses in the region around the anchorage. On the bearing or end surface itself the stress distribution is extremely complex; regions directly under the anchorage carrying very large forces, whilst the remainder of the surface remains almost completely undeformed. However, at distances normally equal to, or greater than, the depth of the beam, only longitudinal normal stresses exist which are usually distributed in a linear format. These longitudinal stresses can be conveniently evaluated using the familiar concepts of strength of material. In the process of progressive transformation from a discontinuous,

irregular and highly localized stress system at the end surface to a regular longitudinal normal distribution at some distance from the end, a complex system of transverse tensile and shear stresses is set up within the body of the end block. "Anchorage zone" is the most commonly used term to designate the length wherein the stress transformation from one stage to another takes place and the part of the member within this zone is known as "anchor block" or "end block". Guyon[1,2] however, has given this zone an alternative name of "Lead-in-Zone".

To be more specific, when a prestressed structural unit is post-tensioned by a group of separate tendons, tensile stresses are set up in the anchor block :

(i) Underneath the anchorages
(ii) Between the anchorages, and
(iii) In areas near the corners of the end face.

The magnitude of the maximum tension in each of the three aforesaid categories can easily be critical in view of the low tensile strength of concrete. This could lead to a tensile failure of the end block if suitable local reinforcement is not designed and detailed to withstand these splitting, bursting and spalling stresses. This entails a precise evaluation of the magnitude and distribution

of the critical stresses as a prerequisite to an optimization of such structural units.

In the anchorage zone of the prestressed beams, for example, the state of stress is of an exceedingly complex three-dimensional nature and is entirely different from that prevailing in the remaining length of the beam. As the critical end zone stresses are located in the immediate vicinity of the anchorages, Navier's classical theory of bending proves to be inadequate to provide a reasonable evaluation of the magnitude and distribution of those essentially parasitic complex transverse tensile stresses in the bursting and spalling zones of the anchor block.

The precise nature and pattern of the transverse stress distribution in the anchorage zone is influenced by a large number of factors including :

1) The ratio of the loaded area to the area of cross-section of the end block (hereafter called concentration ratio k and defined as A_1/A).
2) The proximity and interaction of other anchorages.
3) The method of anchoring the tendons.
4) The shape and position of the anchorage unit.
5) The geometry of the cross-section of end block and that of the structural unit adjoining it.

Several instances of the failures of the anchor blocks, some from the construction of a few major structures, have been reported. Due to the complexity of the stress distribution system associated with the anchorage zone as well as because of a large number of commonly interactive parameters present in the design situation, codes of practices on structural prestressed concrete in most of the countries, even to this day, either do not include any recommendations or at best make some general comments or suggest some empirical formulae which have little relevance to this problem.

1.2 COMMENTS ON THE PRESENT STATUS OF KNOWLEDGE ON THE ANCHORAGE ZONE PROBLEM

Several theoretical solutions have been presented which are in fact approximate or exact solutions of the mathematical models assumed to simulate the anchorage zone problem. Most of these are based on a two-dimensional approach[1,2,3,4,5,6,7,8] and on assumptions which represent a highly simplified form of the actual physical situation with respect to almost all the parameters which are known to affect the magnitude and distribution of the critical stresses in the anchorage zone. The two-dimensional approach alone, made to simplify the theoretical derivation, introduces considerable inaccuracies in the magnitude of the resulting stresses. The transverse

stresses in the direction of the depth of the beam are significantly decreased and the tensions across the width of the beam are completely ignored. In almost every theory there are other approximations and assumptions which although primarily introduced to simplify the mathematical approach, inevitably lead to a less accurate description of the actual behaviour. It is probably on this account that considerable discrepancies exist between these theories. To the author's knowledge only four theoretical solutions[9,10,11,12] have been formulated todate which take into account the three-dimensional nature of the problem; two of these conceive the mathematical model as axisymmetric, having a co-axial cable duct under a circular load - an idealization far from being realistic. The other two are closer to the actual geometrical configurations with respect to the endblock and the loading pad. However, the results of these solutions are contradictory with respect to certain important considerations and, more significantly, are shown by tests on concrete endblocks to seriously underestimate the critical stresses.

Table 1.1 compares the results of the better known theoretical solutions with the measurements made by Zielinski and Rowe[13], and Taylor[14] on concrete endblock test

specimens. This data indicate that the theoretical predictions for the maximum elastic tensions in the surface are invariably low and confirm the need to undertake a more detailed examination of the elastic stresses in typical end anchorage units.

The experimental investigations on actual or model concrete endblocks are mostly piecemeal and fail to provide comprehensive test data to enable satisfactory conclusions to be drawn on the behaviour, design and failure characteristics. The two exceptions are the tests carried out by Zielinski and Rowe[13] at the Cement and Concrete Association Laboratories and by Taylor[14] at the University of London. The strain measurements made were,however, confined to surface planes and therefore provide little insight into the complexities of the internal distributions of the critical tensile and shear stresses.

Two-dimensional photoelastic investigations have been carried out by several investigators but comprehensive three-dimensional photoelastic tests have been made only by S.P.Christodoulides[15] whose work has been widely reported and used by designers and researches. Unfortunately, the analysis contains an error in the signs of the shear slope contributions which have resulted in considerable distortion

of the stress distributions in the anchorage zone. There are other shortcomings in the experimental techniques used in this work which are likely to induct serious inaccuracies. These are discussed in detail in Chapter

1.3 THE SCOPE OF THE PRESENT WORK

The work presented in this thesis consists of :

(i) Three-dimensional photoelastic investigations on end block models prestressed by single and multiple anchorages of the external and embedded types with and without cable ducts; and

(ii) Tests on concrete endblock models.

The content of the photoelastic work can be enumerated as follows:

Firstly, it is a study to establish the qualitative and quantitative picture of stress distribution in the anchorage zone when the anchor block is post-tensioned with single and multiple anchorage units. The magnitude and nature of all the important stress components on critical planes are obtained. The principal stress trajectories are drawn for typical cases to examine the diffusion of transverse tensile stresses and the longitudinal stresses in the whole body of the end block. The external anchorages

used correspond to CCL compact plate, Lee McCall or Magnel-Blaton Systems, all of which employ a rectangular thrust plate acting on the face of the concrete end block. The embedded anchorage units simulate the Freyssinet system of prestressing which employs a cylindrical thrust block. The justification for adopting the anchorage units of the type described for a comparative study is in the sharp contrast of their several essential characteristic features; geometric, positioning in the member, method of anchoring wires and in the mode of transmitting the forces to the body of the end block.

Secondly, the degree of stress concentration (hereafter called concentration ratio) expressed by the ratio of the loaded area(A_l) to the area of the anchorage block,(A) being the most important parameter influencing the magnitude of the tensile stresses, one special series of tests have been so planned as to establish a relationship between the value and position of the maximum transverse tensile stresses and the concentration ratio.

Thirdly, all photoelastic work and most of the concrete testing that have been carried out hitherto, use external rectangular or circular thrust plates to simulate the anchorage units of all types. These experimental techniques

tend to ignore a vital difference which occurs in the mode of transmitting the forces to the body of the end block if the anchorage unit is embedded within the body of the anchor block instead of being external to it. Whereas in the case of the later, the total applied load is transferred by bearing action in the case of the former part of the load will almost certainly be transferred by the shear action and only the balance by bearing. One series of the present photoelastic investigations employs the embedded anchorage unit and the results of this series tend to establish the precise mode of load transfer to the end block when an embedded anchorage unit is used for prestressing. The ratio of loads transferred by shear and bearing has been established and the magnitude and pattern of the critical tensile and shear stresses have been established on surface and internal planes for purposes of comparison with the corresponding values for the end block employing the external type of anchorage.

Fourthly, photoelastic tests have been planned in one series to enable the effect of cable duct to be established on the magnitude and location of the critical stresses. As there are very substantial difficulties in successfully obtaining internal measurements in concrete end blocks, it

is noteworthy that information on the effect of cable duct or on the mode of load transfer on internal planes is unlikely to be reliable from that source.

Fifthly, a series of three-dimensional photoelastic tests has been planned to study the interactive effect of multiple anchorages. The model of a prestressed concrete beam end block has been post-tensioned using a group of three external plate anchorages. The configuration of these loading pads has also been varied with respect to the width of the beam to obtain information on the magnitude and location of critical tensile stresses in the surface plane as affected by the proximity of the loading pad to this plane.

Sixthly, tests have been carried out on model concrete end blocks to establish the failure characteristics of concrete situated in the complex three-dimensional stress system of the anchorage zone. Actual concrete is a two-phase heterogeneous, anisotropic, material showing noticeable quasi-elastic deformational responses to loads in all ranges but specially so in the range obtainable in anchor blocks. It would be a gross over simplification to think in terms of a limiting tensile strain or stress as a criterion of concrete failure when subjected to complex states of stress

such as those exist in the anchorage zone. Actual concrete tests under realistic conditions will go a long way to provide valuable guidance in establishing a viable empirical design methodology which appears to be the best approach to this problem with the existing state of knowledge on the subject.

The strain measurements from concrete tests were also used with the supplementary purpose to establish the degree of influence of the Poisson's ratio effect by comparing the computed concrete surface stresses with those obtained from photoelastic tests and models.

Further, the data obtained from the photoelastic and concrete tests has been analyzed and arranged in such formats as to be of direct use to the designer of the end block. Guyon's[12] symmeterical prism method is the most commonly adopted concept for computing maximum tensile stresses and the magnitude of tensile forces along critical planes in multi-anchorage applications. The data obtained in the present investigations seeks to test this concept.

Finally, in the whole range of the experimental programme an attempt has been made to seek refinements and innovations in the techniques. Unlike other researchers, techniques have been developed and used:

(i) to represent correct physical features,

(ii) to allow for the appropriate stiffnesses of anchorage unit and end block material, and

(iii) eliminate differential thermal expansion at the metal-epoxy interface which is likely to introduce high local shear stresses and thus distort the stress distribution in the vicinity of the anchorage unit.

In concrete testing pulse velocity techniques were used to identify the onset of cracking and photostress techniques have been used to provide a full field visual picture of the strains on the surface plane and the loaded end face of the anchor block.

1.4 SPECIAL FEATURES AND POSSIBLE LIMITATIONS OF THE INVESTIGATIONS

The anchorage zone problem invariably incorporates significant features which can only be clarified and covered by a three-dimensional study. Amongst others, these features include the effect of the cable ducts, stress concentrations near the edges of the loading pad, shears developed under the surface of the anchorage due to the restraining action resulting from the friction between the loading pad and the end block, stress distribution in the controversial

spalling zones, the proportion of load transferred by shear in the case of the embedded anchorage, the mode of stress diffusion into the body of the end block, and the evaluation of the magnitude and distribution of stress on internal planes. The anchorage zone problem falls in the following two of the several categories which are specially suited to the genius of the three-dimensional photoelastic technique[16].

(i) the analysis of three-dimensional structures too complex to be modelled numerically within the limitations of the available programmes and machines, and

(ii) modelling structures composed of two or more contacting components and in which the contact boundary conditions change with increased load.

It was felt that photoelastic method at present is the only possible experimental approach to the anchorage zone problem if its three-dimensional constitution based on aforesaid factors (listed in para 1 of this section) is to be examined adequately. Further the photoelastic method proved to be a quick and inexpensive technique and it enabled a complete and full investigation of all the features listed in para 1 of this section. Almost 2500 observations were recorded on a large number of slices

removed from light photoelastic models which manufactured for this investigation.

The photoelastic method suffers from the obvious disadvantage that the models have to be made from material having special optical properties and having little resemblance to concrete. The later is a two-phase heterogenous, anisotropic, quasi-elastic material of a most complicated nature which does not show a simple response to the action of applied loads. The photoelastic material used, however, may be treated as elastic and isotropic for all practical purposes. As failure conditions are approached in concrete structures, the deformation behaviour becomes exceedingly complex and there is considerable uncertainty as to the true nature of the mechanics of internal stresses. To this general difficulty is added the specific complication that the failure conditions of concrete are undoubtedly modified under the action of combined compressive and tensile stresses as is the case in the anchorage zone.

In view of these difficulties an attempt has been made to design an experimental programme which meets some of the aforesaid limitations and difficulties effectively. The belief that photoelastic measurements will predict the stresses in actual concrete end blocks fairly accurately

in the working range is based on the following justifications:

(i) Although very few materials are homogenous and isotropic, but the average behaviour over a sufficiently large sample very often corresponds to the ideal condition. In metals, over a few hundred grain sizes, in concrete over ten times the maximum aggregate size, and even in soils on samples of hundreds of particles, measured strains have been shown to agree with the ideal states.

(ii) Differential Poisson's ratio effect usually figures in a three-dimensional analysis and is the usual factor causing concern to the photoelastician. The value of Poisson's ratio for concrete is usually 0.15 to 0.20, while the value for Araldite B is about 0.45. This difference, it is generally believed[17,18] only influences the minor stresses in such a way that the effect does not exceed the usual experimental error of $\pm$ 10 percent.Previous work by Iyengar[9] on the anchorage problem as well as favourable outcome of comparisons made in this thesis between the photoelastic results and measurements on concrete end blocks tend to substantiate this conclusion.

It is,however, true that the behaviour of concrete near failure cannot be predicted on the basis of photoelastic tests. Here, the photoelastic data is only useful in exposing the critical stress conditions in the vicinity of the anchorage unit. Therefore, tests on actual concrete end blocks have been carried out to study the specific aspect of the failure mechanism of anchorage zone. The lucid stress picture provided by photoelastic tests in conjunction with the observations on concrete end blocks provide a tenable failure mechanism which has been presented in Chapter

It may also be noted that the present investigations are related to rectangular end blocks carried at the end of rectangular beams. For rectangular end blocks carried at the end of I-shaped beams, although the stress distribution near the loaded end remains similar to the one presented here, an additional zone of tension is reproted in the region of juncture between the I-section of the beam and the rectangular end block.

TABLE 1.1

Comparison of maximum transverse stress in anchor blocks subjected to isolated concentric post-tensioning force

A_1/A	Maximum transverse tension expressed as a ratio of mean axial compression					
	Experimental		Theoretical Solutions			
	Zielinski and Rowe	Taylor	Guyon (2-dimensional)	Magnol (2-dimensional)	Iyengar (3-dimensional)	Yettram & Robbins (3-dimensional)
0.1	0.71	-	0.34	0.36	0.13	0.30
0.25	0.56	0.5	0.25	0.28	0.096	0.21
0.35	0.485	-	0.18	0.22	0.07	0.15
0.5	0.44	-	0.15	0.18	0.059	0.066

chapter **2**

REVIEW OF PREVIOUS WORK

The problem of calculating stresses associated with the application of concentrated forces received attention as early as 1888 when concrete hinges were used in bridge construction. Many theories have been presented since then to date which are applicable to the anchorage zone problem in varying degrees. Also, experimental work, mostly confined to the measurement of strains on the surfaces of concrete end blocks has been reported by some investigators. This chapter briefly reviews the theoretical and experimental work carried out to date on the anchorage zone problem.

2.1 REVIEW OF THEORETICAL SOLUTIONS

Bleich[7](1923) considered the problem as two-dimensional and has obtained a solution in the form of Fourier Series. Bleich's solution, however, does not satisfy the compatability conditions.

Morsch[3](1924) has proposed an empirical formula for the computation of the total tensile force on the basis of the assumption that the resultant compressive stress

trajectories on either side of the central axis have the form of a second degree parabola. The total tension is computed from

$$Z = \tfrac{1}{4}P \frac{(a-a_1)}{h}$$

Figure 2.1 taken from Morsh's original paper shows the pattern of stress trajectories adopted to calculate the transverse tensions.

Bortsch[4] (1935) has made a theoretical study of the problem of stress concentration in a rather general way. He has considered the block as a deep beam of infinite depth and the load distribution on the contact area as a cosine function of amplitude $p_1 = \frac{\pi p}{2a_1}$ (Figure 2.2). The solution has been obtained with the help of an Airy's stress function. Results of this solution are not completely valid for the end block problem as the effect of longitudinal boundaries on the stress distribution has been ignored.

Magnel's[5] (1949) method of calculating the stresses in the anchorage zone is based on a foundation block analogy. His fundamental assumption is in regard to the nature of stress distribution along planes parallel to the central axis of the beam. He assumes the transverse stress

distribution due to a bending moment M on a plane AB to be a cubic parabola (Figure 2.3). The constants in the cubic equation for transverse stress are determined from boundary conditions. Magnel's solution is approximate as it does not satisfy the two-dimensional elasticity equations.

Guyon's[1,2](1951) analysis of stress distribution under anchorages is the most widely used method of designing the end blocks. Guyon has considered the end block as a two-dimensional semi-infinite strip subjected to the action of normal or oblique fo-ces on a narrow edge. An approximate solution is first obtained by means of a Fourier's series which is then improved for normal symmetrical loads by a process of reiteration of calculations. It may be mentioned here that Guyon has corrected only the transverse normal stress fy. The longitudinal stress fx and the shear stress have not been corrected. This implies that the calculation of principal stresses would be in error. The general case considered by Guyon, the variation of transverse stresses along the longitudinal axis for varying values of concentration ratios and the general form of the transverse stress distribution are shown in Figures 2.4, 2.5 and 2.6 respectively. To calculate the anchorage zone stresses due to several prestressing forces Guyon has introduced the

concept of "symmetrical prism (Figures 2.7 and 2.8). Sievers[8] (1952-1956) modified Bleich's solution by considering a modified block of variable thickness (Figure 2.9). The expression for the transverse stress fy is derived only for the central section of the end block. He has further concluded that the position of zero and maximum transverse stress does not change with the type of loading.

Ramaswamy et al[19] (1957) and Gilder[20] (1953) have proposed the solutions of the two-dimensional anchorage zone problem by the method of lattice analogy (Figures 2.10 and 2.11). The analogy consists in replacing the solid body of the end block in a two-dimensional problem with an articulated framework.

Douglas and Trahair[9] (1960) have reported a three-dimensional solution for an axisymmetric case. The effect of concentration of the prestressing forces has been evaluated theoretically in an idealized problem where a circular concentrated load is applied at one end of a cylinder having a central duct (Figure 2.12). Formulae have been derived for the calculation of shear and normal stresses in terms of cylindrical co-ordinates from which the distribution of principal stresses is determined (Figure 2.13).

Gerstner and Zienkiewicz[21] carried out two-dimensional analysis of the stress distribution caused by a line load on a semi-infinite medium, using a theory of elasticity approach. The results agreed well with Guyon.

Rydzewski and Whitbread[22] have proposed an approximate method for evaluating the tensile stresses in short rectangular end blocks carried at the ends of I-beams (Figure 2.14). The analytical results have been compared with those obtained from three-dimensional photoelastic models as well as mortar models.

Schlech[23] treated the anchorage zone as a deep girder and analyzed the transverse and longitudinal stresses by the application of Fourier series. The value of the total tension force on the line of axis between anchorages for various values of bearing width to spacing ratios has been calculated.

Som and Ghosh[24] have obtained a solution in the form of Fourier series. The solution does not satisfy some boundary conditions. Both concentric and eccentric loads have been dealt with and numerical results presented. Their estimation of the maximum tensile stress is lower than those of Guyon and Maguel.

Lenschow and Sozen[25] (1965) using a physical analog (Figure 2.15) have presented a simple equation for the distribution of transverse stress in the anchorage zone. The transverse stress distribution obtained has been shown to agree fairly well with that given by Guyon.

Iyengar and Yogananda[10] (1966), using similar idealization as Douglas and Trahair, obtained an exact solution for the axisymmetric problem.

Gaynor[26] (1966) assumed the existence of a crack on the centre-line of an axially loaded prism and used a beam on elastic support analysis approach to determine the transverse stress distribution. He concluded that the total bursting force is higher than that predicted by Guyon.

Yettram and Robbins[12](1970) have obtained a solution considering the problem as three-dimensional and using the finite element procedure. The transverse stress distribution along the centroid and surface has been obtained for a wide range of load concentration ratios.

Iyengar and Prabhakara[11](1971) formulated a three-dimensional elasticity solution for a finite rectangular prism subjected to end concentric and eccentric loads. The results obtained by this solution for the magnitude of the transverse tensile stress and force are considerably lower

than the values obtained by tests on concrete end blocks.

Gergely and Sozen [27] (1967) considered the equilibrium of the end zone, assuming a horizontal crack at the critical level. They have proposed a method for determining the amount of vertical steel based on assumed length of crack and limiting strain across the crack.

2.2 REVIEW OF EXPERIMENTAL INVESTIGATIONS

Christodoulides[28] (1957) was the first to obtain systematically the stress distribution in the anchorage using photoelasticity on two-dimensional models. Results were obtained for single concentric and double symmetrically placed loads.

Christodoulides[15] (1957) obtained the three-dimensional stress distribution in the anchorage zone of a prestressed concrete crane girder using frozen stress technique (Figure 2.16). His results showed that the two-dimensional solutions underestimate the magnitude of the maximum transverse tension. He also obtained strain measurements at internal points of the prototype gantry beam using embedded electric strain gauges. The good agreement of the photoelastic results and concrete measurements made him to conclude that Poisson's ratio has no significant effect on

the stress distribution.

Ban et al[27] conducted tests on 40 rectangular concrete end blocks and in all these tests surface strains were measured using electrical strain gauges. The studied variables included the load concentration ratio, thickness of the anchorage plate, dimensions of the anchor unit, amount and position of reinforcement and strength of concrete. The influence of those variables on the stress distribution as well as on the cracking and ultimate load was studied. It has been concluded that the measured strain distribution agrees well with the results of the Bleich-Sievers theory.

Sargious[30] (1960) conducted an investigation on the stress distribution of the stresses in the end block using two-dimensional photoelastic techniques. He considered the effect of prestressing force applied through a single or group of anchorages - concentric as well as eccentric - and the vertical reaction in determining the stress distribution.

Zielinski and Rowe[13] (1960,1962) were the first to carry out a comprehensive investigation on the actual concrete end blocks carried on rectangular and I-beams and post-tensioned by single and multiple anchorages. On the basis of their test data the authors have proposed methods for

evaluating the total tensile force and the maximum transverse tensile stresses. Zielinski and Rowe have shown that the values of tensile stresses and forces observed on surface planes were considerably higher than the corresponding values predicted by the theoretical solutions.

Rydzewski and Whitbread[31] used frozen stress photoelastic technique to study the three-dimensional stress distribution in a short rectangular end block carried on I-beam. These tests were to confirm a suggested theoretical solution for the anchorage zone problem.

Huang[32] (1964) tested on I-beam with rectangular end blocks, where internal and surface strains were measured using electrical resistance strain gauges. No general conclusions are presented but it was observed that the results obtained from Magnel and Guyon's two-dimensional theories can error considerably in the evaluation of maximum transverse stresses.

Taylor[14] (1967) made a detailed study on the stress distribution using concrete prisms with a central duct. The load was applied through steel plates and surface strains were measured using electrical strain gauges. His results indicate the maximum transverse surface tensions to be much higher than those predicted by the two-dimensional

theories. His computed stresses were,however, somewhat lower than those observed by Zielinski and Rowe.

Tassi and Windisch[33] tested stepped end blocks with an overall depth of about 1 m. The reinforcement for the different specimens was designed by different methods: those of Guyon, Zielinski and Rowe, and Yettram and Robbins. The specimens designed by the latter two methods showed insignificant cracking at the design prestress load, while the reinforcement designed by the Guyon's method appeared to be insufficient to the authors in view of the recorded actual widths of the cracks.

Higashida and Nakajima[34] tested large blocks, each stressed by 18 bars, in three vertical lines of six. They concluded that the theories for single anchorages could be extended to multiple anchorages but suggested that the majority of the steel should be situated on the outside of the section.

Abdullah Al-Musallam[44] carried out photoelastic investigations at the University of Petroleum & Minerals of the stress distribution in the anchorage zones of post-tensioned concrete slabs. The general form of stress diffusion was established and the critical tension zones have been identified.

The critical shear and tensile stresses as well as tensile forces have been evaluated and their sensitivity to the interactive load positions established. The results of critical values are compared with the various theoretical solutions in common use for design purposes. A mechanism of failure was suggested and recommendations were made for the design of the anchorage zone.

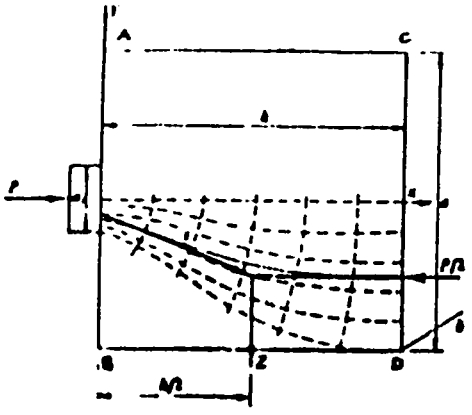

FIGURE 2.1 - Stress trajectories in Morsch's theory.

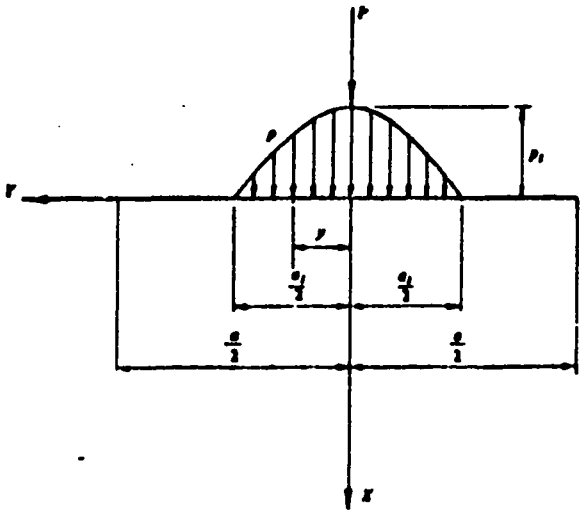

FIGURE 2.2 - Load distribution in Bortsch's theory.

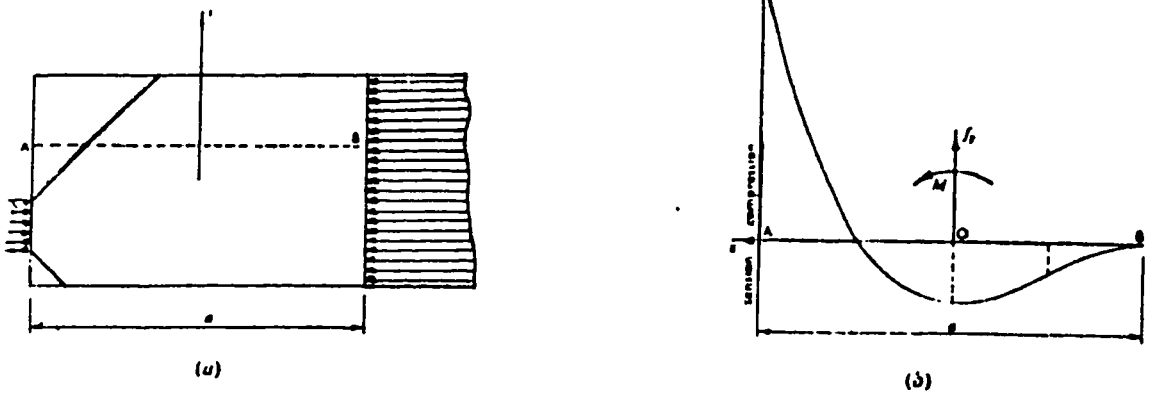

FIGURE 2.3 - End block and transverse stress distribution in Magnel's theory.

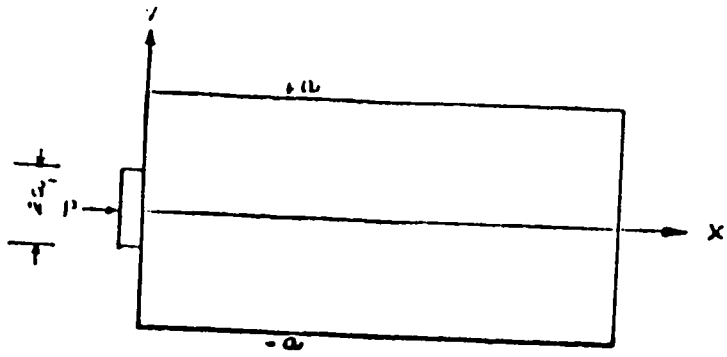

FIGURE 2.4 - Single centrally applied force on rectangular end block.

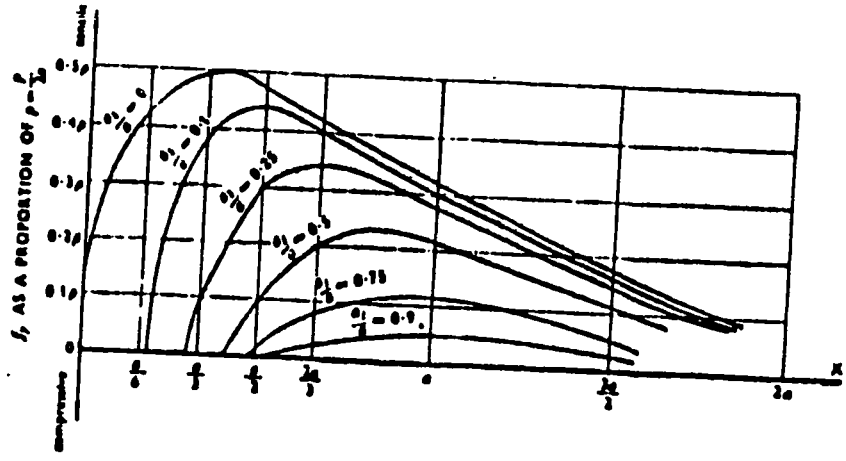

FIGURE 2.5 - Stress distribution according to Guyon's theory.

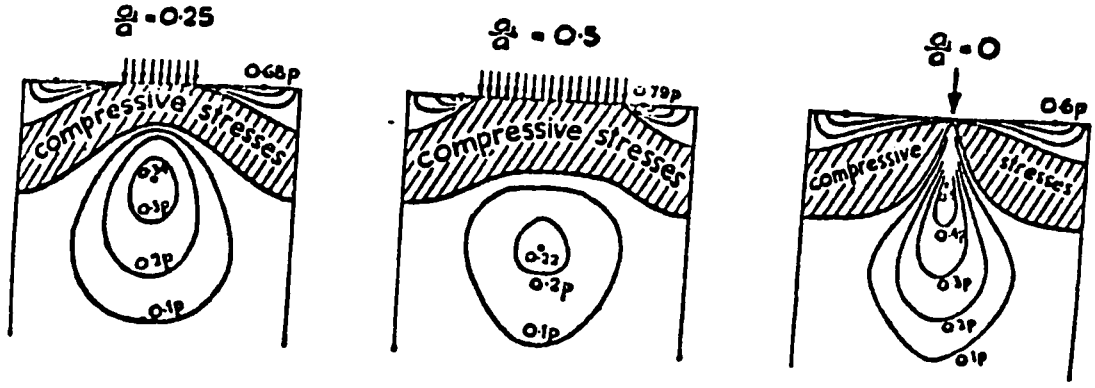

FIGURE 2.6 - Stress distribution according to Guyon's theory.

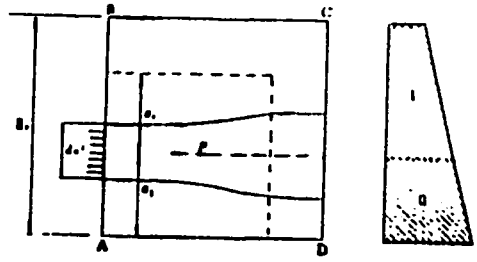

FIGURE 2.7 - Symmetrical Prism method of analysis for a rectangular end block stressed by a single eccentrically applied force.

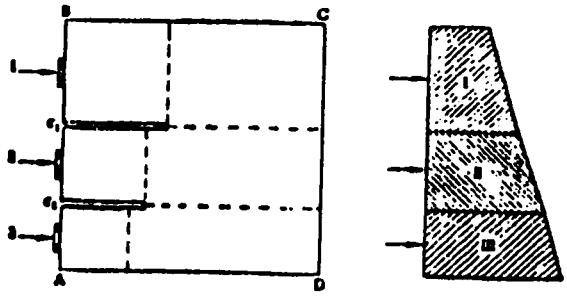

FIGURE 2.8 - Symmetrical prism method for several applied forces giving a linear distribution of prestress.

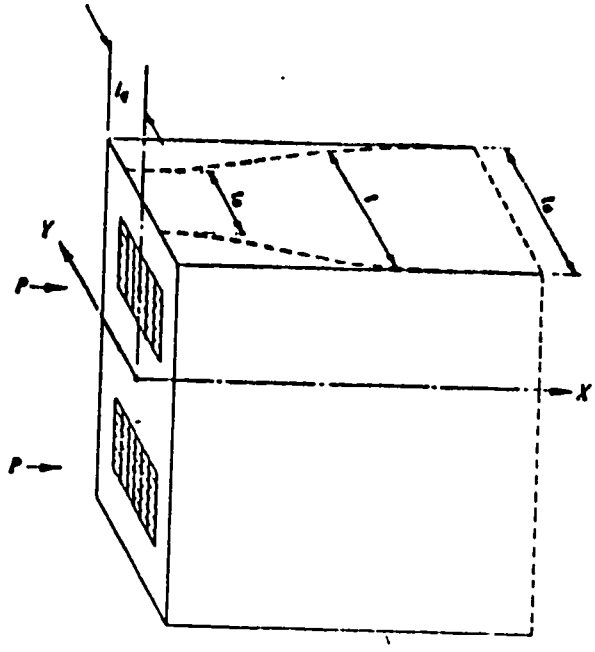

FIGURE 2.9 - Variation of t in end block (Sievers' theory).

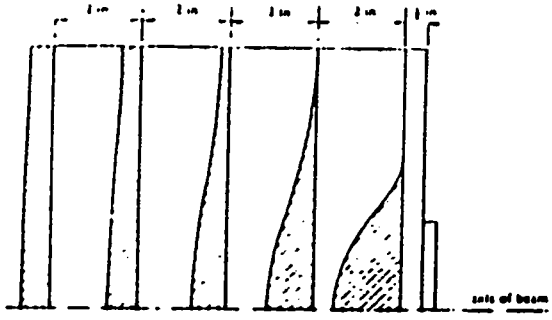

FIGURE 2.10(a) - Distribution of longitudinal stresses on transverse planes (lattice analogy solution by Gilder).

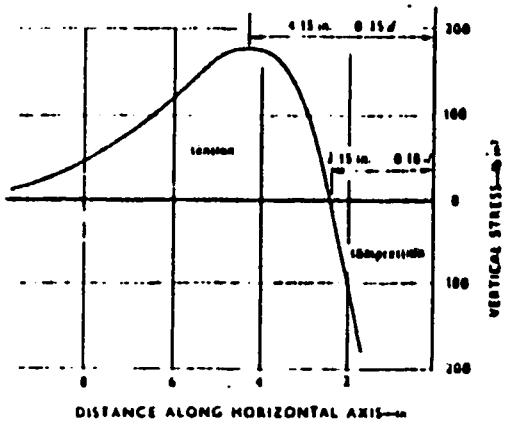

FIGURE 2.10(b) - Distribution of transverse stresses on the longitudinal axis of the beam (lattice analogy solution by Gilder).

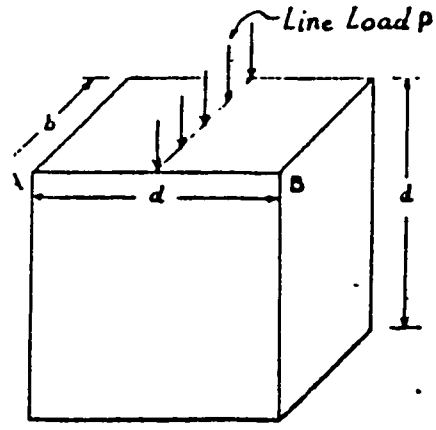

FIGURE 2.11(a) Case investigated by Ramaswamy and Goel.

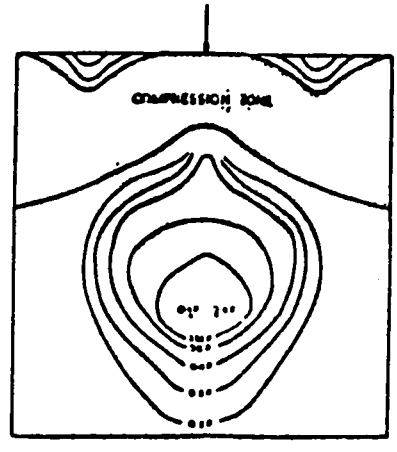

FIGURE 2.11(b) Stress distribution obtained by lattice analogy solution (Ramaswamy and Goel).

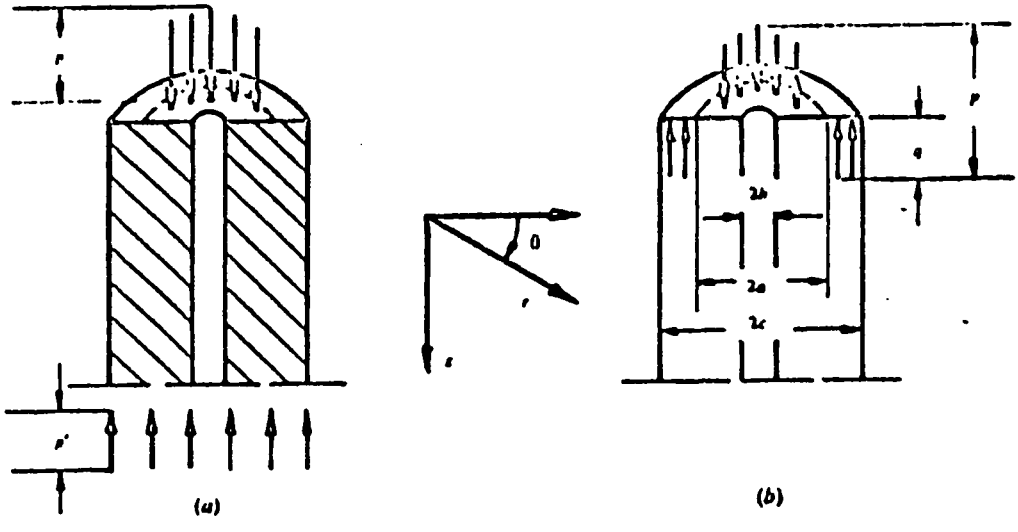

FIGURE 2.12 - Problem selected by Douglas and Trahair.

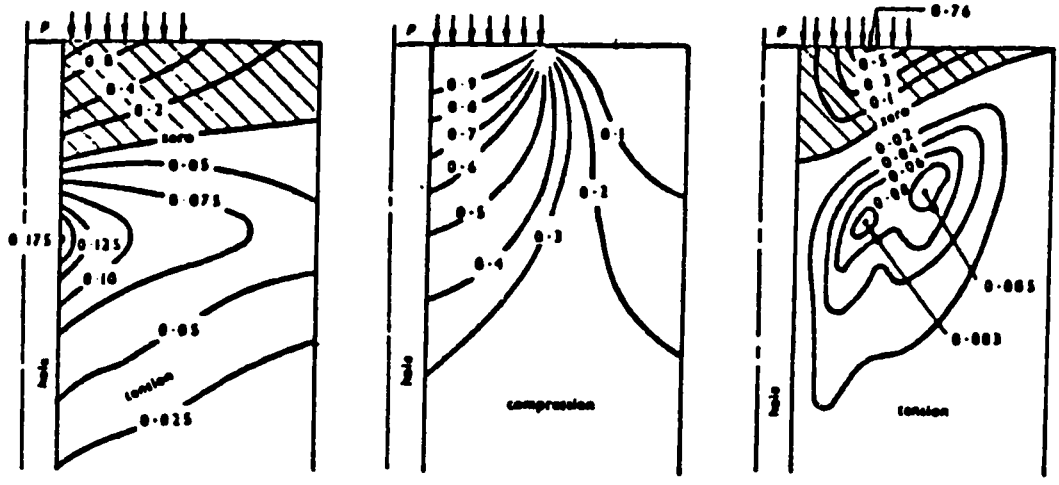

FIGURE 2.13 - Contours of principal stresses (Douglas and Trahair's theory).

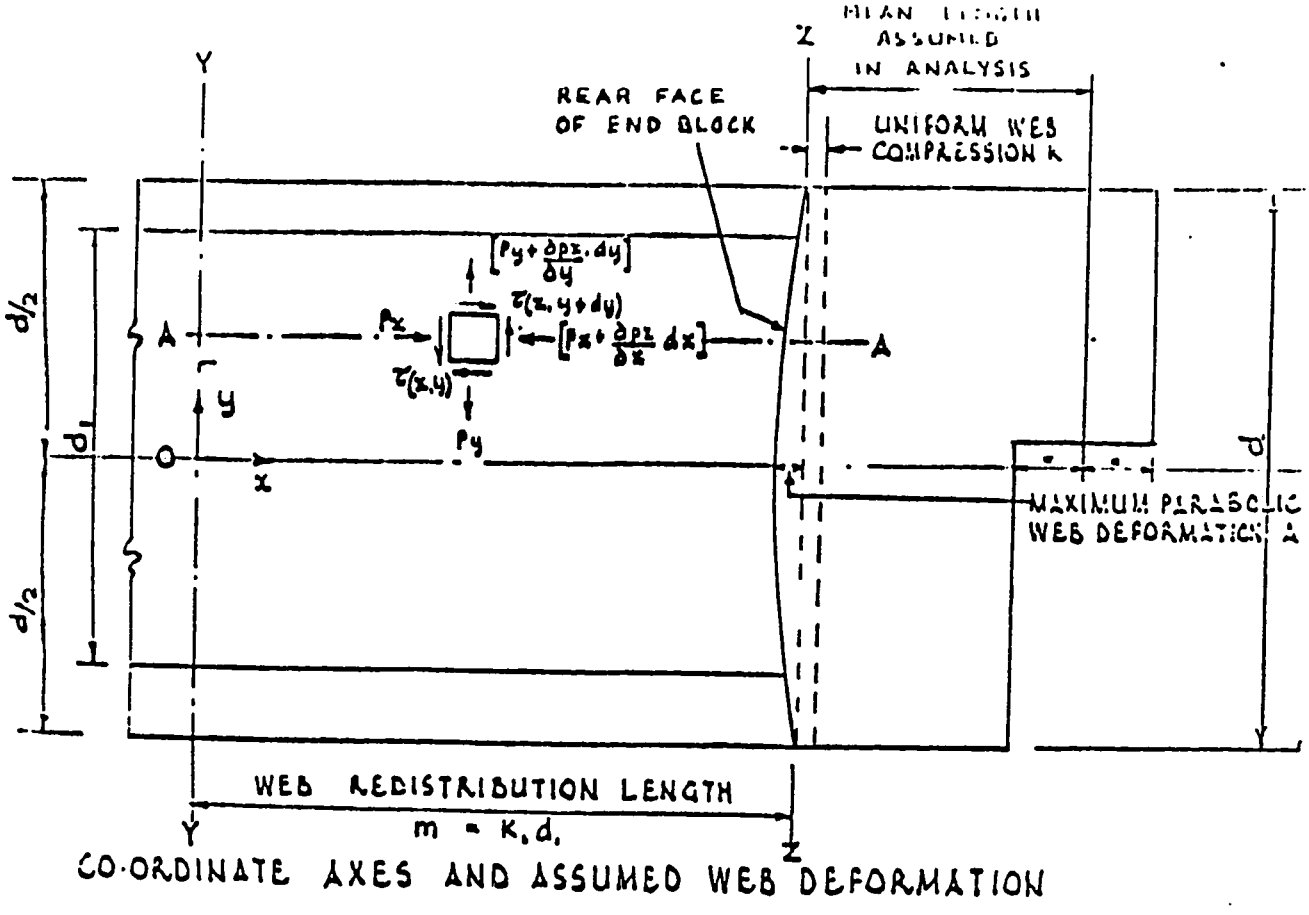

FIGURE 2.14 - Details of end block analysis (Whitbread).

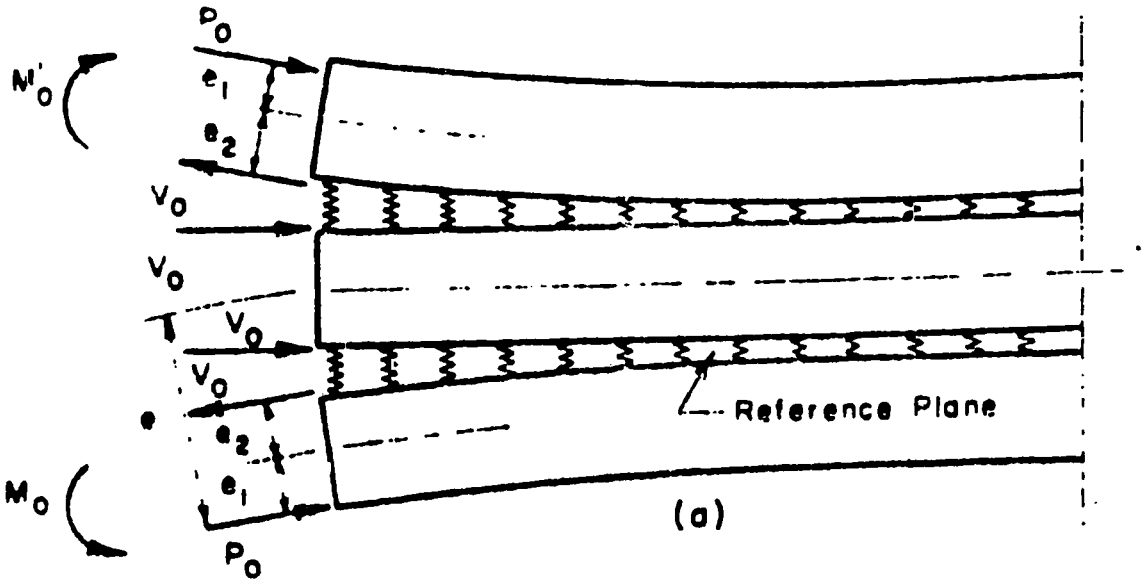

FIGURE 2.15 : Sozen's physical analog

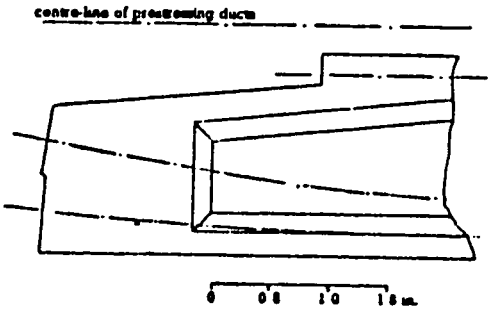

FIGURE 2.16 - Model end block tested by Christodoulidis.

chapter 3

EXPERIMENTAL TECHNIQUES

3.1 APPARATUS

The apparatus used in this investigation consisted of the following items:

(i) A transmission polariscope specially suited for observations on frozen slices removed from the three-dimensional models (Figure 3.1).

(ii) A 17-inch diffused light transmission polariscope (Figure 3.2).

(iii) A telemicroscope consisting of a 4 x digitive lens, 10 x eyepiece, f/3.5 43-86 mm zoom lens giving an overall maximum magnification of approximately 15 x (Figure 3.2).

(iv) A casting and stress-freezing oven (Figure 3.3).

(v) Loading frames to load the single and multiple anchorage models (Figure 3.4).

(vi) Instron 250 k Newton capacity universal testing

machine for loading the concrete end blocks (Figure 3.5).

(vii) Ultrasonic pulse velocity equipment for detecting the cracking of concrete end blocks (Figure 3.6).

The transmission polariscope (Figure 3.1) which was used most of the time for recording photoelastic data is a specially designed equipment which is admirably functional for normal incidence photoelastic measurements. The slice is simply supported on a precision x-y table and without any further adjustments all measurements can be performed. The built-in magnification (calibrated 10X) enables the examination of details on the slices with a clear bright image of the photoelastic pattern appearing on a 12-inch screen.

The assembly of the diffused light polariscope and the telemicroscope is shown in Figure 3.2. This equipment was used from time to time to discern the movement of isoclinics in a wider field. The diffused light polariscope consists of a polarizing assembly, analyzing assembly, diffused white light source, mechanical drive coupling system for remote control of all four filters.

The special features of both the transmission polariscopes are:

(i) Suitability for reading fractional fringes by the Tardy method.

(ii) The analyzer is independently rotatable ensuring accurate measurement of fraction of fringe order within 1/100 of a fringe on a specially graduated dial.

(iii) Monochromatic light is obtained by an efficient narrow and interferential filter. It provides a bandpass of less than $100^{o}A$ at the wavelength of the tint of passage, producing an almost black fringe at every location at which the tint of passage is observed in white light.

The telemicroscope is mounted in position on x-y rack and the front zoom lens permits observation of a relatively wide area to locate the point of interest and then zooms to high magnification forthe desired detail by projecting the image at the focal point of the rear mounted microscope.

The casting and stress-freezing oven is a highly efficient model which has a 12" x 12" stress free viewing window with built in polarizers. It has a cam programme, variable from 25 to 600 hours with heating or cooling rate continuously adjustable from $1/2^{o}F$/hour to $25^{o}F$/hour with

pen recorder. Horizontal forced air circulation ensures a reasonable uniformity of temperature.

Three loading frames shown in Figure 3.4 were specially designed and fabricated for this research project. In the design of each frame special attention was paid to three considerations. Firstly that model is properly and rigidly supported; secondly, the forces applied are correct in magnitude and direction and continue to maintain the prescribed values for sometime at high temperatures of 130-140^{o}C when the models are being stress-frozen; and thirdly, that the auxiliary members transmitting forces and reactions to the model are designed kinematically, so that straining movements do not affect the loading conditions. Figure 3.4(a) shows a loading device wherein the model is very securely supported on a rigid platform which can be moved up and down. The load is applied to the model by means of a lever and weights, and several holes are provided in both lever and frame so that a suitable positioning of the lever with respect to the model can be obtained. A vernier adjustment with the help of a screw is incorporated in the frame for levelling the lever after the load is applied. The levelling position is monitored by a level

affixed to the lever arm. This adjustment ensures constancy in the lever ratio and the truly vertical direction of the applied load.

The frame shown in Figure 3.4(b) has a rigid load supporting base with the loading plate mounted on four pillars through highly efficient bearings. Loads are placed on predetermined position which ensures a truly central and vertical force application.

The end block of the beam wherein multiple anchorages were used was post-tensioned in the frame shown in Figure 3.4(c). This is a simple rigid frame with carefully located holes through which hang the cables which carried plate anchorages at the upper end and were loaded with weights on discs at the lower end.

The detection of onset of cracking in concrete was made using an ultrasonic pulse technique. The apparatus used was a portable ultrasonic non-destructive digital indicating tester shown in Figure 3.6 and Figure 3.7 describes the system. Two transducers of 80 HZ frequency were used. An ultrasonic pulse of longitudinal vibrations is produced by one of the electro-acoustical transducer, which is held in contact with one surface of the concrete

member under test. After traversing a known path length in the concrete the pulse vibration is converted into an electrical signal by the second electro-acoustical transducer, and the electronic timing circuits enable the transmit time of the pulse to be measured and displayed. Knowing the path length and time, the pulse velocity is computed. As pulses cannot traverse cracks, they take a longer path and hence more time to reach the second transducer. This causes a sudden decrease in the pulse velocity signalling the onset of cracking. Figure 3.7 shows the end block models in instron compression testing machine with the transducers in position.

3.2 MODEL MATERIALS

The properties of Araldite B have been studied extensively by Baud and Racke,[35] Spooner and McConnel[36] and also Dixon.[37] At room temperature the resin in combination with 30 percent by weight of hardener HT901 has an average values of Young's Modulus of 4.2×10^5 lb/sq. inch and a material fringe value of 59 lb/in fringe. At 135°C it has an average value of Young's Modulus of about 1950 lb/sq. in, a fringe value of 1.28 lb/in fringe, and a figure of merit, defined by Leven[38] as E/f, of 1300. On the basis of

this criterion the stress-optical sensitivity of Araldite B is higher than most other materials in use. Moreover,it can be cast relatively free from initial stress if the model is not large size as it has low curing shrinkage and exotherm and unlike Araldite MY 753 has a high stability of stress pattern. Its machinability is good and the time edge effects can be eliminated by maintaining the models at a room temperature of about 60°C. For these reasons, all the models used in the present investigation were made from Araldite B in combination with 30 percent by weight of hardener HT 901. The resin and the hardener were heated separately to 130° - 140°C in an oven till both were melted. The hardener was then added to the liquid resin through a very fine mesh sieve and stirred thoroughly till a homogeneous and clear mixture was obtained. It was poured through the fine mesh into the moulds which were preheated to a temperature of 130°C. After 10 minutes of cooling the moulds were placed in the casting oven, the temperature having been set to 120°C, where they were held for about 16-20 hours for the curing of the castings. After the curing period was over, the oven was cooled down to room temperature at the rate of 2°C/hour and finally examined to ensure that the initial stresses did not excee one fringe per inch.

3.3 MODELS

The three-dimensional photoelastic models of the rectangular prestressed concrete beams were machined from oversize blocks of Araldite B, previously annealed to remove initial stresses. Various machining operations were performed with the normal workshop equipment using tungsten carbide tipped tools. In general, sharp tools, very light cuts (0.001 - 0.003 inch per revolution), moderate cutting speeds and proper support of the model were always employed to avoid introducing undesirable machining stresses.

The specimens were first finished a little oversize by cutting on a band saw using moderate speed and a blade having about 18 teeth per inch. The feed was kept extremely low and the temperature rise of the blade was closely controlled using a vacuum cleaner with nozzle set above the work. The models were then finished by careful milling ~~milling~~ operations using a normal high speed steel helical milling cutter 2" diameter. The surfaces obtained were found to be completely satisfactory. Holes to simulate cable ducts were drilled using long spiral drills and the cavities for the plug simulating the Freyssinet anchorage unit were formed by cutters specially made for this

purpose. The tension pieces for calibration purposes were made from the same material block as used for model making.

The finished models were kept in a temperature controlled oven at 60°C to prevent the development of time edge stresses. Typical models used are shown in Figure 3.9.

3.4 ANCHORAGE UNITS

The Lee-McCall, CCL compact plate,Magnel-Blaton and Gifford-Udall systems employ some form of anchor or thrust plate which is usually rectangular in shape and is positioned external to the concrete. The load in all these systems is thus transferred to the beam through a plate or bearing action. In the photoelastic tests the external anchorage was therefore simulated by steel plates which were, however, applied to the photoelastic model material through a pad of silica filled Araldite (100 parts by weight) for two reasons. Firstly, the coefficient of thermal expansion of steel is about 1/5 times that of Araldite B. The use of the pad would avoid excessive shears due to differential thermal expansion. Secondly, the value of E for steel is about 4-5 times that of concrete used in prestressing, whilst it is 15 x 10^3 times that of Araldite B at 140°C. The direct application of steel plates to

the Araldite blocks would therefore cause a very deep indentation at the edges of the loading pads, causing effects which are unrepresentative of the real situation in the prototype. The Young's Modulus of silica filled Araldite at 140°C was determined in a loading test (Figure 3.10) and was found to be about 8000 lb/sq. in. This is about four times that of unfilled Araldite and the combination is comparable to that of steel and concrete.

The prototype Freyssinet anchorage unit consists of a heavily reinforced concrete cylinder with a conical hole running through it. The prestressing wires lie around the surface of this hole and are firmly held by a tapered concrete plug that is driven tightly home. The whole unit is basically of a cylindrical form with the wires passing through a central hole. The conical shape of the hole and the action of the inserted plug are only important in that they may give rise to some bursting stresses in the female cone. These stresses,however, are amply resisted by the heavy spiral steel reinforcement round the outside of the female cone. It is for this reason that the Freyssinet unit has been simulated by a simple cylinder glued into the female cavity of the Araldite model of the end block by means of a cold setting epoxy resin, leaving a central hole

in the anchorage unit through which the stressing cable may pass. The load at the top of this unit is applied through a round steel washer of the same diameter as the inserted cylinder. To avoid the direct contact between the steel of the washer and the material of the end block, the anchorage is left slightly proud of the beam section.

The actual Freyssinet anchorage unit is much more strongly reinforced than the concrete surrounding it. It would be,therefore, as a whole stiffer than the concrete of the adjoining beam. For this reason the model of the anchorage used in the photoelastic tests was made of Araldite B reinforced with 50 parts by weight of silica flour used as a filler. It was found that the value of Young's Modulus was raised to about twice the value of unfilled Araldite at 140^{o}C. This was considered to be adequate.

The concrete models of end blocks were 4" x 4" x 8" and were cast from the concrete in a wooden form. The poured concrete was vibrated on a vibration table for 30 seconds. The specimens were stripped after 24 hours and were then kept in a curing tank at room temperature for 28 days.

3.5 LOADING ARRANGEMENT

The single anchorage external and embedded models were loaded in a vertical position in either of the two loading frames shown in Figures 3.4(a) and 3.4(b). Every precaution was taken to align the models properly.

The base plate of the frame was made perfectly horizontal with the help of a sensitive level after the loads had been imposed. The models were always placed on a platform made up of three flat layers of Araldite B sheets to allow freedom of lateral expansion at the base. The prestressing force was applied either through the lever arm (Figure 3.11a) or thorugh the loads located on the top steel plate (Figure 3.11b). In either case the load was applied through balls housed in suitable recesses in the anchorage plates as well as in the lever arm (frame of Figure 3.4a) and the loading plate(frame of Figure 3.4b).

The loading in the case of the multiple anchorage end block was done in the manner shown in Figure 3.4 (c). The positioning of the block was done in the same manner as in the single anchorage models. However, the prestressing was applied by cables passing through the ducts.

3.6 FREEZING CYCLE

The temperature in the oven, after the models were properly aligned and loaded, was raised to 140°C at the rate of about 2°C.hour. The oven was maintained at this temperature for 6-8 hours allowing the model to soak in this environment to ensure that uniform temperature was achieved throughout the thickness of the model. Throughout the freezing cycle, a fan inside the oven circulated the air freely, reducing the temperature gradients. The oven was cooled down at a rate of 2°C.hour to room temperature. This sequence of operations formed the complete freezing cycle after which the model was ready for slicing. A typical freezing temperature regime is shown in Figure 3.12.

3.7 SLICING PROCEDURE

Before carrying out the freezing cycle on the models, the boundaries and the centre lines of the required slices were scribed on them by means of a precision vernier height gauge. The gauge used and the scribed models are shown in Figures 3.13 and 3.14. Slices from the frozen model were sawn roughly on a band saw to an average thickness of about 0.10 inches. They were subsequently finished by a

milling operation to the required thickness using sharp tipped tools and extremely low feeds. These were then ground lightly on a fine and then polishing emery paper.

The thicknesses of the prepared slices varied from 0.06 to 0.08 inches. For convenience of location of the points for observation, a suitable grid of horizontal and vertical lines was inscribed on the surface of each slice. Slices were stored in oven at $60^{o}C$ until immediately prior to examination to eliminate the induction of edge stress effects.

3.8 EXAMINATION OF SLICES

Most of the slices were examined for stress exploration in a normal incidence position. The slices were placed on the precision X-Y table and the isochromatics and isoclinics were observed on the glass screen at grid points (Figure 3.1). The transmission polariscope was operated in accordance with Tardy method to record the fractional fringe numbers at the predetermined grid points.

3.9 TESTING OF CONCRETE ENDBLOCK MODELS

The concrete models were listed till failure in the Instron compression testing machine. SR-4 strain gauges

were fixed on the two faces (Figure 3.15) to measure the lateral and longitudinal strains at pre-determined locations. The onset of cracking was monitored by ultrasonic pulse velocity measuring equipment. The failure pattern was carefully examined to study the failure characteristics of the end block.

3.10 DETAILS OF PHOTOELASTIC MODELS INVESTIGATED

For ready reference the details of the photoelastic models investigated are given in Table 3.1.

3.11 CHECKS ON ACCURACY

It is customary to establish the accuracy of a photoelastic analysis by applying equilibirum checks to the forces at various sections in the body. A static check is obtained at points where the longitudinal stress YY has been calculated by a numerical integration procedure along a longitudinal line which ends in a free surface. At such closing points the calculated value should be zero. In the models tested in this investigation the maximum closing error is 0.5 lb/sq.in. in a case where the starting value of yy at the base was about 24.5 lb/sq.in. In terms of the mean compression this error is about 2%. In all the other

cases the closing error is less than 3%.

The second check is provided by the requirement that at any section the applied force must be equal to the corresponding force obtained by integration over the cross-section. The values of yy obtained photoelastically for concentric and multianchorage units have been compared with the theoretical values. It was found that in all cases the error was within 3 percent.

TABLE 3.1

Model Dimensions and Loading

Model No.	Model Dimension in inches	Position of load	Load Concentration $K_A=A_1/A$	Load Concentration $K_a=a_1/a$	Load Applied (lb)	Remarks Type of anchorage unit
1	1.5x1.5x3	Concentric	0.1	0.316	55.1	External
2	1.5x1.5x3	"	0.25	0.5	55.1	"
3	1.5x1.5x3	"	0.35	0.592	59.4	"
4	1.5x1.5x3	"	0.5	0.707	59.4	"
5	1.5x1.5x3	"	0.35	0.592	58.3	"
6	1.5x1.5x3	"	0.25	0.5	58.9	Embedded
7	1.5x1.5x3	"	0.25	0.5	58.9	Embedded
8	1.5x3x6	3 loads are applied at distances of 0.392",1.269" and 2.344 from the bottom	-	-	3 equal loads 55 lb each	External

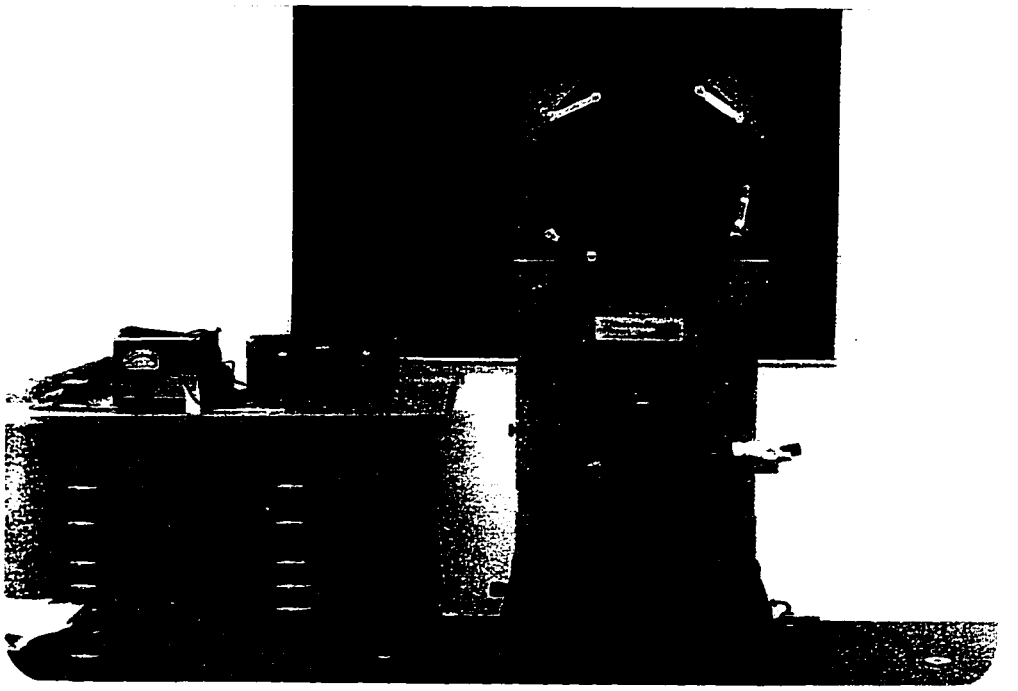

FIGURE 3.1 : A transmission polariscope

FIGURE 3.2 A 17-inch diffused light transmission polariscope with the telemicroscope

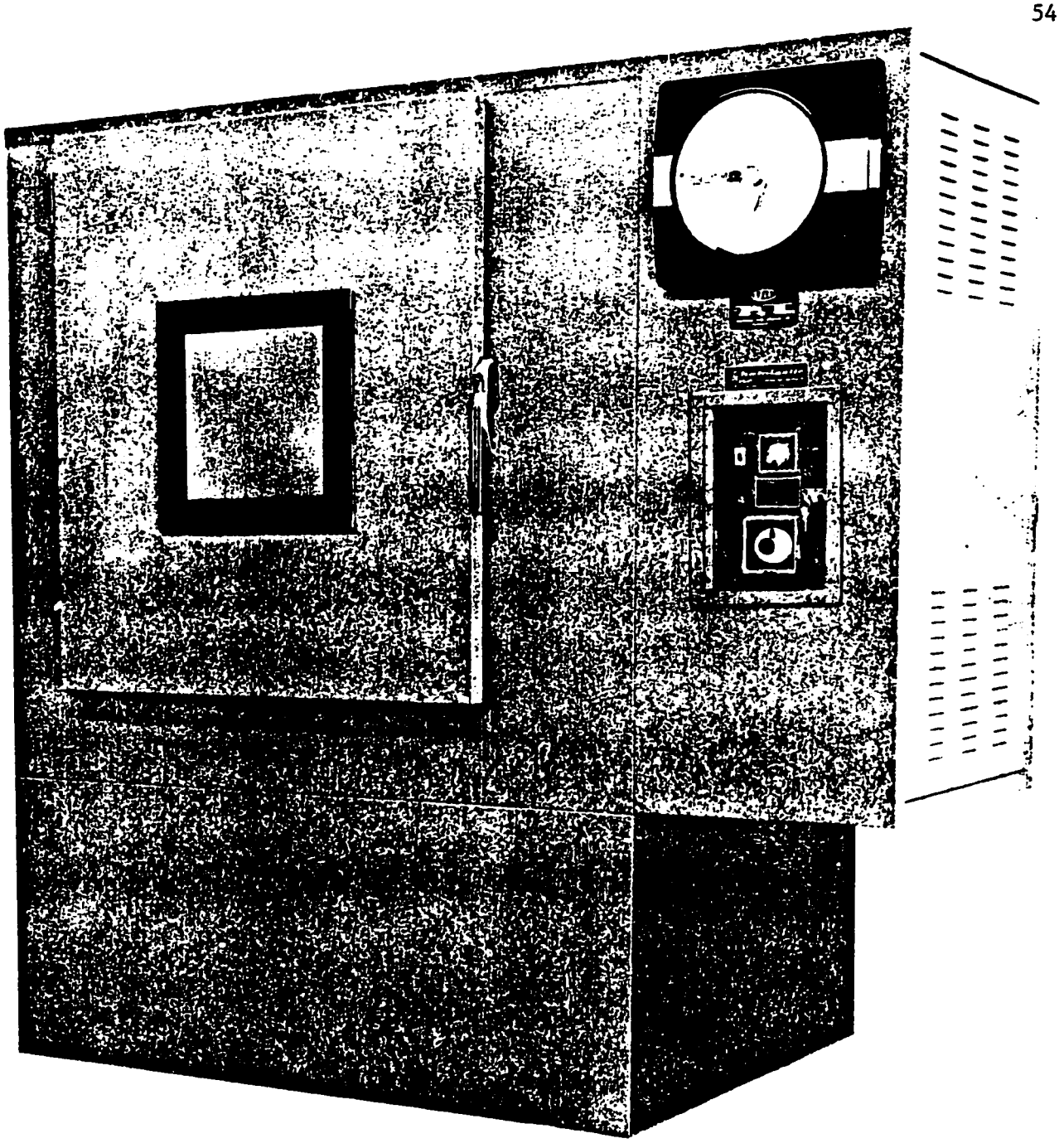

FIGURE 3.3 : Casting and stress-freezing oven

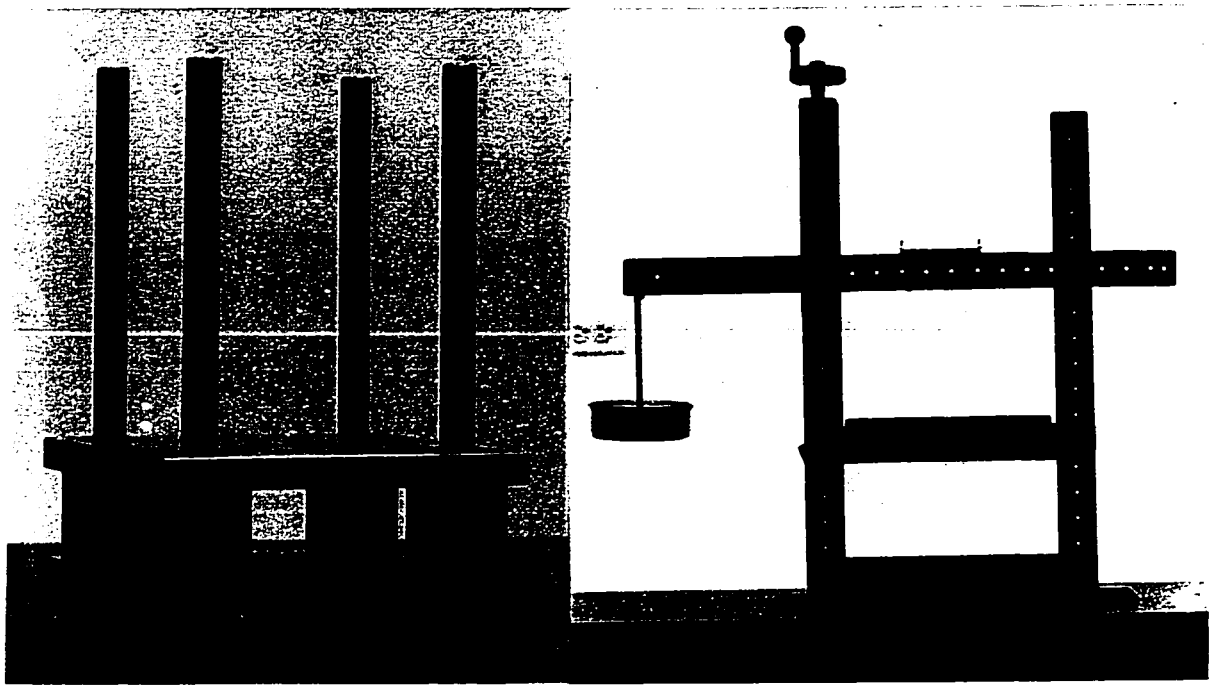

(a) (b)

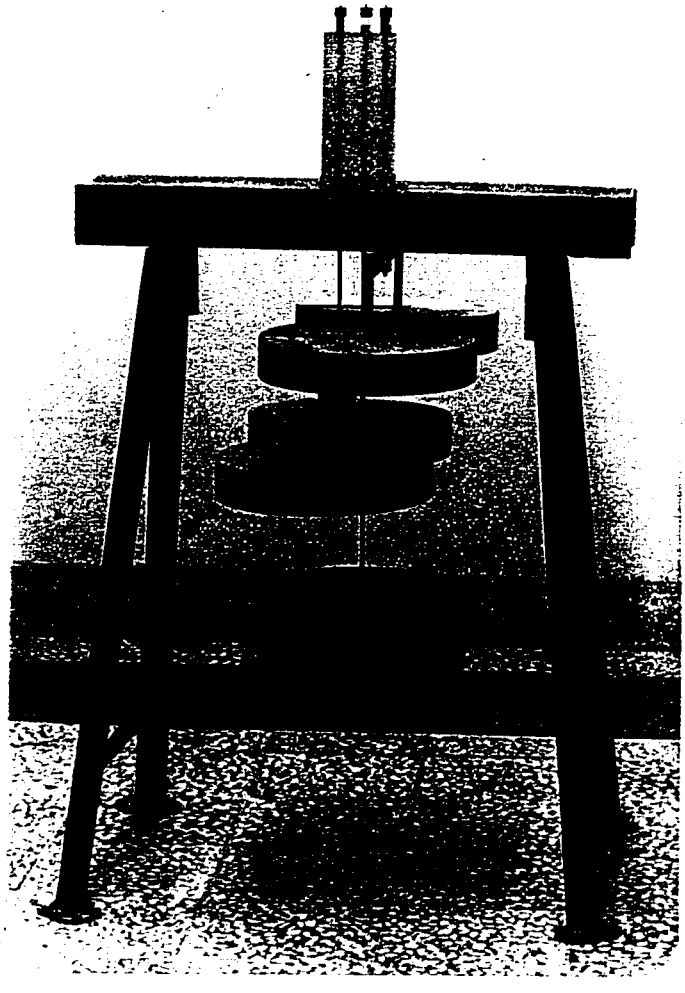

(c)

FIGURE 3.4 : Loading frames

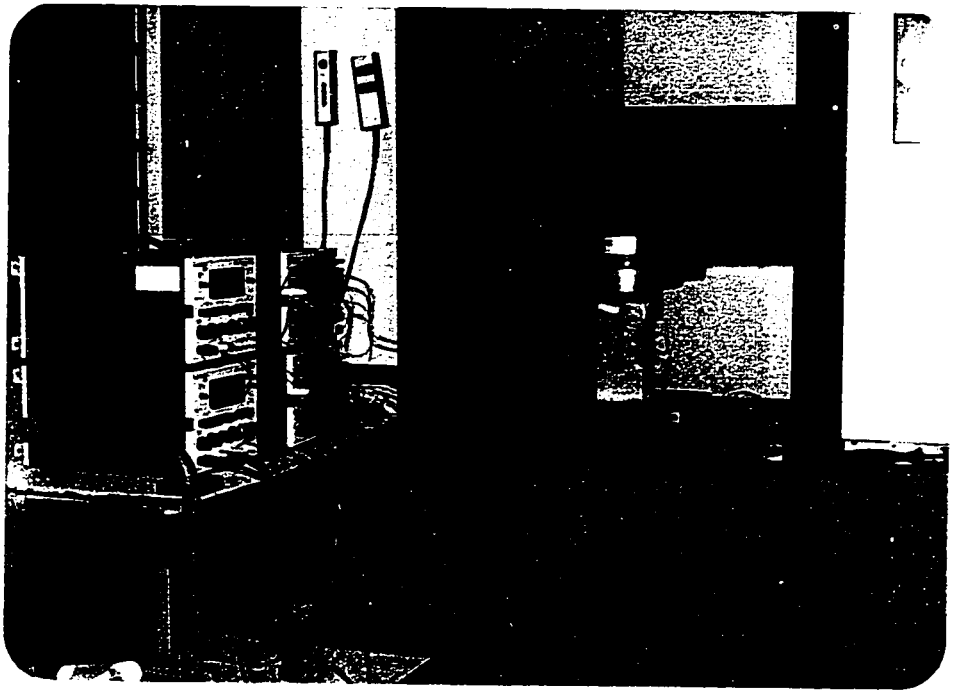

FIGURE 3.5 : Instron unviersal testing machine

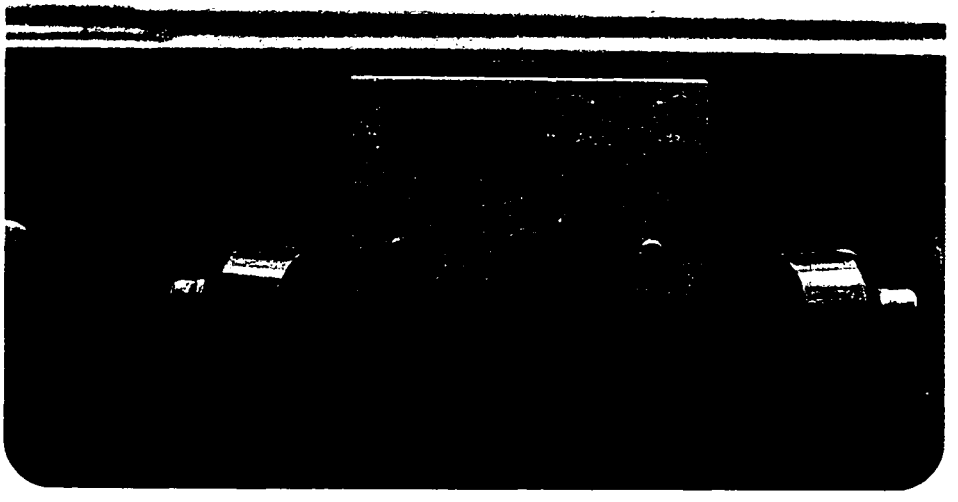

FIGURE 3.6 : Ultrasonic pulse velocity equipment

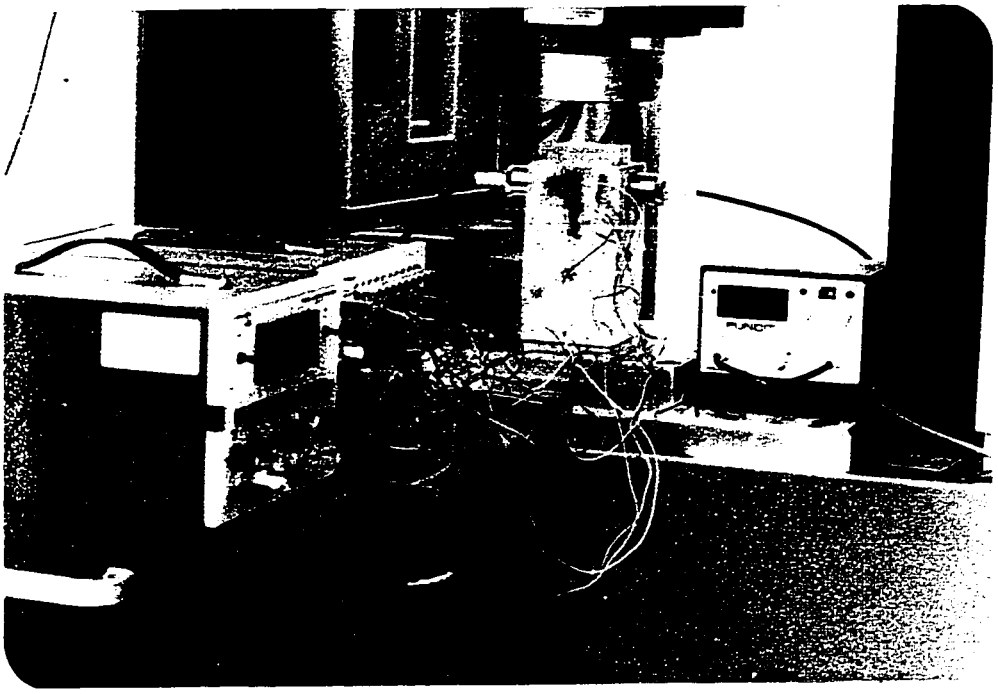

FIGURE 3.7 : The end-block model in the instron compression testing machine with the transducers in position

FIGURE 3.8 : The moulds used for casting the photoelastic end block models

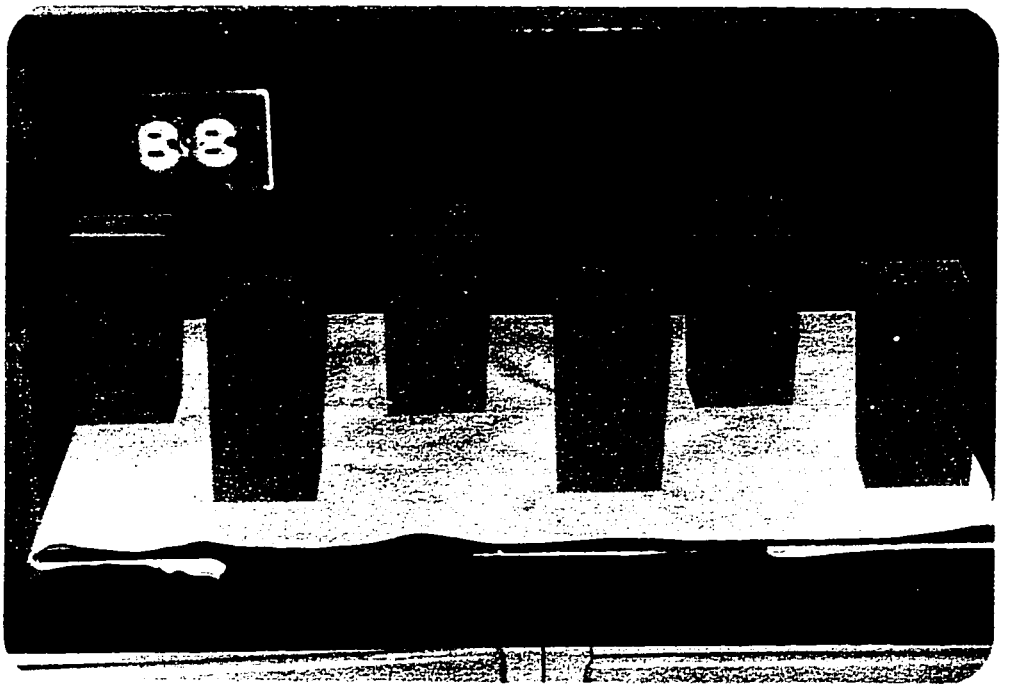

FIGURE 3.9 : Typical models

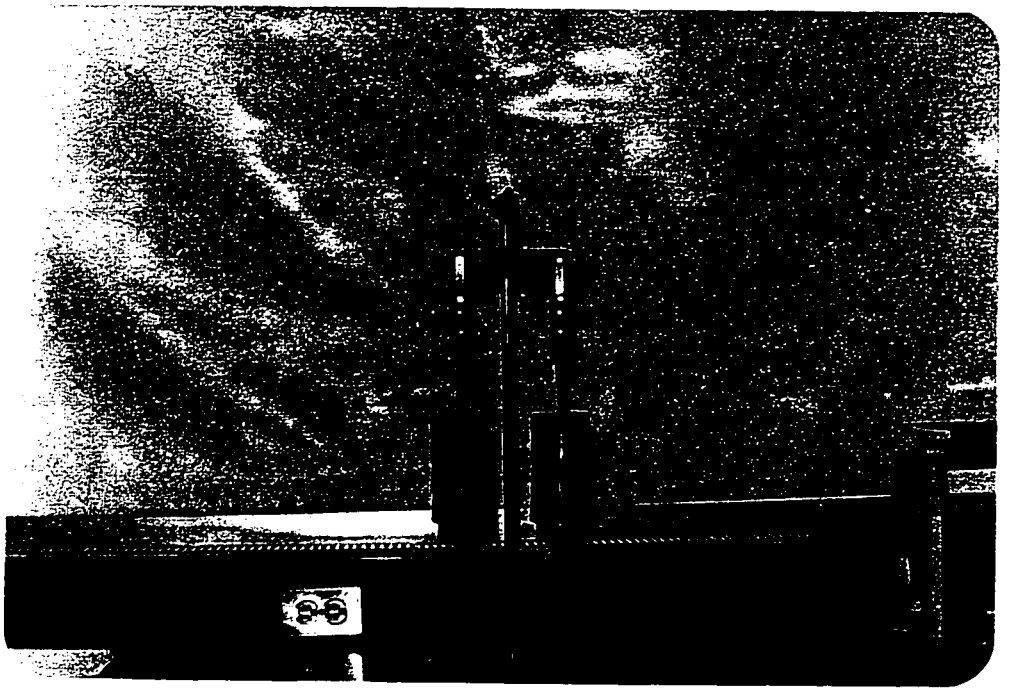

FIGURE 3.10 : Loading test done to determine the Young's Modulus of silica filled Araldite at 190°C

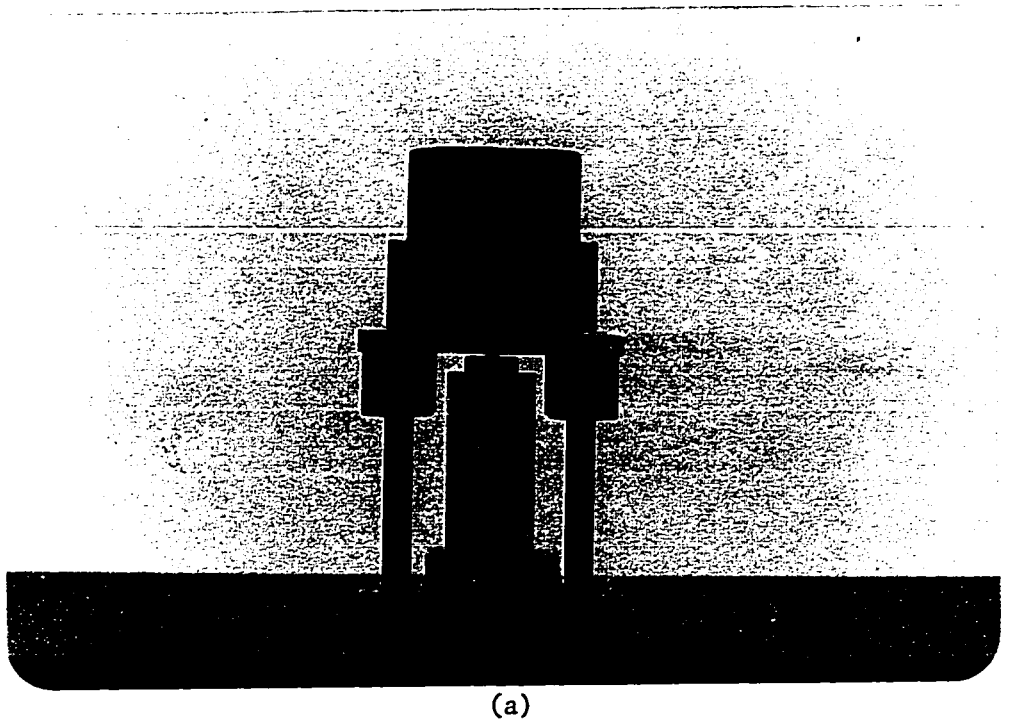

(a)

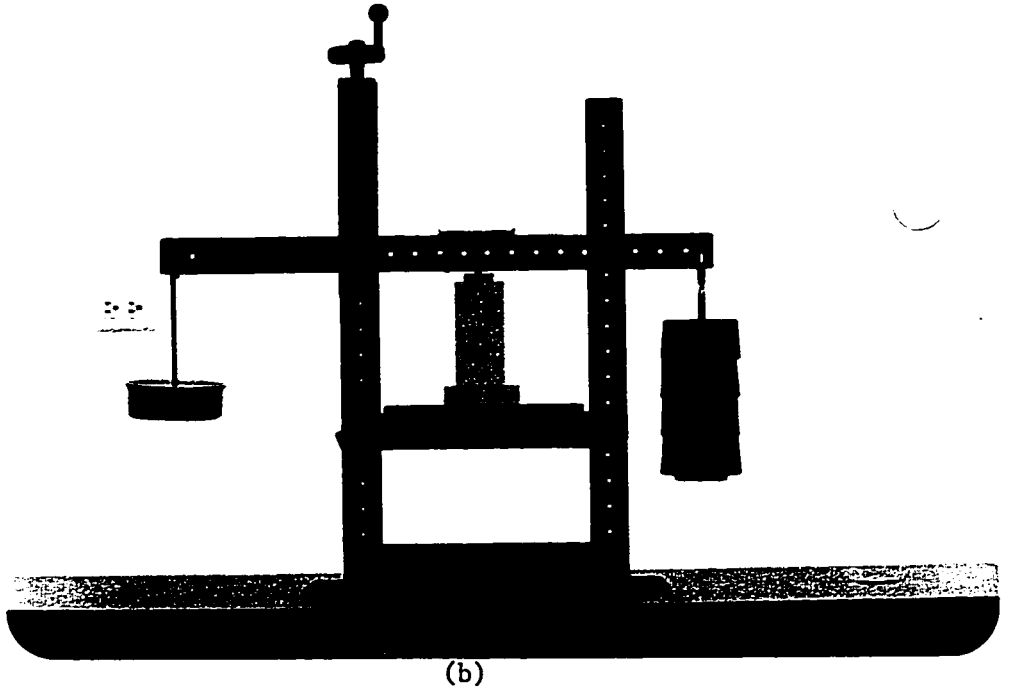

(b)

FIGURE 3.11 : The frames in loading position

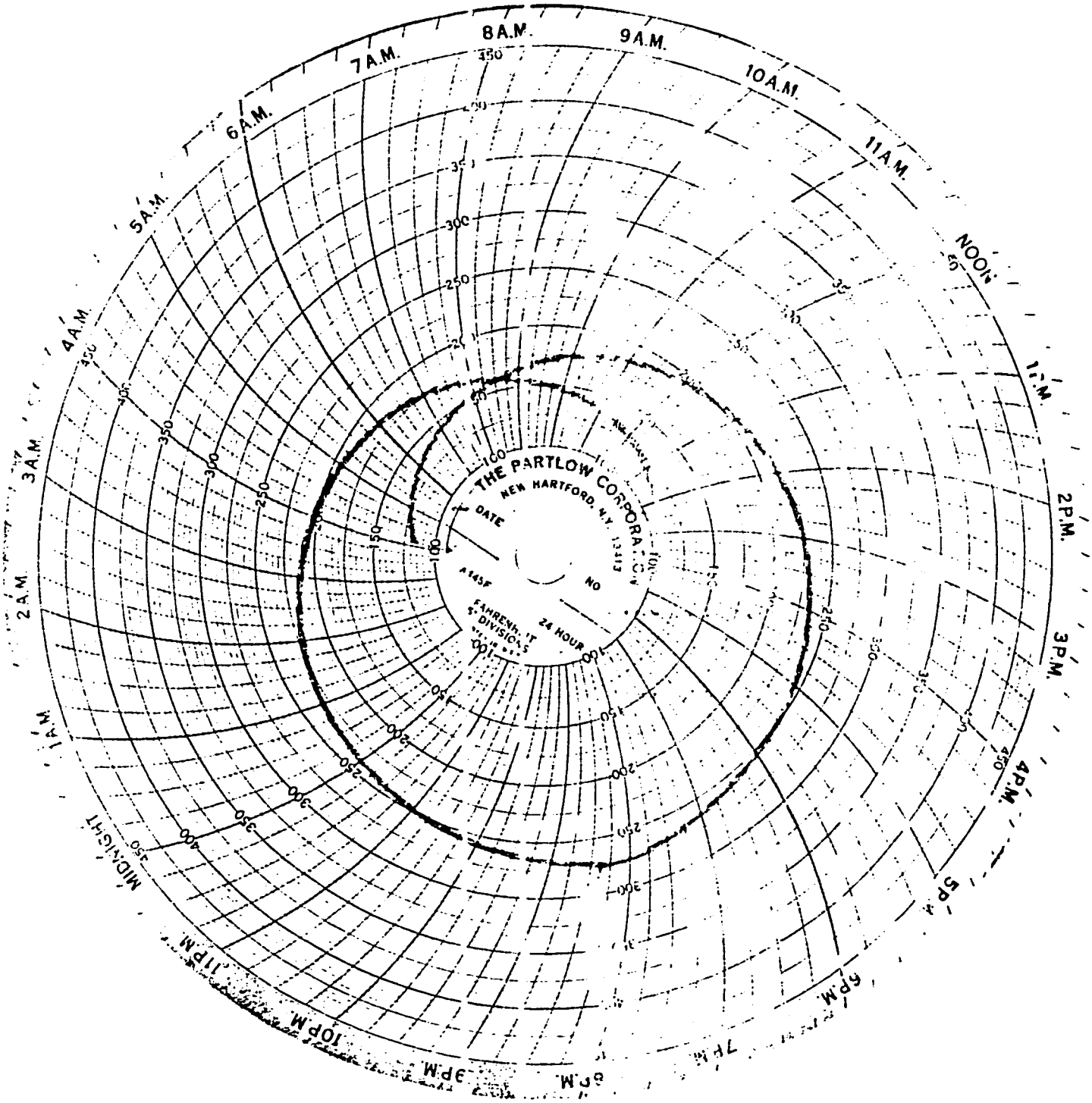

FIGURE 3.12 : A typical freezing temperature regime

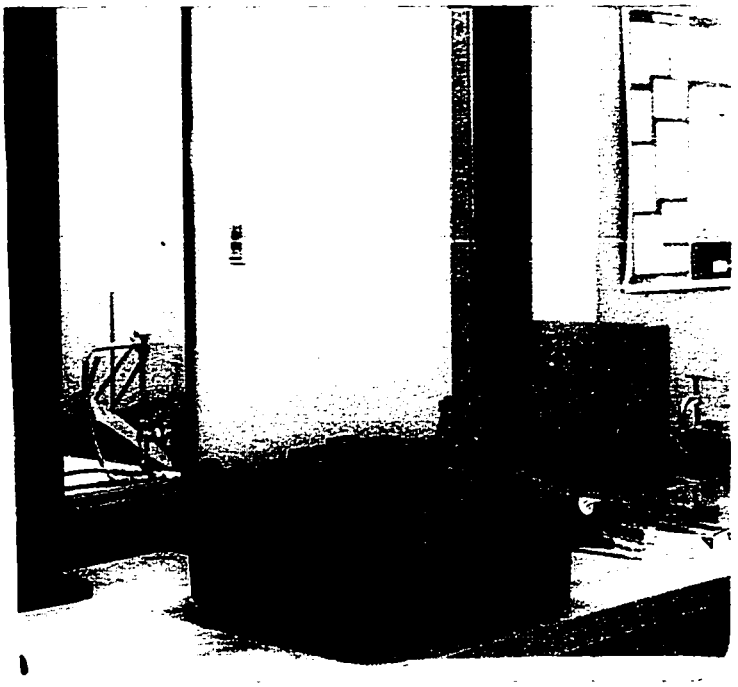

FIGURE 3.13 : The gauge used in scribing the models and slices

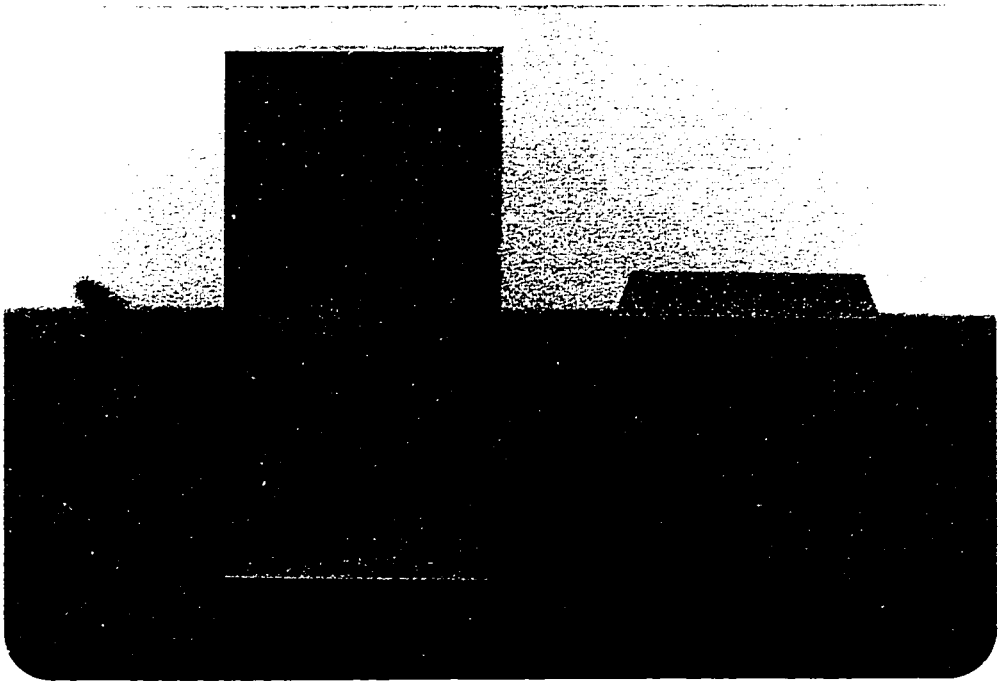

FIGURE 3.14 : The scribed models

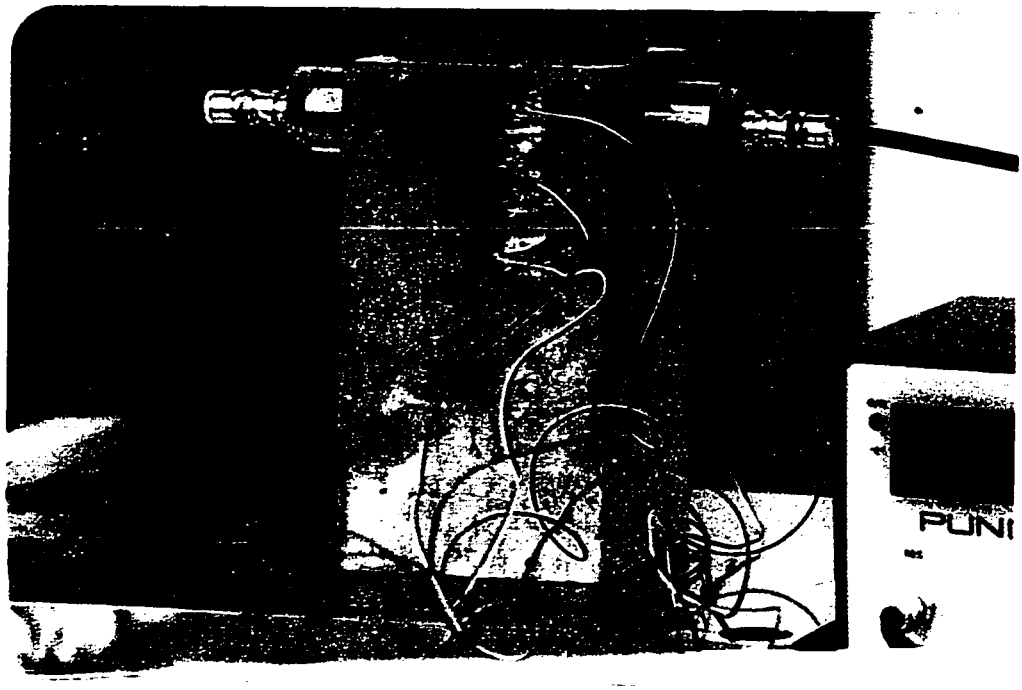

FIGURE 3.15 : SR-4 strain gauges fixed on the end block beam

chapter 4

THREE-DIMENSIONAL ANALYSIS OF STRESSES

The three-dimensional analysis of stresses has been made using the "frozen-stress" technique. This amazing phneomenon which results in fixing or freezing the stresses pertaining to an applied load system is attributed to the diphasic make-up of certain resins and polymers used as photoelastic material. The stress-freezing techniques are now well known for their flexibility and versatility and have been frequently applied to the analysis and design of an exceptionally wide variety of complicated three-dimensional parts. The mechanism leading to stress-freezing is explained in detail elsewhere.

If a three-dimensional frozen stress model is observed in a polariscope, an isochromatic pattern can be seen which in general cannot be directly interpreted. This is because the light passing through the thickness of the model integrates the stress difference over the length of the path of the light and presents it as a weighted average which is meaningless with respect to the state of stress at a point

or along a specific plane.

To obviate this difficulty the three-dimensional stress frozen model is sliced along chosen planes of interest and these slices are then analyzed individually to obtain the state of stress existing along the sliced planes.

From the point of view of analysis one can recognize generally two types of slices:

(i) Internal slices taken from the interior of the model.
(ii) Surface slices removed at the surface of the model.

Generally speaking, a slice which is taken from the interior of a model does not coincide with the principal plane. A plane of symmetry, with respect to both the applied loads and the geometric shape of the model,however, is an exception. Such a plane is a principal plane of stress at all points and observation of a thin slice containing the plane of symmetry will give us the distribution of principal stresses in the plane. However, in all other interior sliced planes the stresses are referred to as secondary principal stresses and are denoted by P',Q' and R' which do not coincide with the principal stresses P, Q and R. Also, the solution of the general three-dimmensional

problem at internal points not situated in a plane of symmetry necessitates the calculation of six catesian stress components by means of photoelastic observations.

Of all the methods proposed for stress separation, the integration of the body-stress equations is the most convenient and versatile. In the form it is used with reference to cartesian axes and in this research it is called the "shear difference" method as proposed by Frocht[39,40,41] and described in detail elsewhere. For ready reference it is briefly recounted here with reference to Figure 4.1.

The equations of equilibrium for a three-dimensional body (without body forces) are written as:

$$\frac{\partial xx}{\partial x} + \frac{\partial xy}{\partial y} + \frac{\partial xz}{\partial z} = 0 \qquad (1)$$

$$\frac{\partial xy}{\partial x} + \frac{\partial yy}{\partial y} + \frac{\partial yz}{\partial z} = 0 \qquad (2)$$

$$\frac{\partial xz}{\partial x} + \frac{\partial yz}{\partial y} + \frac{\partial zz}{\partial z} = 0 \qquad (3)$$

Referring to Figure 4.1 consider the determination of the state of stress at a point B on the line AB in a three-dimensional mode (Figure 4.1a). Firstly, the normal stress yy at the point B can be obtained by integrating the second

equilibrium equation :

$$\int_A^B \frac{\partial xy}{\partial x}\, dy + \int_A^B \frac{\partial yy}{\partial y}\, dy + \int_A^B \frac{\partial yz}{\partial z}\, dy = 0$$

which can be written as

$$yy_B = YY_A - \int_A^B \frac{\partial xy}{\partial x}\, dy - \int_A^B \frac{\partial yz}{\partial z}\, dy = 0$$

In the above equation

YY_B = normal vertical stress at point B

yy_A = normal vertical stress at point

$\frac{\partial xy}{\partial x}$ = rate of change of shear xy with respect to x.

$\frac{\partial yz}{\partial z}$ = rate of change of shear yz with respect to z.

The values of $\frac{\partial xy}{\partial x}$ and $\frac{\partial yz}{\partial z}$ can be obtained at any point by observing the slopes of xy and yz shear curves drawn along x and z respectively. For small intervals dx and dz the values of xy and yz are obtained from the slices taken in the xy-plane (Figure 4.1b) and in the yz-plane (Figure 4.1c) respectively. The xy shear curves $[\frac{1}{2}(P-Q)\sin 2\alpha)]$ are drawn along x at all levels knowing

the principal stress difference (P-Q) and the directions of the principal stress (α_1) from the photoelastic data in the xy slice plane. Similarly the yz shear curves [$\frac{1}{2}$(R-Q)sin $2\alpha_2$)] are drawn along z at all levels knowing the principal stress difference (R-Q) and the directions of the principal stress (α_2) from the photoelastic data in the yz sliced plane. In the present investigation values of ∂xy and ∂yz for fixed small values of dx and dz (cols 3 and 8 Table 4.1) were obtained by drawing tangents on the xy and yz shear curves and these recorded values of xy and yz (cols 2 and 7 of Table 4.1) were plotted against the y-distance along the vertical section BA. A typical plot of ∂xy and ∂yz values against Y-distance for Model M_2 is shown in Figure 4.2. The evaluation of quantities ∂xydy; and ∂yzdy is carried out on the plots of ∂xy and ∂yz against y (cols 4 and 9 of Table 4.1) and the final integration is done in column 12 of Table 4.1. The entire computation is done in a tabulated form a typical sample of which is shown in Tabde 4.1. The value of YY_{AA} is known at a sufficiently low level where the vertical normal stresses have become uniform. YY_B is,therefore, conveniently computed.

Knowing yy, (P-Q) and α_1 in the xy-plane, the value of separate principal stresses P and Q are obtained by the following formulae

$$xx = (P-Q) \cos 2\alpha_1 + yy \qquad (1)$$

$$P = \tfrac{1}{2}xx + \tfrac{1}{2}yy + \tfrac{1}{2}(P-Q) \qquad (2)$$

$$Q = P-(P-Q) \qquad (3)$$

At a point on the surface, the normal stress zz (which is also the principal stress R) and the two shear components xz and yz being zero, the state of stress is essentially two-dimensional in nature and can be specified by normal photoelastic observations on the surface slice together with the information for the distribution of vertical pressures obtained previously. Use is made of the following stress relationships

$$xx = \tfrac{1}{2}(P+Q) + \tfrac{1}{2}(P-Q) \cos 2\alpha \qquad (4)$$

$$yy = \tfrac{1}{2}(P+Q) - \tfrac{1}{2}(P-Q) \cos 2\alpha \qquad (5)$$

$$P+Q = xx + yy \qquad (6)$$

Substituting xx from (4) in the right hand side of (6)

$$P = \tfrac{1}{2}(P-Q) + \tfrac{1}{2}(P-Q) \cos 2\alpha + yy$$

$$Q = \tfrac{1}{2}(P-Q) - \tfrac{1}{2}(P-Q) \cos 2\alpha - yy$$

Knowing (P-Q) and α from photoelastic observations and yy from the boundary observations of an orthogonal slice containing the surface point under consideration, separate principal stress P and Q have been obtained on surface planes.

In the aforesaid analysis it is of utmost importance to substitute shears and shear slopes with correct signs. This necessitates a consistent approach throughout the analysis. The following conventions were adopted:

1. (P-Q) and (R-Q) are considered positive at every point of the xy and yz slices.
2. Tensile stresses are positive and compressive stresses negative.
3. Figure 4.3 shows the xy and yz planes of the plate anchorage model prestressed by one cable. The lines of principal stress P are shown at the top and the sign convention with respect to the isoclinic angle (α_1) is shown. α_1 is positive for the xy-plane when measured from the positive direction of x-axis to the direction of P anticlockwise. For the yz-plane α_2 is positive when measured anticlockwise from the positive direction of Y to the direction R.

4. As (P-Q) and (R-Q) are always considered positive the signs of the shear stresses $\frac{1}{2}(P-Q) \sin 2\alpha_1$ and $\frac{1}{2}(R-Q) \sin 2\alpha_2$ depend on the signs of α_1 and α_2 . Figures 4.2b and 4.2c show the signs of the shear stresses and shear slopes.

TABLE 4.1

Calculation of Vertical Normal Stress yy in lb/in^2 Along
Vertical Section H_7 in XY Plane A
Model M_2

	Average dxy	dy	dx	dxy.dy	$\frac{dxy.dy}{dx}$	$\int\frac{dxy.dy}{dx}$	Average dyz	dy	dz	dyz.dy	$\frac{dyz.dy}{dz}$	$\int\frac{dyz.dy}{dz}$	$yy_B = yy_A - \int\frac{dxy.dy}{dx} - \int\frac{dyz.dy}{dz}$
	1	2	3	4	5	6	7	8	9	10	11	12	13
V_0													
V_1	2.7	0.125	0.5	0.3375	0.675	10.525	3.3	0.125	0.5	.4123	0.825	8.05	-24.5-10.525-8.05=-43.075
V_2	10.9	0.125	0.5	1.3	2.6	9.85	8.8	0.125	0.5	1.1	2.2	7.225	-24.5-9.85-7.225=-41.575
V_3	11.6	0.125	0.5	1.45	2.9	7.25	7.5	0.125	0.5	.9375	1.875	5.025	-24.5-7.25-5.025=-36.775
V_4	7.4	0.125	0.5	0.925	1.85	4.35	5	0.125	0.5	.625	1.25	3.15	-24.5-4.35-3.15=-32
V_5	4.2	0.125	0.5	0.525	1.05	2.5	3.1	0.125	0.5	.3875	0.775	1.9	-24.5-2.5-1.9=-28.9
V_6	2.6	0.125	0.5	0.325	0.65	1.45	2	0.125	0.5	.25	0.5	1.125	-24.5-1.45-1.125=-27.075
V_7	1.3	0.25	0.5	0.325	0.65	0.8	1	0.25	0.5	.25	0.5	0.625	-24.5-0.8-0.625=25.925
V_8	0.3	0.25	0.5	0.075	0.15	0.15	0.25	0.25	0.5	.0625	0.125	0.125	-24.5-.15-.125=-24.775
V_9													-24.5

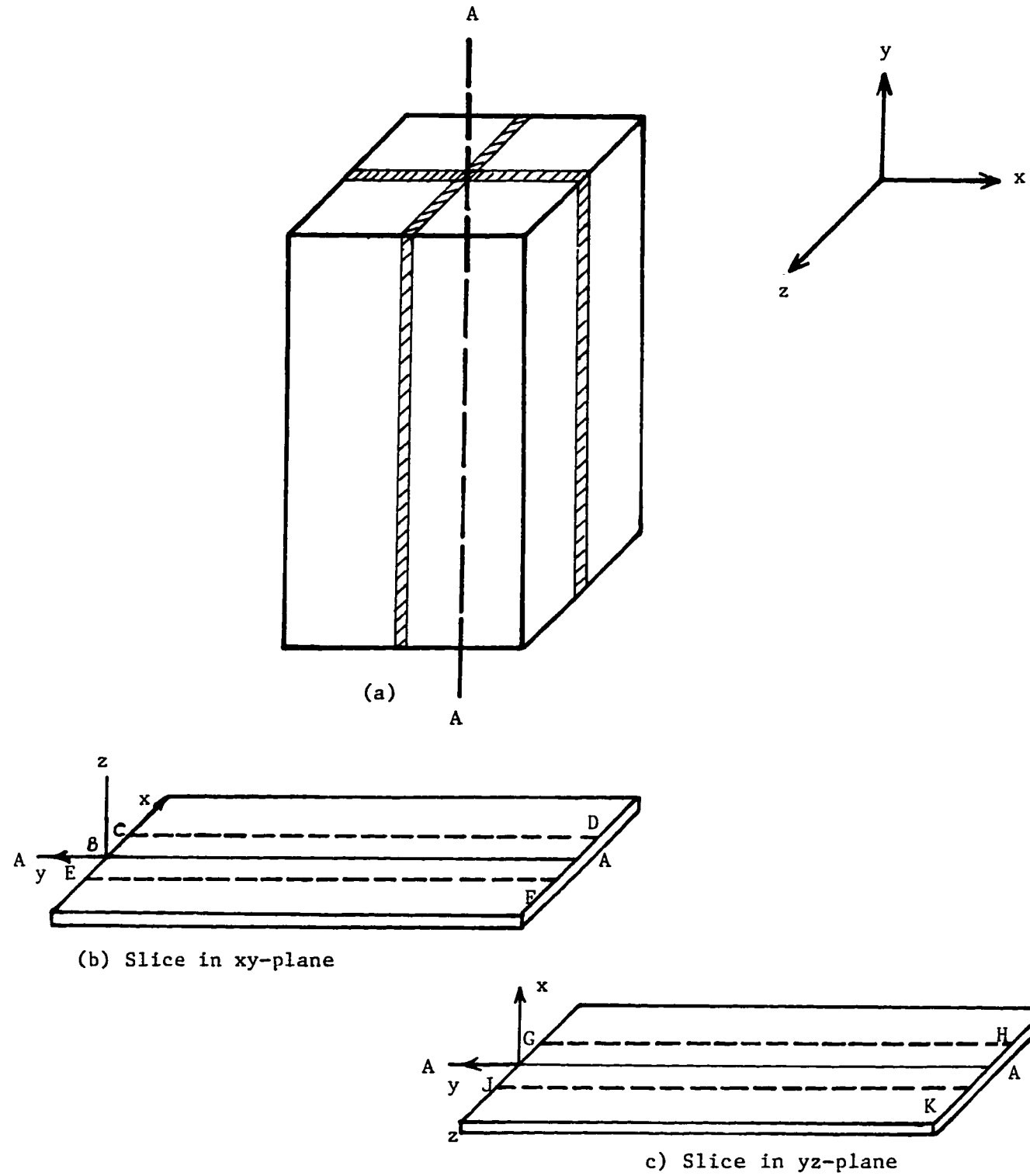

FIGURE 4.1 : Slicing scheme for shear difference method

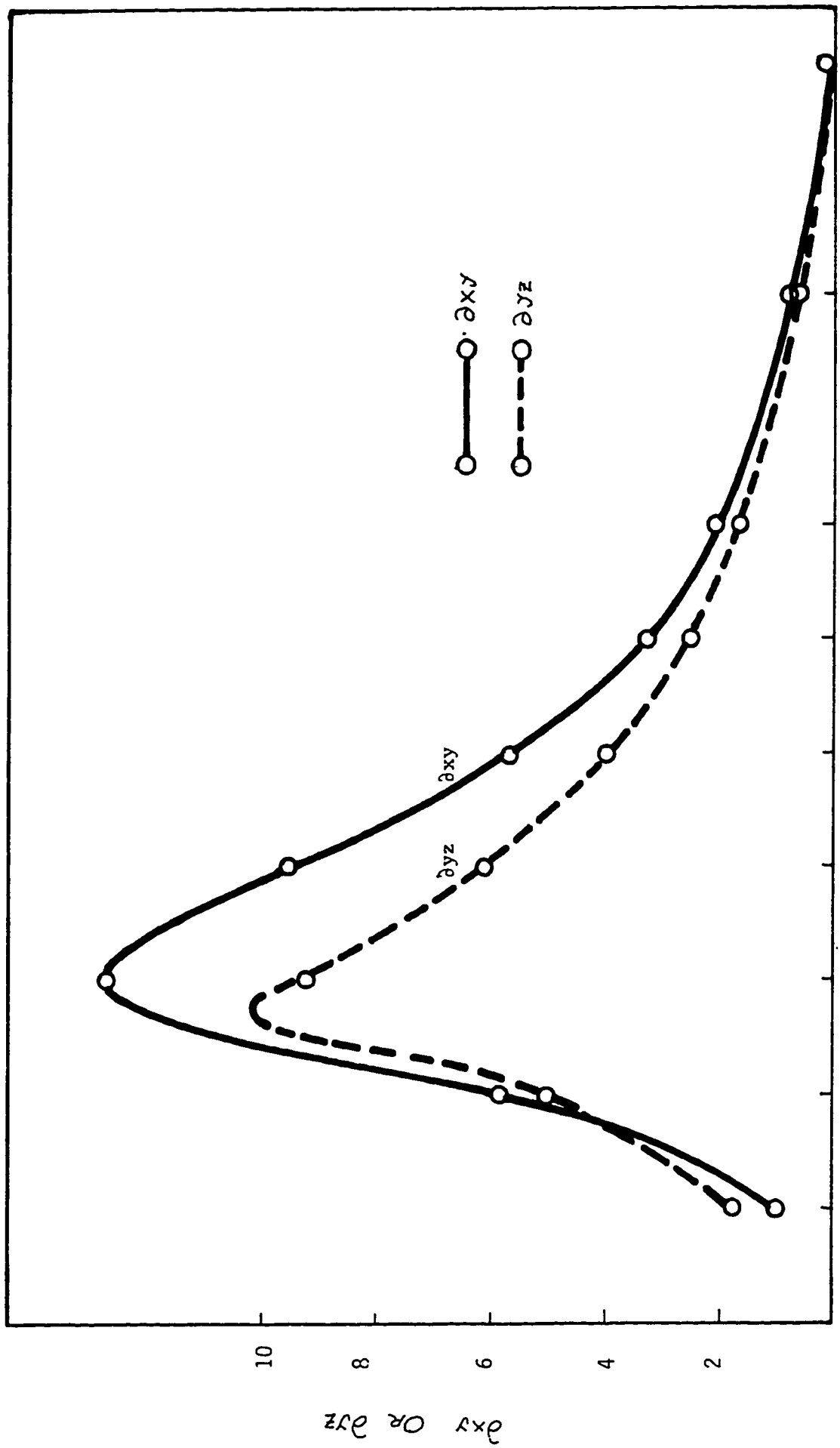

FIGURE 4.2 : ∂xy and ∂yz values against y-distance for fixed values of ∂x and ∂z equal to 0.5" for model M_2

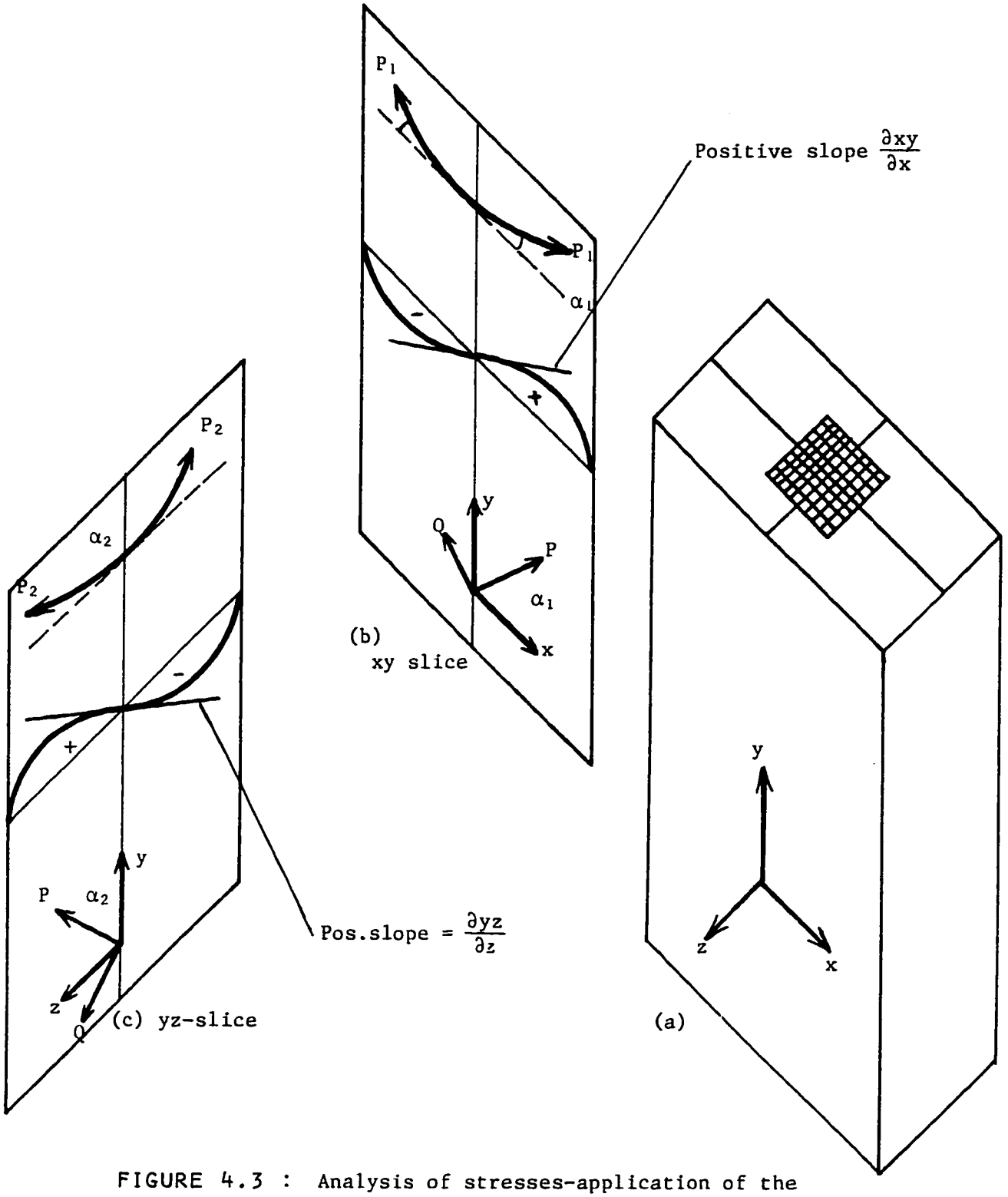

FIGURE 4.3 : Analysis of stresses-application of the shear difference method to the general three-dimensional problem

chapter **5**

THREE-DIMENSIONAL INVESTIGATION OF SINGLE EXTERNAL ANCHORAGE MODELS

5.1 INTRODUCTION

This chapter describes the three-dimensional investigation carried out using the "frozen stress" photoelastic technique on five rectangular end blocks which were prestressed by single concenterically situated cables, acting through external anchorage units. Four models of varying concentration ratios had no cable duct, as work on this series was carried out to establish a relationship between the concentration ratio and the maximum tensile stresses and forces. One model was loaded through a cable duct to investigate the effect of the duct on the magnitude and distribution of the critical stresses. The stress system has been fully explored on several planes removed from the models in the form of thin slices in an attempt to define the general behaviour and with a view to locating the regions of critical stresses.

5.2 EXPERIMENTAL PROCEDURE

5.2.1 General Details

The photoelastic models were made of Araldite B having a square cross section 1½ x 1½ and a length of 3" (Figures 5.1 and 5.2). As the object was to explore the stress distribution only in the anchorage zone, the length of which usually does not exceed the depth of the end block, only a small length of the adjoining beam was cast into the model.

The prestressing forces of 55.1 and 59.4 lb were applied on two sets of models, were concentric in all the five cases (Figure 5.1) and were applied vertically in loading frames already described in section 5 of chapter 3.

The dimensions of the anchorage units are chosen to give concentration ratios of 0.10, 0.25, 0.35 and 0.50 in terms of the ratio of loaded area to the area of cross section ($\frac{A_1}{A}$) as shown in Figure 5.3(a). These ratios correspond to values of 0.316, 0.5, 0.592 and 0.707 in terms of the frequently used terminology of $\frac{a_1}{a}$ as explained in Figure 5.3 (b). The anchorage unit simulates the CCL compact, Lee McCall or Magnel Blaton Systems. In all the cases the steel loading pad was applied through a silica

filled Araldite pad for the reasons described in section 3.4, chapter 3.

The thermal cycle for freezing the stresses is also described in chapter 3 (section 6).

5.2.2 Method of Slicing

The details of the slices cut from the frozen models are shown in Figure 5.1. Stress distribution has been obtained for the internal plane A and the surface plane B and the slicing scheme is determined from considerations detailed in chapter 4 and also on the basis that there should be enough slices to enable a satisfactory picture of stress distribution to be obtained. Advantage has been taken of symmetry with respect to the geometrical form and the system of applied loads to take most of the important slices from the same model. Therefore the slices in XY and YZ planes, which were required for a complete solution of the stress system on the surface (B) and on the plane of symmetry (A), were obtained from the same model. The width of the transverse slices was reduced by approximately 0.05 inches since a complete slice containing the mid plane of the model had been removed. The symmetry of the stress pattern across the width of the model was verified from typical observations. The thicknesses of the slices varied

from 0.06 to 0.08 inches.

5.2.3 Analysis and Measurement

The grids marked on the XY and YZ slices are shown in Figure 5.1. The calculation of the normal and principal stresses on various planes of the end block has been carried out by the application of the shear difference method to the general three-dimensional problem as explained in detail in chapter 4.

5.3 DISCUSSION OF RESULTS

5.3.1 Stress Trajectories and Shear Stresses

Figures 5.4 and 5.5 show the isoclinics and the lines of principal stress respectively for the central slice for model M_1 ($\frac{a_1}{a} = 0.316$). The pattern obtained for the remaining three models show the expected similarity. In particular the portion of the boundary above the isotropic point I_1 is in tension. The general pattern of the lines of tensile principal stress P is significant in that when local reinforcement is provided in the corners, to be most effective it should follow the lines of principal stress P tying the corners by closed kidney shaped loops rather than being located perpendicular to this direction as suggested by some investigators.

The lines of principal stress show that for all practical purposes the stress distribution becomes uniform at a distance of 1.38 a from the loaded face.

The optical fringe patterns in the important slices are shown in Figure 5.6. The mid-plane and the YZ slice 4 which are directly under the loading pad show large concentrationsof shear stresses under the edges of the anchorage plate. This is also shown very effectively by the fringe patterns on a XZ slice removed directly from under the loading pad (Figure 5.7). This slice also shows how most part of the loaded face away from the anchorage unit is almost unstressed. In the midplane of the model M_2, the maximum shear stress is about 0.81 times the mean compression at the base (Figure 5.6). These stresses, however, decrease rapidly with the distance away from the location of the loading pad. A high build up of the shear stresses under the edges of the loading pad is also indicated by Figure 5.8 which shows the distribution of shear stresses along typical transverse sections in the mid plane.

5.3.2 Internal and Surface Stresses

Separate stresses for all the four models on the internal plane A have been obtained. The principal stress

components P and Q (which are respectively equal to xx and yy for the axis of symmetry) have been calculated for the axis of symmetry across which the tensile stresses would obviously be maximum. The variation of the principal stresses, P and Q for the internal plane A along the axis of symmetry in the direction of the length of the models has been plotted in Figure 5.9 and Figure 5.10 for all the four concentration ratios investigated in this series of tests.

The two stress components P and Q for the surface plane are plotted in Figures 5.11(a) and 5.11 (b).

5.3.3 Transverse Tensile Stresses

Both in the internal and surface planes the maximum transverse tensile stress occurs on the longitudinal line corresponding to the centre line of the loading pad. Figures 5.9 and 5.11 show the distribution of principal tensile stresses respectively in the internal and surface planes along the longitudinal lines containing the maximum values for all the values of $\frac{a_1}{a}$ ratios investigated. Table 5.1 summarizes the positions and values of the maximum stresses on the two planes. In the whole range of load concentration ratio (K_A) investigated (0.1-0.50) for values from 0.12 to 0.50 the largest value of tension

in the anchorage zone occurs on the surface plane (B) where the values are 0.78 and 0.47 times the mean compression for concentration ratios of 0.12 and 0.50 respectively. The corresponding maximum values in the mid plane (A) are 0% and 49% smaller than the maximum values in the surface plane. However, for values of K_A lesser than 0.12 the maximum value of the transverse tensile stress occurs on the mid-plane. For a value of $\frac{A_1}{A}$ = 0.10 the magnitude of the maximum tension on the mid-plane is 0.80 times the mean compression.

Figure 5.12 shows how the difference in the maximum values of transverse tensions in the surface and mid plane narrows down as the concentration ratio decreases and the distance of the loading pad from the face of the anchor block increases. This brings out the fact that transverse tensions on the surface of the end block would usually depend on the proximity of the applied load to the face of the anchor block, and from the trend of the shrinking difference it may be reasonable to assume that at a value of $\frac{a_1}{a}$ less than 0.18 the value of the critical surface tensions may be less than the corresponding value on the internal plane. In fact in the series conducted to study the interaction effect of multianchorage units this

position is strengthened. As pointed out earlier there are only two three-dimensional solutions of the anchorage zone problem which could be considered to be simulating the actual conditions with some degree of accuracy. It is, however, noteworthy that both the solutions give entirely conflicting positions with respect to the surface and internal transverse stresses. Whereas according to Iyengar's solution the maximum transverse stresses on the internal central plane are always higher than those on the surface plane right from a concentration ratio of zero to one (Figure 5.13a). Yettram and Robbins[12] solution indicates the surface stresses to be higher than those in the internal central plane for the concentration ratio of 0.1 to 0.7 after which these probably equalize. However, Yettram's solution shows a reversal in this position for an $\frac{a_1}{a}$ value of 0.1 and for lesser values (Figure 5.13a). The results of the photoelastic tests obtained by the author also show the surface transverse stresses to be higher than the corresponding stress in the central plane for $\frac{a_1}{a}$ values greater than 0.35. However, a reversal in this position occurs for values of K_a less than 0.35. Thus, qualitatively speaking, in this particular respect, the results of this investigation are closer to Yettram and

Robbins[12] results than those of Iyengar's[11]. However, the values of the tensile stresses and forces obtained in this investigation are significantly higher than the corresponding values obtained by Yettram and Robbins (Figure 5.13) as well as those obtained by Iyengar.

Figures 5.14 and Table 5.4 compare the results of the present investigation with all the available two-dimensional solutions. It is quite clear that all the existing analytical two-dimensional theories appear to be grossly inadequate to present a realistic assessment, as the maximum transverse tensile stress found in this three-dimensional investigation is consistently far higher than those predicted by the two-dimensional analytical solutions in the whole range of the $\frac{a_1}{a}$ values which is of practical significance (Figure 5.14). As an example, the variation of the transverse tensile stress P is compared with the existing two-dimensional solutions for the $\frac{a_1}{a}$ value of 0.50 (corresponding to $\frac{A_1}{A} = 0.25$). It is seen that the maximum value of the transverse tensile stress obtained for the present investigation is 3 times the value predicted by Guyon's and Magnels theories; twice that given by Bleich's solution and about one and a half times the value given by Bleich-Sievers' solution. These tests

thus confirm the point made by Ban et al[27] and Zielinski and Rowe, on the basis of their results obtained from tests on concrete end blocks, that amongst the analytical solutions Bleich-Sievers' theory gives the closest approximation.

Figure 5.13 and Table 5.5 show a comparison of the results of the present investigations with those of the relevant three-dimensional analytical solutions and with the test results on concrete end block models reported by Zielinski and Rowe and Taylor. Figure 5.13(a) shows that the values predicted by Iyengar's and Yettram and Robbins' solutions grossly underestimate the values of maximum transverse tensile stress both on the surface and internal planes. The values obtained in the present investigation for the surface plane are 6,7,8.5 and 8 times the corresponding values given by Iyengar for $\frac{a_1}{a}$ values of 0.316, 0.5, 0.592 and 0.707 respectively. Also, author's values are 2.6, 3.2, 4 and 7 times the corresponding values given by Yettram and Robbins analytical solutions. Discrepancies of similar order exist for the internal plane.

Author's surface plane values can be compared with those of Zielinski and Rowe who also measured strains on the surface plane on concrete end block models. It is seen

that the author's values are in fairly good agreement with those of Zielinski and Rowe, the former being about 15% higher. It is also, noteworthy that the values predicted by the three-dimensional solutions of Iyengar and Yettram are 0.18, 0.17, 0.13 and 0.42, 0.375, and 0.15 times the corresponding values observed by Zielinski and Rowe for $\frac{a_1}{a}$ ratios of 0.316, 0.5 and 0.707 respectively. This comparison with observations on actual concrete model confirms the author's earlier view that both investigations underestimate the actual values. Figure 5.13 shows the comparison of the author's values with those of Zielinski and Rowe, Taylor and the three-dimensional solutions.

Figure 5.15 shows the positions of the maximum tensile stress for the external and internal planes. In the present investigation this position is found to vary in a very narrow range of 0.42a - 0.5a for the external plane and in the range of 0.67a to 0.75a for the internal plane. For all practical purposes a value of 0.5a to 0.45a could be considered to be quite acceptable for the surface plane. This is in close agreement with the position of 0.44 a given by Kummuller[42] and of 0.46a given by Zielinski and Rowe for the surface plane. In tests on concrete end blocks Zielinski and Rowe observed that for

all specimens with $\frac{a_1}{a}$ ratio in the range of 0.31 - 0.67, the first crack always appeared on the surface at a point 0.3a-0.5a from the loaded face. This observation is also in excellent agreement with the results obtained in the present investigation. Further, the positions of maximum stress as defined by Magnel and Guyon are substantially in error and misleading. Figure 5.16 shows that the stresses are about half the maximum values at the position of maximum stress suggested by Magnel and about two-third the maximum values at the position suggested by Guyon.

The positions of zero tensile stress near loaded face are shown in Figure 5.17. These values are compared with other investigators in Figure 5.18 and Table 5.2.

5.3.4 Transverse Tensile Force

Figure 5.19 and Table 5.3 show the variation of the total transverse tensile force per unit width for the $\frac{a_1}{a}$ ratios investigated. Figure 5.14b and Tabel 5.4 compare these values with the existing two-dimensional solutions and Figure 5.13b and Tabel 5.5 compares these values with the three-dimensional solutions of Iyengar and Yettram and the concrete tests of Zielinski and Rowe.

All the theoretical solutions and the approach recommended by Zielinski and Rowe on the basis of their test data, suggest a uniform distribution of the tensile force throughout the end block. It is,however, more likely that the tensile force will decrease on planes located between the central and surface plane. However, since the uniformity approach gives somewhat conservative results which may be an acceptable position in the rather complex and uncertain stress situation prevailing in the end block, the same approach is adopted here. Figure 5.19 shows the tensile force based on the stress distributions obtained on both the internal and surface planes.

It is clear from Figures 5.14 and 5.13 and Tables 5.4 and 5.5 that both the two and the three-dimensional solutions give values of tensile force which are a good deal smaller than the values obtained in this investigation. For the load concentration ratio ($\frac{a_1}{a}$) of 0.5 Magnel's and Guyon's values are 37% and 42% of the present values and those of Iyengar and Yettram are 33% and 26% of the author's values for the surface plane and 57% and 45% for the central plane. However, as shown in Figure 5.13 and Table 5.5 the values obtained in the present investigations for the surface plane are in excellent agreement with those

observed by Zielinski and Rowe from their tests on the surface of concrete end block models.

The three-dimensional nature of the problem, therefore, requires a reassessment of the location and total area of reinforcement required for an efficient design. The large difference between the positions of the maximum tensile stress obtained by experiments and those predicted by the commonly used theoretical solutions indicates that transverse reinforcement, if provided strictly on the basis of these theories, would often be located in the wrong place. The three-dimensional tests indicate that 27% of the total tensile force in the central plane and about 15.5% in the surface plane are operative within a distance of 3/4a. The corresponding figures for Guyon's, Magnel's, Iyengar's, and Yettram and Robbins' distributions are 0.115, 0.1,0.09 and 0.08. The comparative figure for Zielinski and Rowe is 0.27 which is in good agreement with the author's results.

5.3.5 Spalling Tensions

Figure 5.20 shows the distribution of spalling tensile stresses on the free surfaces of the corner in the central plane. The tension in the vicinity of the anchorage unit is quite high and varies in the range 0.42 - 0.30 times the uniform compression for $\frac{A_1}{A}$ values of 0.19 to 0.50.

The variation of the spalling tensions with $\frac{a_1}{a}$ ratios is shown in Figure 5.21. The spalling tensions decrease rapidly away from the anchorage plate and become negligibly small near the surface plane. As would be expected, this analysis suggests high tensile stresses on the bearing face in the vicinity of the periphery of the anchroage plate.

5.3.6 Compressive Stresses

The maximum values of the principal compressive stresses are found to occur immediately under the loading pad on the central axis in the central plane A. These values are six times the uniform compression at the base. Figures 5.22 show the distribution of the principal stress Q in the longitudinal direction for the central and surface planes.

5.3.7 Effect of Cable Duct

Table 5.6 summarizes the data which is related to the effect of cable duct on the magnitude and distribution of the transverse tensile stresses. It is seen that there is little difference in the maximum values of the transverse tensile stresses in the two cases. However the presence of the duct modifies the position of the maximum tensile stress in the mid-plane. In the model with the duct the

maximum value in the mid-plane occurs under the edge of the loading pad instead of occuring along the load center line. This is also shown in Figure 5.23 where the peak P value in the mid-plane occurs directly under the edge of the loading pad.

Slices in the xz planes were examined for hoop tension along the duct. It was found that the nature of hoop tension was compressive in the vicinity of the loading pad and became a small tension at some distance from the loaded face. These tensions were too small to be significant.

TABLE 5.1

The positions and values of the maximum stresses on the mid and surface planes

Model	Positions of maximum stresses from the top surface		Values of maximum stresses expressed as a ratio of mean axial compression	
	Mid-plane A	Surface plane B	Mid-plane A	Surface plane B
M_1	0.67a	0.5a	0.8	0.78
M_2	0.67a	0.5a	0.6	0.68
M_3	0.7a	0.5a	0.46	0.6
M_4	0.75a	0.42a	0.26	0.47

TABLE 5.2

The positions of zero tensile stress in comparison with other investigators

a_1/a	Magnel	Guyon	Bleich	Sievers	Author
0.316	0.66a	0.22a	0.3a	0.3a	0.325a
0.5	0.66a	0.33a	0.33a	0.33a	0.32a
0.592	0.66a	0.35a	0.33a	0.33a	0.33a
0.707	0.66a	0.37a	0.31a	0.31a	0.4a

TABLE 5.3

The variation of the total transverse tensile force for the a_1/a investigated

a_1/a	The value of the transverse tensile force as a ratio of the mean axial compression	
	Mid-plane A	Surface plane B
0.316	0.215	0.35
0.5	0.155	0.27
0.592	0.115	0.225
0.707	0.055	0.13

TABLE 5.4

Comparison of the author's results with the available two-dimensional analytical solutions

a_1/a	Maximum transverse tension expressed as a ratio of mean axial compression					Maximum tensile force expressed as a ratio of the applied force				
-	Guyon	Magnel	Bleich	Bleich-Sievers	Author	Guyon	Magnel	Bleich	Bleich-Sievers	Author
0.316	0.34	0.36	0.486	0.71	0.78	0.178	0.15	0.2	0.27	0.35
0.5	0.25	0.28	0.34	0.486	0.68	0.114	0.107	0.14	0.178	0.27
0.592	0.18	0.22	0.286	0.36	0.6	0.095	0.095	0.114	0.14	0.225
0.707	0.15	0.18	0.23	0.21	0.47	0.09	0.083	0.086	0.096	0.13

TABLE 5.5

Comparison of the author's results with the relevant three-dimensional analytical solutions and with the experimental results on concrete and block models

a_1/a	Maximum transverse tension expressed as a ratio of mean axial compression					Maximum tensile force expressed as a ratio of the applied force				
	Theoretical three-dimensional analytical solution		Experimental			Theoretical three-dimensional analytical solution		Experimental		
	Iyengar	Yettram & Robbins	Zelinski and Rowe	Taylor	Author	Iyengar	Yettram & Robbins	Zelinski and Rowe	Taylor	Author
0.316	0.13	0.30	0.71	-	0.78	0.14	0.106	0.38	-	0.35
0.5	0.096	0.21	0.56	0.5	0.68	0.091	0.07	0.26	-	0.27
0.592	0.07	0.15	0.485	-	0.6	0.07	0.057	0.22	-	0.225
0.707	0.059	0.066	0.44	-	0.47	0.05	0.047	0.176	-	0.13

TABLE 5.6

Effect of Cable Duct on the Magnitude and Position of the Maximum Transvers Tensile Stress (a_1/a = 0.592)

	Internal Plane A		Surface Plane (B)	
	Value of max.transverse tensile stress in terms of yy_o	Position of maximum transverse tensile stress	Value of maximum transverse tensile stress in terms of yy_o	Position of maximum transverse tensile stress
Model with duct	0.49	under edge of the loading pad	0.72	Along the load center line
Model without duct	0.46	Along the load centre line	0.63	Along the load centre line

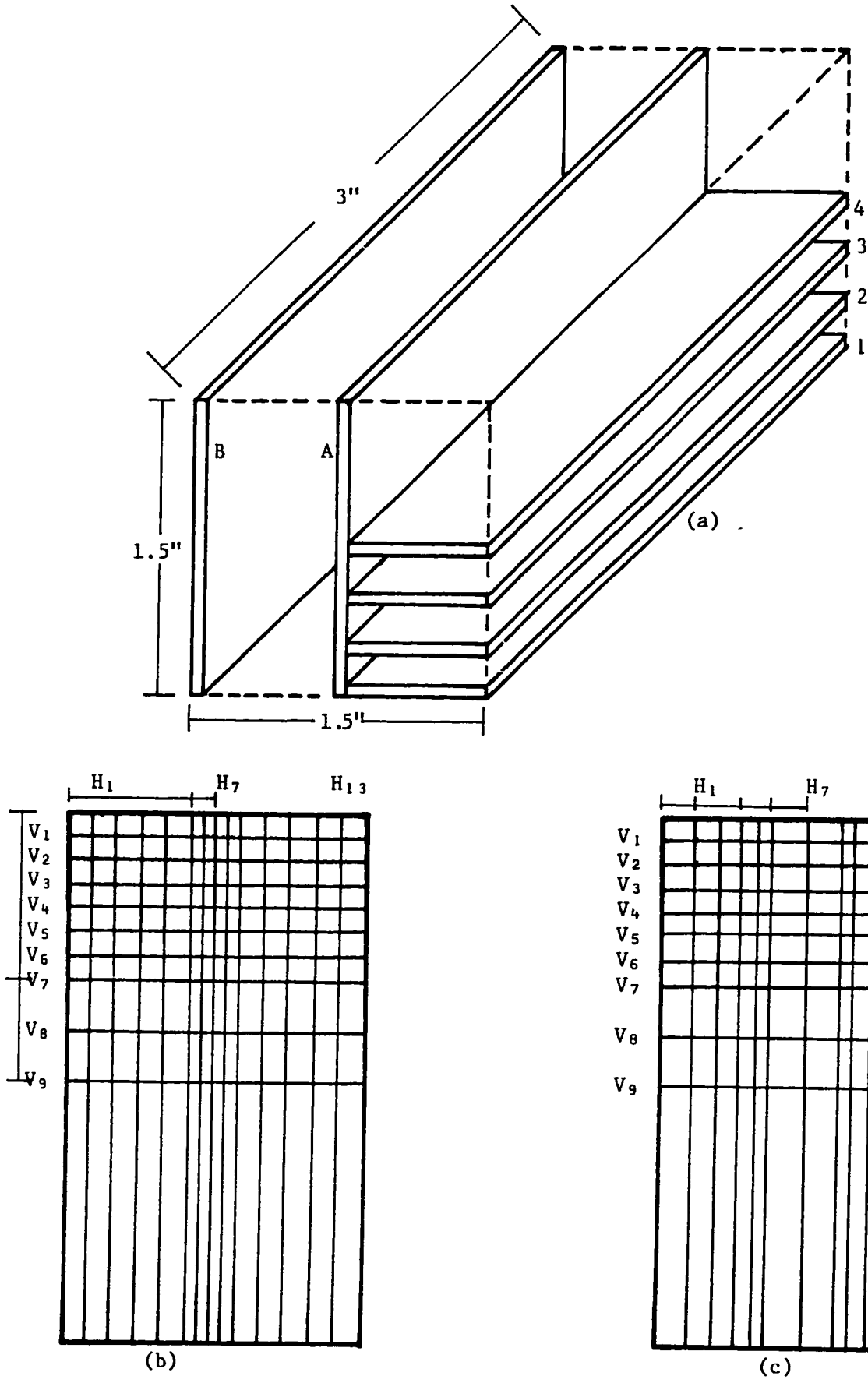

FIGURE 5.1 : (a) Model slicing scheme
(b) xy-plane A slice
(c) yz-plane 4 slice

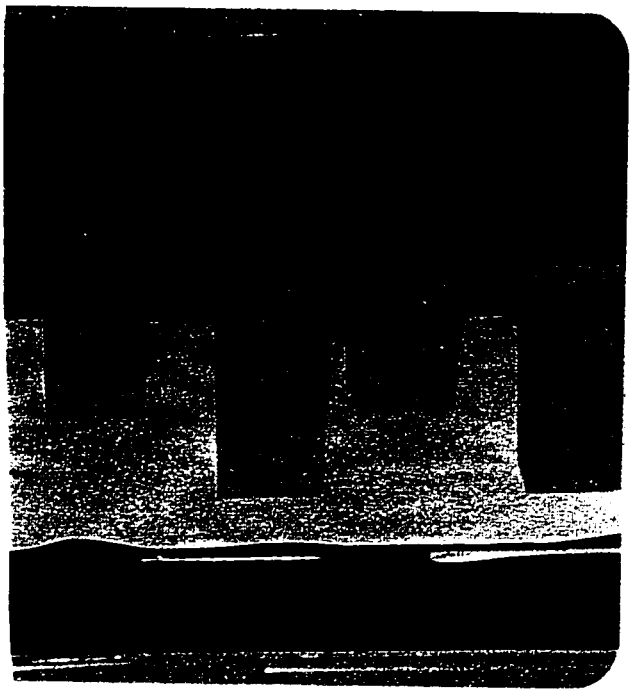

FIGURE 5.2 : Photoelastic models which were made of Araldite B

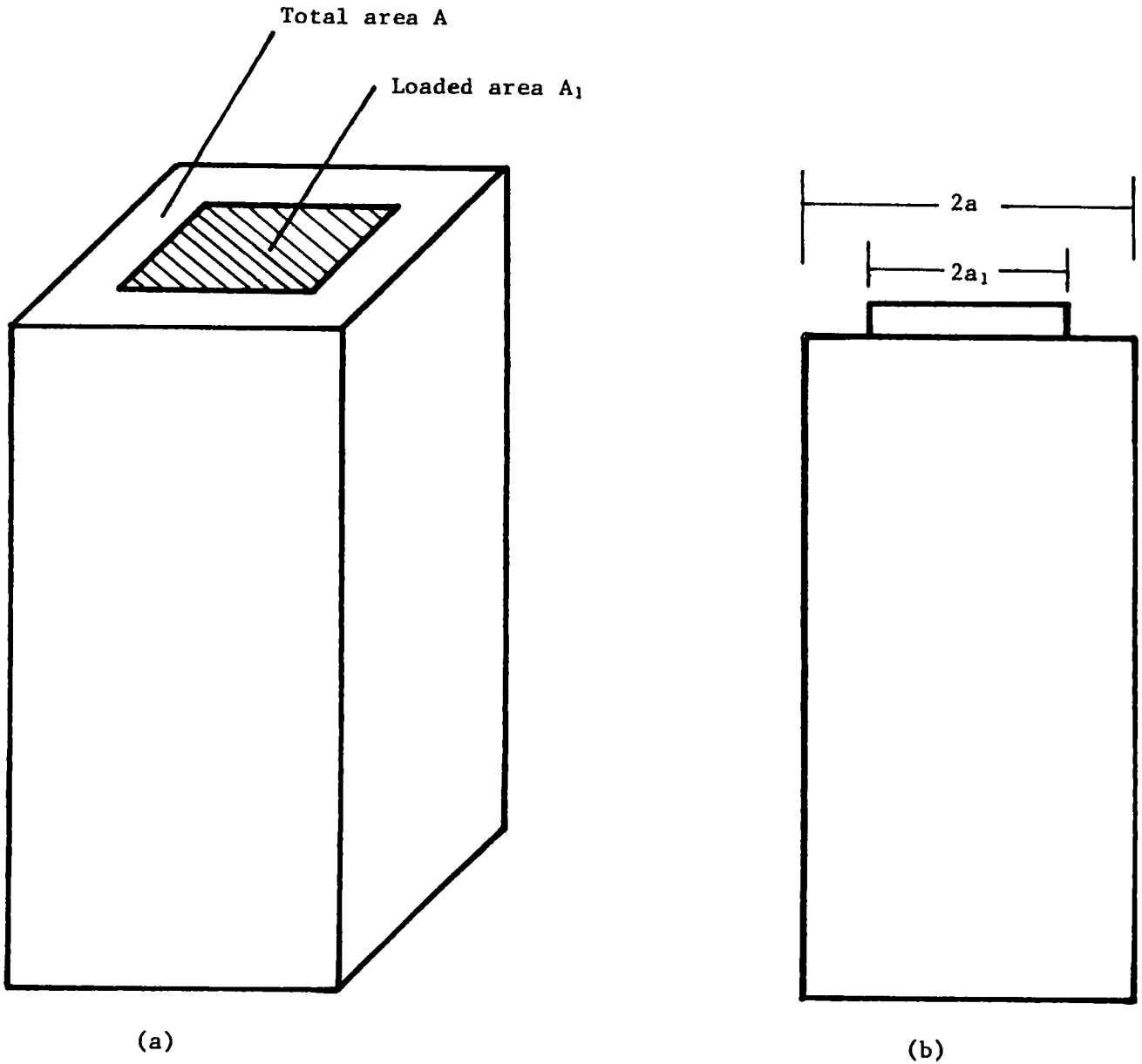

FIGURE 5.3 : The two load concentration $\frac{A_1}{A}$ and $\frac{a_1}{a}$

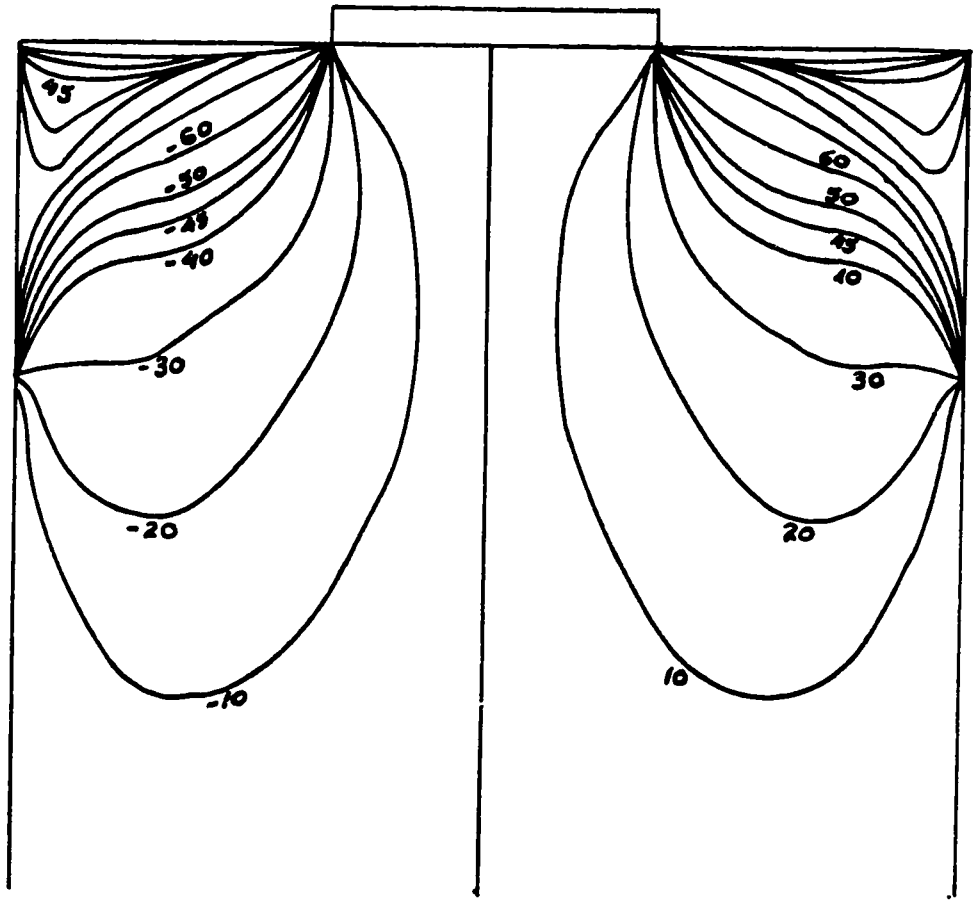

FIGURE 5.4 : Isoclinics for the central slice for model M_1

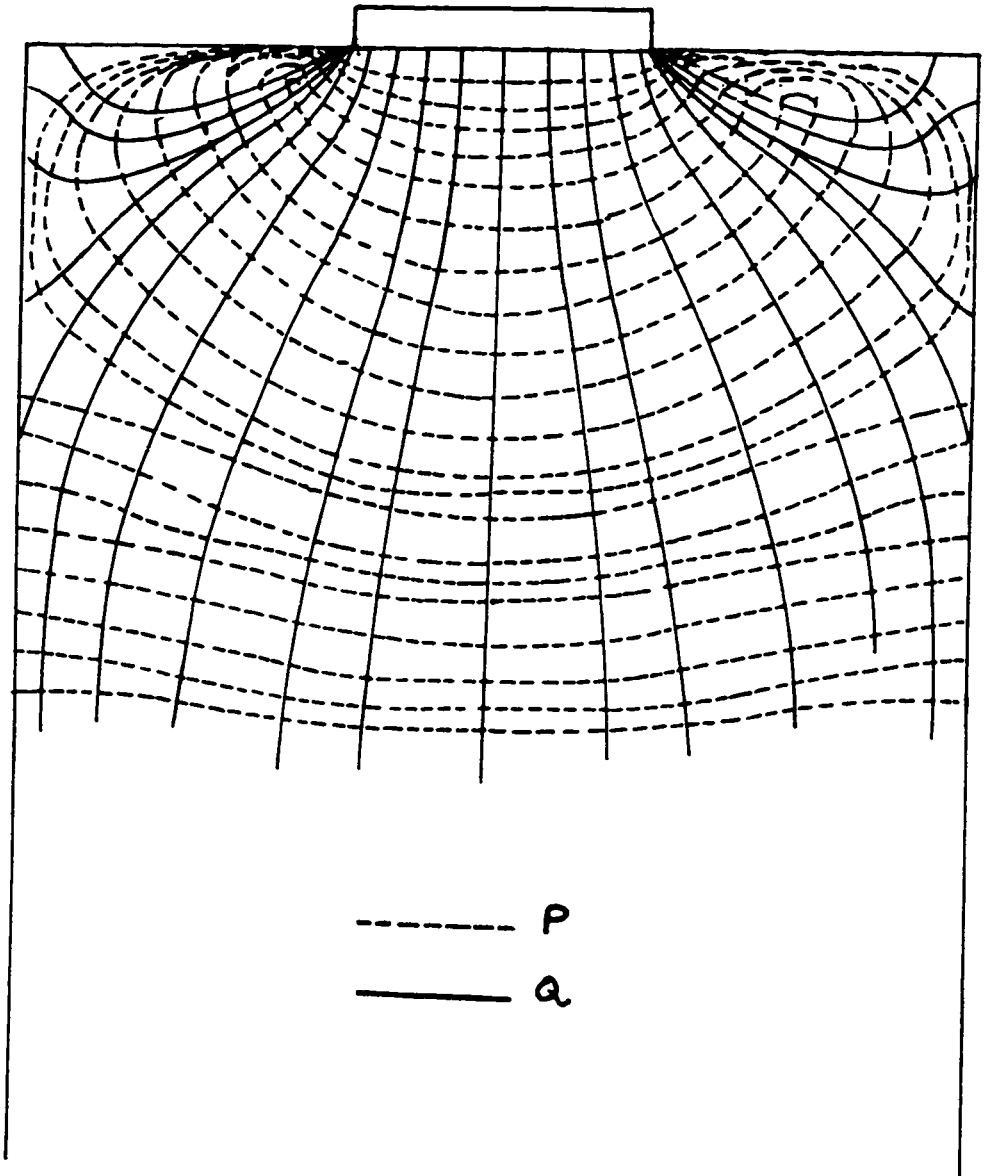

FIGURE 5.5 : The lines of principal stress for the central slice for model M_1

a) Typical isoclinic for $\alpha = 0^{o}$ in xy-plane A(mid-plane) for model M_1

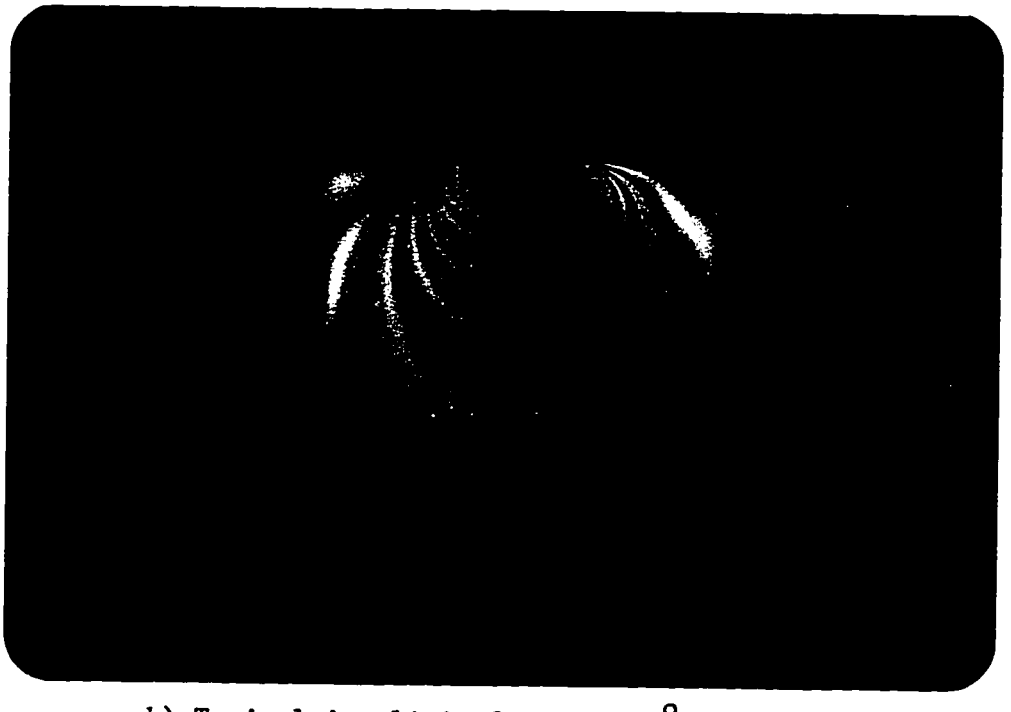

b) Typical isoclinic for $\alpha = 10^{o}$ in xy-plane (mid-plane for model M_1

FIGURE 5.6 : The optical fringe patterns in important slices

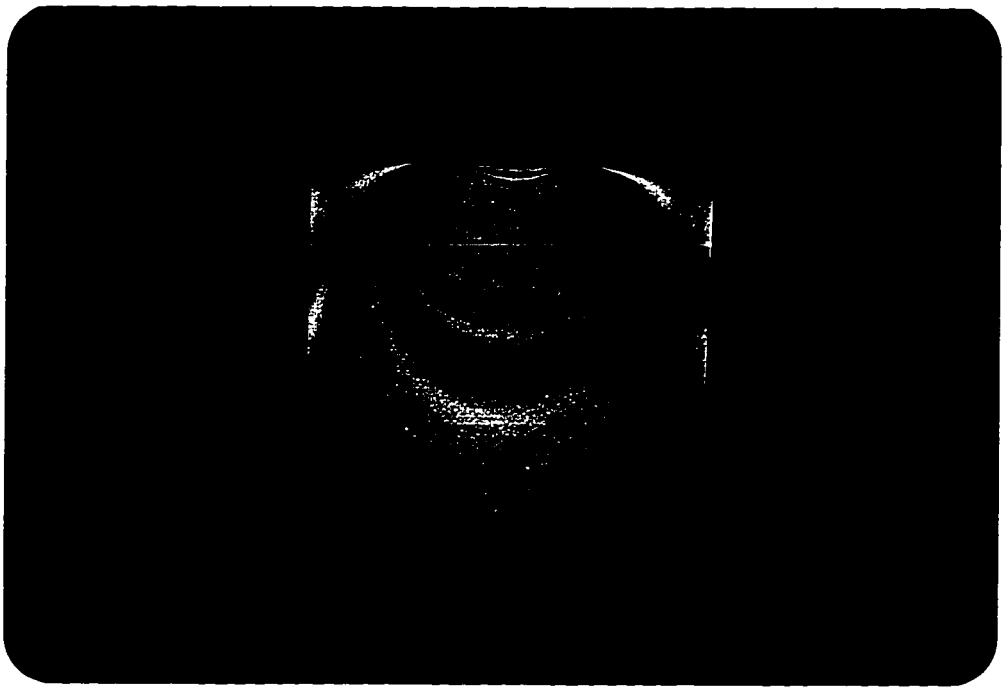

c) Typical isoclinic for $\alpha = 45^{o}$ in xy-plane A(mid-plane for model M_1

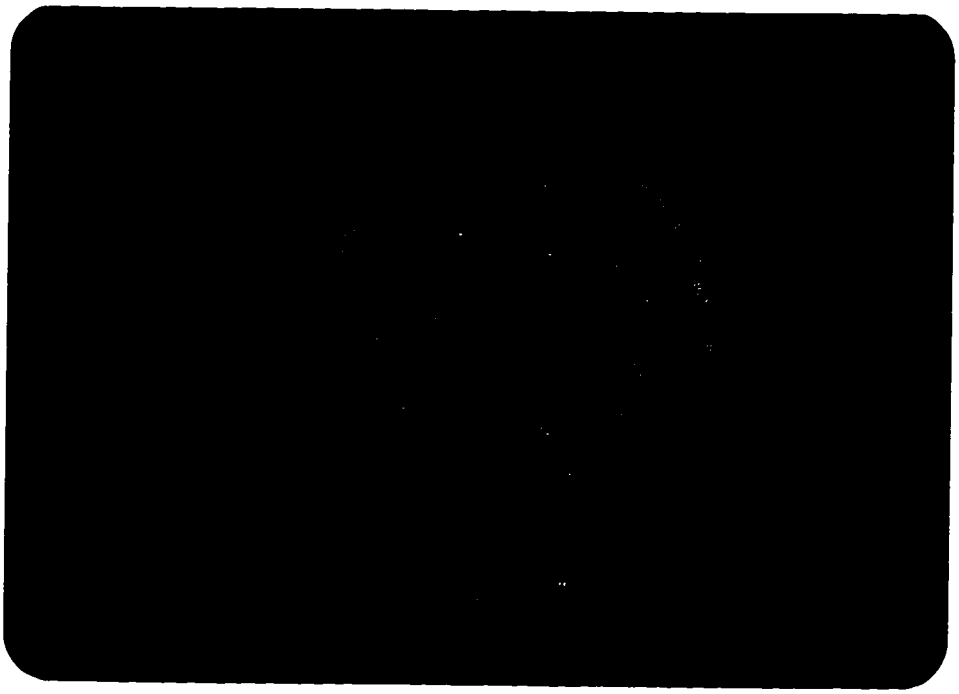

d) Typical isochromatic for xy-plane A (mid-plane)

The optical fringe patterns in important slices

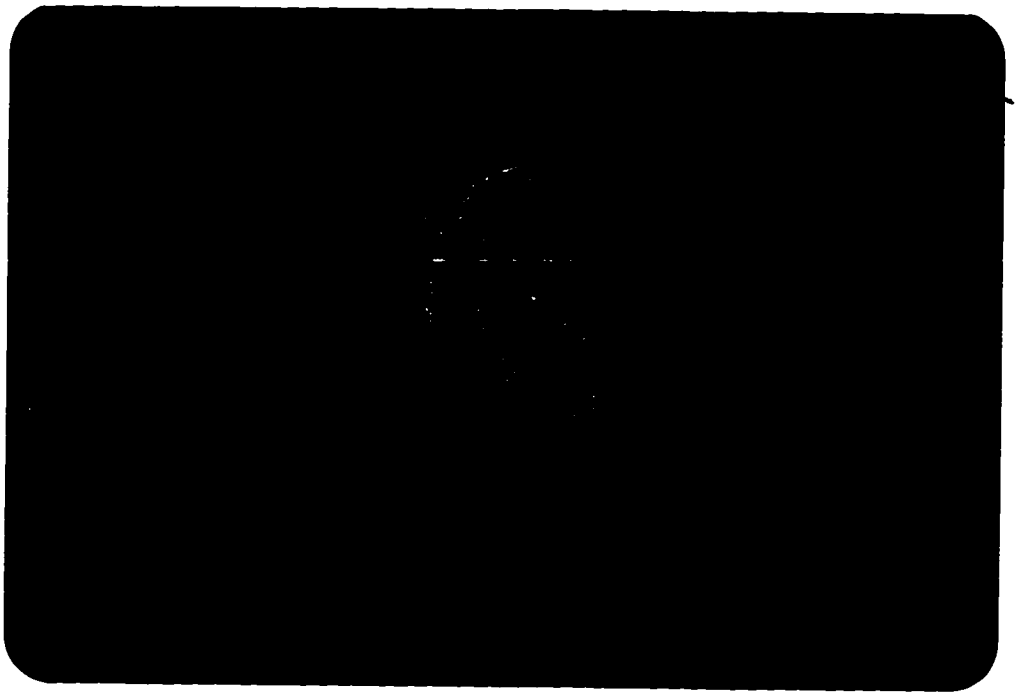

e) Typical isochromatic for yz-plane model M_1

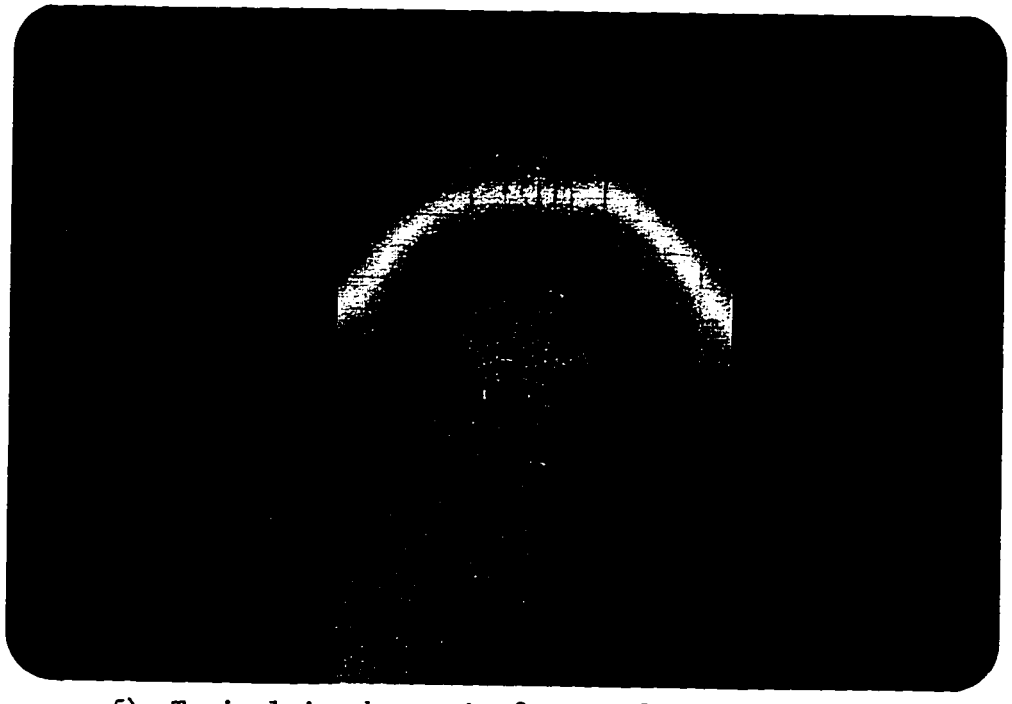

f) Typical isochromatic for xy-plane B model M_2

Optical fringe patterns in important slices

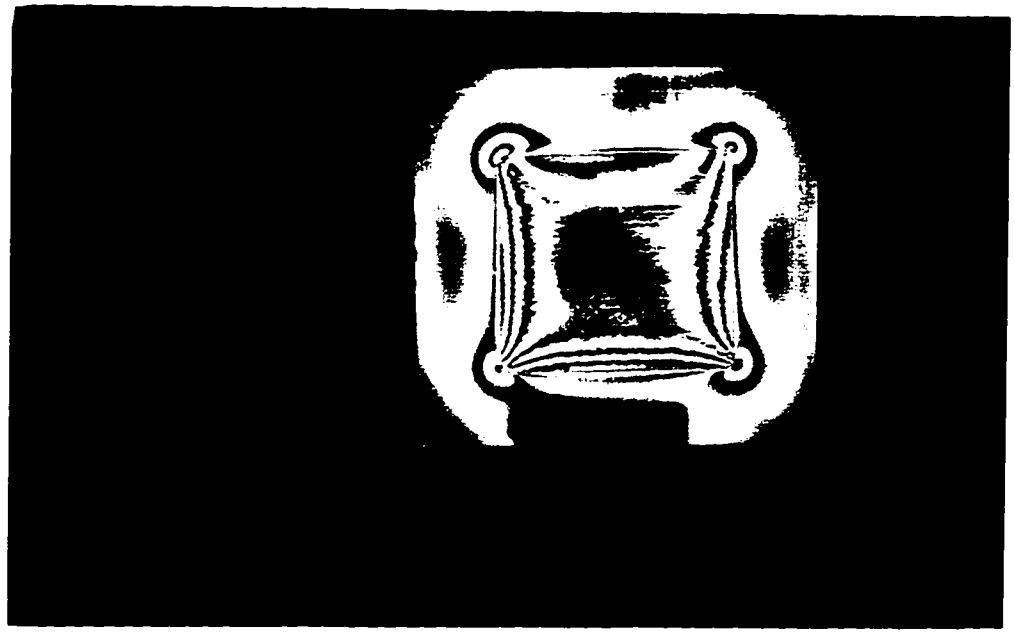

FIGURE 5.7 : The optical fringe patterns in xz slice

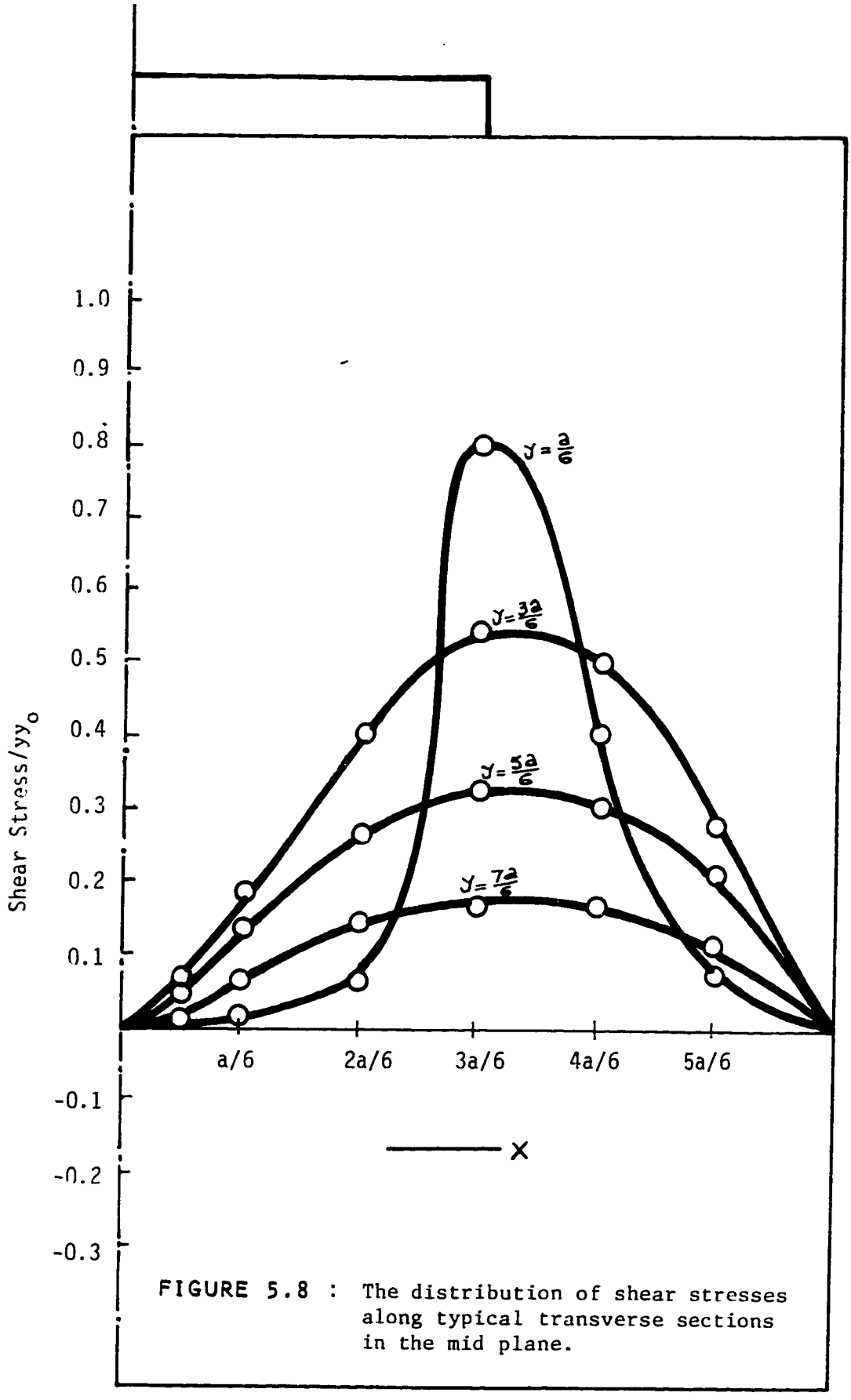

FIGURE 5.8 : The distribution of shear stresses along typical transverse sections in the mid plane.

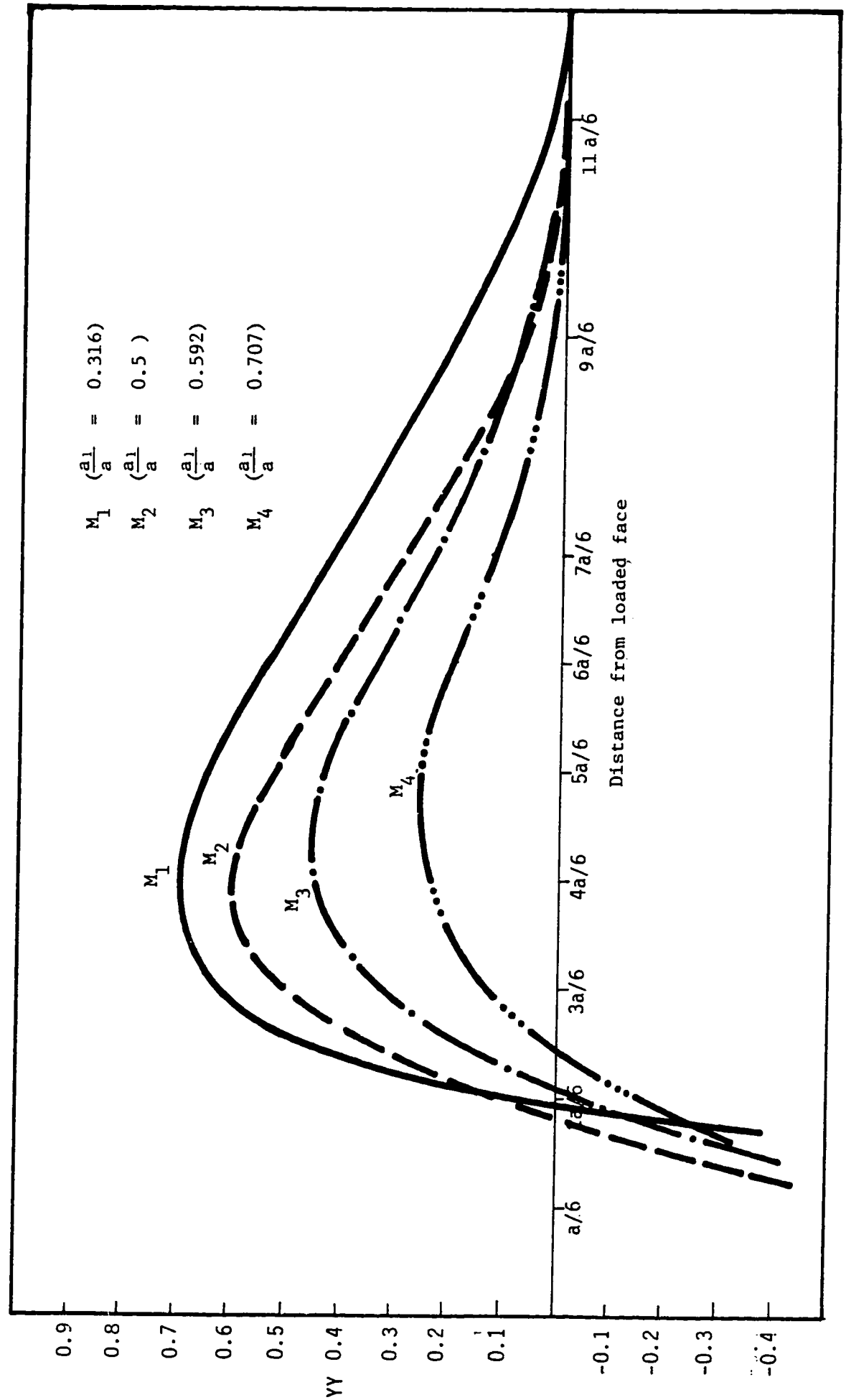

FIGURE 5.9 : The variation of the principal stress P for the internal plane A along the axis of symmetry in the direction of the length of the models.

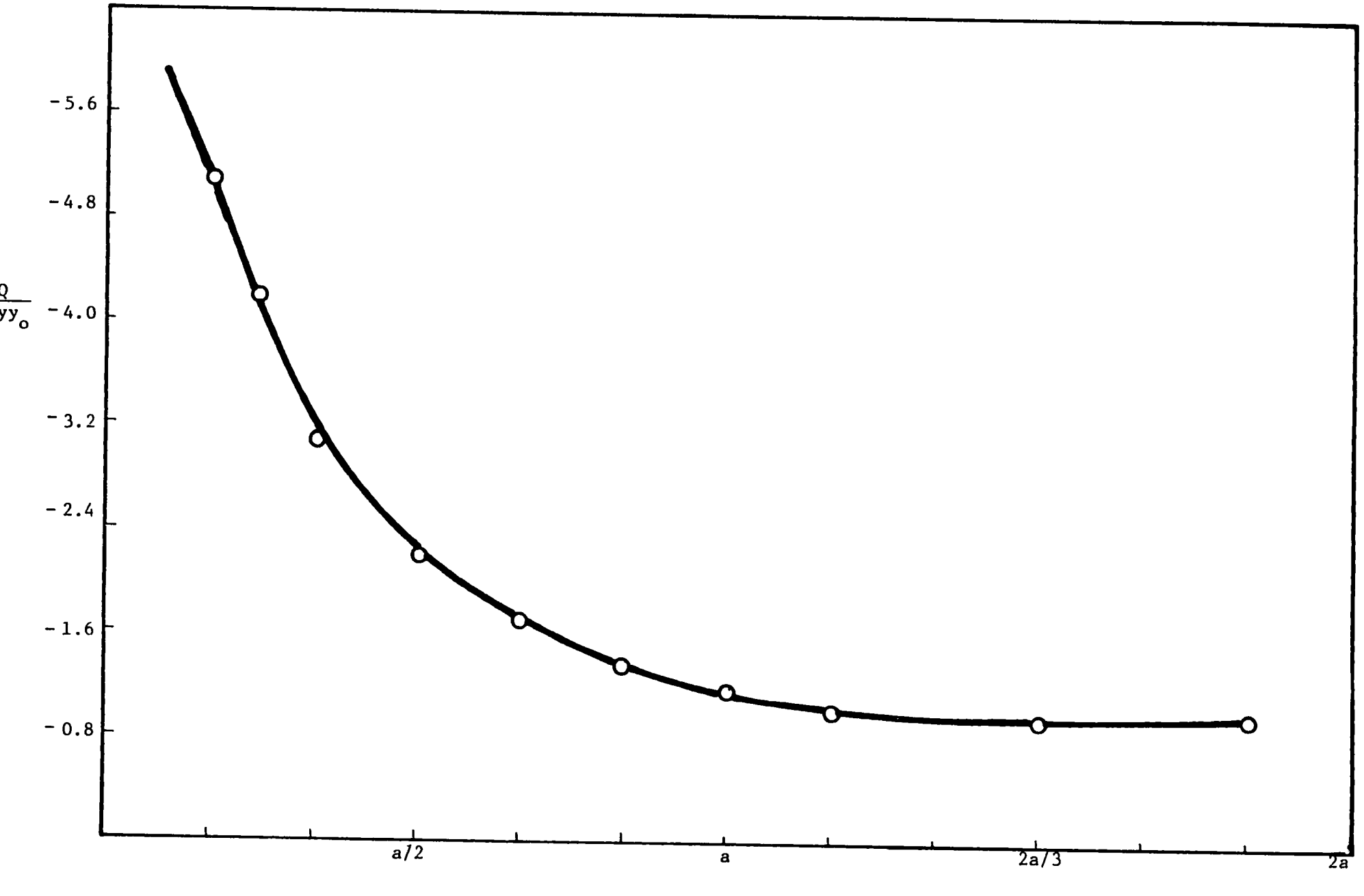

FIGURE 5.10 : The distribution of principal stress Q along y-distance (Model M_1)

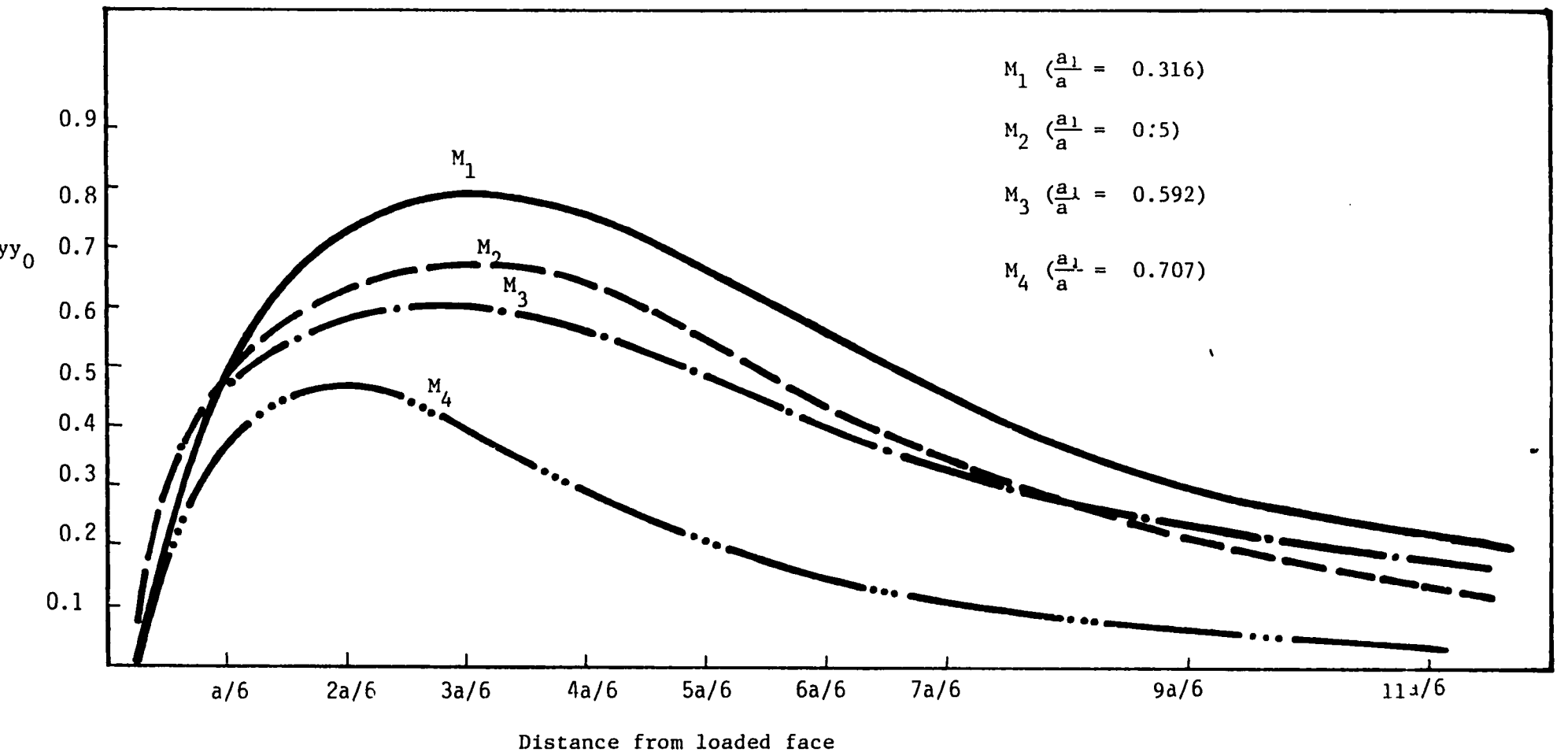

FIGURE 5.11a : The variation of the principal stress P for the surface plane B along the axis of symmetry in the direction of the length of the models.

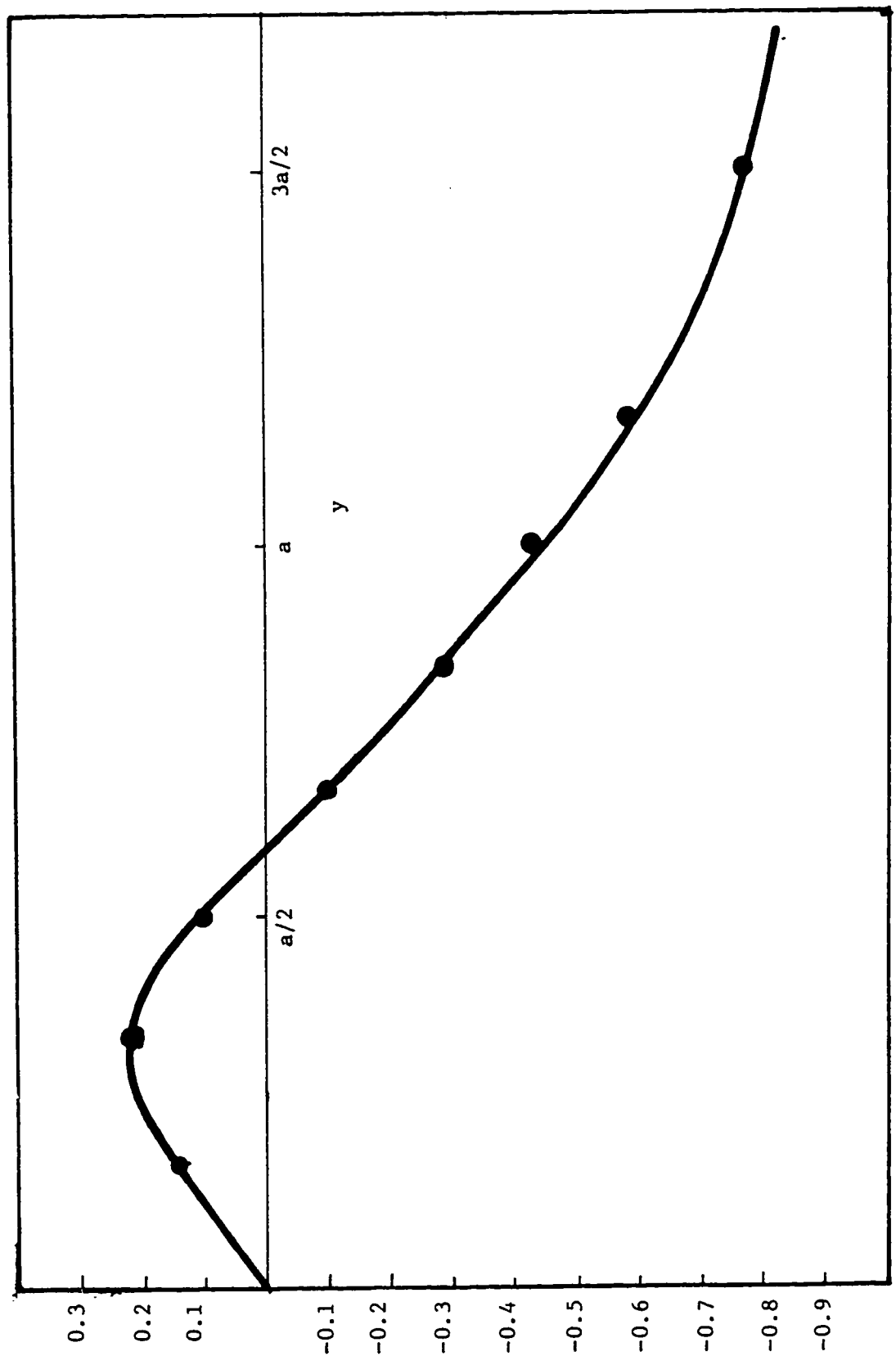

FIGURE 5.11b: The distribution of the principal stress Q along y-distance for xy-plane B (Model M_1)

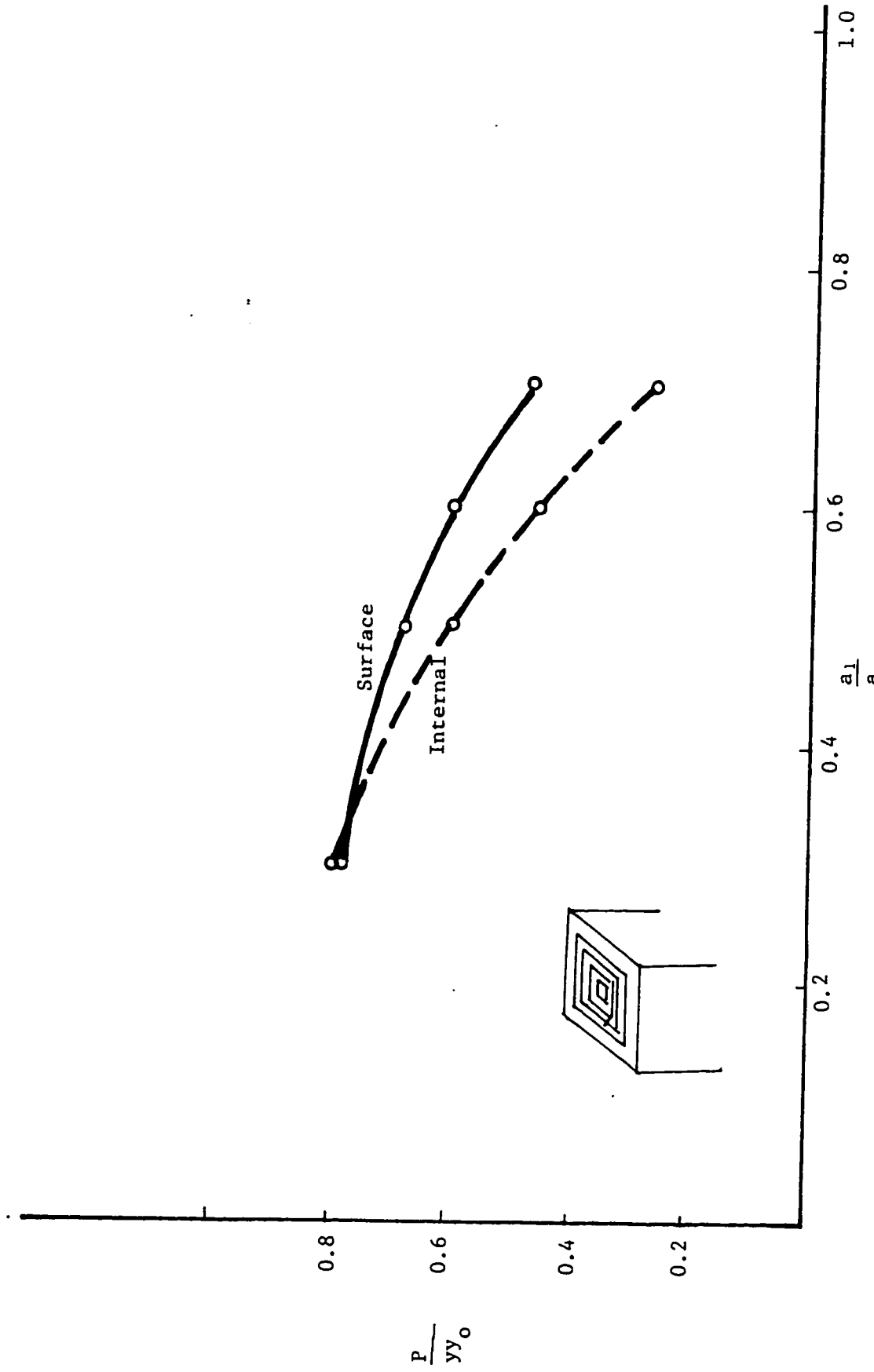

FIGURE 5.12 : Maximum transverse stress as a ratio of uniform compression

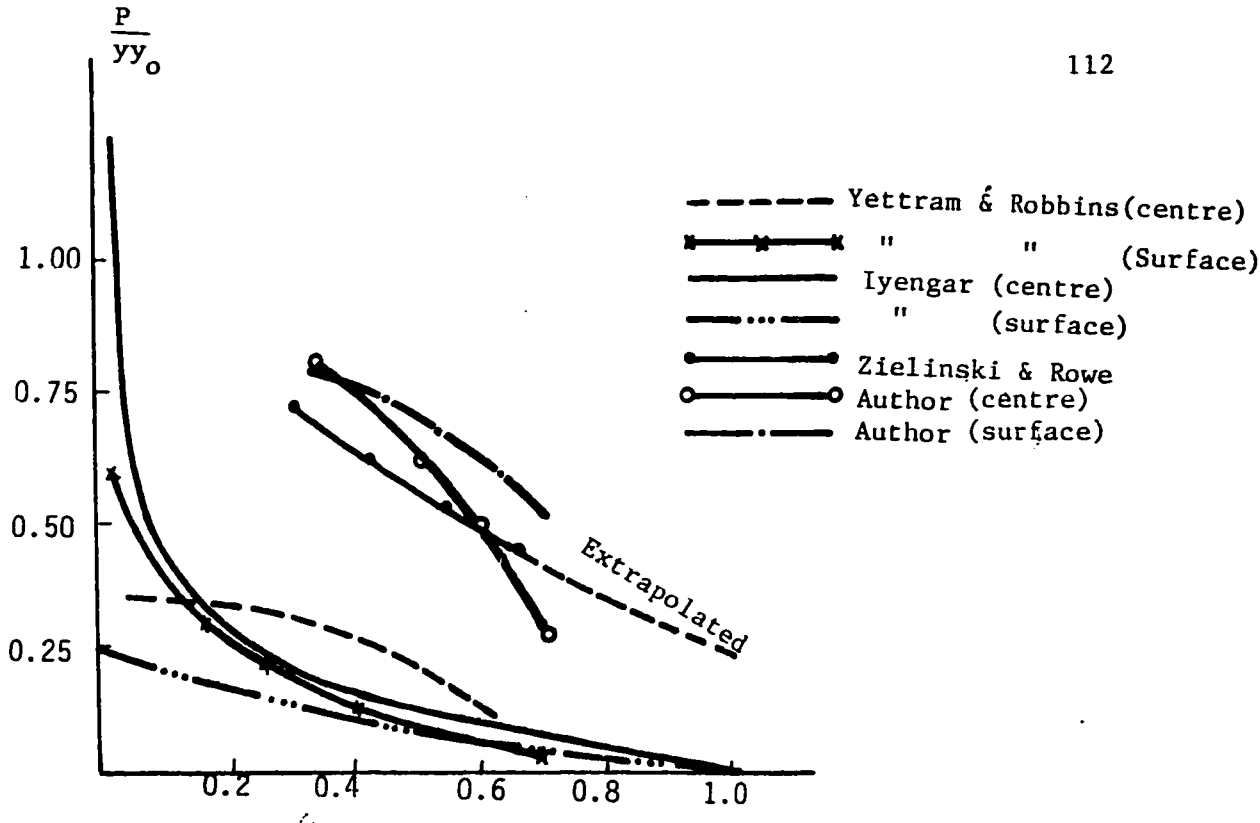

FIGURE 5.13 (a) : Comparison of maximum transverse stresses in anchor blocks subjected to isolated concentric post-tensioning force.

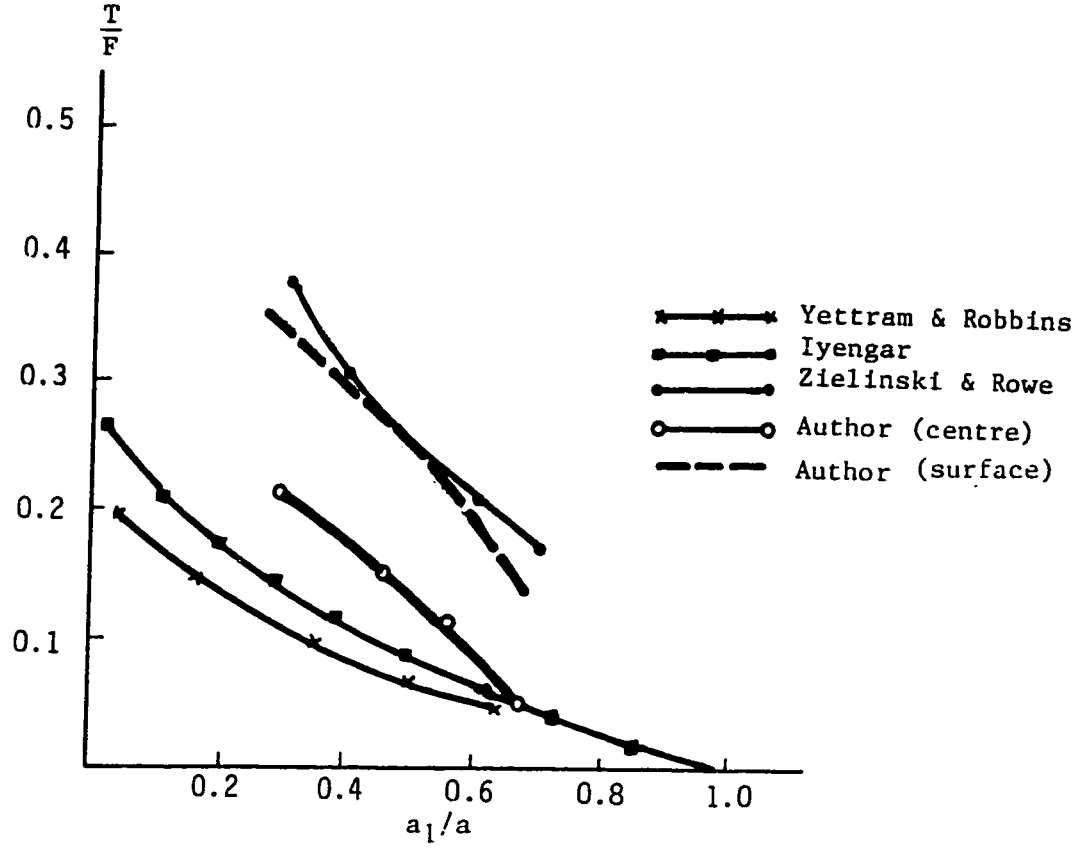

FIGURE 5.13(b) : Comparison of maximum tensile force in anchor blocks subjected to isolated concentric post-tensioning force.

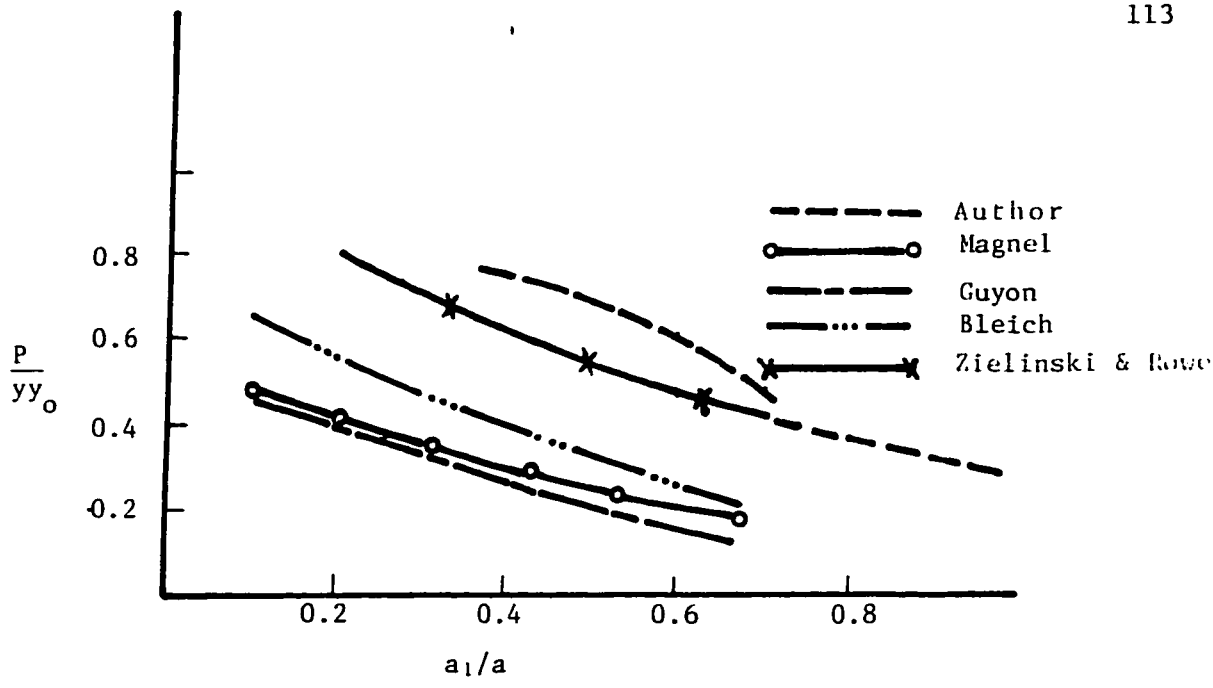

FIGURE 5.14a: Transverse tensile stresses for different a_1/a ratios.

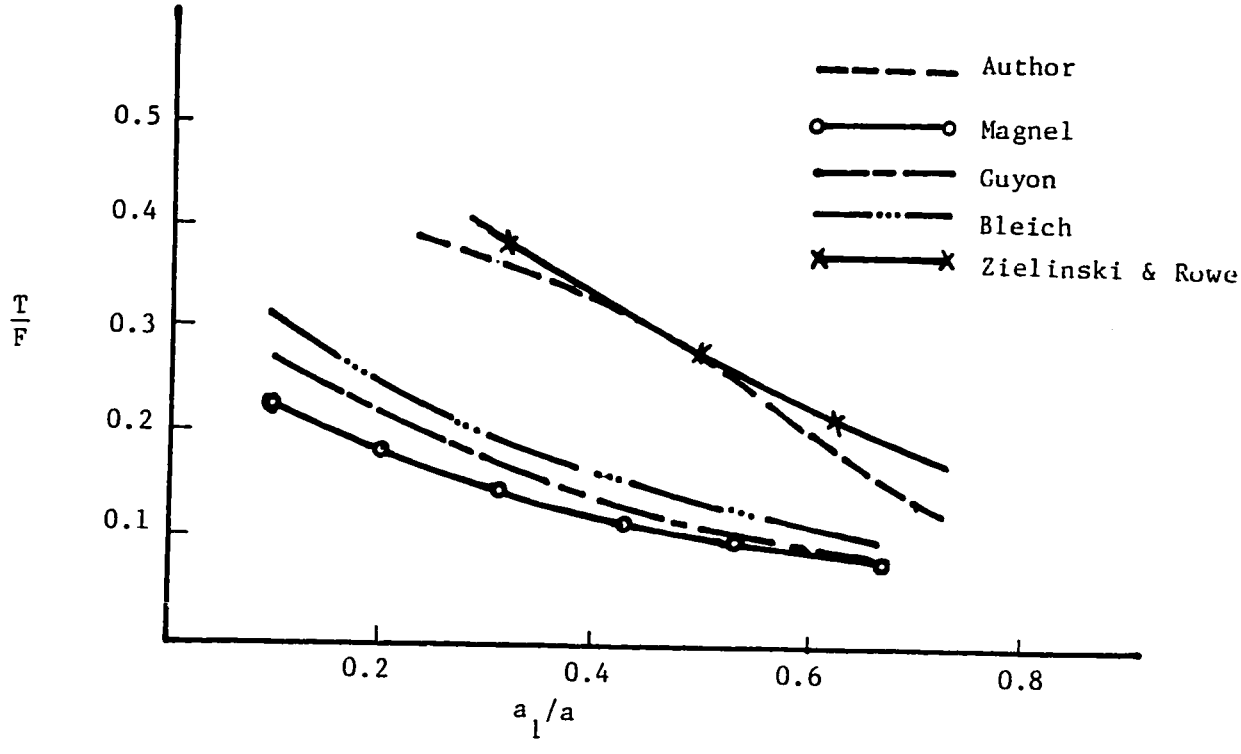

FIGURE 5.14b : Transverse tensile forces for different a_1/a ratios

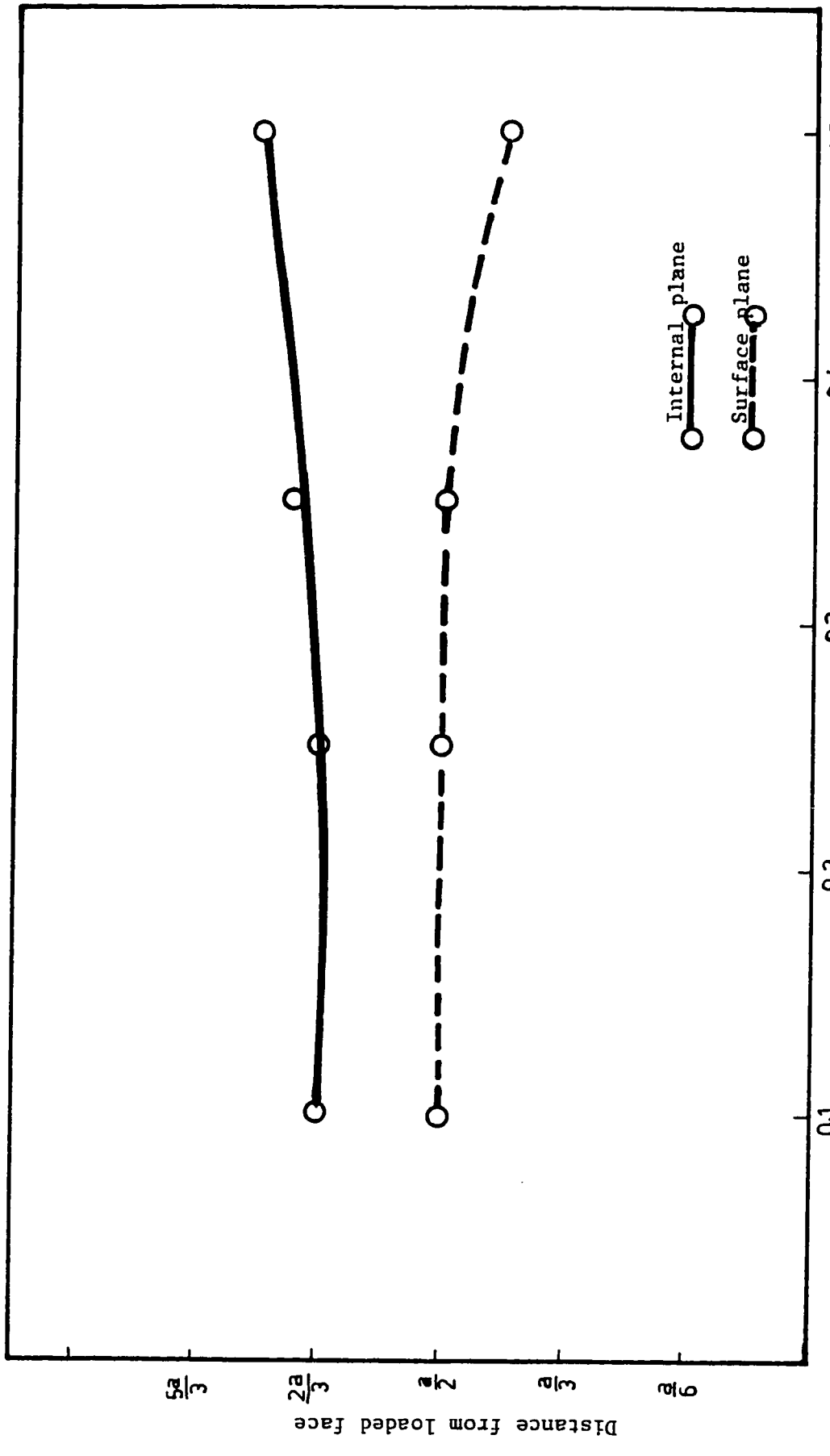

FIGURE 5.15 : The positions of the maximum tensile stress from the loaded surface for external and internal planes.

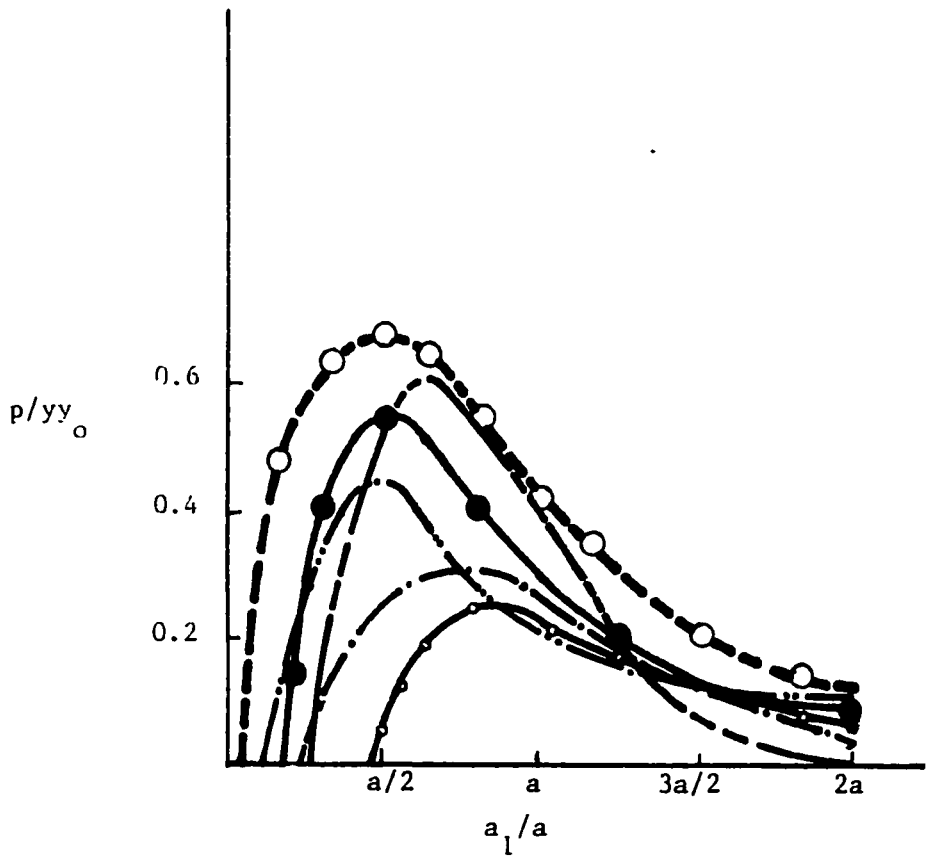

FIGURE 5.16 : Distribution of transverse tensile stress along the longitudinal direction for $a_1/a = 0.5$

Iyenger

Taylor

Yettram & Robbins

Zielinski & Rowe

Author (surface)

Author (centre)

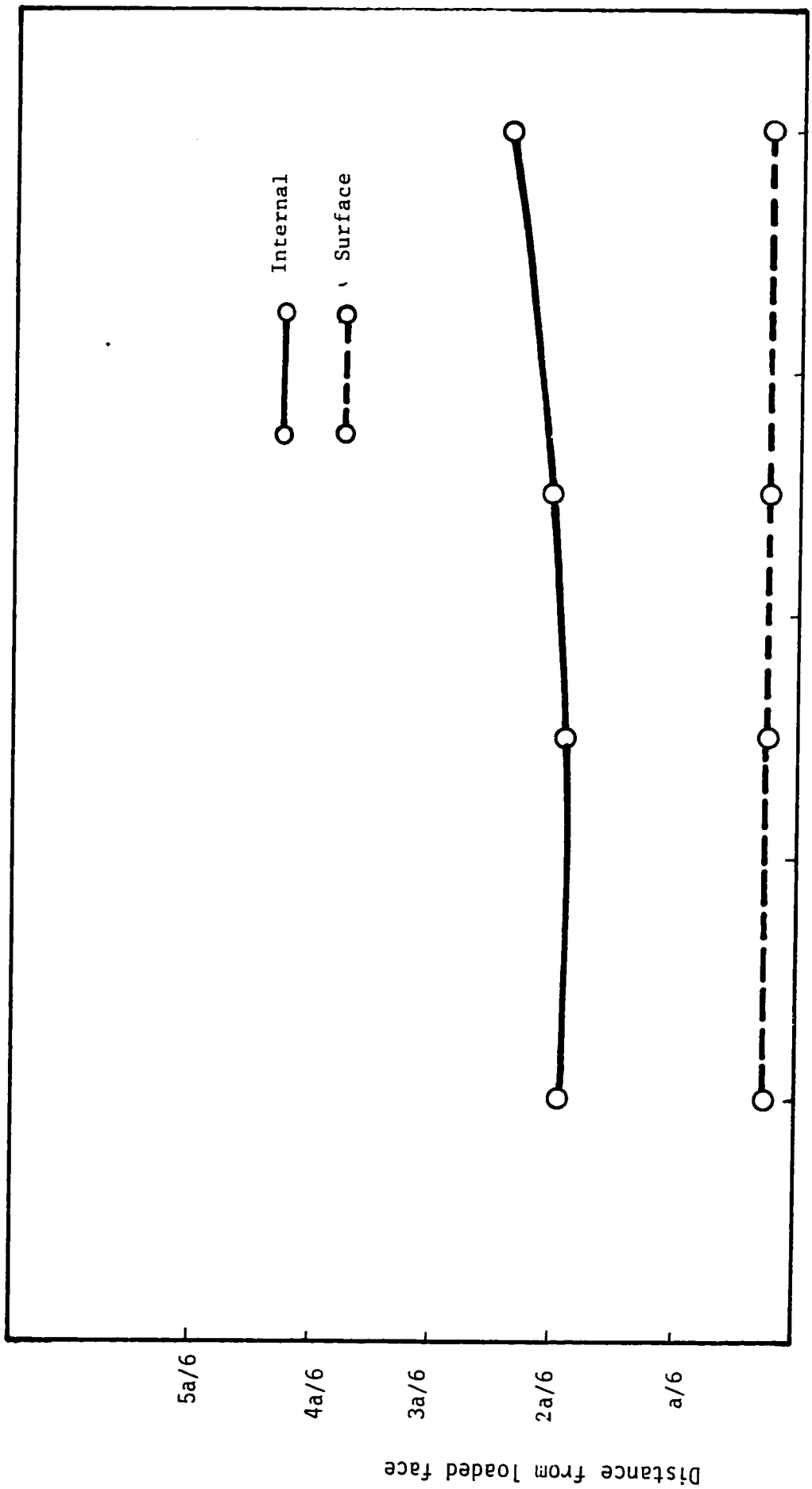

FIGURE 5.17 : The positions of zero tensile stress near loaded face for different $\frac{A_1}{A}$ ratios.

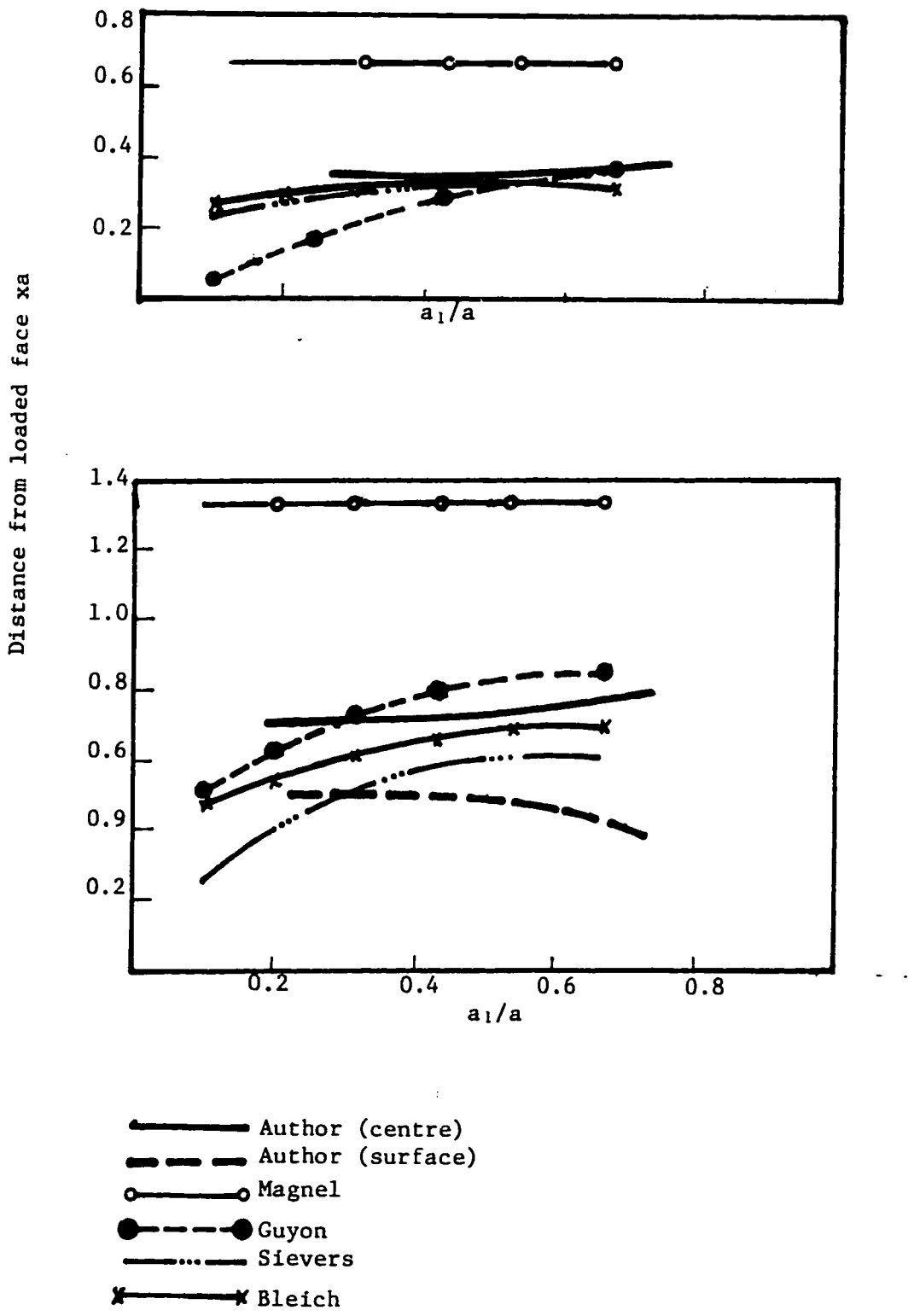

FIGURE 5.18 : Comparison of positions of zero and maximum tensile stresses

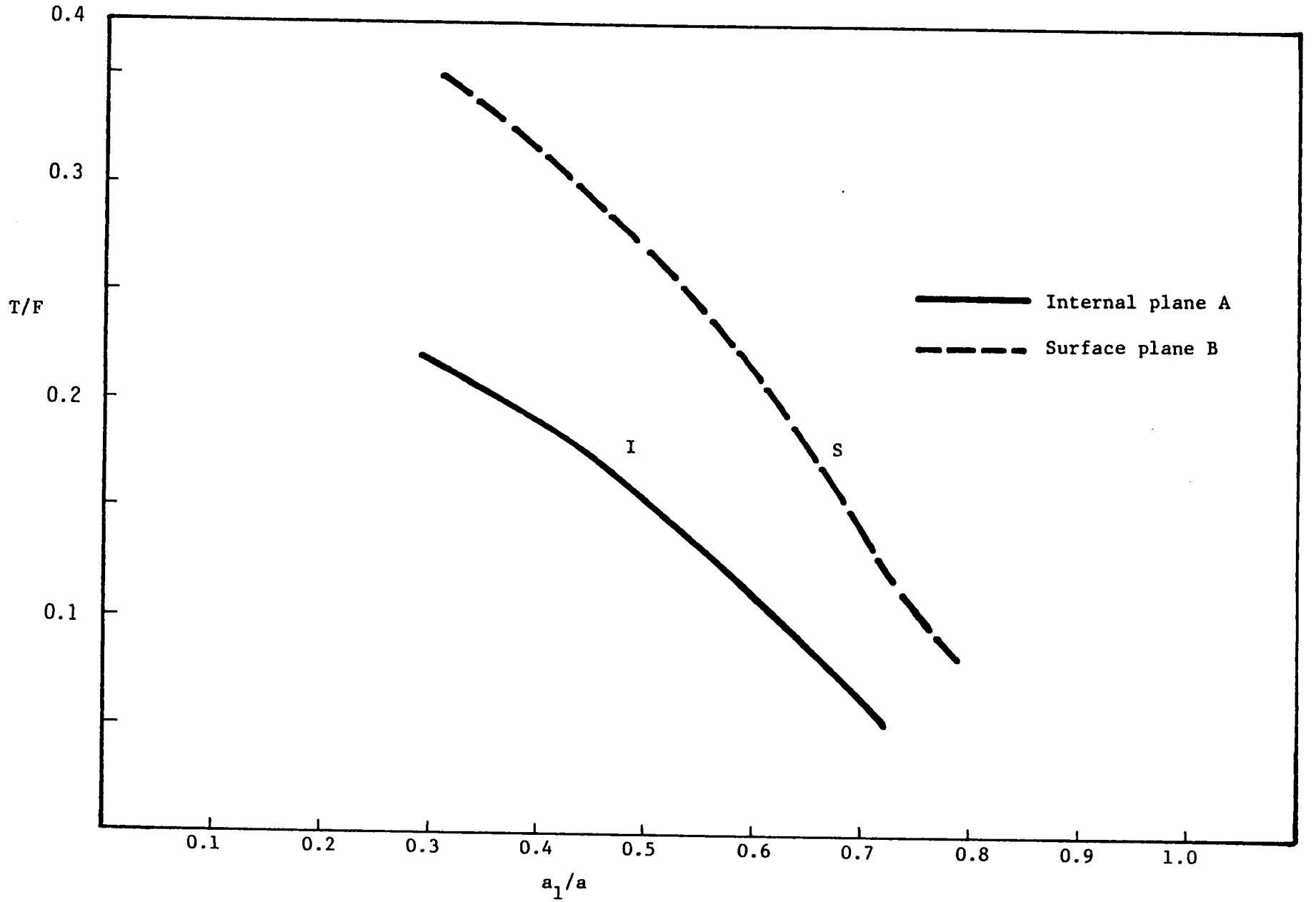

FIGURE 5.19 : The variation of the total transverse tensile force per unit width for a_1/a ratios investigated.

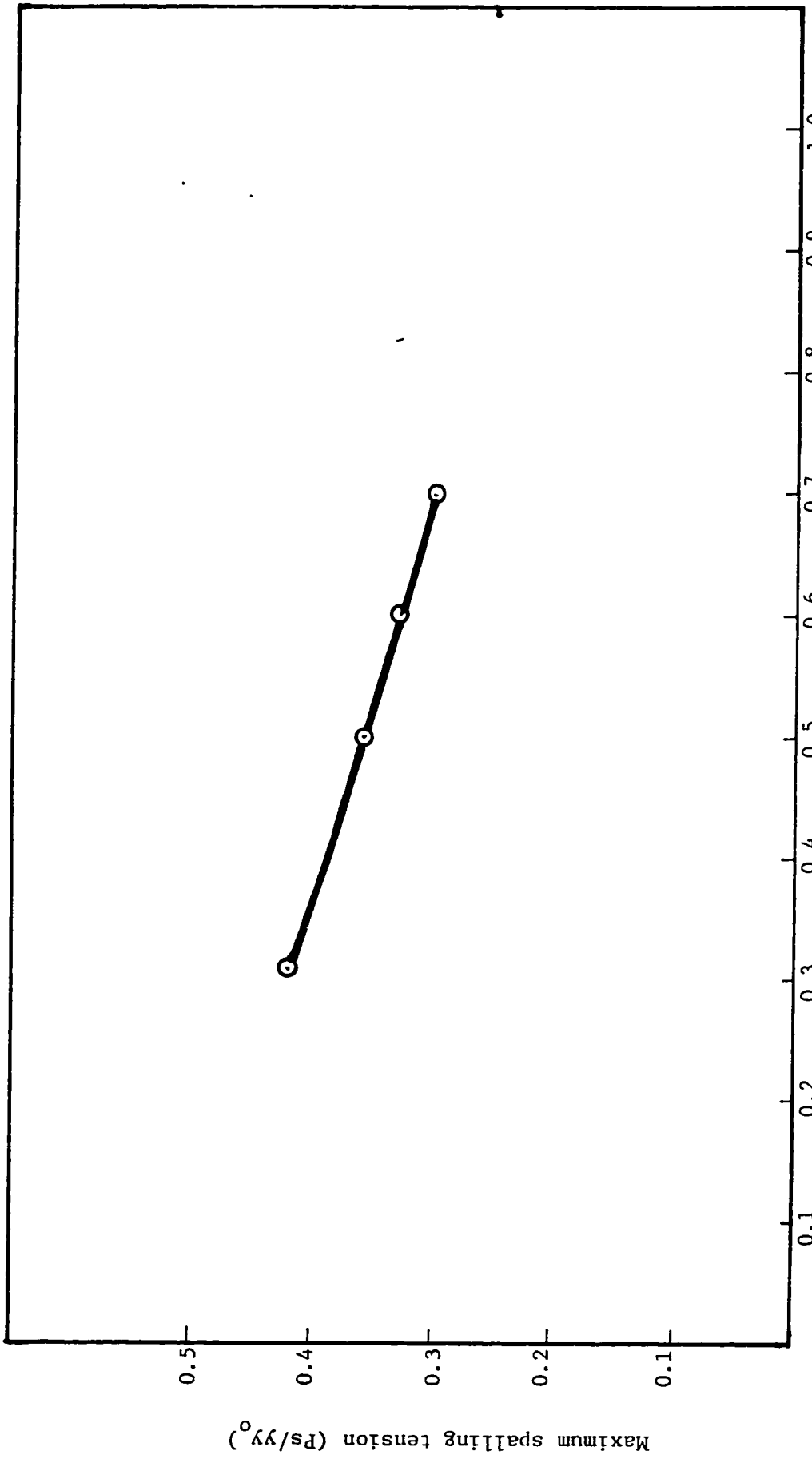

FIGURE 5.20 : Maximum spalling tension for various a_1/a ratios.

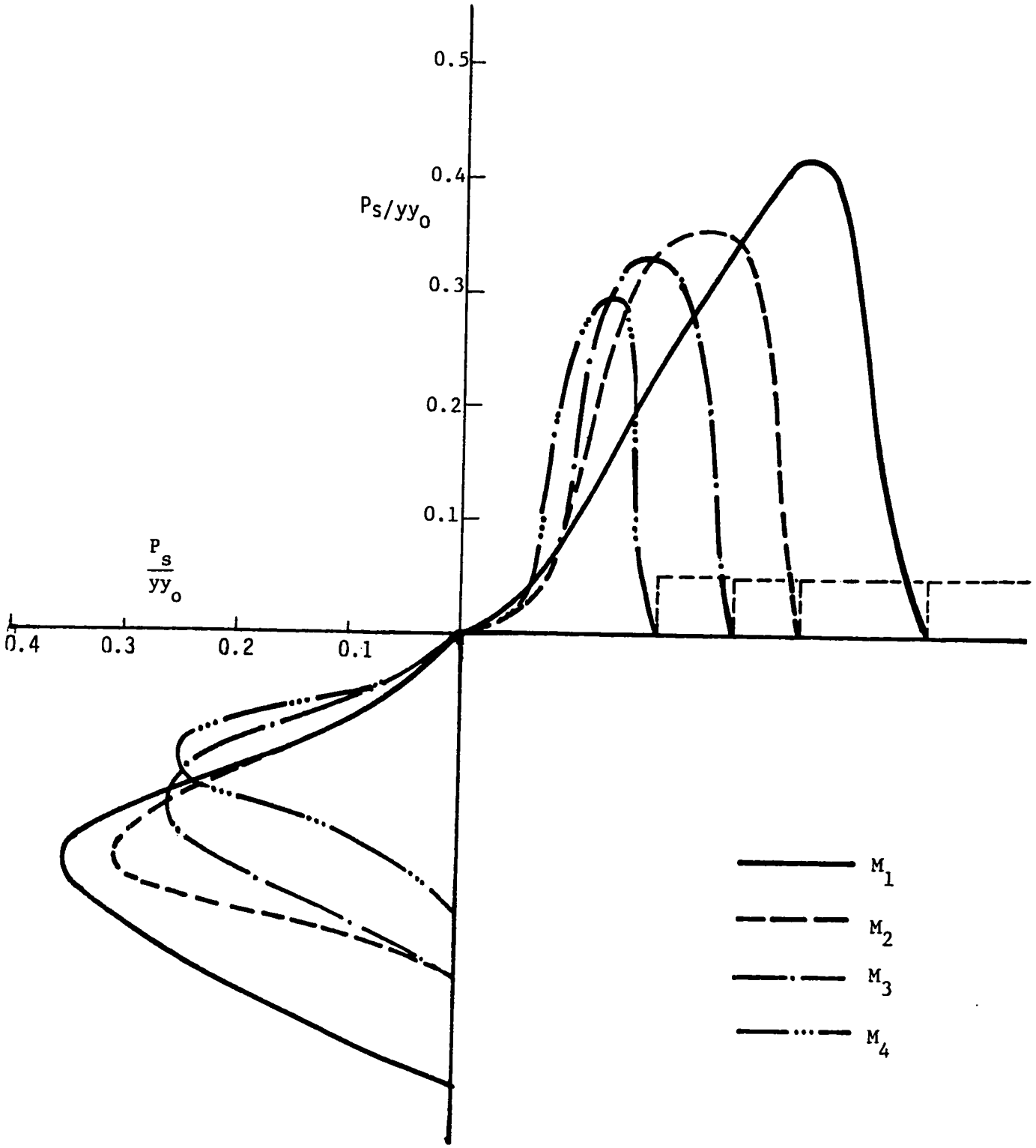

FIGURE 5.21 : The distribution of spalling tensile stress on the free surfaces of the corner in the central plane as a ratio of the mean axial compression.

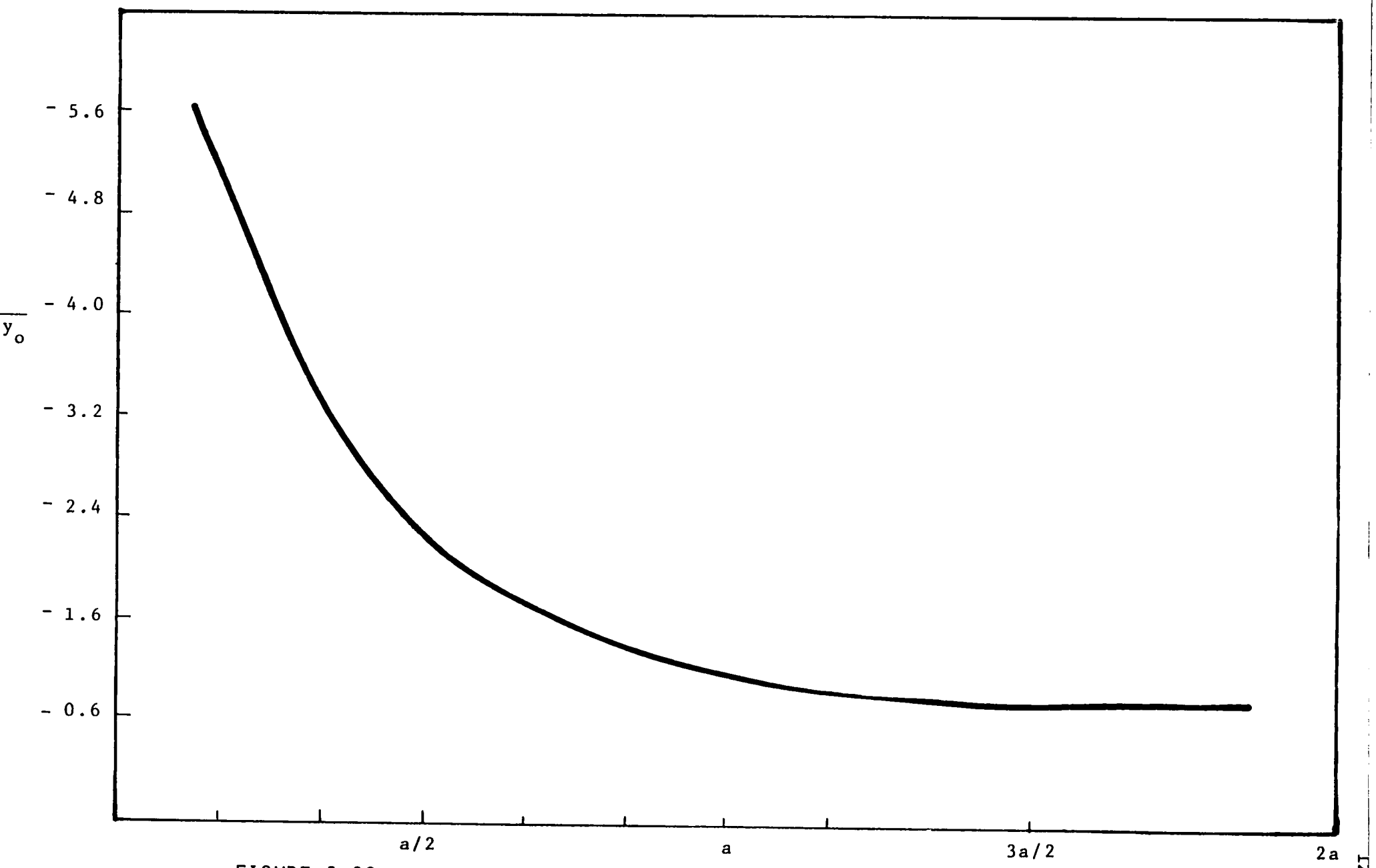

FIGURE 5.22 : The distribution of Q along y-distance for Model M_1 ($a_1/a = 0.316$)

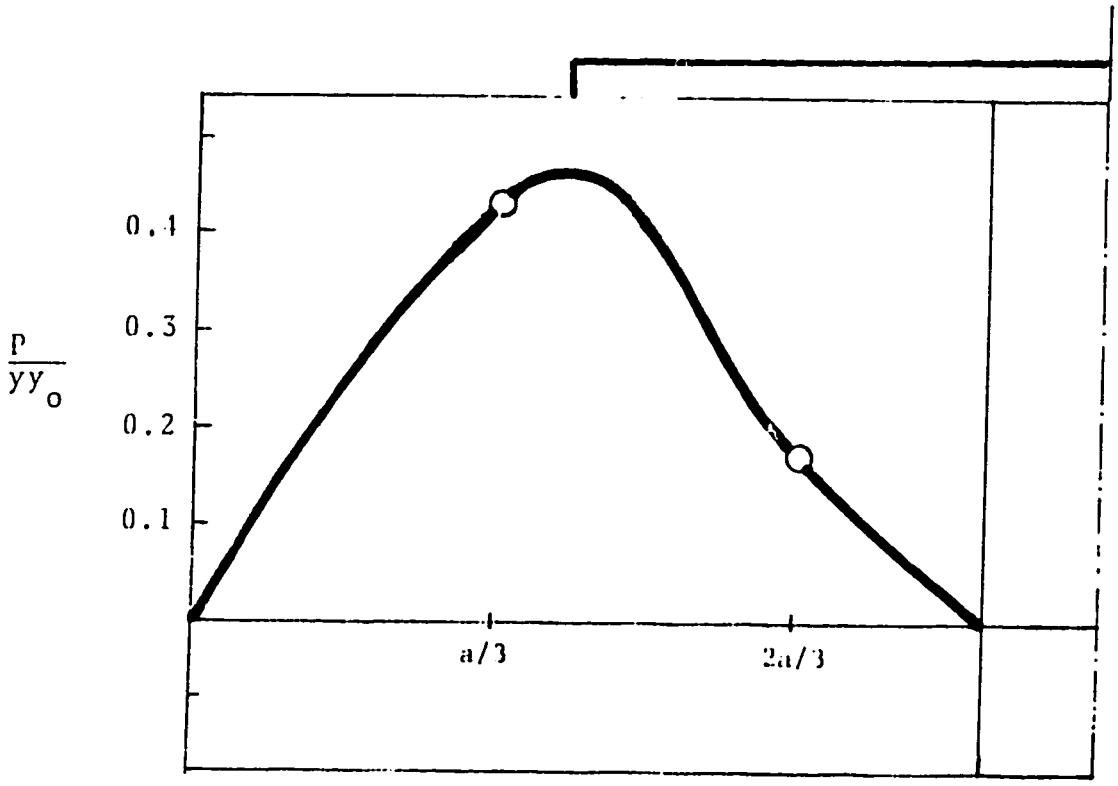

FIGURE 5.23 - The distribution of the transverse principal stress P along X at level V_4 for xy-plane A (Model M_5)

chapter **6**

THREE-DIMENSIONAL INVESTIGATION OF SINGLE EMBEDDED ANCHORAGE MODELS

6.1 INTRODUCTION

This chapter describes the three-dimensional investigation carried out using the frozen stress photoelastic technique on two rectangular end blocks having the same $\frac{A_1}{A}$ ratio, with different embedded anchorage sizes, which were prestressed by single concentrically situated cables, acting through an embedded anchorage unit. The two models till todate no photoelastic tests have been reported which take into account the embeddment of the anchorage unit; also all theoretical derivations essentially presuppose an externally located anchorage. The stress system has been fully explored on the internal mid-plane (A) and the surface plane (B) removed from the models in the form of thin slices in an attempt to define the general behaviour and with a view to establishing the magnitude and location of the maximum tensile stresses, specially in comparison with the external anchorage unit.

The fundamental difference between the external plate and the embedded anchorage unit lies in the mode of load transfer to the end block. The former transfers the prestressing force entirely by a bearing action while the latter which is cast into the anchorage zone transfers this partly through the bearing action at its base and partly by shear around its lateral surface. This investigation seeks to establish the proportions of the loads transferred by shear and bearing respectively.

The cylindrical embedded anchorage unit simulates the Freyssinet system and is made of silica filled Araldite. It corresponds to $\frac{A_1}{A} = 0.25$. The details regarding ensuring the compatibility of stiffness and temperature are given in section 4 of chapter 3.

6.2 MODE OF LOAD TRANSFER

In order to illustrate the mode of load transfer the shear force per unit length of the embedded anchorage has been evaluated by integrating the shear stress around the circumference of the embedded anchorage unit. Figure 6.1 shows the distribution of the shear force per unit length against distance from the surface of the end block for model M_6. The integral of the area beneath this curve

corresponds to the load transferred by means of shear tractions at the surface of the anchorage unit. The second curve in Figure 6.2 is a plot of the proportion of the total load which has been transmitted by shear at each longitudinal station. It is apparent that 33% of the total load is transferred by shear and the remaining by a bearing action. This result is in fairly good agreement with Guyon's assumption that one-third of the total anchorage force is transmitted to the concrete by the lateral surface of the anchorage.

6.3 SHEAR STRESSES

Figures 6.3 to 6.6 show the optical fringe patterns in som- important slices removed from the embedded anchorage end block. The maximum shear stresses occur very near the top surface around the anchorage and also immediately under the anchorage. These values,however, are 0.63 times the maximum values in the external plate anchorage end block. These comparatively lower values are understandable and are obviously due to a more diffused transfer of load from the unit to the end block. Figure 6.7 shows the distribution of shear stress on typical transverse sections in the mid-plane.

6.4 TRANSVERSE TENSILE STRESSES

The distribution of the principal tensile stress P in the transverse direction along the sections at which maximum values are found to occur in the surface and mid-plane are drawn for both these planes in comparison with the corresponding values for the external anchorage in Figures 6.8 and 6.9. The magnitudes of the maximum transverse tensile stresses are respectively 0.58 and 0.52 times the mean compression for the surface and central planes. Both these values occur below the base of the anchorage unit.

Unlike the external plate anchorage model the maximum value of the transverse tensile stress for the embedded anchorage is almost equal in the central and surface planes.

Table 6.1 compares the values of the tensile stresses in the central and surface planes for the two types of anchorage units. These values and a comparison at other typical sections in the central and surface planes indicate that the overall stress level in the embedded anchorage end block is considerably lower than that for the external anchorage end block.

It is obvious that the 15-20% differences in the stress distributions for the two types of prestressing systems are basically due to the difference in the mode of load transfer by the anchorage units. In the embedded anchorage end block, 33% of the total load is carried by the lateral surface of the anchorage unit. Thus the total load being transferred in parts is more thoroughly diffused in the body of the end block and the effect achieved is more or less identical to the effect of decreasing the degree of load concentration with the consequence that the resulting maximum tensile stress is significantly smaller than that for the external plate anchorage.

The existing theoretical solutions, irrespective of the fact that all of these are obtained for loading through externally applied anchorage units, are very frequently used for predicting the distribution of the tensile stresses in the anchorage zones of end blocks stressed by embedded anchorage units.

It is obvious from this investigation that these solutions considerably underestimate the tensile stress in the embedded anchorage zones also. Table 6.2 compares

the maximum values found in this investigation with those predicted by the various theoretical solutions for the $\frac{a_1}{a} = 0.5$. The $\frac{a_1}{a}$ for the circular loading has been obtained by the usual method of replacing the circularly loaded area by its equivalent square area. Bleich and Siever's solution provides the closest approximation. Zileinski and Rowe have not conducted tests on end blocks with embedded anchorage units for this $\frac{a_1}{a}$ ratio.

The positions of the maximum stresses on the two planes are also different from those predicted by the various theoretical solutions. The conclusion for these tests is that the maximum stresses on both the surface and central planes occur only a short distance away from the base of the anchorage unit. This conclusion is in agreement with Guyon's view that with the Freyssinet embedded anchorage unit the maximum tensile stress in the anchorage zone will occur at a certain distance from the end of the anchorage and not from the loaded face.

6.5 TRANSVERSE TENSILE FORCE

The tensile forces per unit width on the mid-plane and the surface plane are 0.06 and 0.12 times the total load. These tensile forces on the surface and mid-plane are

40% and 44% smaller than the corresponding values for the external anchorage unit.

6.6 SPALLING TENSIONS

The spalling tensions in the case of the embedded anchorage end block are found to be negligibly small. This is contrary to the state observed for the external anchorage end block when the maximum tensile stresses adjacent to the edges of the anchorage plate on the bearing surface in the central plane were found to be 0.42 and 0.3 times the mean compression.

6.7 COMPRESSIVE STRESSES

The maximum compressive stress occurs in the longitudinal direction immediately below the base of the anchorage unit. Since part of the applied load is transferred to the end block as shear force at the lateral surface of the embedded unit the maximum principal compressive stress Q in this case is only about 1.7 times the average compression. The maximum compressive stresses for the external anchorage end block for this $\frac{a_1}{a}$ ratio was found to be 5 times this value. Figure 6.10 shows the distribution of Q along the longitudinal axis.

6.8 EFFECT OF ANCHORAGE SIZE

Another model was investigated (M_7) which had a longer anchorage unit embedded in it to study the effect of anchorage size on the load percentage transferred by the shear action. The second model had the same $\frac{A_1}{A}$ ratio as the first one but the length of the anchorage was twice the length of the first anchorage. It was found that in the second case the load transferred by the shearing action was measured to 49%. This evidently resulted in the reduction of the value of the transverse tensile stress from 0.52 times mean compression to 0.42 times mean compression. Figure 6.11 shows the transverse tensile stresses drawn along the longitudinal sections of the mid-plane of the two embedded anchorage models.

TABLE 6.1

The maximum tensile stress and tensile force values for external and embedded anchorage units ($a_1/a = 0.5$)

Type of anchorage	Tensile stress expressed as a ratio of the mean compression		Tensile force expressed as a ratio of the prestressing force	
	Mid-plane	Surface	Mid-plane	Surface
External	0.6	0.68	0.155	0.27
Embedded	0.5	0.57	0.06	0.12

TABLE 6.2

Comparison of the maximum tensile stress values for the embedded anchorage unit

	Iyengar	Yettram & Robbins	Zeilinski & Rowe	Rowe	Bleich & Sievers	Author
Maximum tensile stress expressed as a ratio of the mean compression	0.096	0.21	0.56	0.5	0.986	0.57

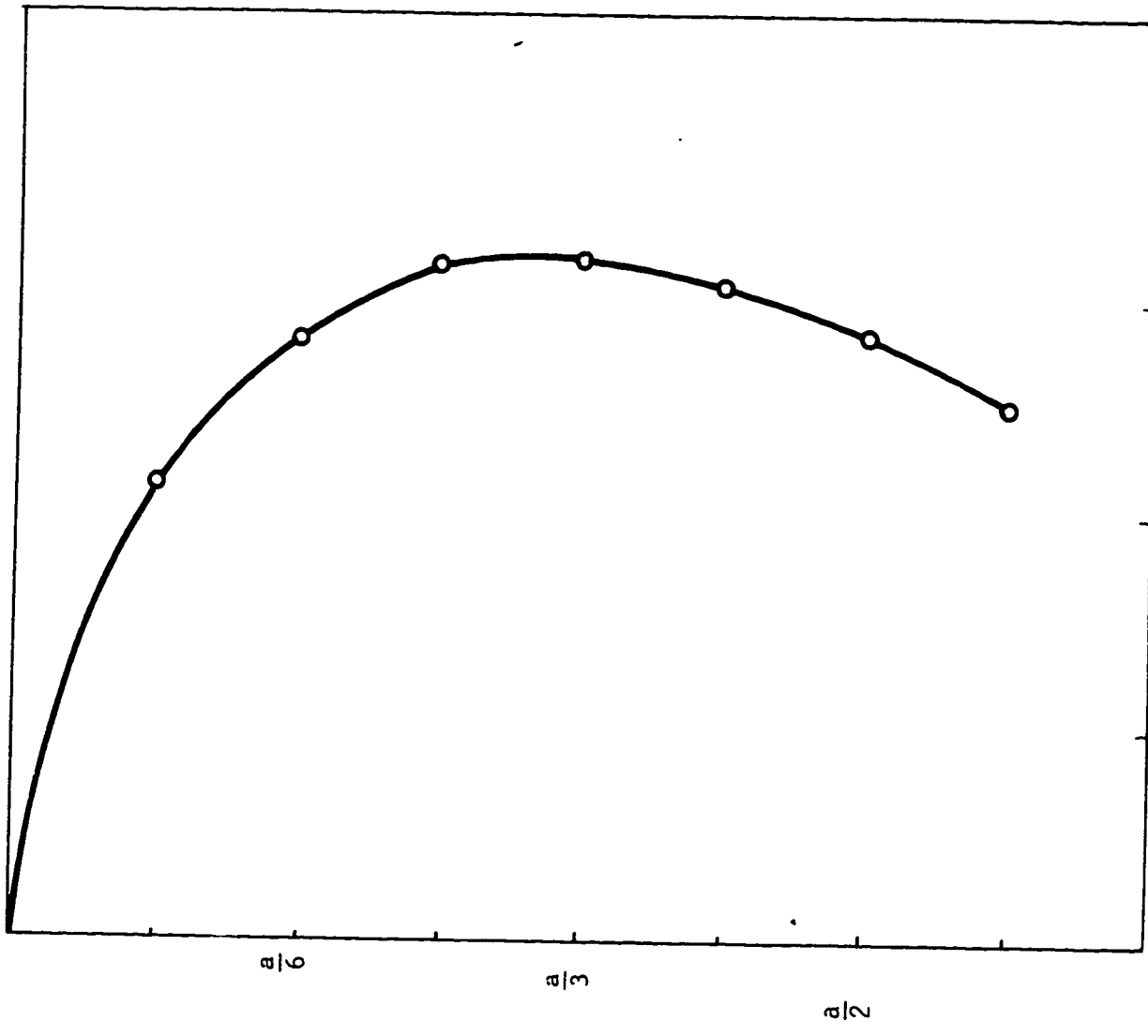

FIGURE 6.1 : The distribution of the shear force per unit length against distance from the surface of the end block (M6)

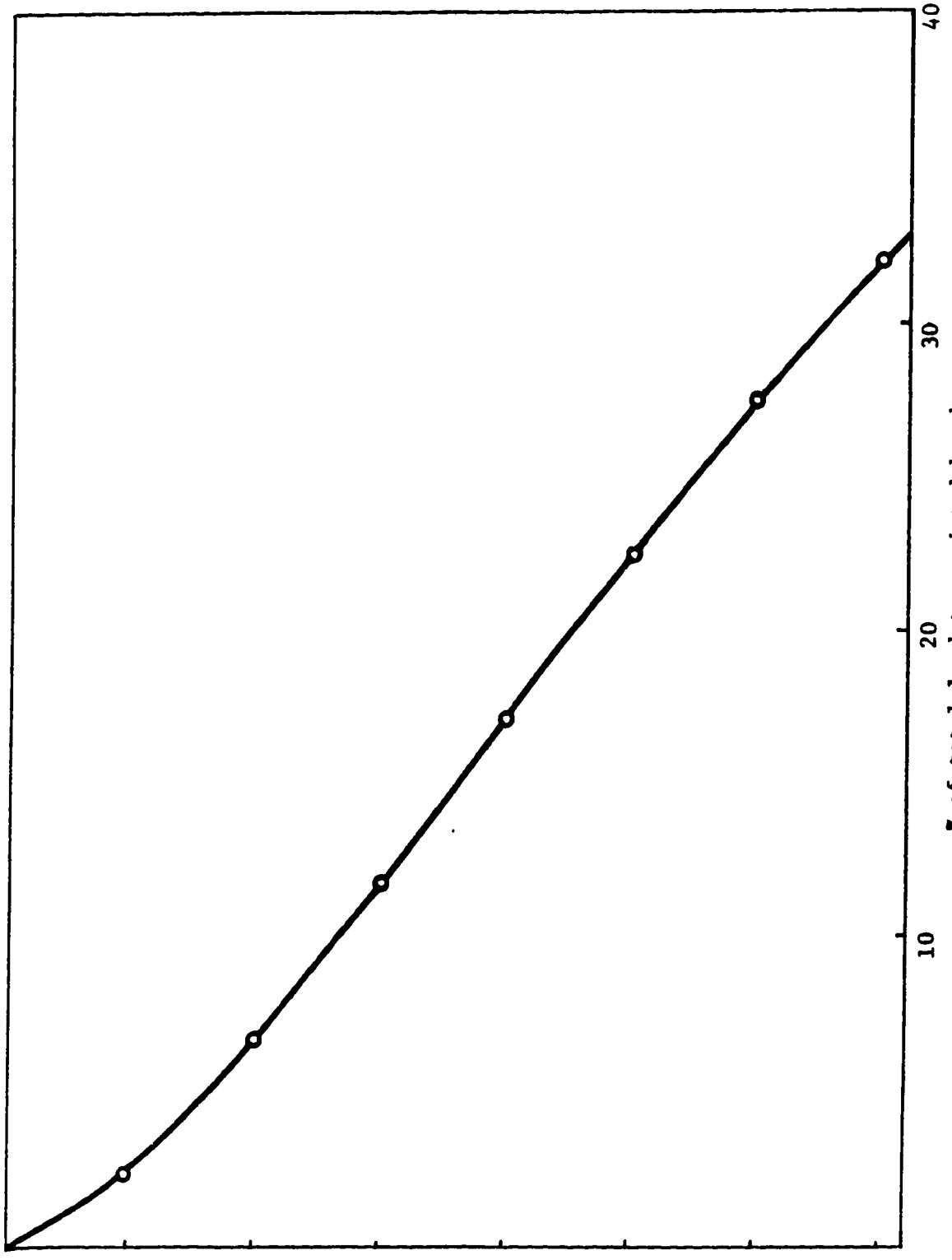

FIGURE 6.2 : The proportion of the total load transmitted by shear at each longitudinal section (%)

FIGURE 6.3 : Typical isochromatic for xy-plane A for the embedded anchorage model

FIGURE 6.4 Typical isochromatic for yz-plane 4 for the embedded anchorage model

FIGURE 6.5 : Typical isochromatic for radial plane for the embedded anchorage model

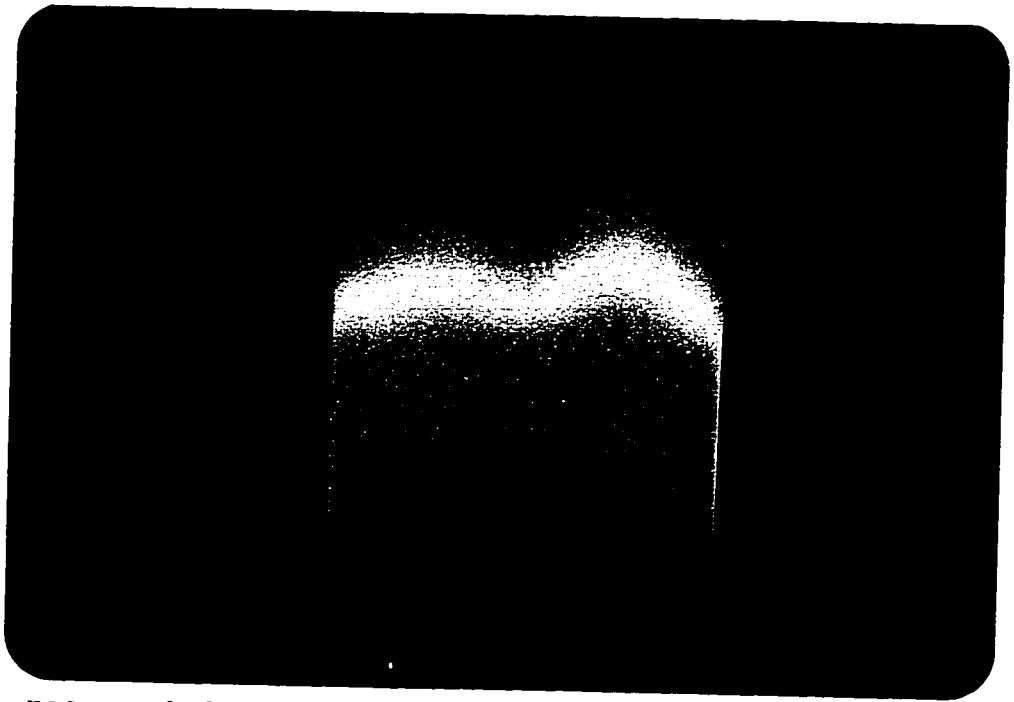

FIGURE 6.6 : Typical isochromatic for xy-plane B for the embedded anchorage model

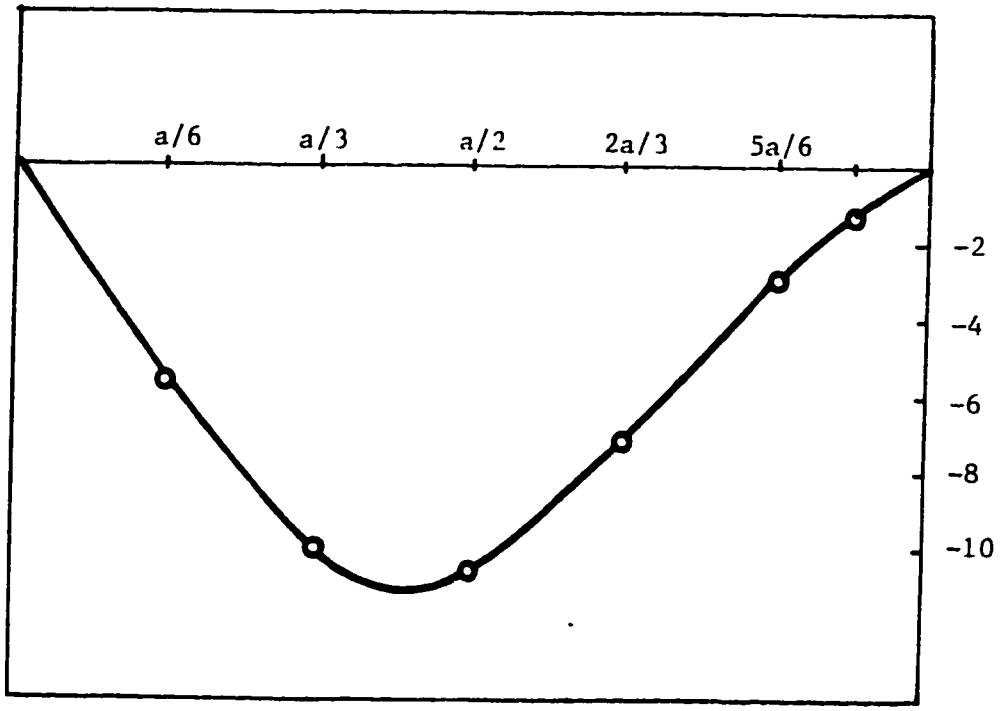

FIGURE 6.7a - Shear stress distribution along X at level V_{10} for xy-plane A (Model M_6)

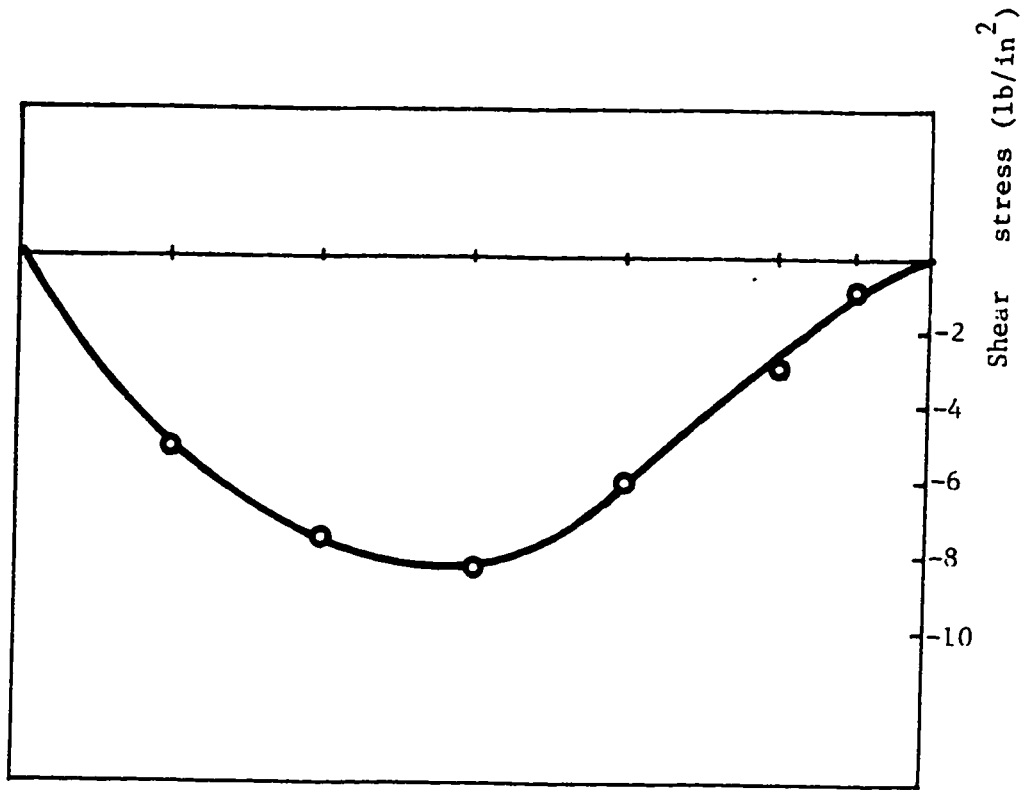

FIGURE 6.7b - Shear stress distribution along X at level V_{11} for xy-plane A (Model M_6)

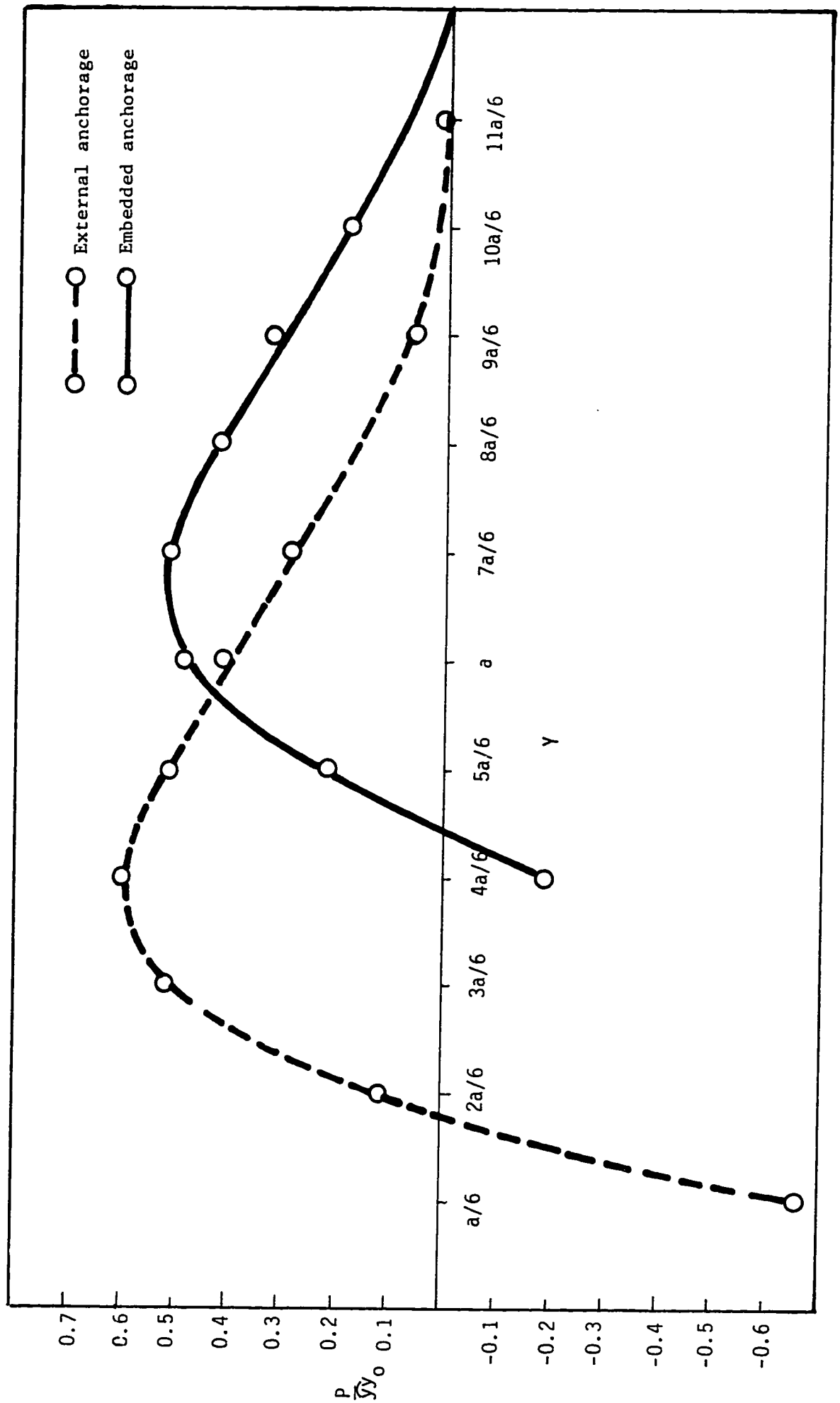

FIGURE 6.8 : The distribution of the principal tensile stress P in the transverse direction along the longitudinal section in the mid-plane for the embedded and external anchorages.

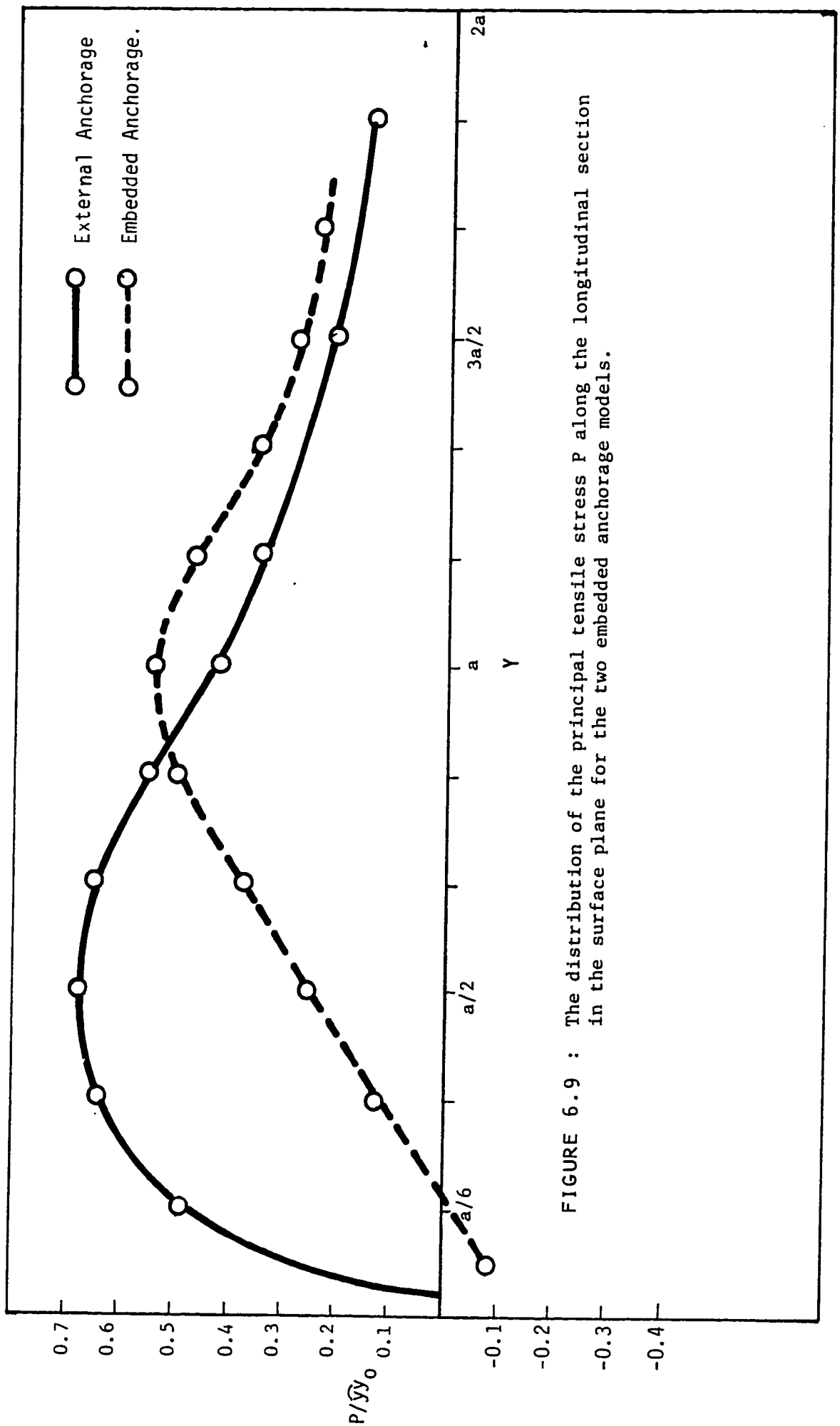

FIGURE 6.9 : The distribution of the principal tensile stress P along the longitudinal section in the surface plane for the two embedded anchorage models.

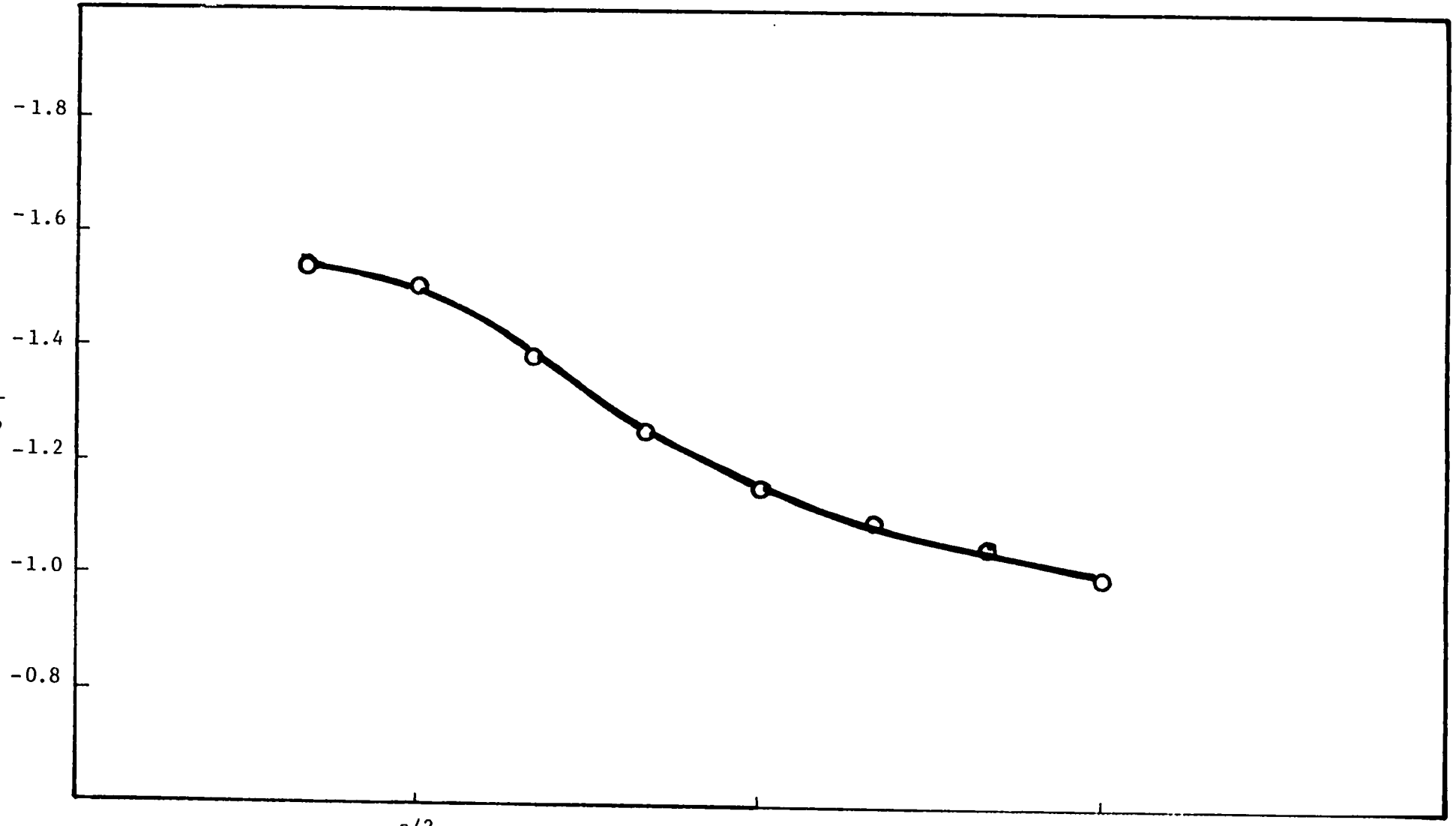

FIGURE 6.10 : The distribution of Q along y-distance for Model M_6

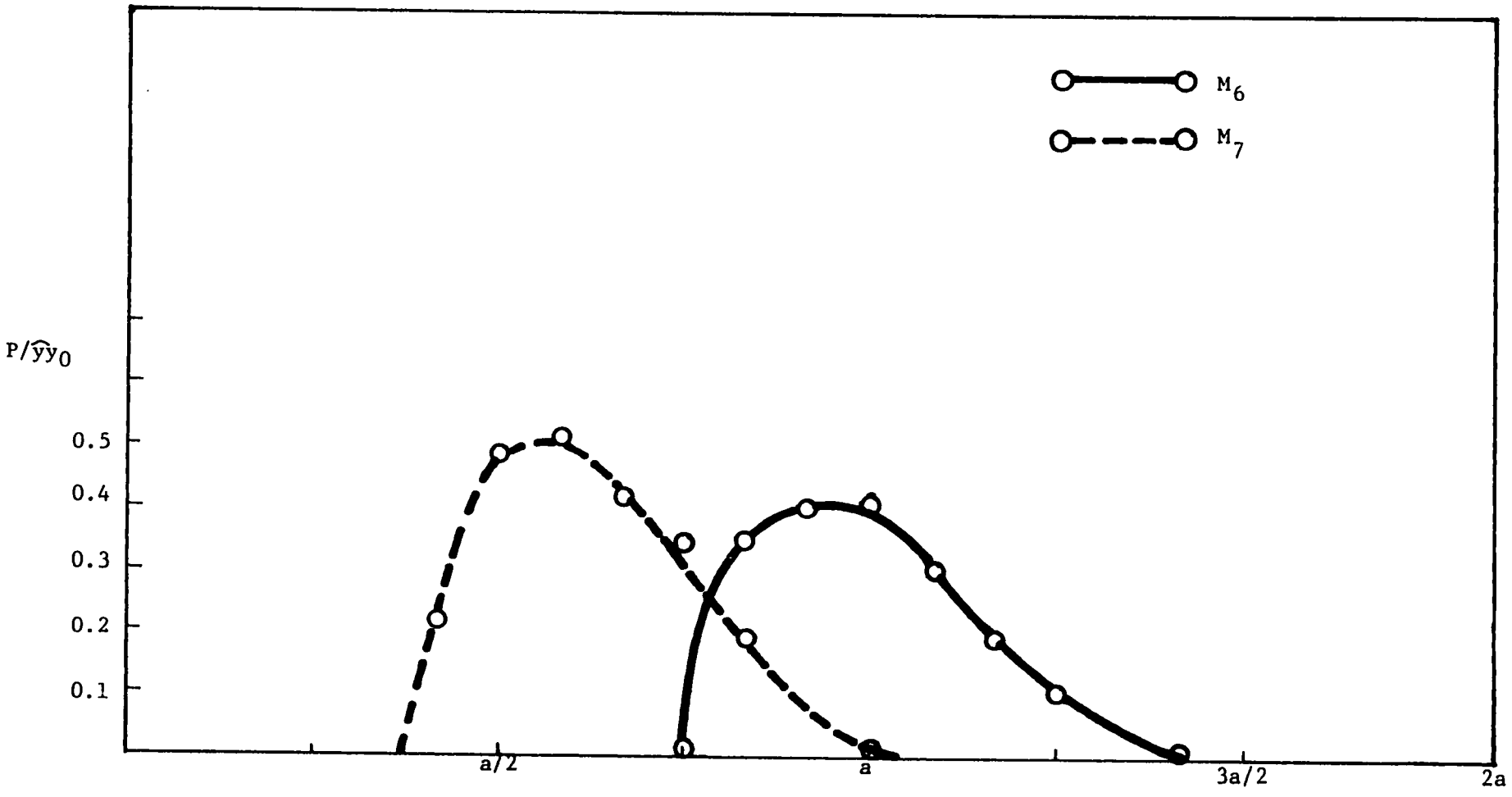

FIGURE 6.11 : The distribution of the principal tensile stress P along the longitudinal section in the mid-plane for the two embedded anchorage models

chapter **7**

THREE-DIMENSIONAL INVESTIGATION OF MULTI-ANCHORAGE END BLOCK MODEL

7.1 INTRODUCTION

This chapter describes the three-dimensional photoelastic analysis of a rectangular end block subjected to three post-tensioning forces and considered to be an integral part of a long rectangular beam. The post-tensioning of the model studied here was carried out by three cables acting through external anchorage units carrying equal prestressing forces (Figure 7.1). The overall concentration ratio in this case is 0.26, although based on symmetrical prism approach the concentration ratios are 0.16, 0.32, and 0.45 for individual anchorages I, II and III respectively (Figure 7.2). In this study the distribution in the anchorage zone has been fully explored. The magnitudes of all the important stress components have been obtained on internal and surface planes in the XY and YZ directions. The lines of principal stress and the contours of the principal tensile stress P are drawn on the internal

and surface planes.

The analysis of this study has been deepened in the direction of verifying the application of single concentric test results to the multi-anchorage case on the basis of the symmetrical prism method proposed by Guyon and slightly modified by Zielinski and Rowe. Moreover, some other potential directions useful to the designer have been explored on the basis of the behaviour results of the multi-anchorage end block.

7.2 EXPERIMENTAL PROCEDURE

7.2.1 General Details

The photoelastic model was made of cast Araldite B having a rectangular cross section 3" x 1½" and a length of 6" (Figure 7.3). As in the case of three-dimensional single anchorage models only a small part of the length of the adjoining beam was cast into the model. The applied post-tensioning forces were 55 lb for each anchorage and were applied vertically by means of cables passing through ducts as shown in Figure 7.1. The manner of loading and the forms of anchorage units employed have been described in detail in chapter 3 where the experimental procedure is outlined for these tests. The ratio of the total loaded

area to the gross area of cross-section of the end block is 0.26.

7.2.2 Method of Slicing

The details of the slices removed from the frozen model for observations are shown in Figure 7.3. The general scheme and the procedurefor removing the slices is similar to the one adopted in the preceeding investigation with the difference that far more slices were removed and analyzed in this case than in the preceeding case of single anchorage models; the reason being that an in-depth study of the behaviour was considered essential to be able to make recommendations for the design. The thickness of the slices varied from 0.06 inches to 0.08 inches for observations of fringe numbers.

7.2.3 Analysis and Measurement

The grid marked on XY-slices is shown in Figure 7.4. The grid on the YZ-slices is shown in Figure 7.5. The computation of the normal and principal stresses on various planes was carried out by the application of the shear difference method to the general three-dimensional problem as described in chapter 4.

7.3 DISCUSSION OF RESULTS

7.3.1 Shear Stresses and Lines of Principal Stresses

The optical fringe patterns in the important slices are shown in Figures 7.6 and 7.7. In all the planes shown, the shear stresses are seen to be concentrated along the edges of the anchorage plate. The variations of shear stresses in the XY and YZ planes in the directions of x and z respectively were drawn along the horizontal grid lines for all the XY and YZ planes removed from the "frozen" models in order to obtain the contributions required for the evaluation of the normal stresses. On the basis of the observations it may be concluded that the peak values of shear stresses in the end block at all levels along the longitudinal direction occurred under the edges of the anchorage plates. Typical shear variations for the XY- and YZ- planes are shown in Figures 7.8 and 7.9.

Figures 7.10 and 7.11 show the isoclinics and the stress trajectories for the plane of symmetry.

7.3.2 Transverse Stresses

For the internal and the surface XY-planes transverse stresses XX and P have been obtained along eleven

longitudinal lines corresponding to the internal YZ-slices (2 to 12; Figure 7.1). As the stress level in the intermediate planes between internal and surface planes is expected to be lower, the separate principal stresses have been obtained for the internal and surface planes only.

7.3.3 General Form of Stress Distribution

The contours of the principal tensile stresses P in the mid-plane and on the surface are shown in Figures 7.12 and 7.13. These contours show bursting zones beneath and between the anchorage units and spalling zones in the corners.

7.3.4 Bursting Zones

7.3.4.1 Tension zone between the anchorage units : The contours of the principal tensions on the surface and mid-planes indicate tension zones between the anchorage units. The creation of a tensile zone between the anchorage units in akin to the existence of spalling zones in the two corners and could be explained by the mode of load dispersion for each individual end prestressing force (Figure 7.14).

The present analysis indicates that the tension zone between the anchroage unit exists throughout the width of

the end block and that the value of the maximum tensile stress in this region at the mid-plane is fairly high. Figures 7.15 and 7.16 show the distribution of P for the mid and surface planes along section 8 which lies between the anchorages I and II. It is seen that the maximum tension between the anchorages is of the order of 0.5 and .48 times the mean compression for the mid and surface planes respectively, and that these values occur at the surface of loading. The tension zone is confined on section 8 to a shallow depth of (d/25) in the direction of y. Also, the maximum value of the tensile stress in this zone decreases towards the surface where it is about 0.48 the maximum value in the mid-plane. In investigation of section 2 which is close to the edge of the loading pad indicates very high tensions of the order of 1.35 times the mean compression at the free surface on the loaded face close to the edge of the anchorage unit. These high values also,however, correspond to a shallow zone of tension as indicated in Figure 7.17 which shows the distribution of P along the longitudinal axis Y for section 2.

An analysis for the principal stress R along the Z direction at the loaded face point L of section A8 also shows tensile stress of 0.6 times the mean compression.

The distribution of R along y direction for the section A8 shown in Figure 7.18. This indicates that in shallow zones between the anchorages in the mid-plane A there exists a stale of bi-axial tension.

The sustained high values of transverse splitting tensions in most part of the width between the anchorage units and the static of bi-axial tension in this shallow zone render this region between the anchorage units potentially vulnerable to cracking and failure. Figure 7.19 shows the mode of failure in rectangular concrete end blocks post-tensioned by two and three cables. In either case a crack is indicated on the surface between the anchorage units confirming the strong tendency of a splitting failure in this region.

The maximum total tensile force per unit width in this region is 0.02 times the total applied prestressing force. This being small the tensile reinforcement to be provided in this region should be concentrated just below the bearing surface where large tensions are developed in most parts of the end block width.

7.3.4.2 Tensile zones beneath the anchorage units: The contours of the principal tensions in the mid-and surface planes indicate that tensile zones are found to exist

beneath the anchorage units in the XY-planes which tend to cause a bursting or splitting failure in the direction of the height.

A comparison of the mid-plane and surface contours pinpoints a significant fact which was also indicated by the series relating to the single concentric models: that the comparative magnitude of the tensile bursting stress for the internal and surface planes depends mainly on the proximity of the loading pad to the surface plane.

Table 7.1 : Maximum tensions under the anchorages, for mid and surface planes

	Anchorage I	Anchorage II	Anchorage III
Distance of the edge of loading pad from the surface plane	0.375	0.158	0
Maximum tension in surface plane	0.70	0.80	1.20
Maximum tension mid plane	0.9	0.75	0.80

Table 7.1 shows that the position of the mid-plane showing greater tensions in the region of the end block under anchorage I is gradually dialated as the proximity of the loading pad to the surface increases and is reversed under

under anchorage II and the reversal becomes strengthened under anchorage III where the edge of the loading pad is actually located at the surface. This type of potential reversal is indicated in Figure 5.12 of chapter 5 where the difference in the magnitude of traverse tensions between surface and mid planes is shown to progressively shrink with increasing values of $\frac{A_1}{A}$.

This finding is very substantive in indicating that in many situations the concentration ratio, either expressed comprehensively as $\frac{A_1}{A}$ or expressed as $\frac{a_1}{a}$ in the vertical and horizontal directions, may not prove to be a sufficient parameter for evaluating the maximum transverse tension values on the critical surface or mid-planes. The actual geometry of the anchorage with respect to the end block cross section configuration will play an important part as a complementary parameter.

Table 7.2 gives the values and positions of the maximum transverse tensile stresses and the tensile forces on the surface and mid-planes in the zones beneath the anchorage units on various sections. These results should be interpreted in the light of data indicated in Figure 7.13.

It appears from the optical fringe patterns that the behaviour of adjacent anchorage units is sensibly independent, except in the case of the bursting tension in the zones between the anchorages. In view of this conclusion it is reasonable to assign zones of influence to each anchorage unit. This is done in Figure 7.2 on the basis of the symmetrical prism method proposed by Guyon and somewhat modified by Zielinski and Rowe. This gives the load concentration ratios ($\frac{A_1}{A}$) of 0.16, 0.32 and 0.45 for prestressing forces I, II and III respectively. This position is reflected in the values of maximum transverse tensile stresses under the various anchorage units. Table 5.2 and the contours of principal stress P for the mid-plane (Figure 7.12) indicate a higher level of tensile stresses under load I. The stress level, however, falls gradually downward toward load III. It is, however, interesting that an identical position is not obtainable for the surface plane. In fact the maximum transverse tensile stress level follows a reverse trend on the surface plane as indicated by Table 5.2 and the contours for the surface plane. It is clear from this data that the value of the maximum transverse tension in the surface plane is goverened by an additional factor : the proximity of the loading pad. The value of P

is maximum in the whole surface plane at section 3 because the anchorage unit III is closest to the surface there. The value on section 10 is lower than the corresponding values at sections 6 and 3, although the $\frac{A}{A}$ ratios for anchorage units II and III are higher. This can be explained on the grounds that at section 10 the edge of the loading pad is farthest from the surface plane. It therefore seems that the critical stresses in the vicinity of an anchorage unit are also a function of thelocal geometry and are not solely determined by the load concentration ratio parameter. This effect emphasizes the three-dimensional nature of the anchorage zone problem.

A comparison of the positions of maximum transverse tensions in the plane of symmetry with those in the surface plane (Figures 7.12 and 7.13) indicates the effect of the cable duct on the form of tranverse stress distribution in the mid-plane. In a plane which does not contain the duct, the maximum principal tensile stresses (P) are found to occur on lines corresponding to the centre lines of the anchorage units. However, in the mid-plane, the maximum principal tensile stresses occur under the edges of the anchorage units.

The locations of the maximum tensile stresses in the direction of the length for the central and surface planes

are given in Tabel 7.2. For the mid-plane the position is given by 0.03 d from the loaded face and for the surface plane the corresponding value is 0.021 d.

In the single external anchorage having $\frac{A_1}{A} = 0.25$ the total tensile force per unit width worked out on the basis of the maximum transverse tensile stress distribution on the surface plane was found to be 0.27F. The multi-anchorage end block has an almost identical $\frac{A_1}{A}$ ratio (0.26). The corresponding average value for the total tensile force per unit width also worked out for the surface plane on the basis of the maximum values under the individual anchorages is found to be.109F. This value is only about 50% of the value when the similar force was applied using triple anchorages instead of a single anchorage. It may be concluded from this observation that the effect of dividing the forces into smaller units is to affect a reduction in the total tensile force for which the reinforcement is provided.

7.3.4.3 Tensile force : Table 7.2 shows the variation of the total tensile force under the various anchorage units in the internal and surface planes. As discussed earlier the total tensile force in the mid-plane is mainly governed by load concentration ratio. The

tensile force level is higher under the anchorage unit representing a lower load concentration ratio. This position, however, is not true for the surface plane where the proximity of the anchorage unit is also a substantive influencing parameter. This leads to the conclusion that for those geometric configurations of the anchorage units which result in reduced proximity of the loading pad to the surface plane the critical values will not be necessarily found on the surface plane but will occur in the mid plane.

7.3.4.4 Tensile stress ZZ in the direction of the width : The values of ZZ (which are equal to the principal stress R for the mid-plane) were evaluated for the surface planes 1 and 13 and for internal planes 8 and 9. On the surface plane 13 the maximum value go the tensile stress is of the order of 0.54 times the mean compression. On internal plane 9 this value was found to be 0.12 times the mean compression respectively. This suggests that a sizeable part of the region under the anchorage unit is in bi-axial tension. Figure 7.20 shows a typical plot of ZZ for the external plane 13.

7.3.4.5 Compressive stresses : High compressive stresses in the longitudinal direction are found to exist on the planes under the anchorage unit. In the mid-plane

along the hole boundary of load I the value of principal compression Q is found to be four times the mean compression. Figure 7.21 shows a typical plot of Q variation along this section.

TABLE 7.2

The Values of the Maximum Transverse Tensile Stresses and the Tensile Forces on the Surface and Mid-planes on Various Sections

Section	Maximum transverse tensile stress expressed as the mean compression		Maximum tensile force expressed as a ratio of the prestressing force	
	Mid-plane	Surface	Mid-plane	Surface
2	1.3	1.4	0.036	0.268
3	-	1.27	-	0.204
4	0.6	0.6	0.0087	0.148
5	0.29	0.5	0.025	0.02
6	-	1.0	-	0.06
7	0.34	0.54	0.03	0.034
8	0.7	0.45	0.0348	0.008
12	0.19	0.2	0.014	0.02

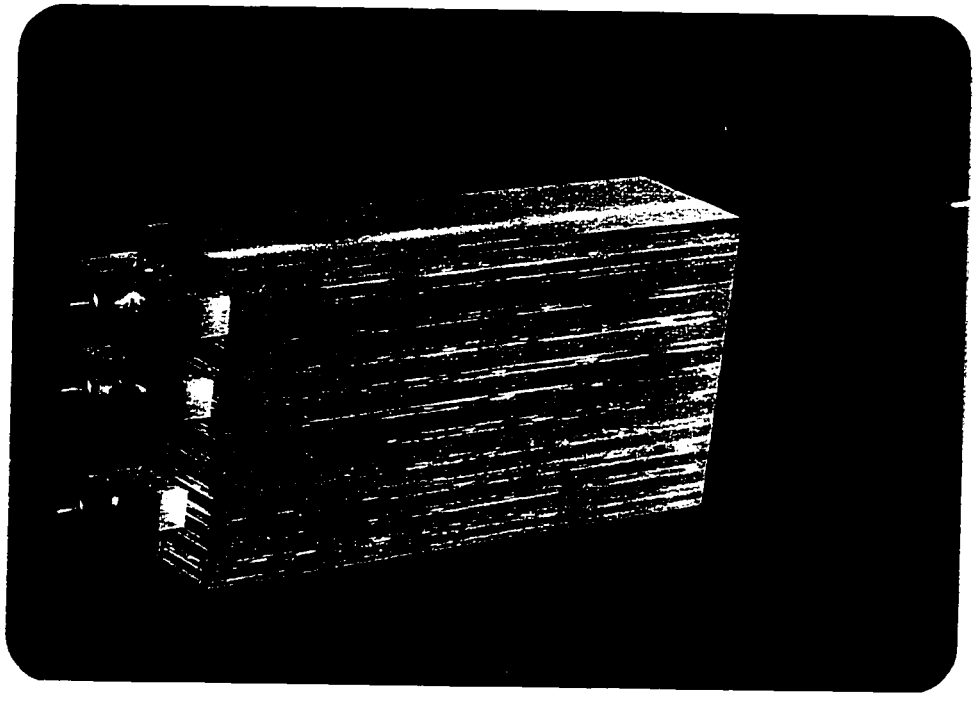

FIGURE 7.1 : The end block beam made from Areldite B with the anchorage units

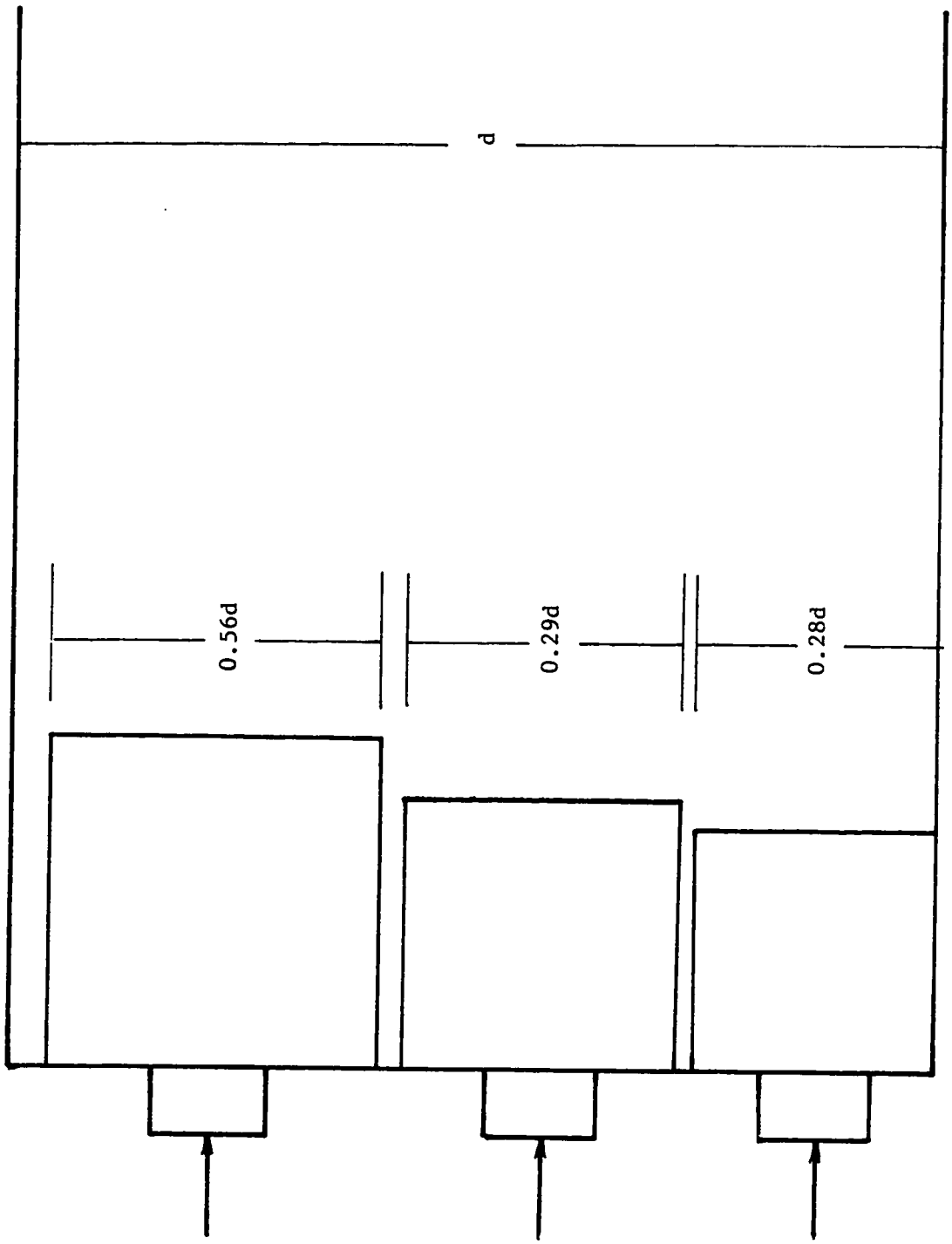

FIGURE 7.2 : Description of the symmetrical prism approach

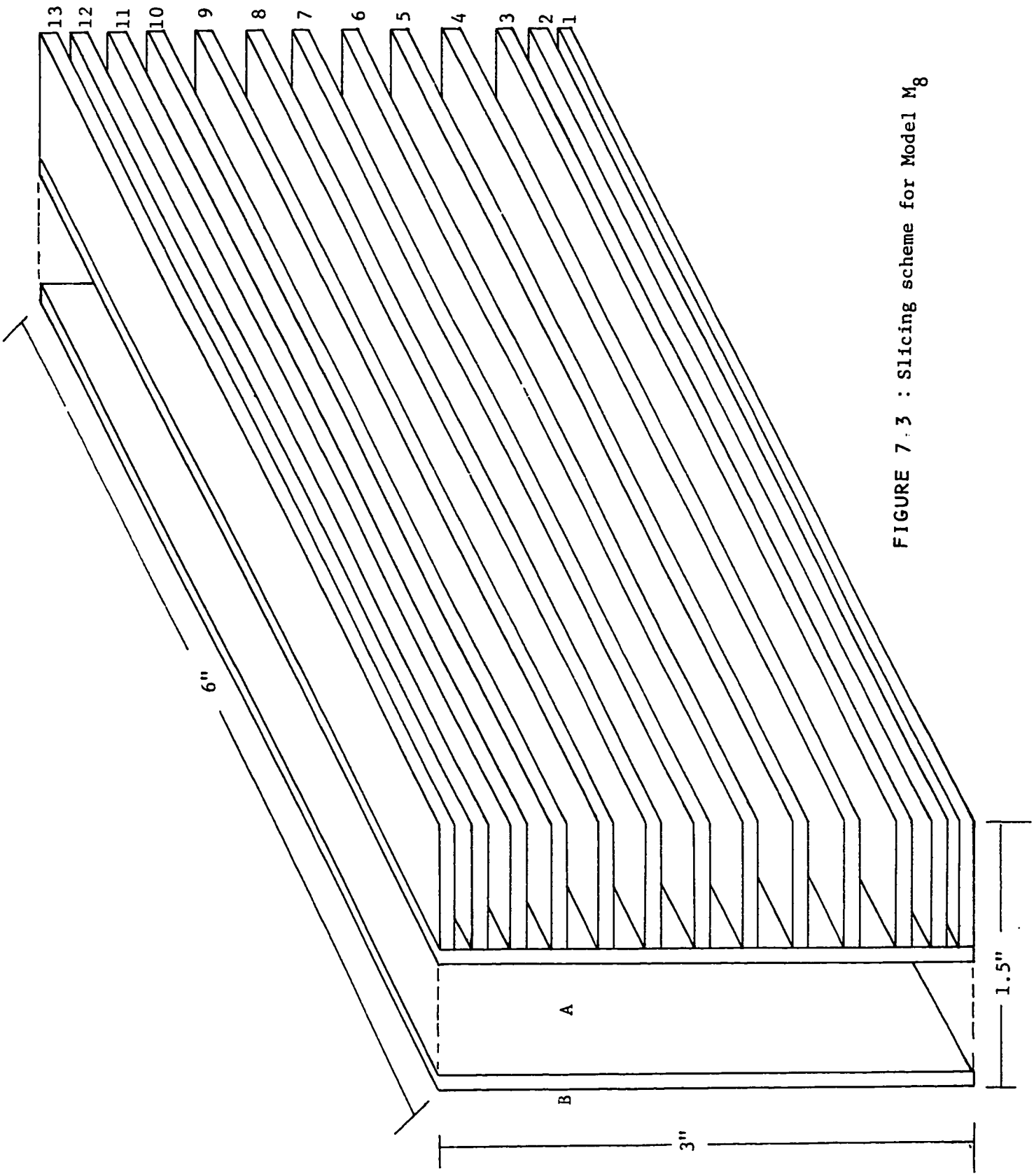

FIGURE 7.3 : Slicing scheme for Model M_8

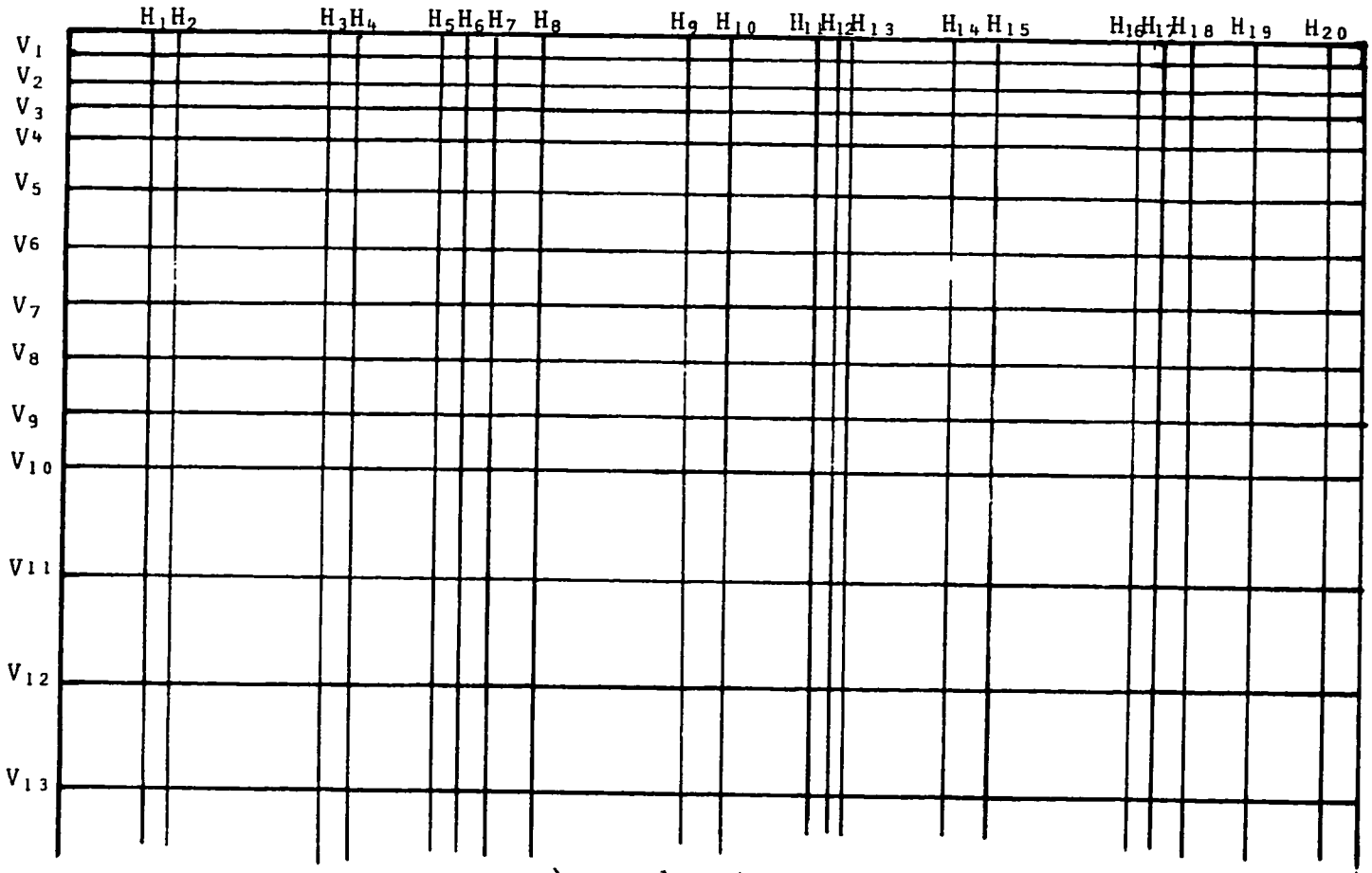

a) xy-plane A

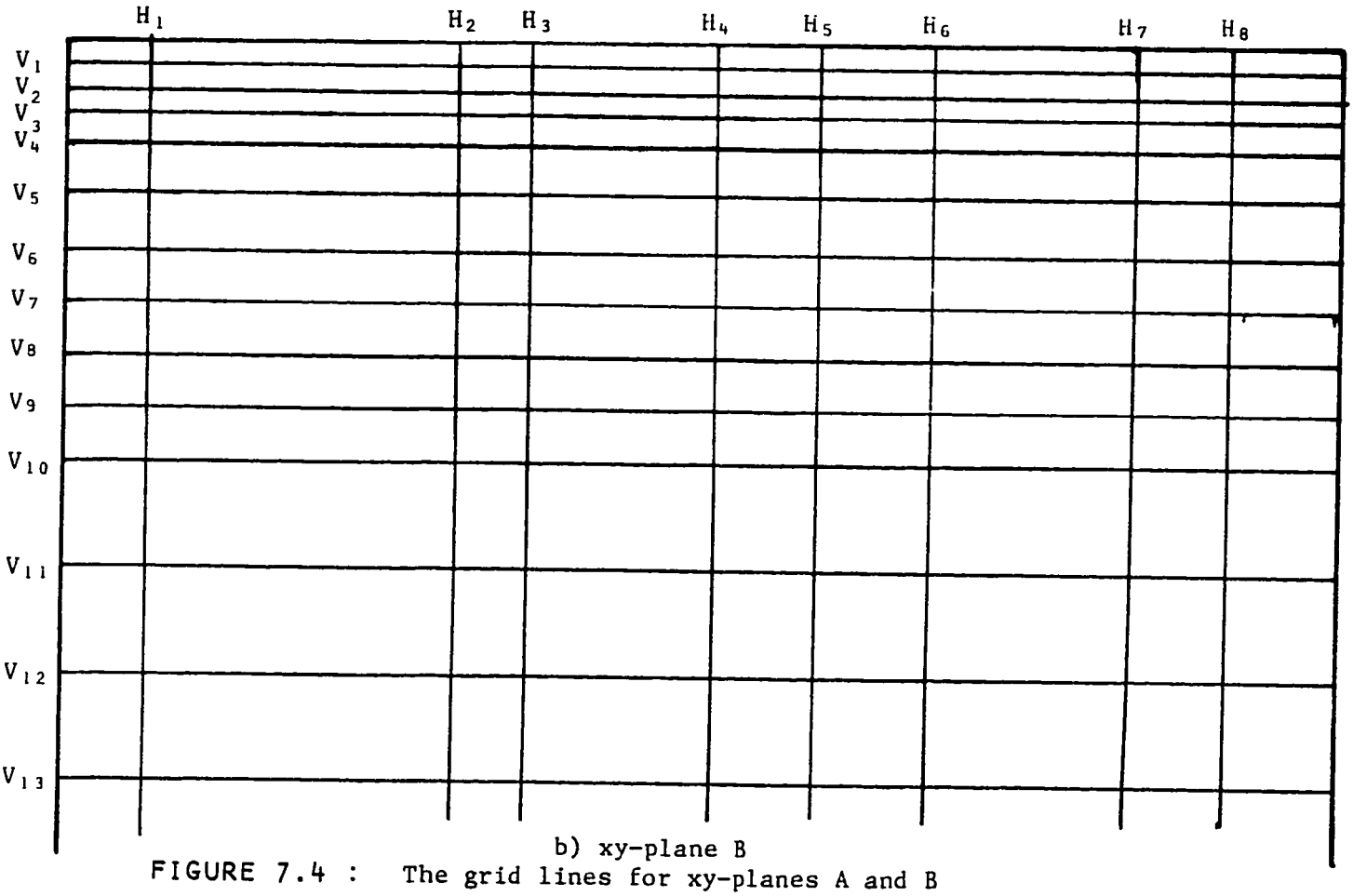

b) xy-plane B

FIGURE 7.4 : The grid lines for xy-planes A and B

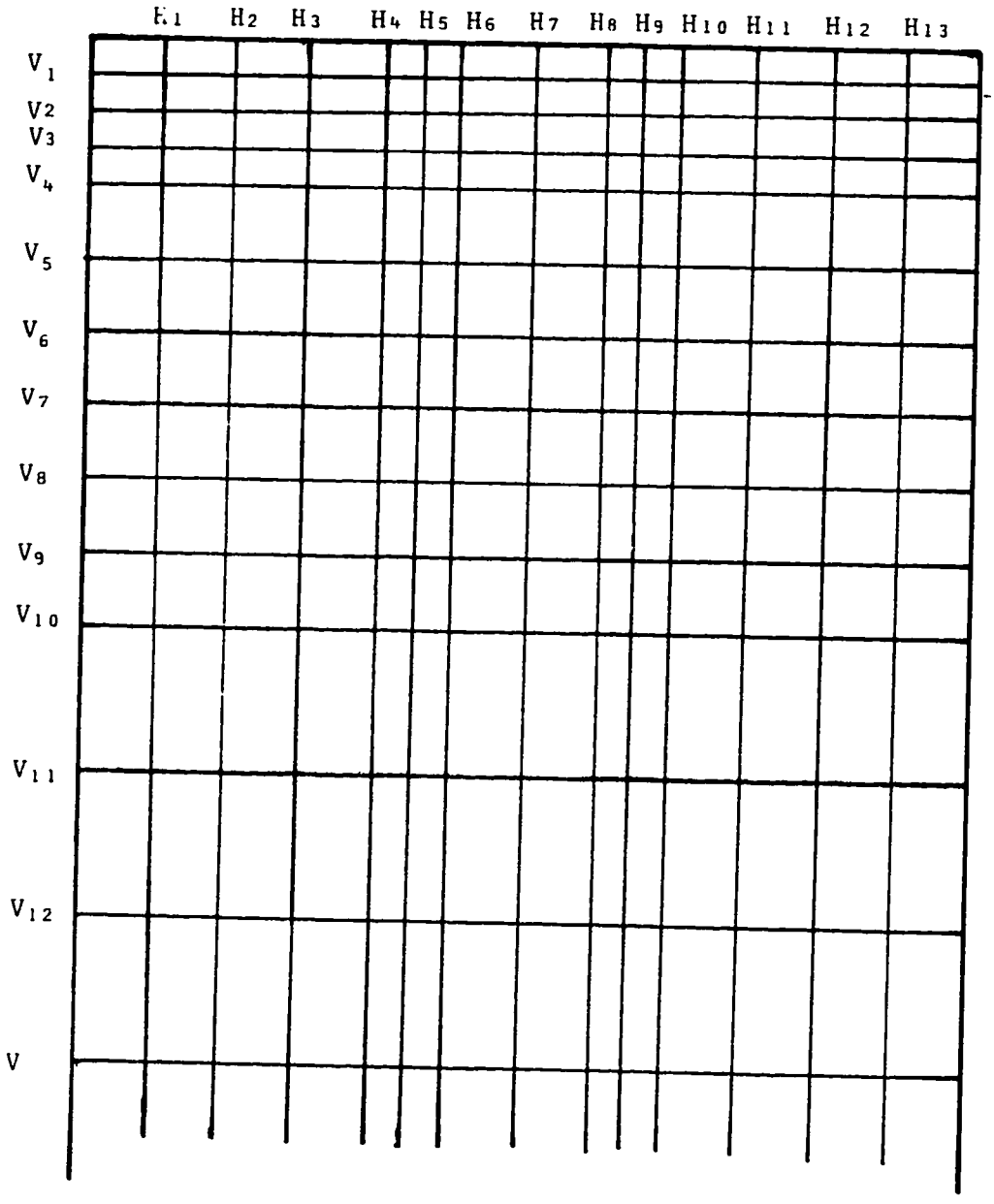

FIGURE 7.5 : Grid lines for yz-planes

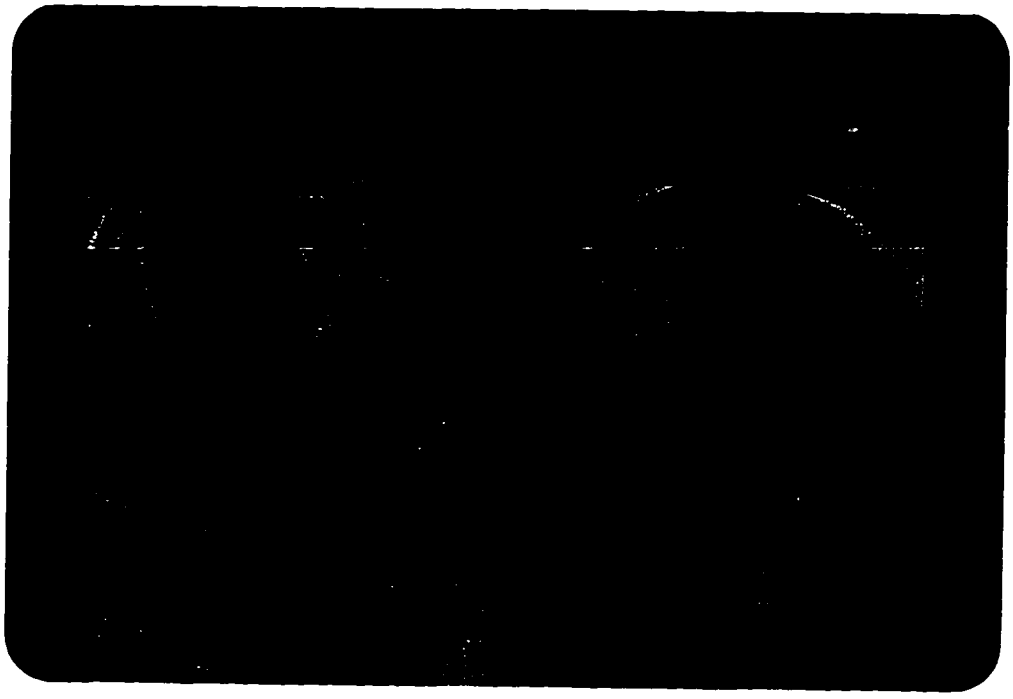

FIGURE 7.6 : Typical isoclinic $\alpha = 25^{o}$ for the mid-plane (xy-plane A) Model M_8

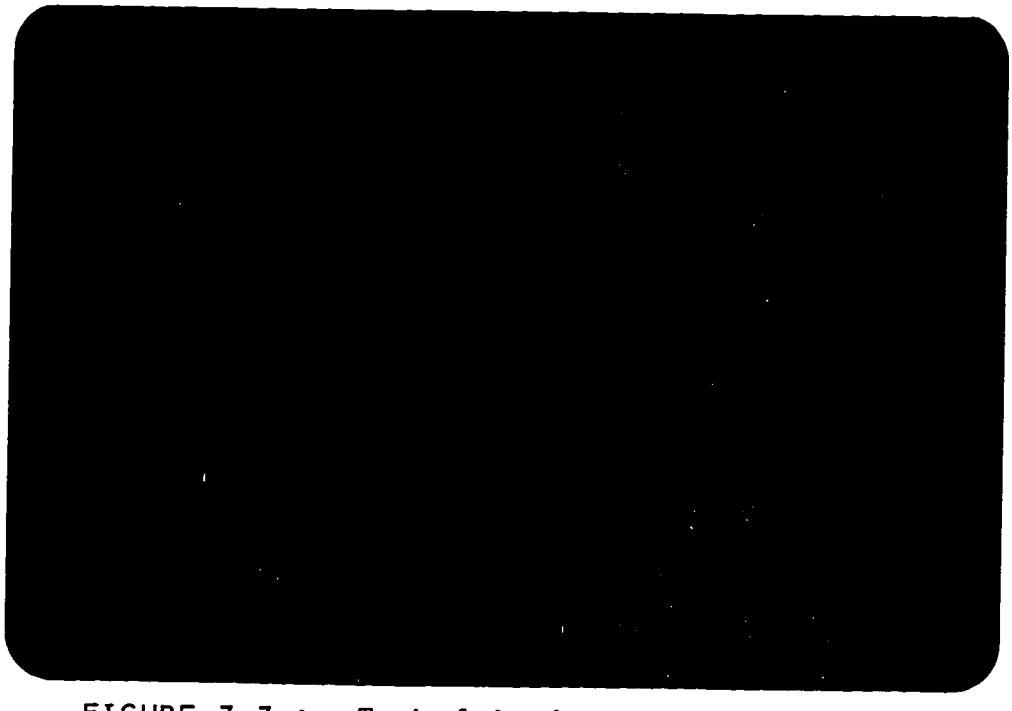

FIGURE 7.7 : Typical isochromatic for the surface plane (xy-plane A) Model M_8

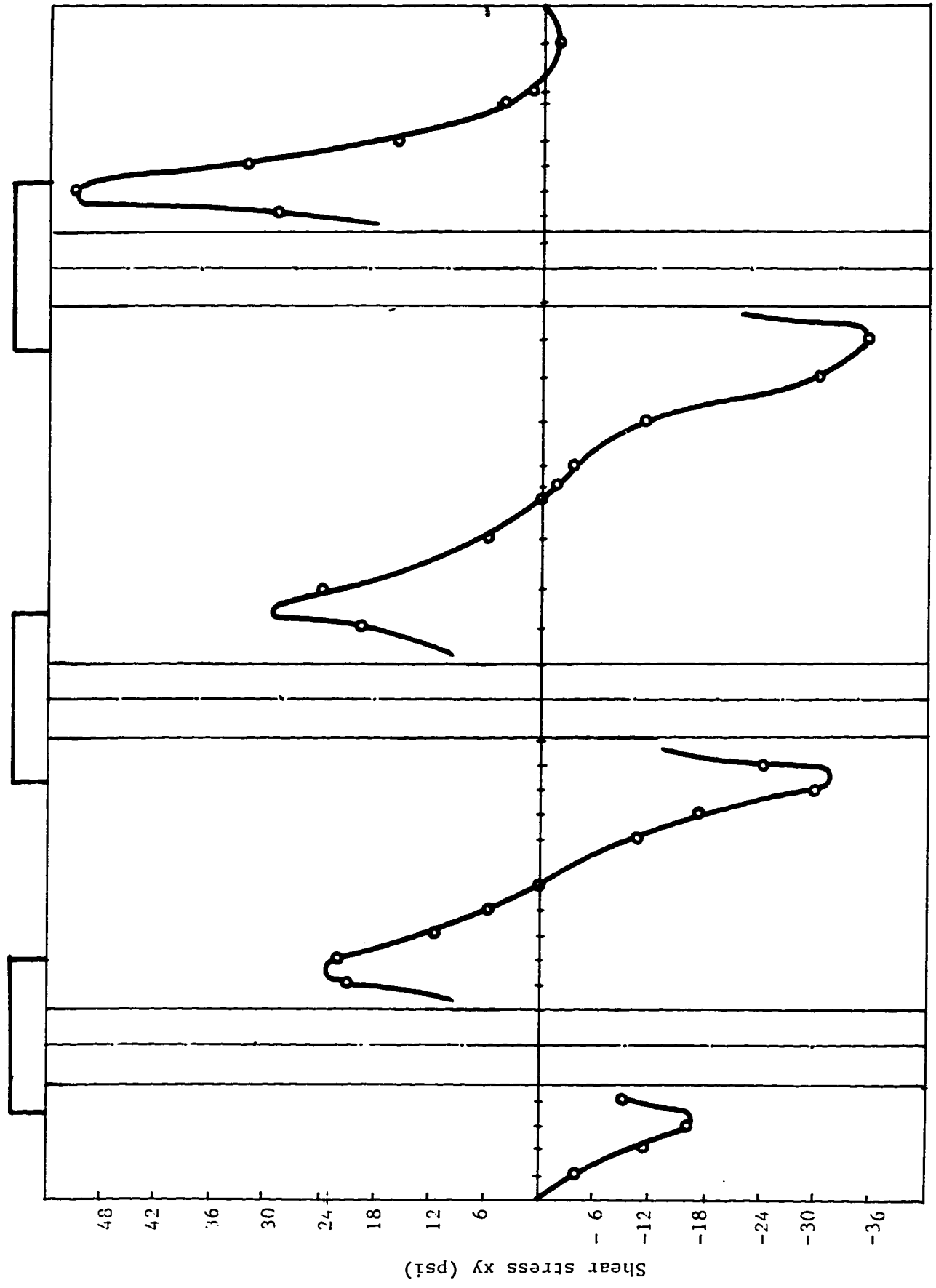

FIGURE 7.8 : Shear stress distribution along x at level V_2 of xy-plane A (Model M_8)

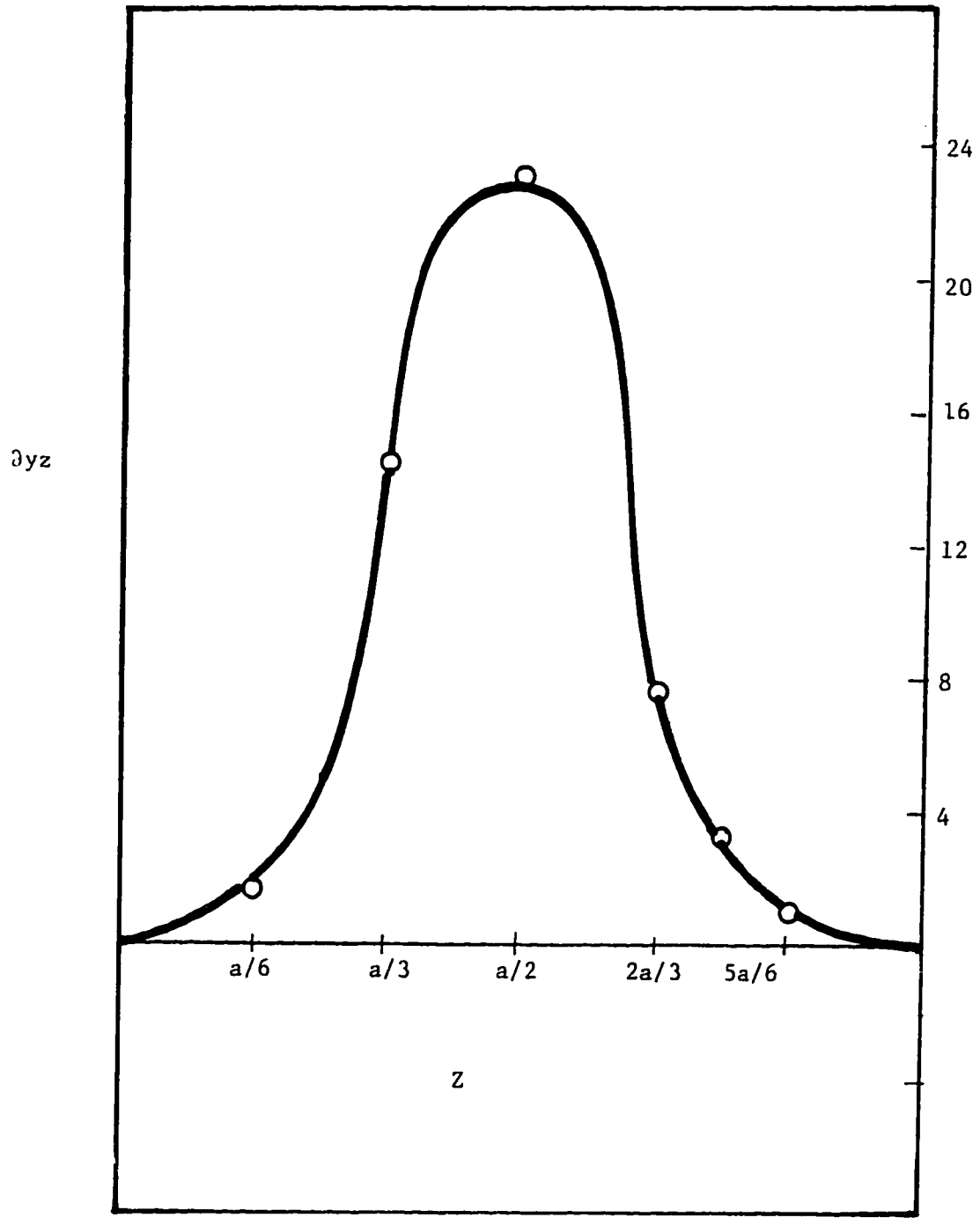

FIGURE 7.9 : Shear stress distribution along Z at level V_2 for yz-plane 11

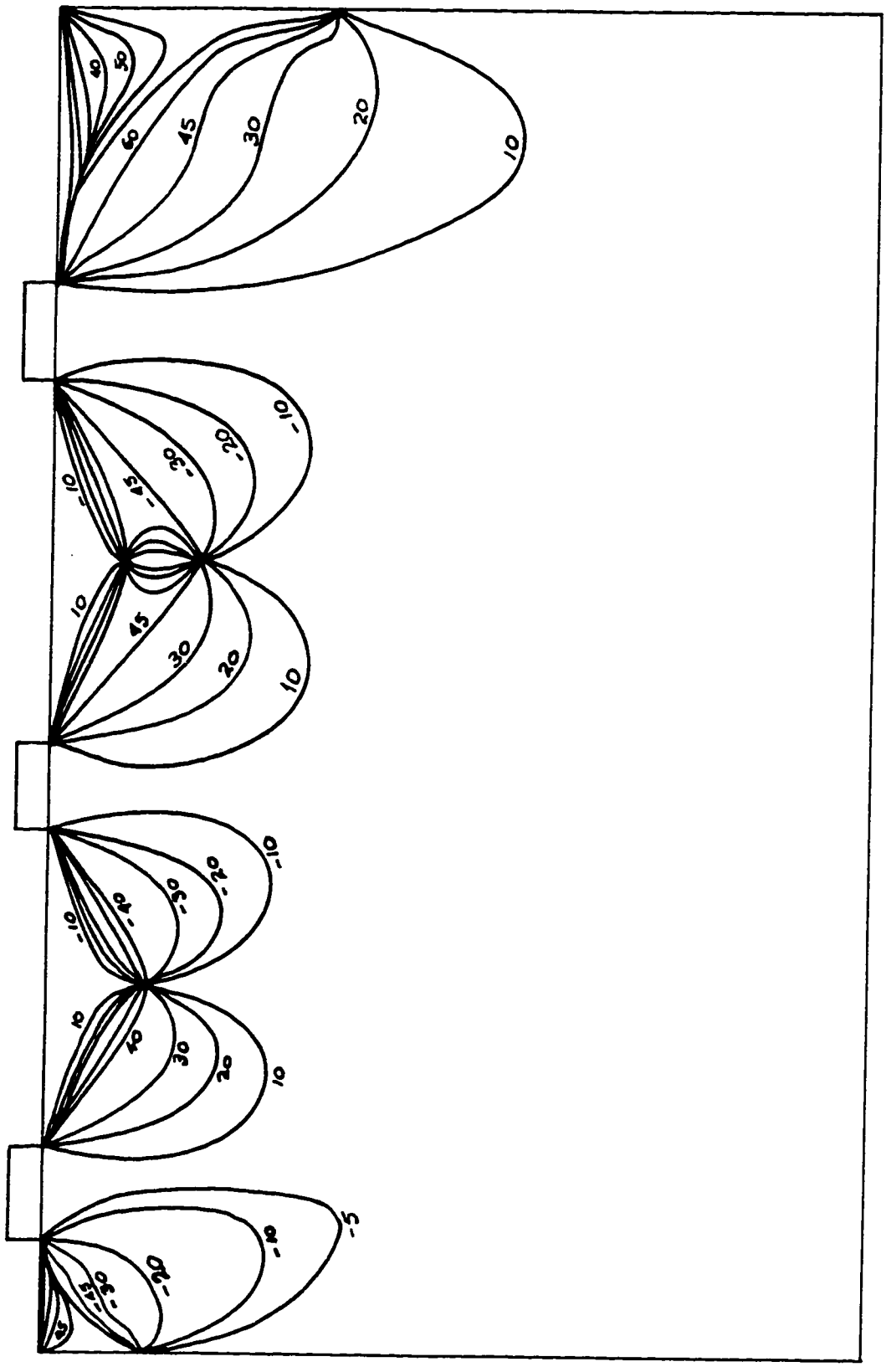

FIGURE 7.10 : The isoclinics for the xy-plane A Model M_8

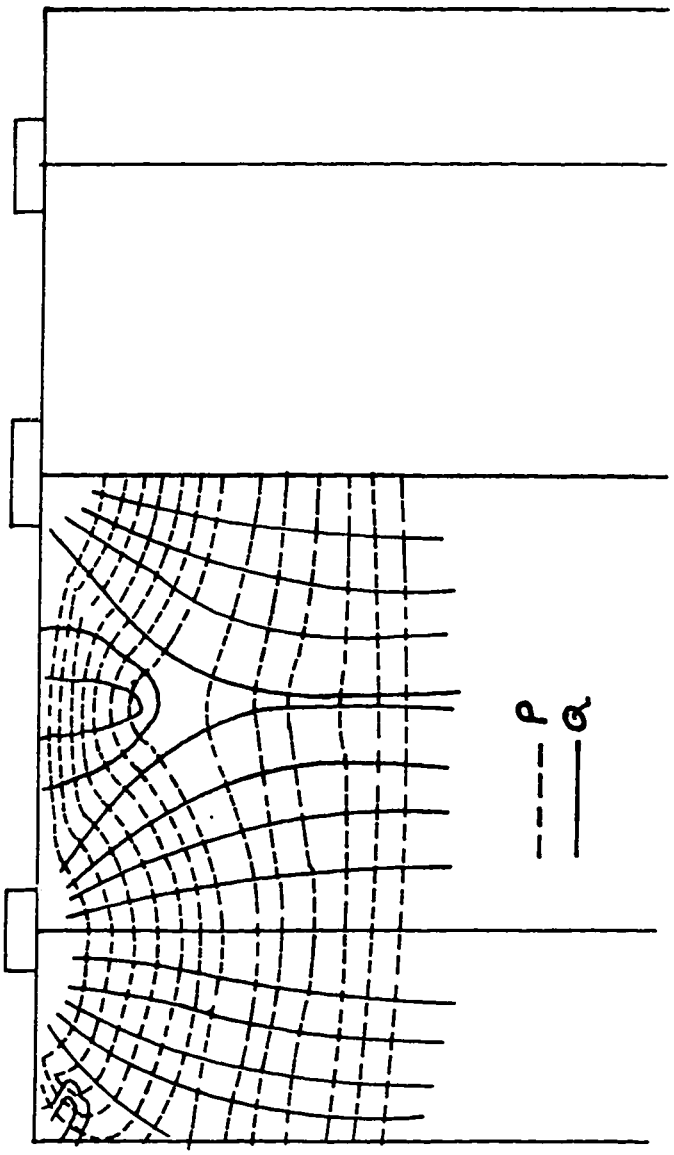

FIGURE 7.11 : The stress trajectories for xy-plane A Model M_8

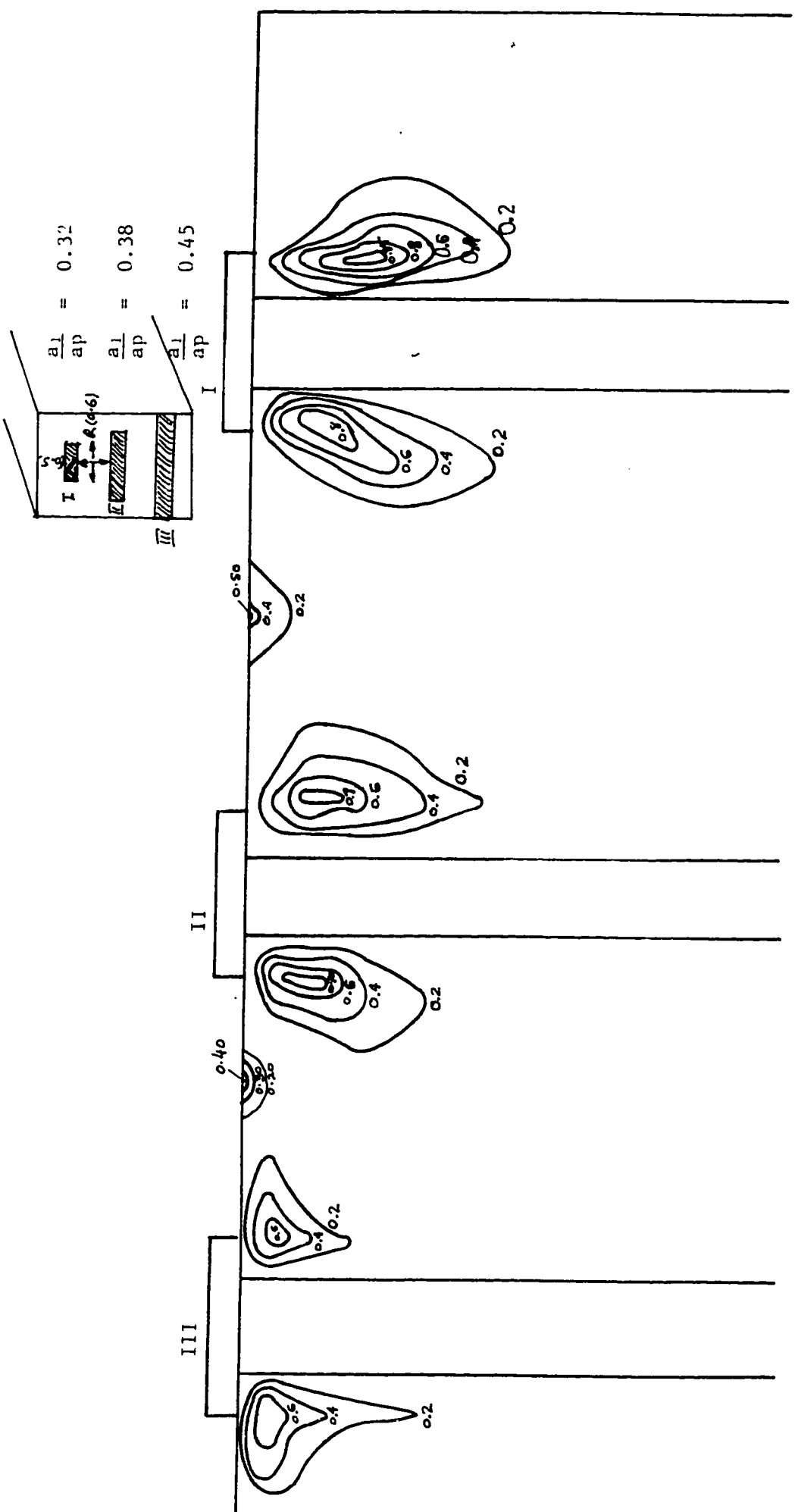

FIGURE 7.12 : The contours of the principal tensile stress P in the mid plane (xy-plane A)

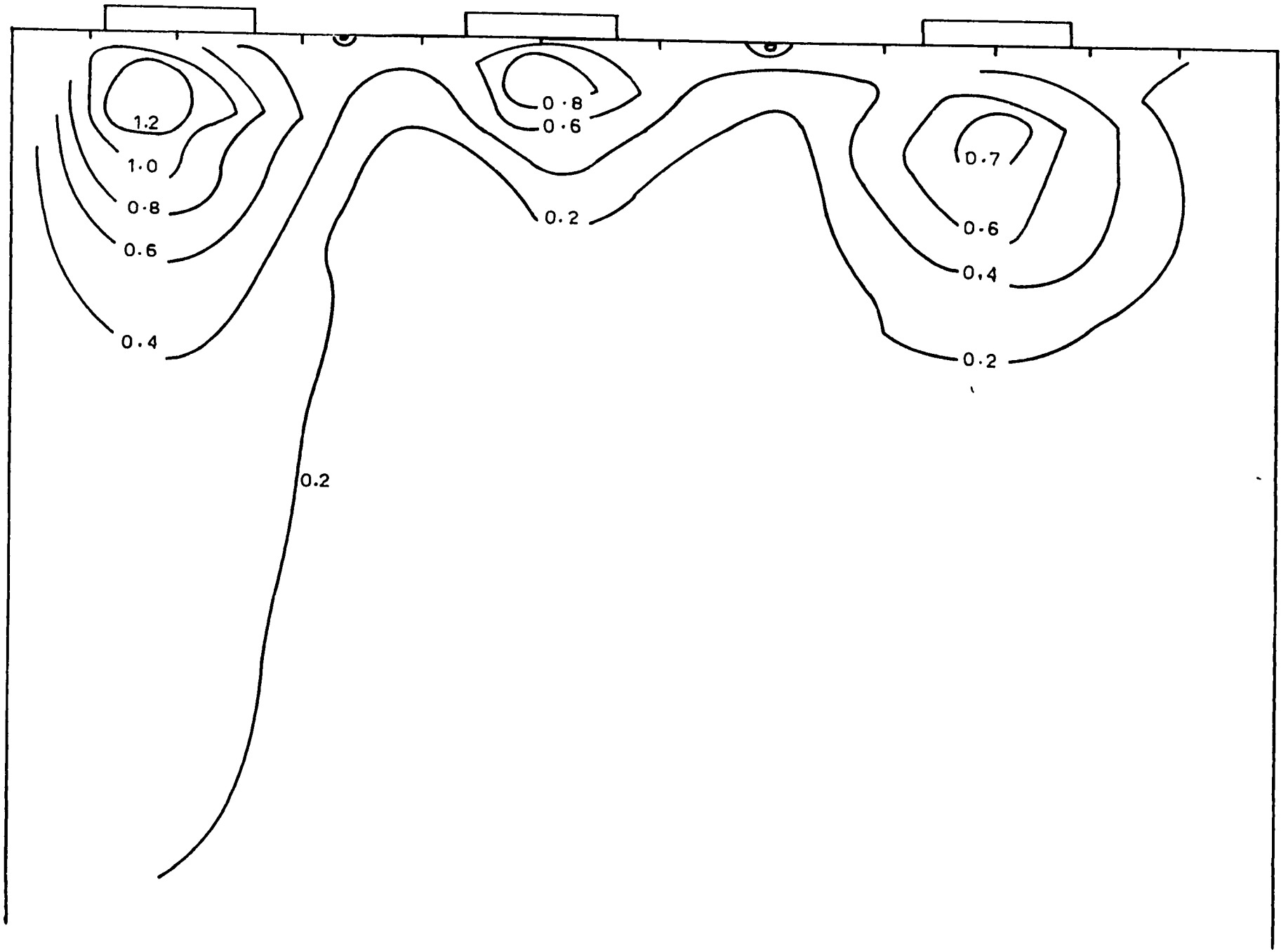

FIGURE 7.13 : The contours of the principal tensile stress P in the surface plane (xy-plane B)

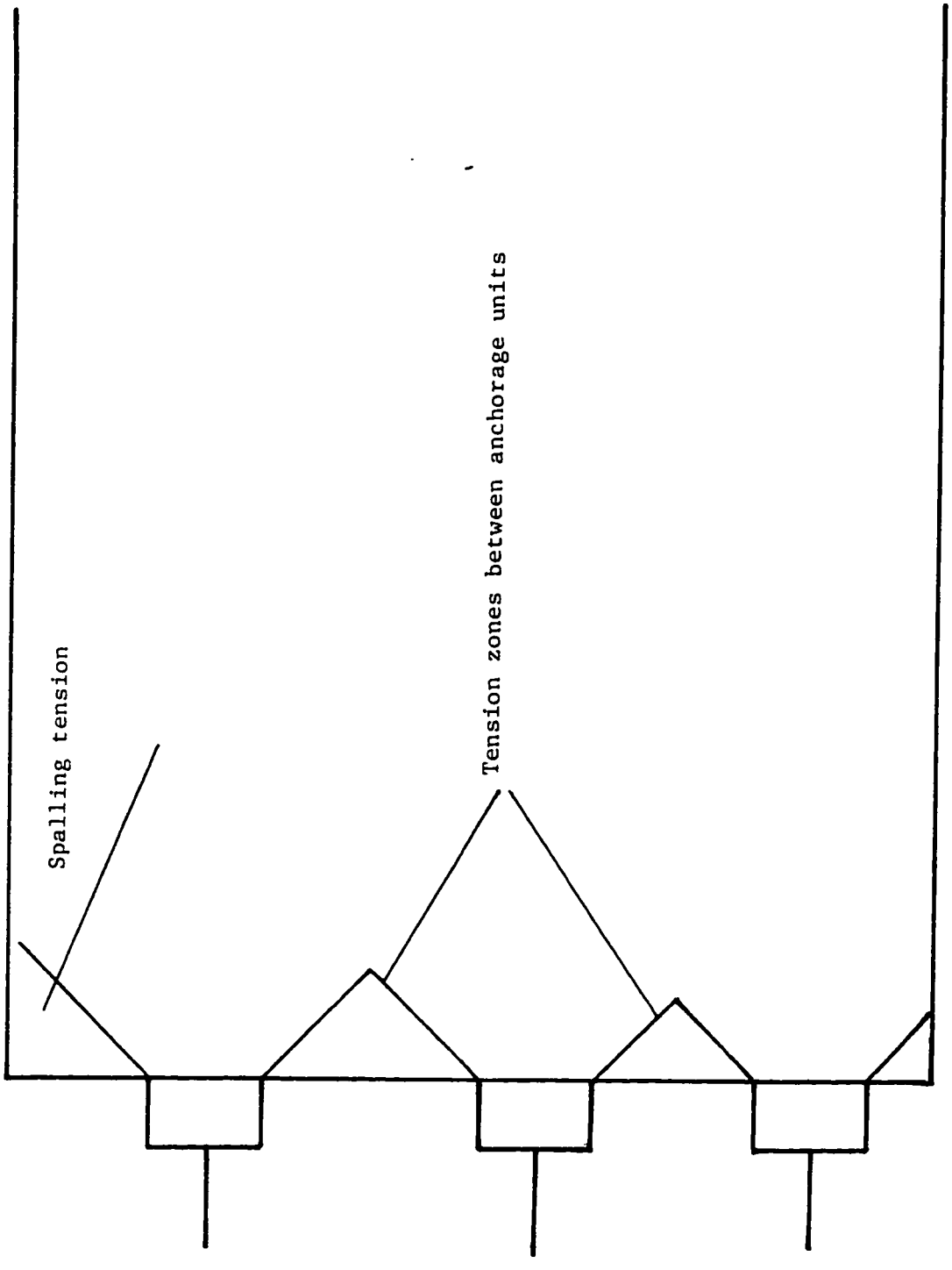

FIGURE 7.14 : The spalling tension and the tension between anchorage units

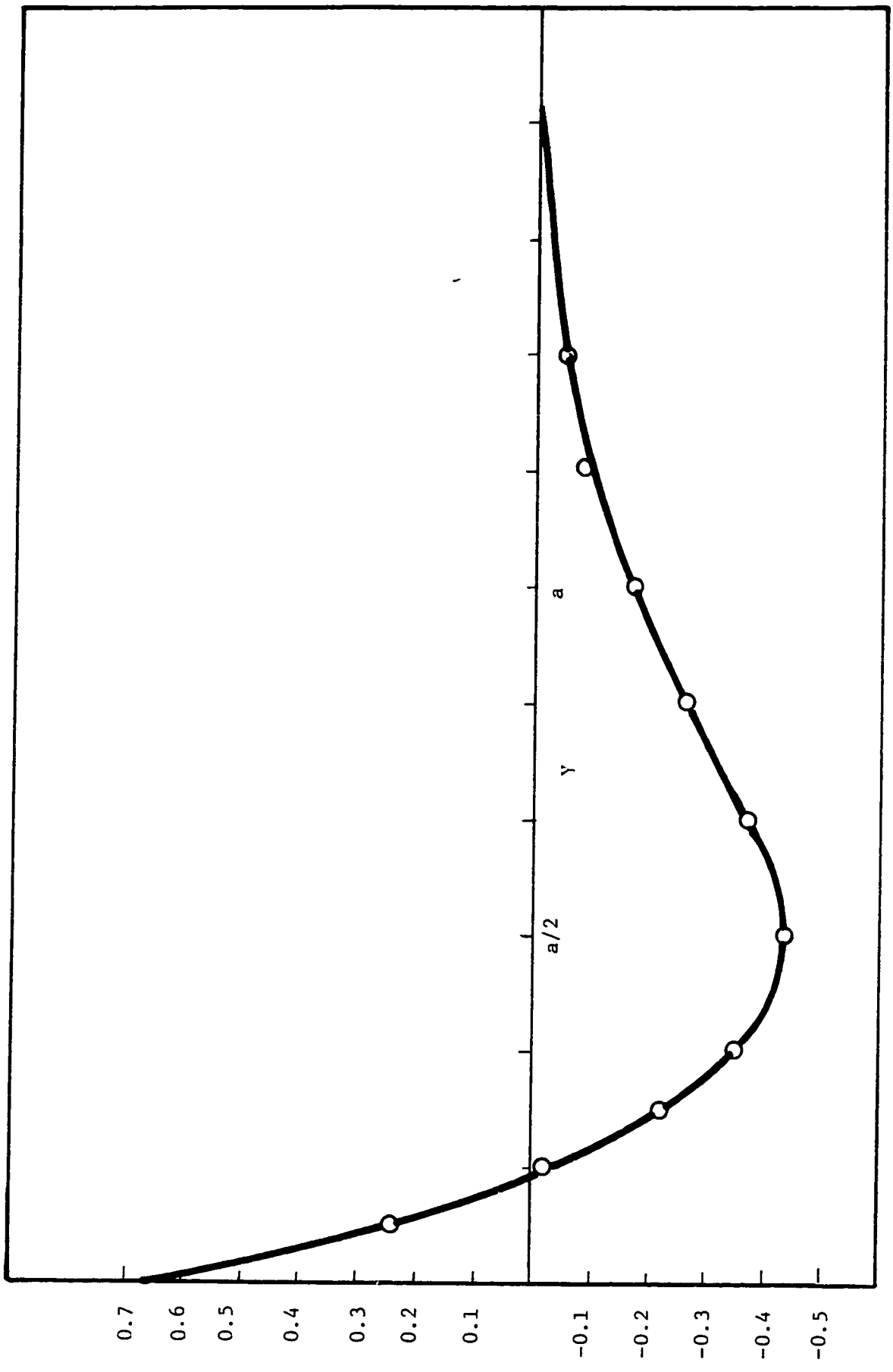

FIGURE 7.15 : The distribution of the transverse principal stress P along y axis for xy-plane A

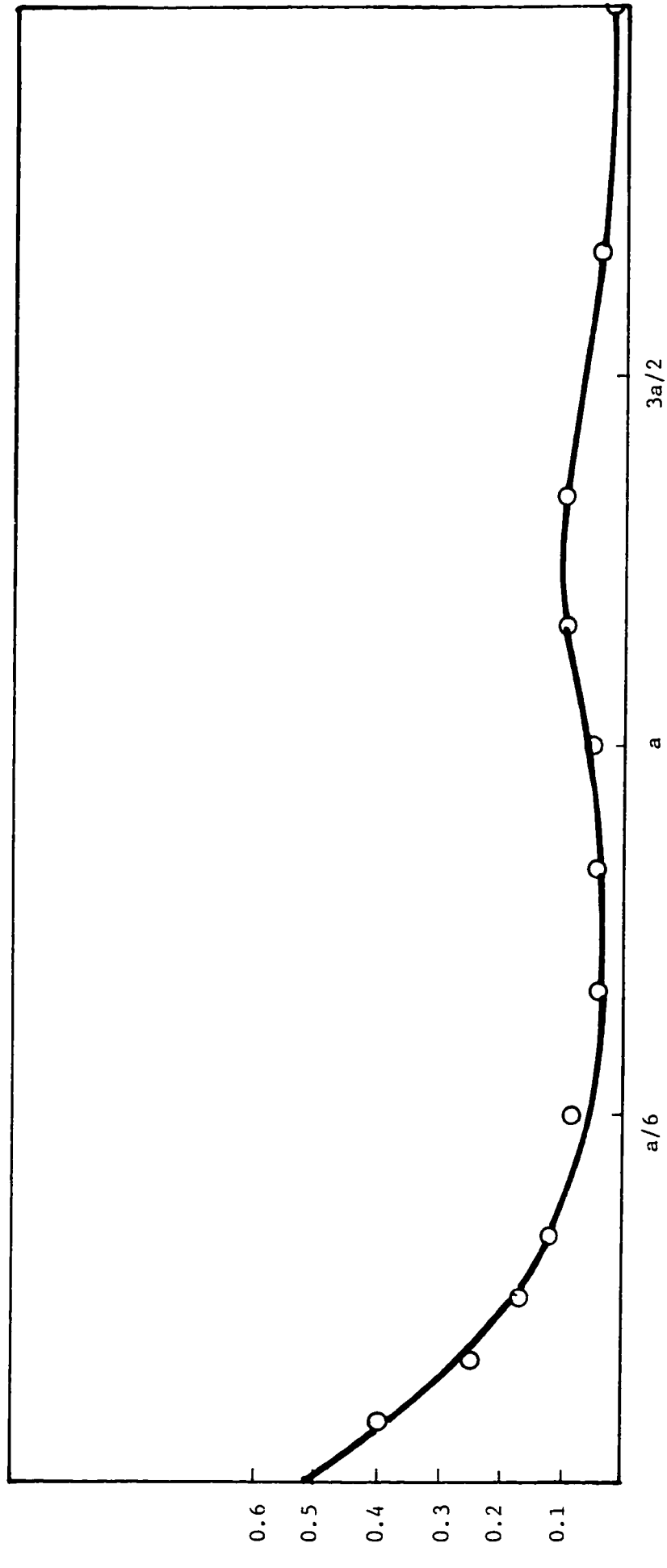

FIGURE 7.16 : The distribution of the principal stress P along y-distance for section B8 (xy-plane B)

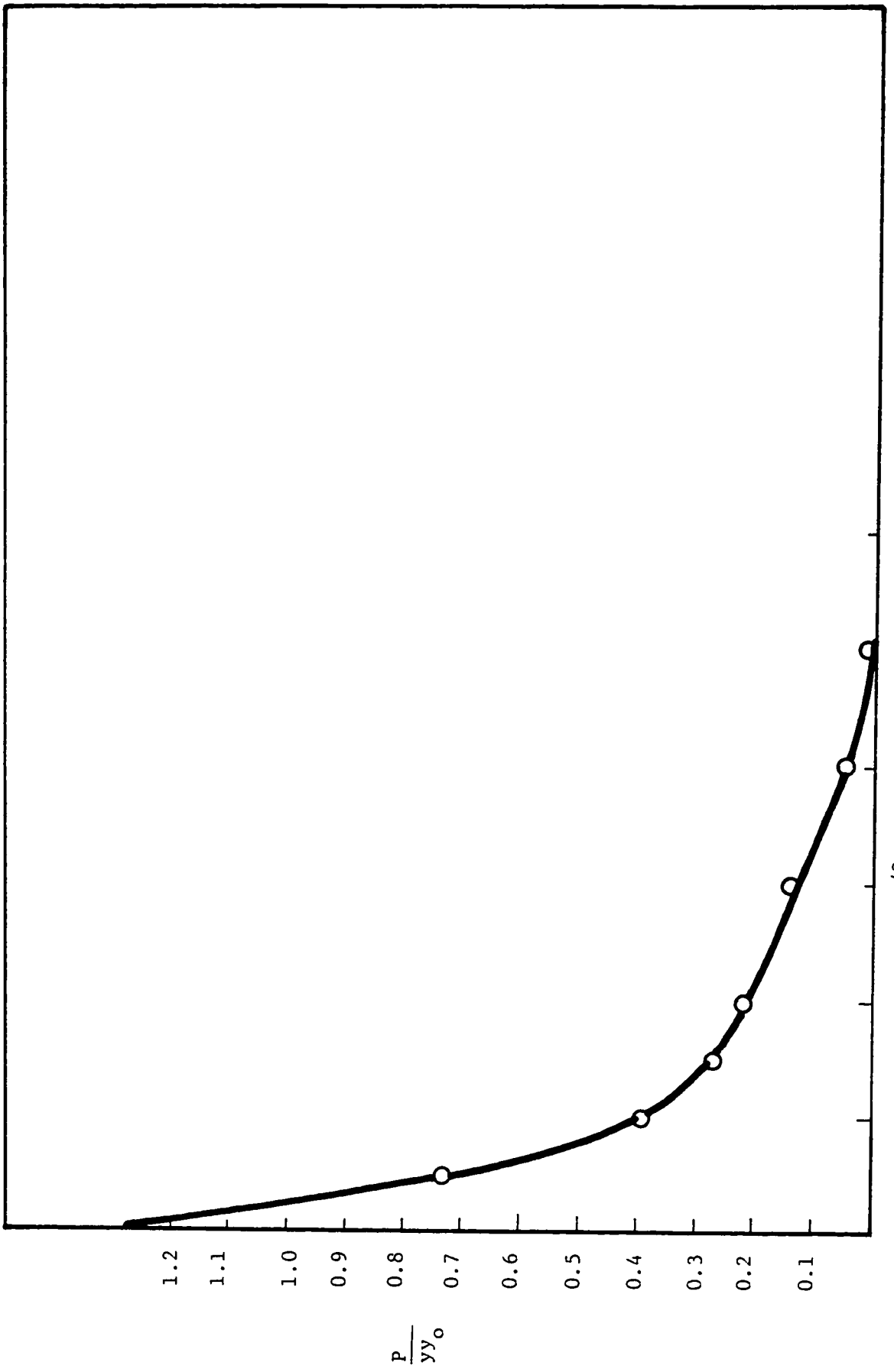

FIGURE 7.17 : The distribution of principal stress P along y-distance for section A2

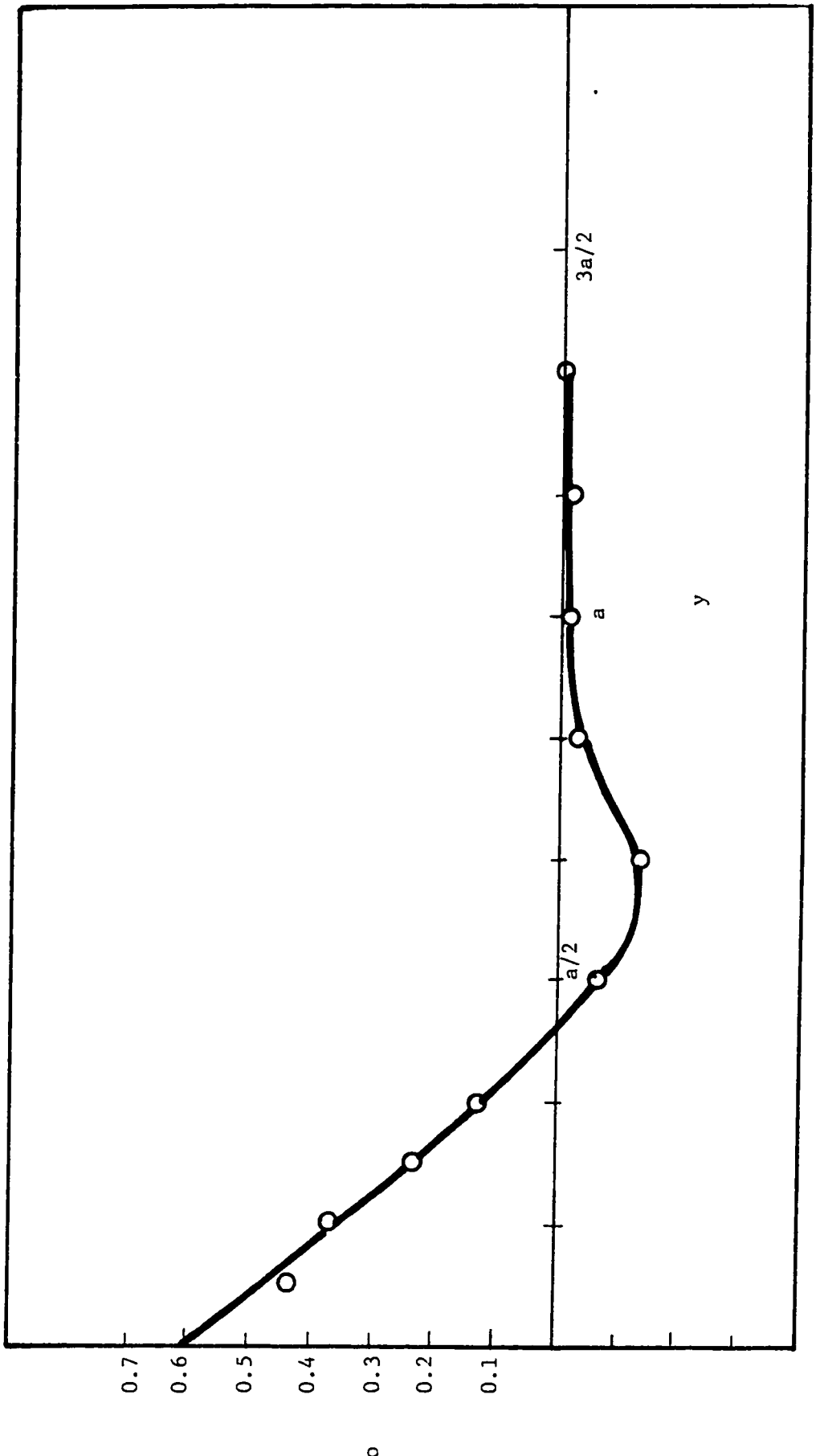

FIGURE 7.18 : The distribution of the transverse principal stress R along y-distance for yz-plane 8

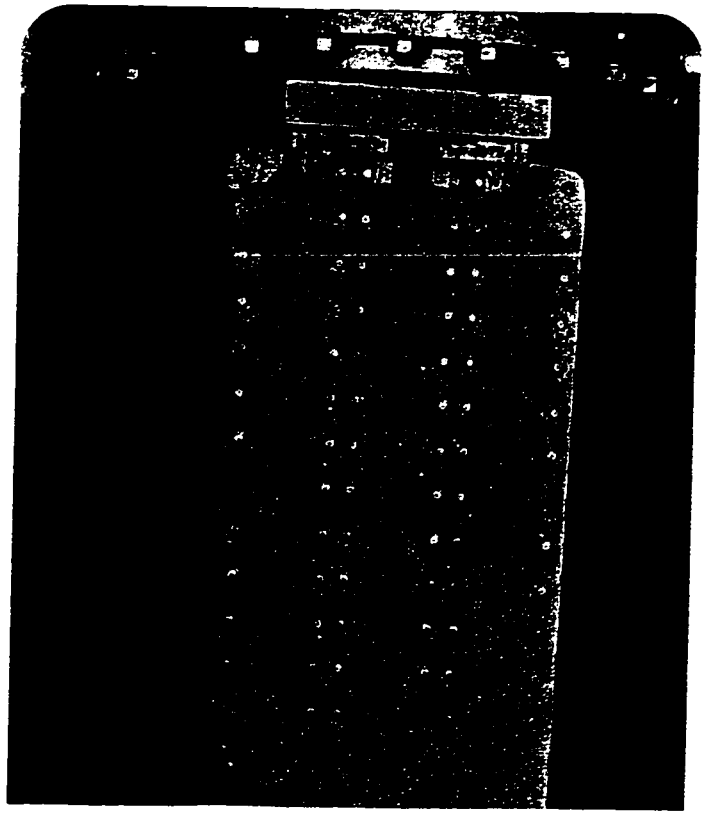

FIGURE 7.19 a : The mode of failure in rectangular concrete end blocks by two cables

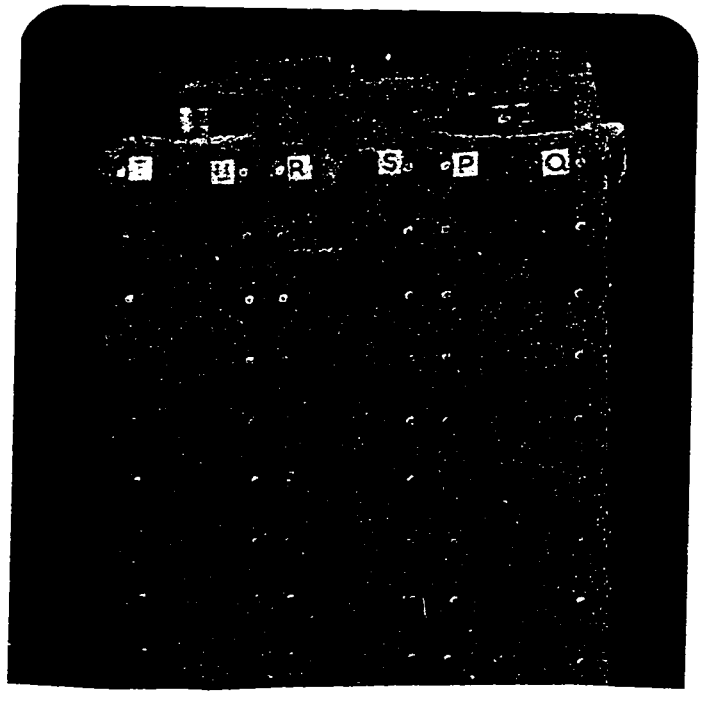

FIGURE 7.19 b : The mode of failure in rectangular concrete end blocks by three cables

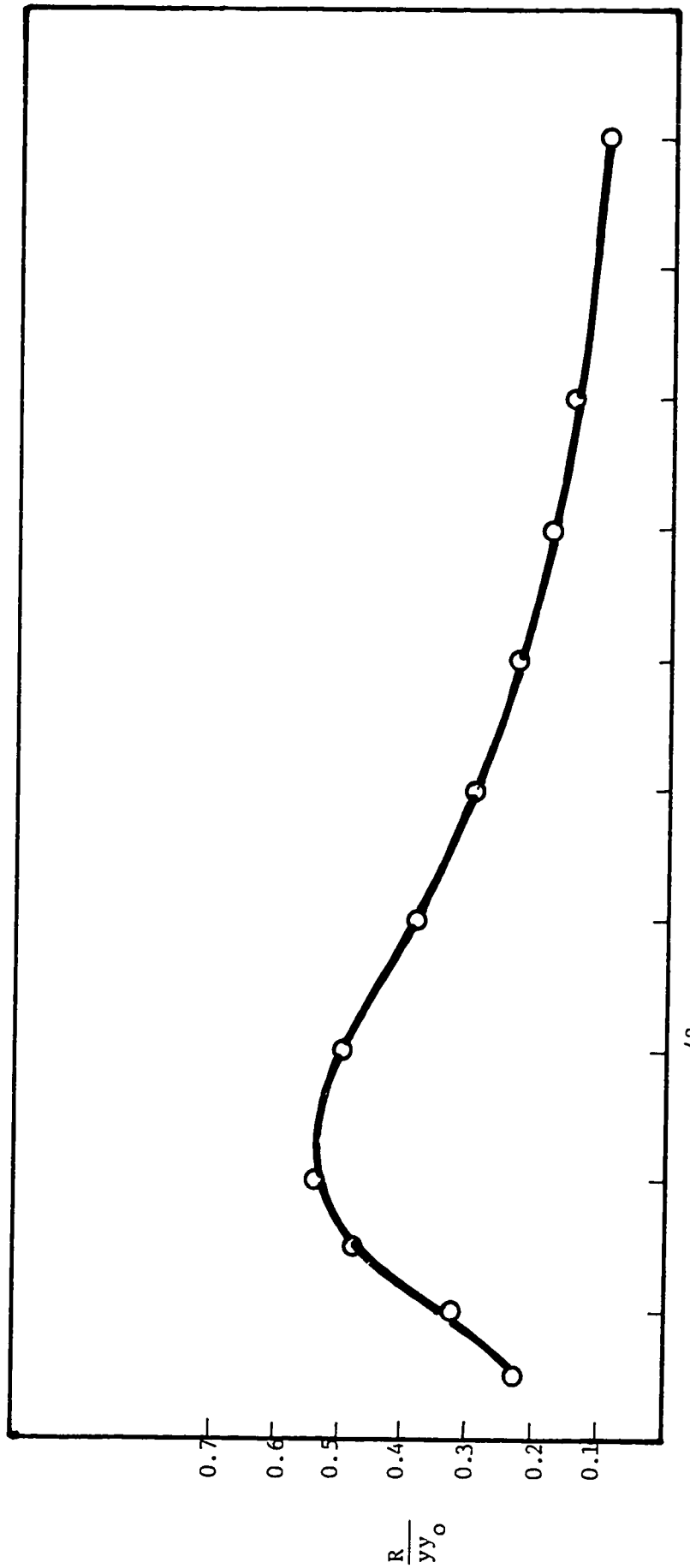

FIGURE 7.20 : The distribution of the principal stress R along y-distance for yz-plane 13

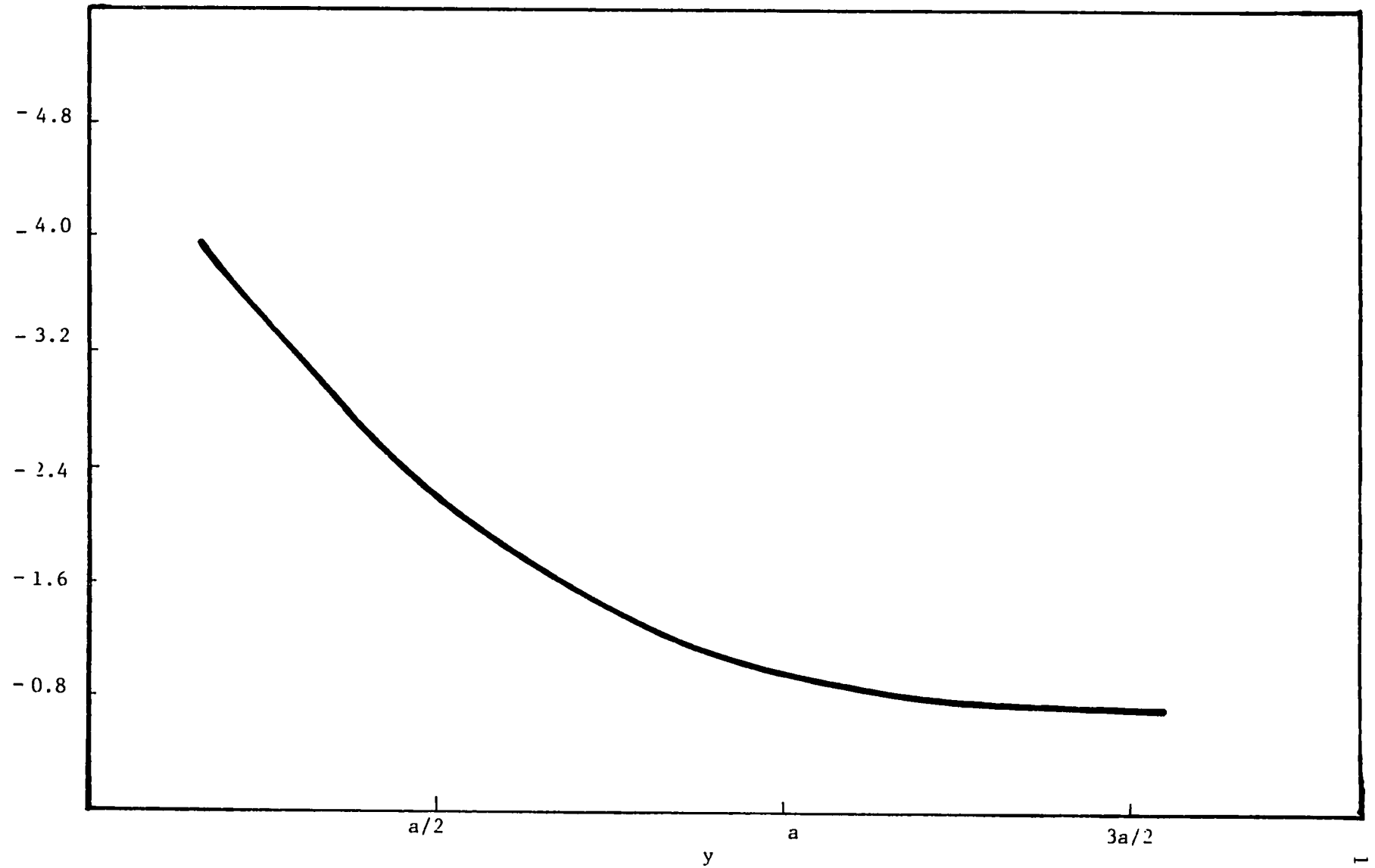

FIGURE 7.21 : The distribution of the compressive stress Q along y-distance under load I.

chapter **8**

FAILURE MECHANISM OF END BLOCKS

8.1 INTRODUCTION

As pointed out at the end of chapter 1 (section 1.4) photoelastic tests fail to predict the behaviour of concrete near the ultimate conditions on account of the differentials in the characteristics of concrete and the photoelastic model material. A test series was,therefore, carried out to investigate the failure mechanism of concrete under the anchorage zone conditions. Tests were carried out on 4" x 4" x 8" concrete prisms which were loaded in the Instron testing machine through externally located steel plates. All the $\frac{A_1}{A}$ ratios investigated in the photoelastic tests were employed. Since the various stages of cracking were of considerable significance, the monitoring of the onset of cracking was carried out using ultrasonic pulse velocity technique rather than the hitherto more common and less precise methodology of visual crack defection. Two 80HZ transducers were fixed on the opposite faces of the specimen using a sticking

grease to provide an effective contact with the concrete surface. The pulse transmission time was recorded at the initiation of the test and was continually monitored during the progress of the test. Microcracking inside concrete increased the pulse transmission time and substantive cracking subsequently caused a further sharp increase.

8.2 FAILURE MECHANISM

There is a general feeling that the limiting transverse tensile strains cause the failure to occur in the form of longitudinal tensile cracks as shown in Figure 8.1. Tests carried out by Zielinski and Rowe show this type of cracking to be occuring very frequently in their concrete end block models tested to failure.

A closer examination of the phenomenon during the author's experimentation, however, suggests a different mechanism. In all the cases the failure mechanism revealed that a downward punching of the concret under the loading pad took place before the appearance of the vertical tensile cracking. This punching action is typically shown in Figure 8.2. A study of the structure

of the specimen after the failure showed that there was a stiff cone of concrete under the bearing plate with the concrete all round it in disintegrated form defined by the shattered aggregates and powdered mortar. The stiff cone under the plate had moved downwards (Figure 8.3) as a wedge opening immediately thereafter a tensile crack of the type shown in Figure 8.1. It seems that the tensile crack appears as a result of the increased tensile strains due to the wedging action of the cone (Figure 8.4) rather than due to the limiting value of the tensile strain as a result of the maximum transverse tensile stress in the anchorage zone.

It appears that due to the different stiffness characteristics of the steel plate and the concrete and due to the localized high compression load the bearing plate restrains the lateral expansion of concrete on all sides putting the concrete behind the anchorage unit into a state of tri-axial compression. This state bestows on the concrete under the anchorage additional strength and stiffness ascribed to confinement. Figures 8.5, 8.6 and 8.7 show the photoelastic observations which invariably indicate very high sub-surface shears in

the vicinity of the edges of the anchorage unit. Figure 8.8 is a plot of the contours of the maximum shear stress. It shows plane AB which represents points of maximum shear at different levels. The failure will therefore initiate along the shear wedge defined by plane AB immediately after the shear resistance of concrete along this plane is overcome.

The failure planes on the two sides of the anchorage unit shape the stiffer concrete into a cone which wedges into the surrounding concrete after the shear failure and consequently setting up high tensile stresses perpendicular to the load and tensile cracking parallel to the load. The propagation of tensile cracks in a complex compression-tension stress field caused by the wedging action of the concrete cone therefore governs the failure of the end block.

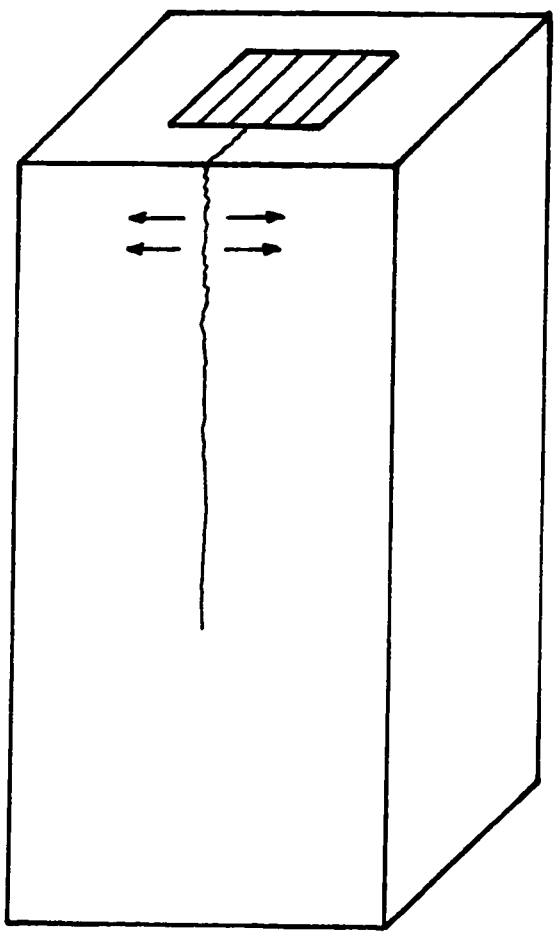

FIGURE 8.1 : Test piece showing the type of crack

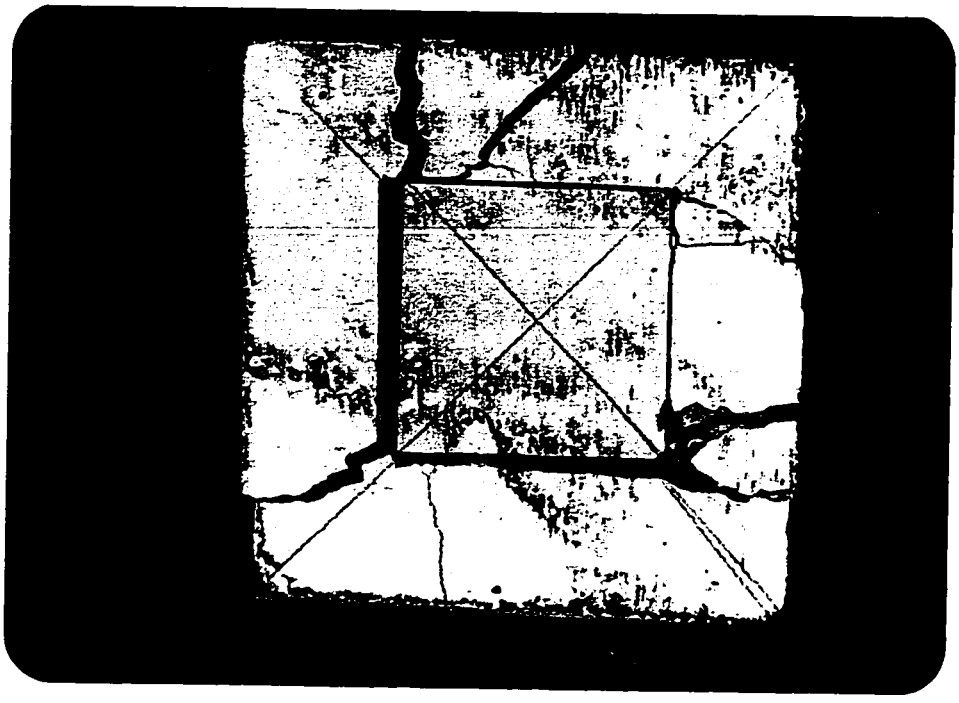

FIGURE 8.2 : Concrete model showing the punching of loaded face

FIGURE 8.3 : The differential levels of surfaces indicate the movement of the stiff cone under the plate

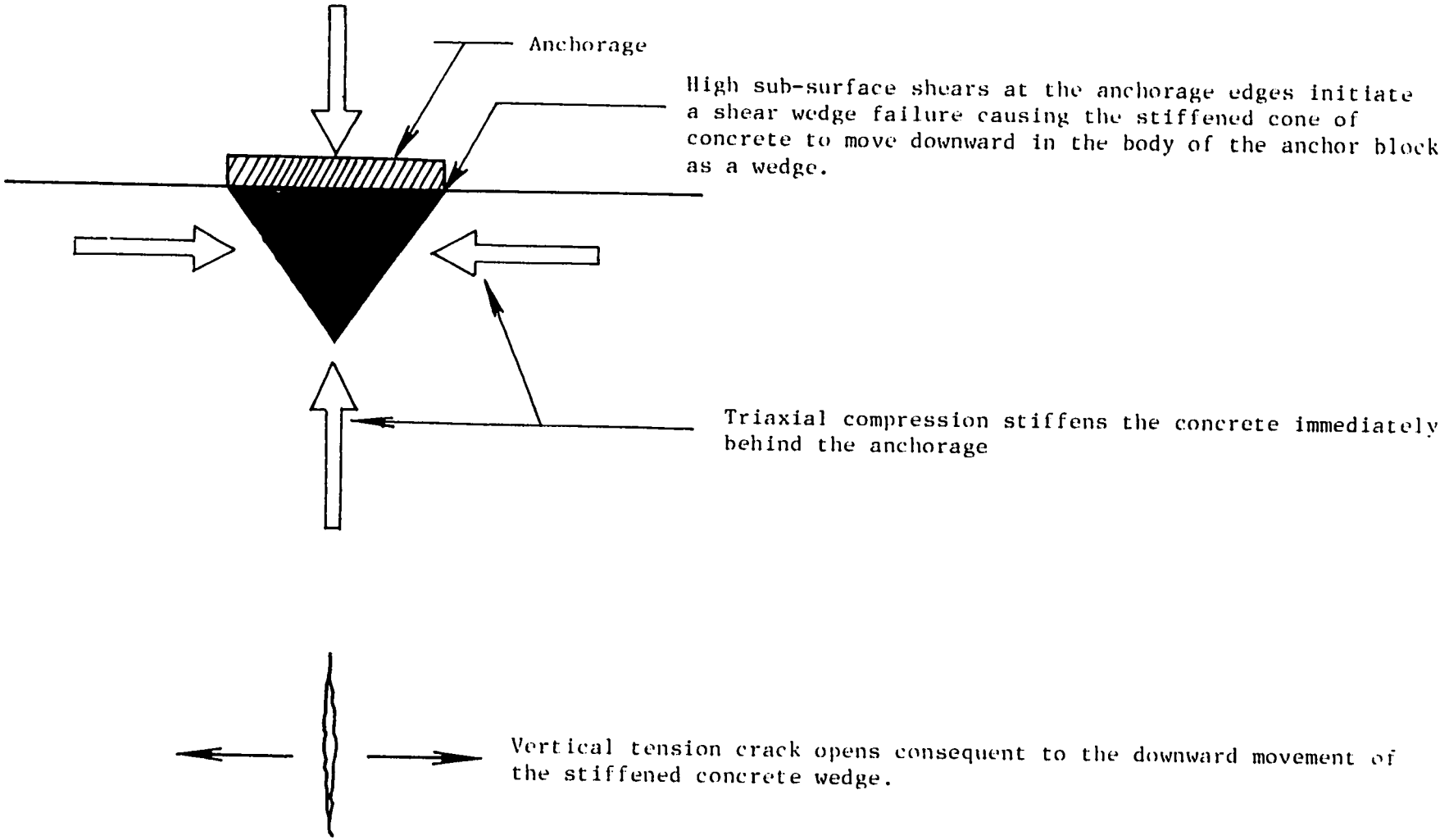

FIGURE 8.4 Proposed failure mechanism of anchor block

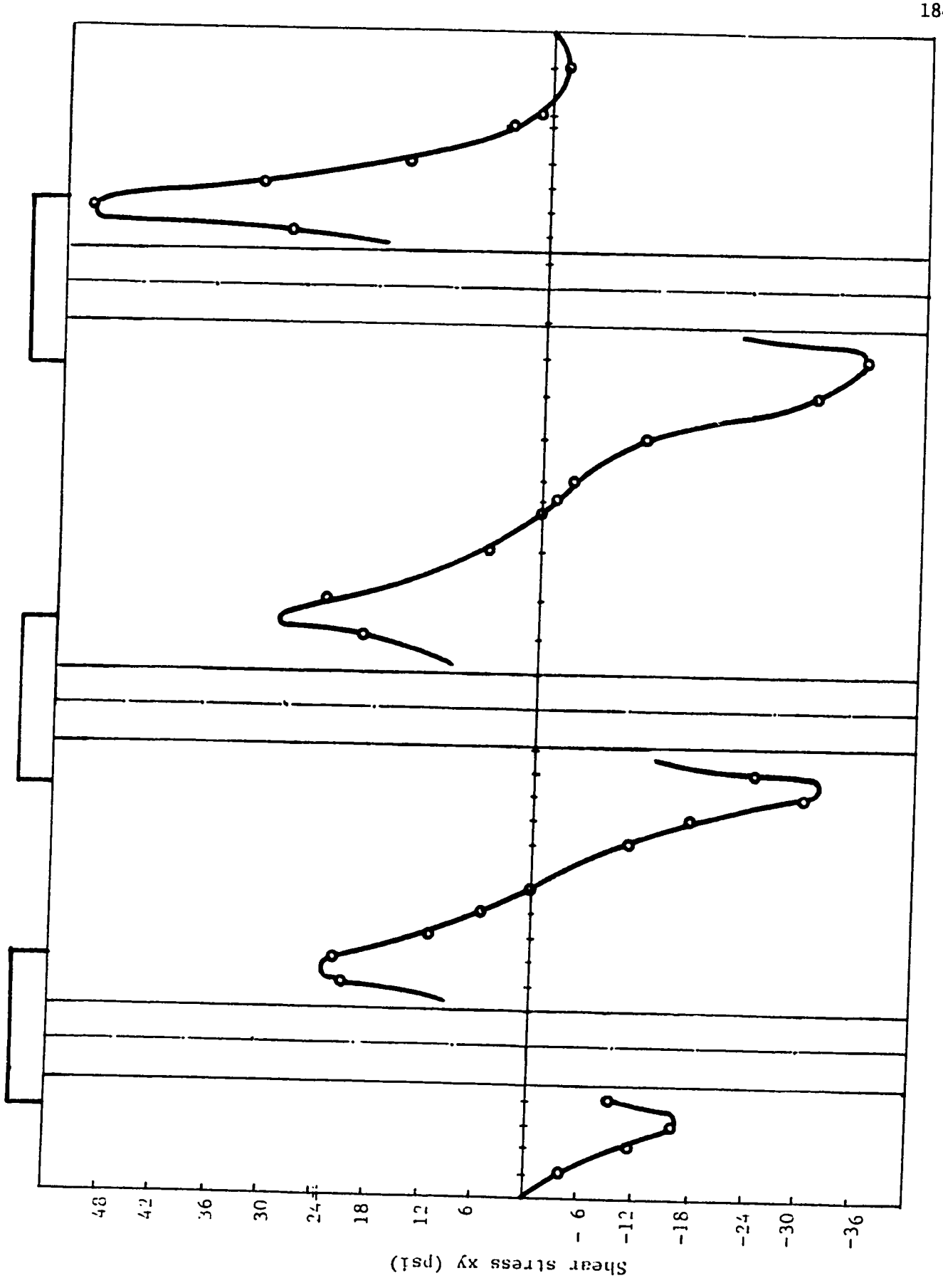

FIGURE 8.5 : Shear stress distribution along x at level V_2 of xy-plane A (Model M_8)

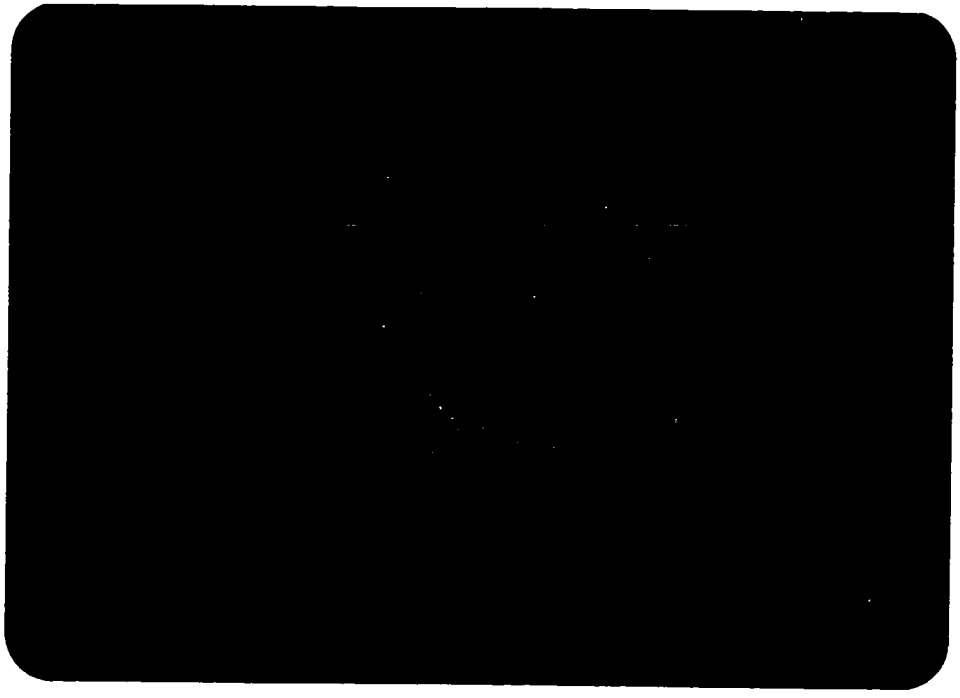

FIGURE 8.6 : Fringe pattern of xy-plane slice under external anchorage unit

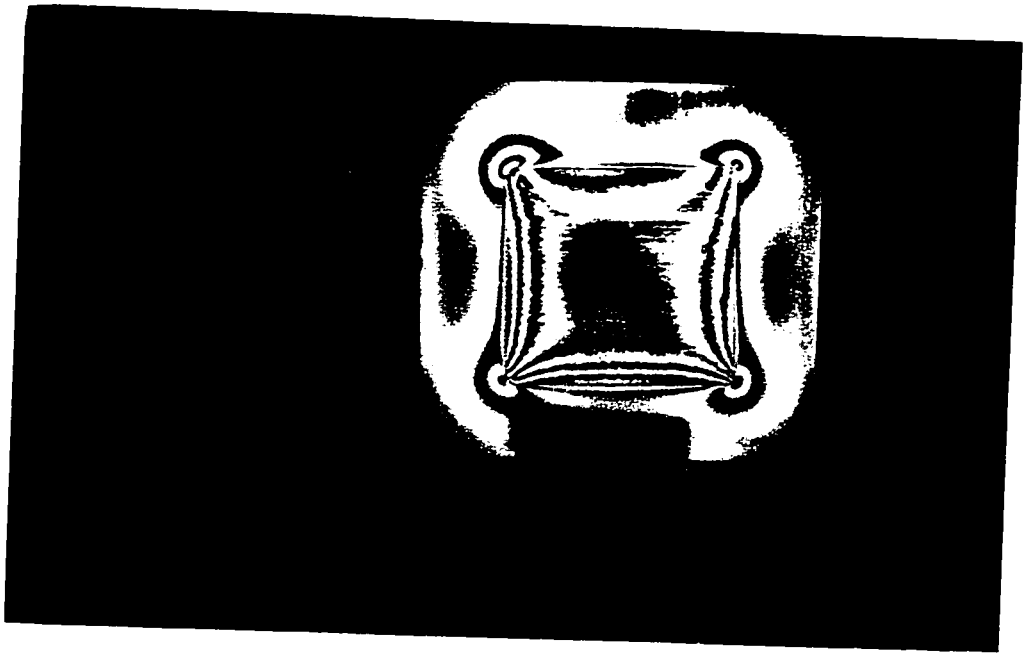

FIGURE 8.7 : Fringe pattern in xz-plane slice under external anchorage

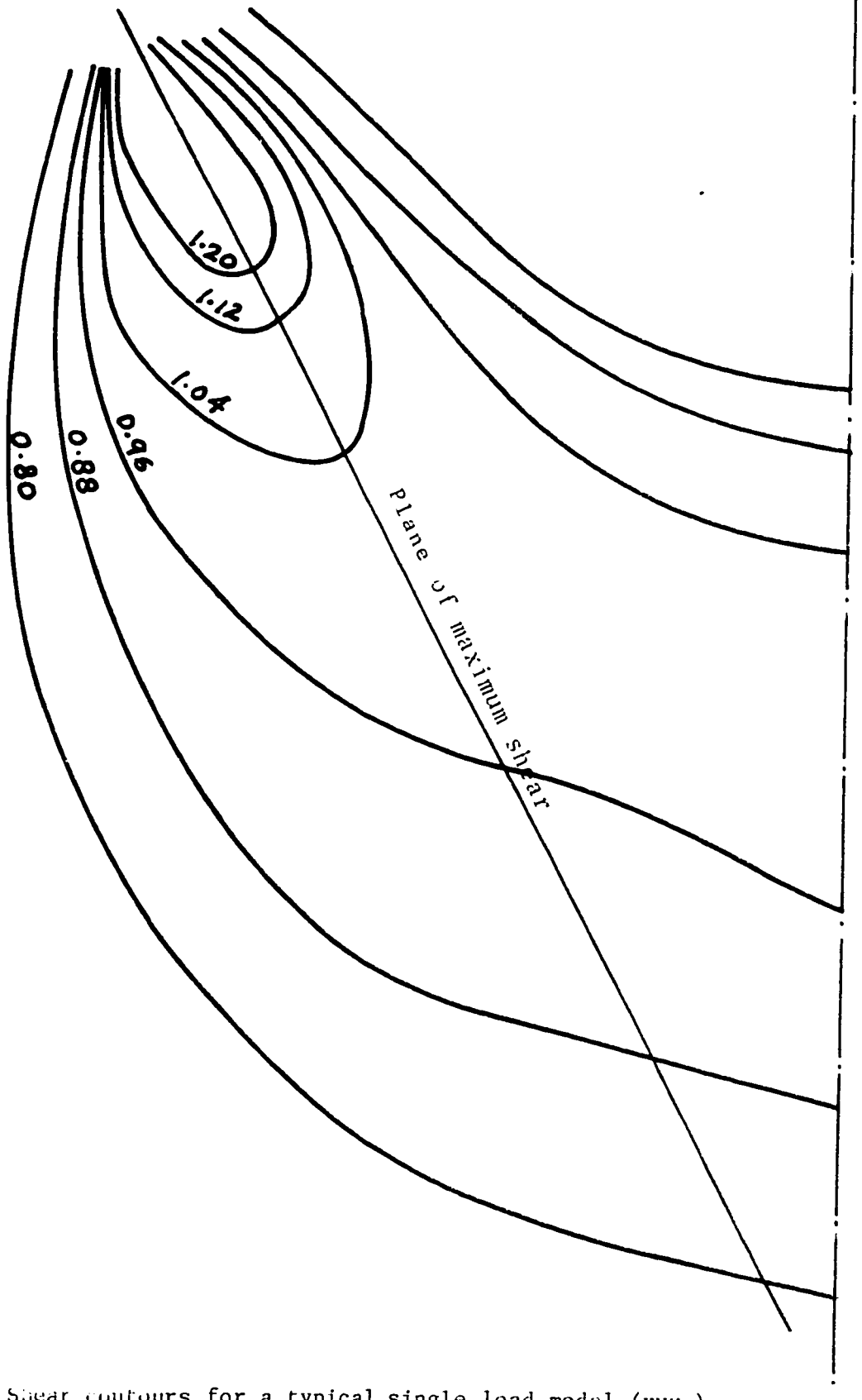

FIGURE 8.8 : Shear contours for a typical single load model (xyy_o)

chapter 9

DESIGN CONSIDERATIONS

9.1 LOAD CONCENTRATION RATIO AND TENSILE FORCE RELATIONSHIP TO BE USED IN DESIGN

On the basis of the test data on concentric models the following format can be recommended :

(a) For External Anchorages

$\frac{a_1}{a}$	0.2	0.3	0.4	0.5	0.6 $\geq$	0.7
$\frac{T}{F}$	0.32	0.28	0.24	0.20	0.15	0.11

(b) For Embedded Anchorages

$\frac{a_1}{a}$	0.2	0.3	0.4	0.5	0.6 $\geq$	0.7
$\frac{T}{F}$	0.22	0.20	0.17	0.14	0.12	0.10

The above tables are expressed in a graphical format in Figure 9.8.

9.2 APPLICATION OF THE SYMMETRICAL PRISM METHOD TO THE MULTI-ANCHORAGE END BLOCK

The results of the investigation on the multi-anchorage end block are applied to a prototype beam end

block 30" x 15" which is post-tensioned by three forces of 180 kips each located as shown in Figure 9.1. This positioning will prestress the beam to a stress of 800 lb/sq in on the upper edge and 1600 lb/sq. in on the lower edge. Symmetrical prisms I,II and III are now delineated in Figure 9.1 according to the consideration that the depth of the symmetrical prism ($2a_p$) is taken to be the lesser of :

(i) distance between the centre lines of adjacent anchors
(ii) twice the distance between the centre line of the anchor and the edge of the concrete.

The data for the symmetrical prisms is tabulated in Table 9.1 for the calculation of vertical reinforcement. Column 4 gives the values of the maximum bursting tensile stresses. It is seen that the actual average values observed from the multi-anchorage end block test are quite close to those predicted by the author's graph which establishes a relationship between the maximum tensile stress and the $\frac{a_1}{a}$ ratio. Further, the values predicted by the author's data are fairly close to the values predicted by the test data of Zielinski and Rowe. However, Guyon's values are seen to make a grossly

underestimated prediction. Column 5 compares the actual values of the bursting tensile forces with those of the author's predictions on the basis of graph which establishes a relationship between the tensile force and the $\frac{a_1}{a}$ ratio. It is seen that the values predicted by author's data, though about 15% conservative, generally are quite close to the actual values in the case of all the three symmetrical prisms. Author's predicted values are very close to those predicted by Zielinski and Rowe on the basis of their tests on concrete end blocks. Again, Guyon's values grossly underestimate the tensile force in the anchorage zone. It is thus seen that, using author's coefficients it is possible to predict the values of maximum tensile stresses and forces reasonably close to the actual values on the basis of the symmetrical prism method. The author, therefore, recommends the adoption of the symmetrical prism method for eccentric single anchorage and for multi-anchorage units.

9.3 DESIGN APPROACH

Having accepted the symmetrical prism approach a design proposal is presented based on the data obtained from this investigation.

9.3.1 Problem Formulation

Refer to Figure 9.2 where anchors of sides $2a_1 x\ 2b_1$, $2a_2 x\ 2b_2$ and $2a_3 x\ 2b_3$ are acting on the beam end block. The symmetrical prisms are delineated according to the consideration outlined in section 9.1

It is seen from Figure 9.2 that rectangular anchors with dimensions $2a_1 x\ 2b_1$, $2a_2 x\ 2b_2$ and $2a_3 x\ 2b_3$ act on symmetrical prisms I, II and III. Considering the three-dimensional nature of the problem two ratios a_1/a_{p_1}, a_2/a_{p_2}, a_3/a_{p_3} and b_1/b, b_2/b, b_3/b can be computed for evaluating different tensile forces in the vertical and horizontal directions respectively. Clearly the prisms will have theoretical depths of $2a_{p_1}$, $2a_{p_2}$, $2a_{p_3}$ for force calculation in the vertical directions and 2b for the force calculation in the horizontal direction. Circular anchors are assumed to act on square prisms in which

$$2a_1 = \sqrt{\text{area of circular anchor}}$$

9.3.2 Formulation for Steel Area Provision

For each prism :

Uniform compression at the base yy_o = $\frac{\text{Prestressing Force (F)}}{\text{Net cross sectional area of the symmetrical prism}}$

$= F/A_p$

It is evident from the investigations that the maximum transverse tensile stress (xx or zz) normal to the central axis of the prism and parallel to a_1 (or b_1) can be expressed as

$$xx = k_f yy_o = k_f \cdot \frac{F}{A_p} \qquad (1)$$

and the total bursting tensile force can be expressed as

$$T_x = k_T F \qquad (2)$$

In relations (1) and (2) the parameters k_f and k_T vary with the ratio a_1/a and have been determined in this investigation in a series of tests described in chapter 5. The variations of k_f and k_T are plotted in Figure 9.3 for ready reference.

Figure 9.4 shows a typical plot showing the distribution of the transverse tensile stress xx. This distribution can reasonably be approximated by a triangle the dimensions of which are shown in Figure 9.4 based

on the results obtained with regard to the position of zero and maximum transverse tensile stress.

Let f_t be the specified permissible tensile stress for concrete. Then the length of end block which requires reinforcement is shown in Figure 9.4 as hatched. Also the tensile force to be resisted by the reinforcement is given by :

$$T_r = T \left[1 - \left(\frac{ft}{xx_{max}}\right)^2 \right] \qquad (3)$$

Zielinski and Rowe carried out tests on prisms loaded over partial areas of their cross-section to establish a relationship between the tensile strength of concrete under this type of loading with the tensile strength of concrete under the splitting cylinder tests. They found that for the same quality of concrete, in a prism loaded over a small area, the apparent tensile strength of the concrete may be between 28 and 47% higher than the splitting tensile strength for values of $\frac{a_1}{a}$ between 0.30 and 0.70 respectively. The ratio of apparent strength to splitting strength (k) being a function of $\frac{a_1}{a}$ ratio, the data obtained by Zielinski and Rowe is shown plotted against $\frac{a_1}{a}$ ratio values in Figure 9.3.

The permissible tensile stress in the anchorage zone situation is,therefore,

$$f_t = \beta kr \qquad (4)$$

where β = a reduction factor

k = ratio of apparent strength to splitting strength

r = tensile splitting strength of the concrete

Tensile stresses greater than f_t must be resisted by the reinforcement at a suitable working stress for steel f_s. Area of steel As required in each direction in any prism containing a single anchorage unit, is then given by

$$A_s = \frac{T_r}{f_s} \qquad (5)$$

Substituting the values of T, f_t and xx in relation (3) and then substituting the value of T_r in relation (5) we get

$$A_s = \frac{k_T F}{f_s} \left[1 - \left(\frac{\beta kr A_p}{k_f F}\right)^2\right] \qquad (6)$$

k_T, k_f and k are plotted in Figure 9.3 for various $\frac{a_1}{a}$ ratios. If suitable values can be specified for f_s and r, the steel area A_s can be calculated for a given prestressing force acting on a prism through a cable duct.

9.3.3 Tensile Splitting Strength for Normal Concretes

It is not yet common practice to specify tensile splitting strength for concrete. Compressive strength of concrete is the usual index for all other design parameters and therefore the tensile splitting strength (r) for use in the aboveformulations has to be expressed as a derivature of the compressive strength of concrete. Because of the sensitivity of concrete tensile strength to variations in compaction and curing conditions, there are obvious difficulties in spelling out a firm or accurate relationship between tensile and compressive strengths of concrete.

In several series of tests carried out at the Cement and Concrete Association an attempt has been made to relate the tensile splitting strength with the cube crushing strength. The data obtained from several reports has been plotted in Figure 9.5. Most of the data relate

to values of cube crushing strength between 5000 and 9000 lb/sq. in. Fortunately this is the range of concrete strength which is of interest in prestressed concrete design and construction.

As suggested by Dorwick it is reasonable to adopt a linear variation between compressive and tensile strengths from Cu = 5000, r = 400 to cu = 10,000, r = 600. To take into account the scatter of the data the value of r used in equation (6) should be adopted from the line r_s = 0.80 r shown drawn in Figure

9.3.4 Design Graphs

In fact having chosen suitable values for the various parameters, a family of curves can be drawn as design aids which will give A_s directly for a given value of prestressing force. This can be conveniently done as shown in Figure 9.6. These curves are made possible by the fact that for any particular prestressing force there is little variation in the sizes of the anchors and the value of $2a_1$ for a given prestressing force is practically constant. Some commonly adopted values for which these curves may be drawn are shown in

a table arranged at the top of Figure 9.6.

9.4 OTHER DESIGN CONSIDERATIONS

9.4.1 Ultimate Load Conditions

The foregoing formulations relate to working load conditions. It is,however, also necessary to ensure that at ultimate load conditions the stress in the anchorage zone reinforcement will not exceed the specified yield value for the steel. The ultimate load condition will be obtainable when a prestressing force equal to the guranteed tensile strength of the tendon multiplied by a suitable load factor (1.1 to 1.2) is assumed to be operative. The calculations can be conducted in the following manner :

Design force in strands = No. of strands x tensile strength per strand x load factor

Ultimate transverse tensile force = k_T x design force

$$\text{Area of steel required from ultimate load considerations} = \frac{k_T \times \text{design force}}{f_y}$$

The area of steel required from ultimate load considerations should be greater than that provided on the basis

of the working load conditions.

9.4.2 End Block Size Selection

There are two considerations. Firstly, the length required to produce a continuous linear distribution of the longitudinal normal stresses; secondly, a size to avoid congestion and wrong positioning of the reinforcement. It is widely recognized that congestion and inappropriate positioning of the reinforcement has largely contributed to the failure of end blocks. The following guidelines emerging from the results of this investigation are relevant :

(i) For cases where single post-tensioning forces are acting it is desirable to make the length of the end block equal to the depth of the beam. This recommendation is made on the basis of the observation that in the case of single concentric test series the distribution of longitudinal normal stress was found to become uniform at a distance of 0.95 d from the back of the anchorage. However, some designers feel that for beams deeper than 4 ft. the ratio of end block length to the beam depth can safely be specified to be less than unity.

In cases where post-tensioning forces are broken up in groups of smaller anchorage units it should be adequate to specify end block length between 0.5d to 0.65d. This recommendation emerges from the observation that in the multi-anchorage end block tested the longitudinal normal stress became linear at a distance of 0.42d from the back of the anchorage.

(ii) The centroid of the bursting steel should be a distance 0.5 to 0.55a from the back of the anchorage in the y direction where the maximum transverse tensile stress occurs, and most of the reinforcement should be close on either side of this position as the transverse tensile force is concentrated in a small length (Figure 9.4).

The size of the end block should,therefore, be selected to satisfy the foregoing conditions without creating a congestion of reinforcement thereby making it difficult to concrete the block properly.

9.4.3 Reinforcement Detailing

Each prism should be properly reinforced behind the anchorage unit and the reinforcement should be provided in such a manner as to interconnect the various prisms.

Most of the reinforcement should be located so that its centroid is close to a distance 0.5a to 0.55a from the back of the anchorage unit. This may necessitate the provision of lesser bars of bigger diameter rather than more bars of smaller diameter. Such a choice may also avoid the most undesirable congestion which hinders effective compaction of concrete behind the anchorage unit.

Reinforcement is most effective a maximum distance laterally from the tendon. Most manufacturers provide a small helix behind the anchorage unit. The diameter of this helix being too small to be effective against bursting tensions,it is mostly an undesirable hinderance for effective compaction.

A convenient and effective form of reinforcement is rectangular stirrups (Figure 9.7) or layers of welded mesh spaced out from the end of the beam.

Between the anchorages a shallow zone of tension exists which has to be reinforced adequately. This zone being shallow, the reinforcement in this region should be provided as close to the surface as possible.

TABLE 9.1

Application of the Symmetrical Prism Method to the Multi-anchorage End Blocks

Symetrical Prism	$k_a = \frac{a_1}{a}$ (for vertical reinforcement along x-direction)	Mean compressive stress at the base of the symmetrical prism (psi)	Maximum value of the bursting tensile stress (P) as a fraction of the mean compression at the base of the symmetrical prism						Bursting Tensile Force(T) as a fraction of the applied force			
			Guyon	Zilinski & Rowe	Author				Guyon	Zielinski & Rowe	Author	
					Coeffi-cients*	Actual					Coeffi-cients	Actual (average)
						Mid-plane B	Surface Plane A	Ave.				
1	2	3	4						5			
I	0.32	1531	0.30	0.70	0.78	0.97	0.80	0.88	0.146	0.36	0.35	0.30
II	0.38	1376	0.26	0.65	0.75	0.70	0.87	0.80	0.127	0.32	0.33	0.27
III	0.45	1111	0.24	0.59	0.71	0.55	0.99	0.77	0.115	0.28	0.29	0.24

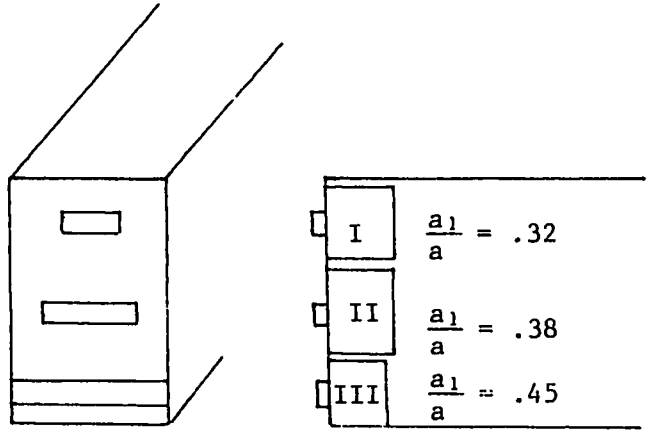

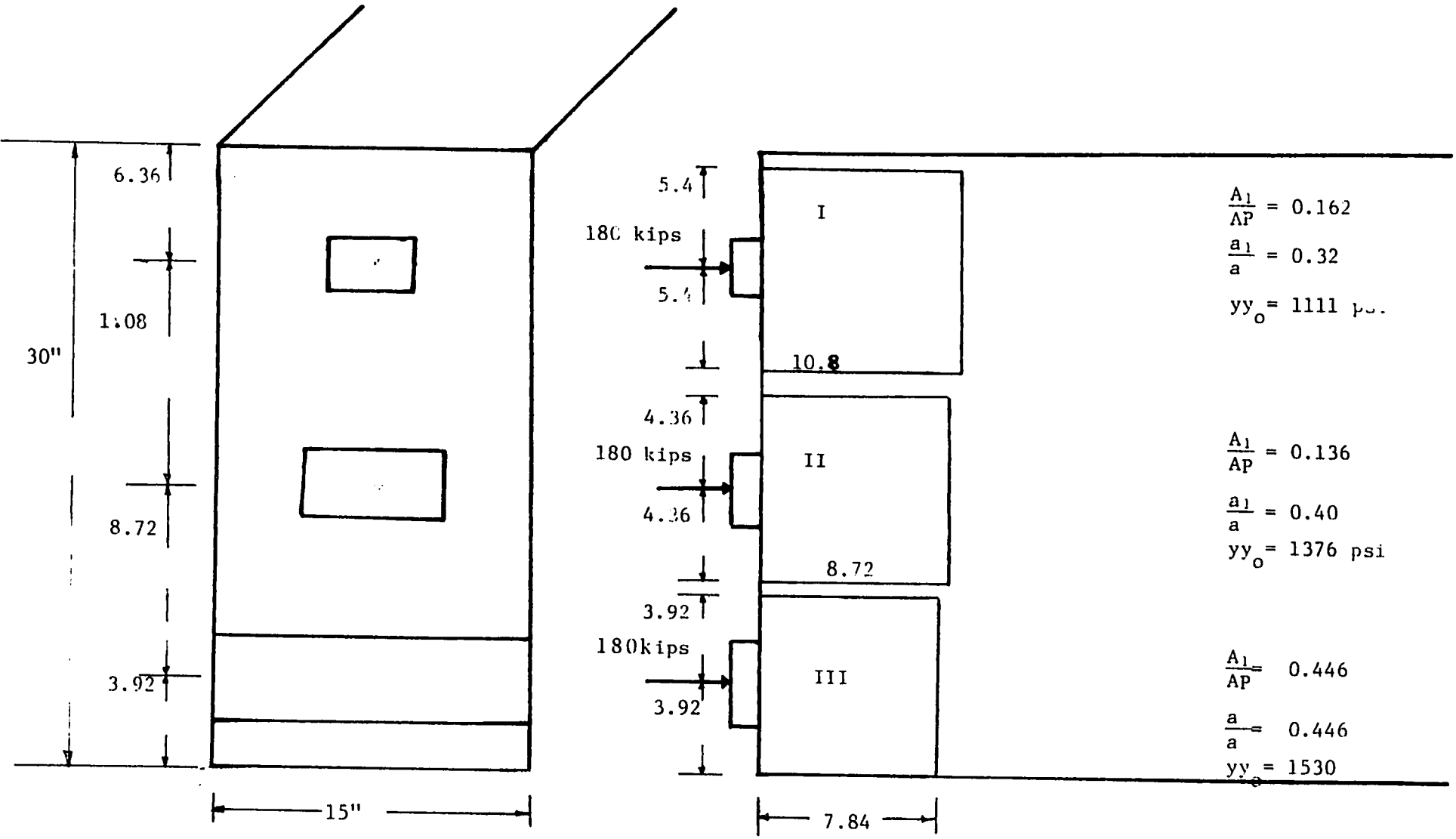

FIGURE 9.1 : The results of the investigation applied on a prototype beam end block of 30"x15"

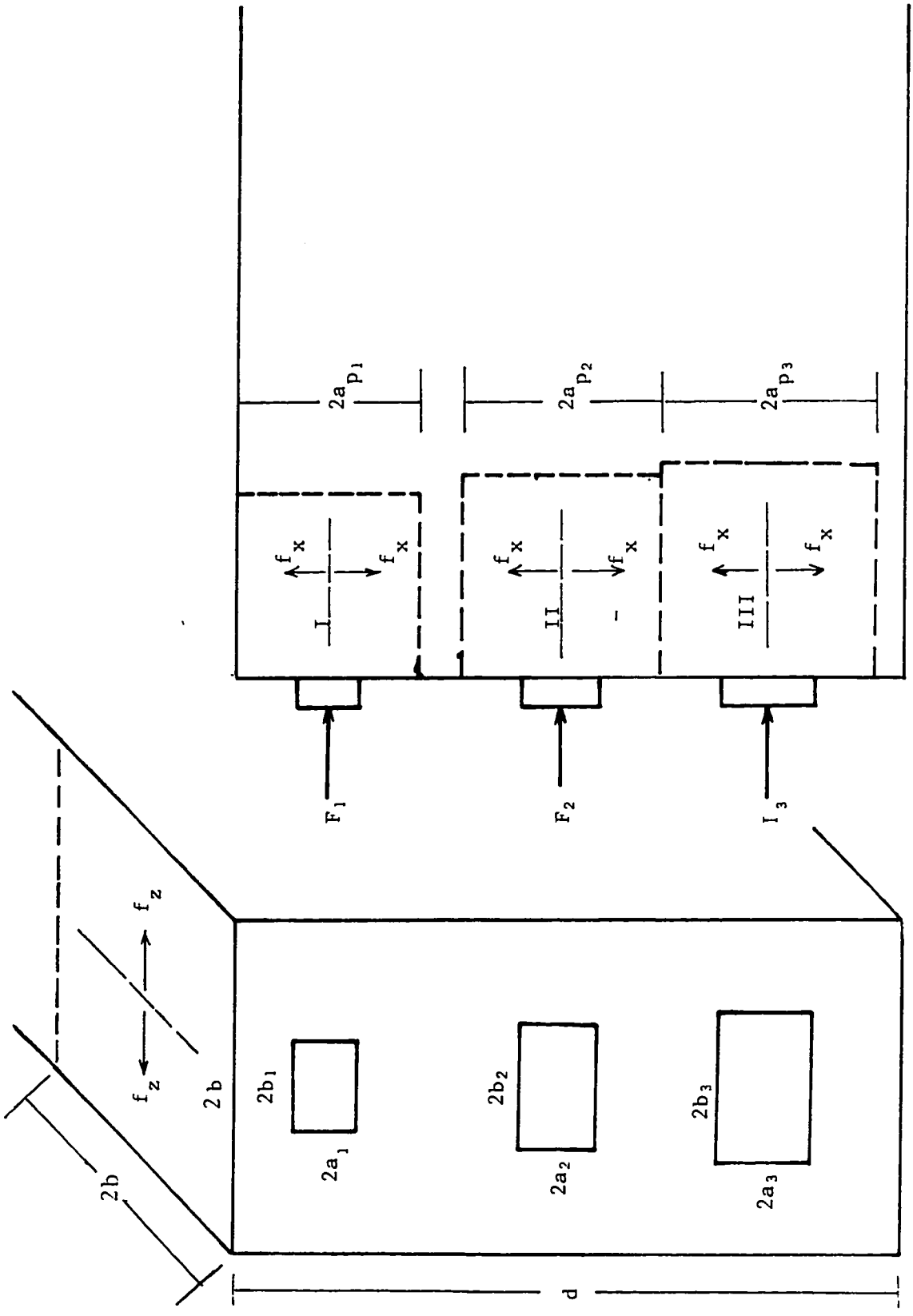

FIGURE 9.2 : General beam

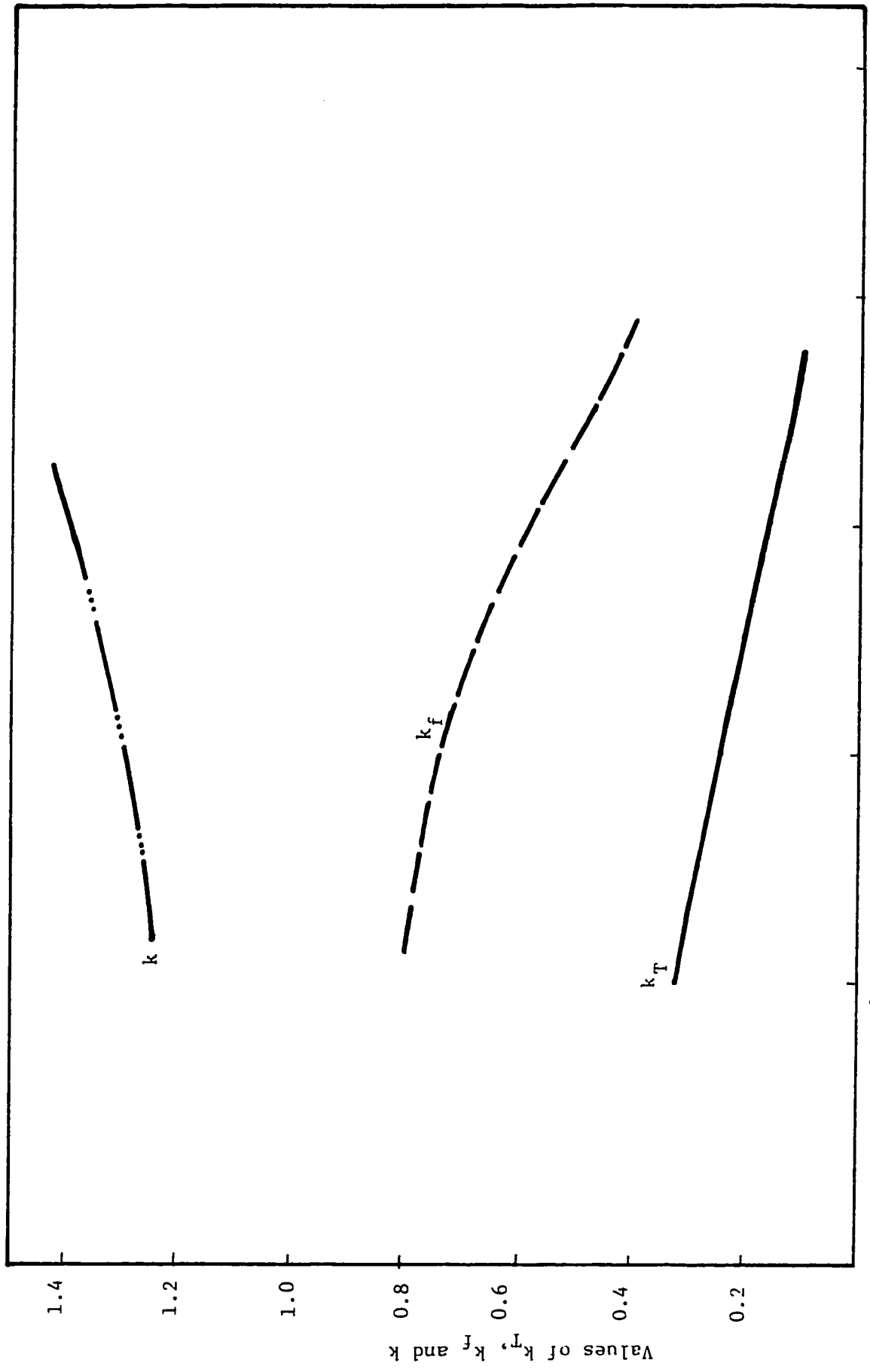

FIGURE 9.3 : Values of k_T, k_f and k

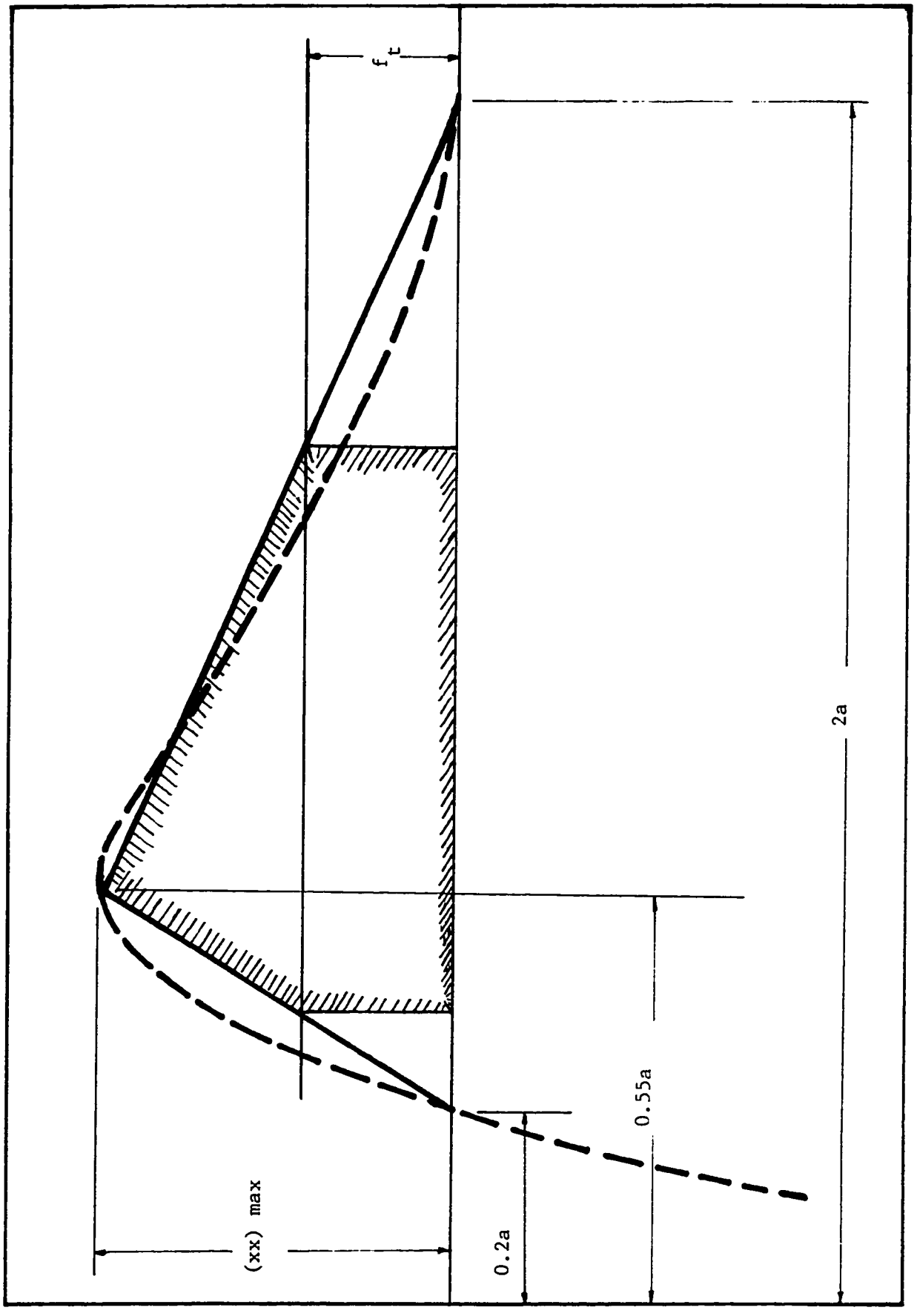

FIGURE 9.4 : Typical plot showing the distribution of the transverse tensile stress which can be approximated by a triangle

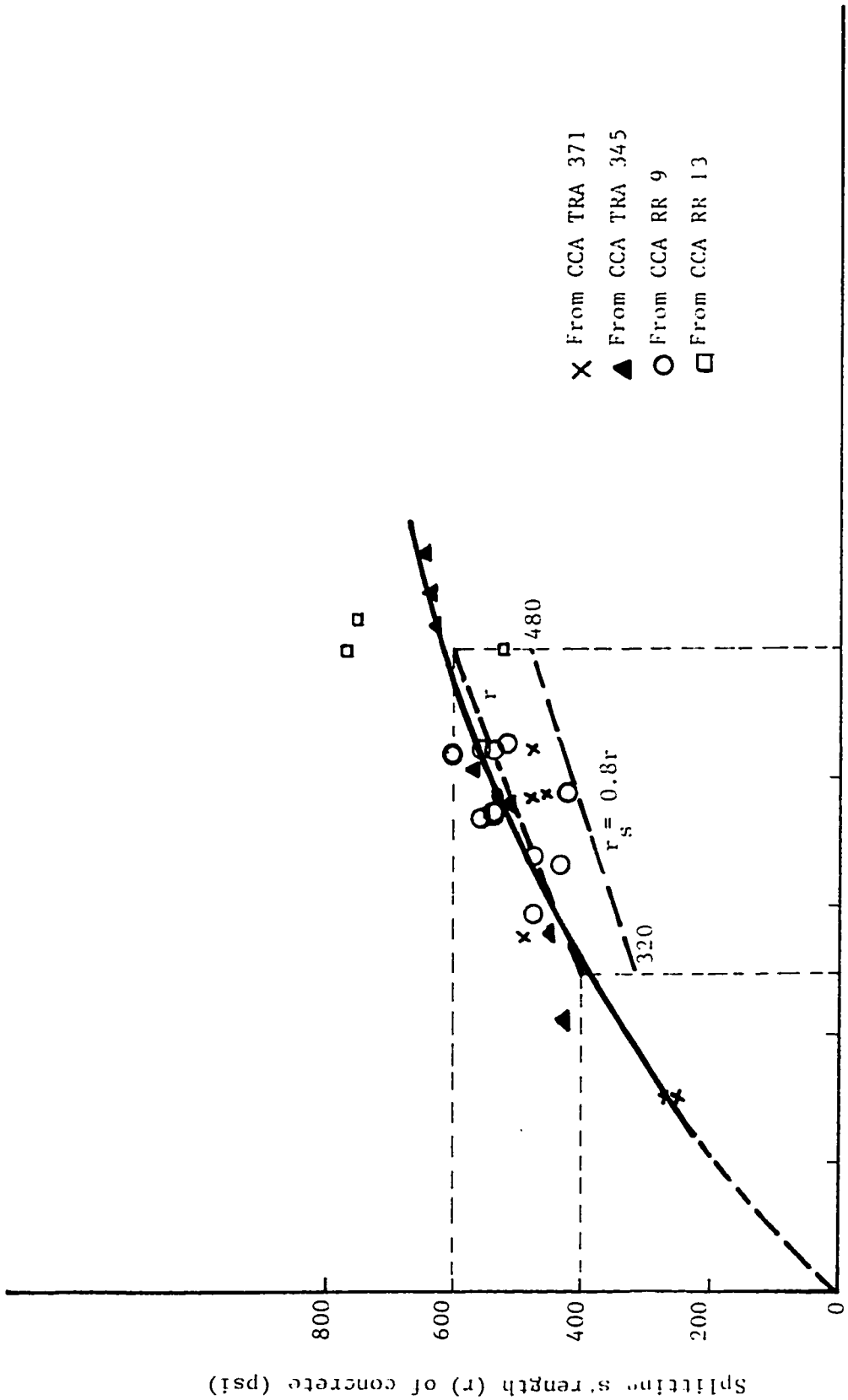

FIGURE 9.5 : Relationship of cube crushing strength and tensile splitting strength

Restressing Force (lb)	100,000	200,000	300,000	400,000	500,000
$2a_1$ (in)	5	6	7	$8\frac{1}{2}$	9
Diameter of Duct (in)	2	2	3	$3\frac{1}{2}$	4

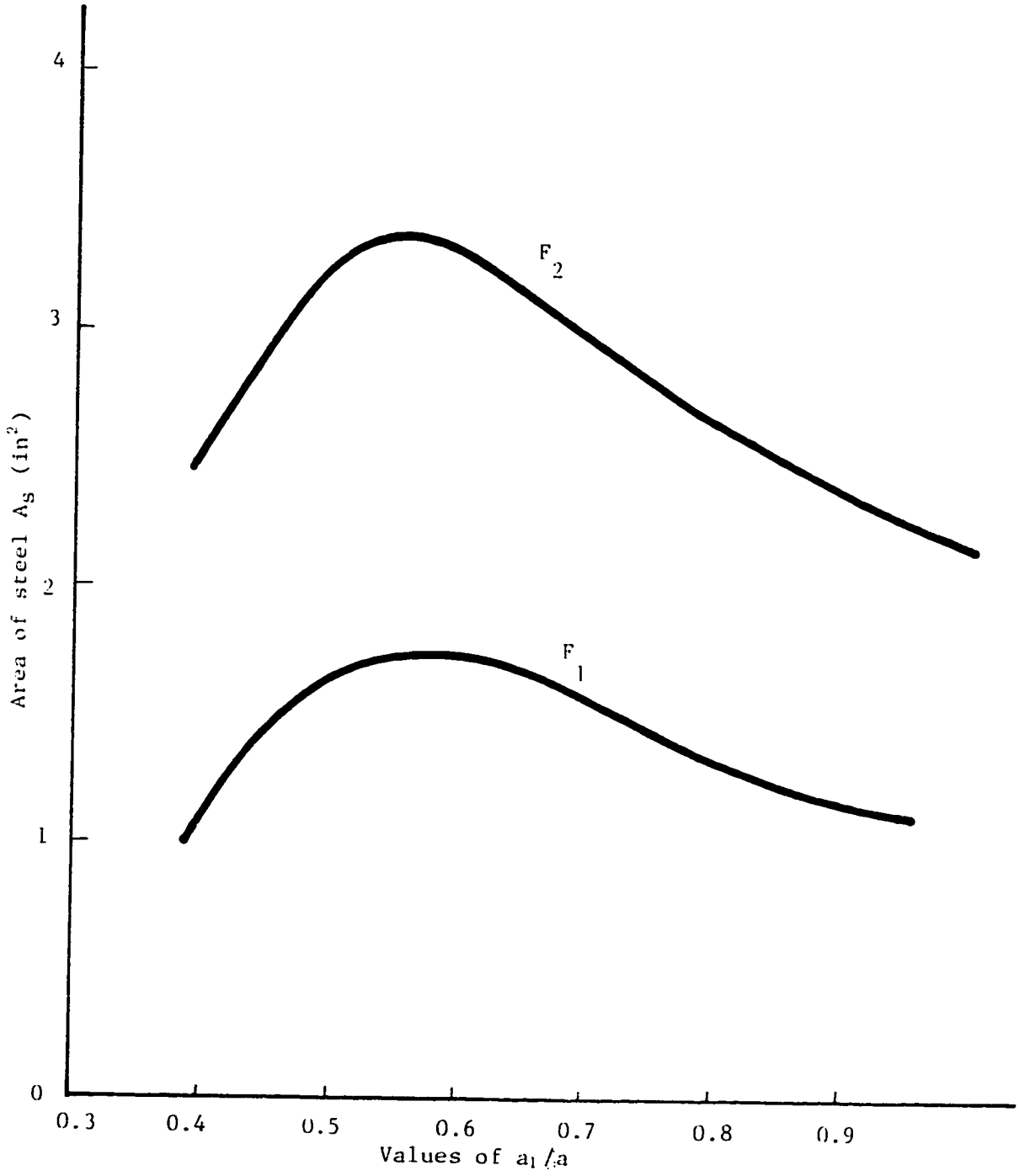

FIGURE 9.6 : Duct calculation of area of steel for the anchorage zone for given values of prestressing zone

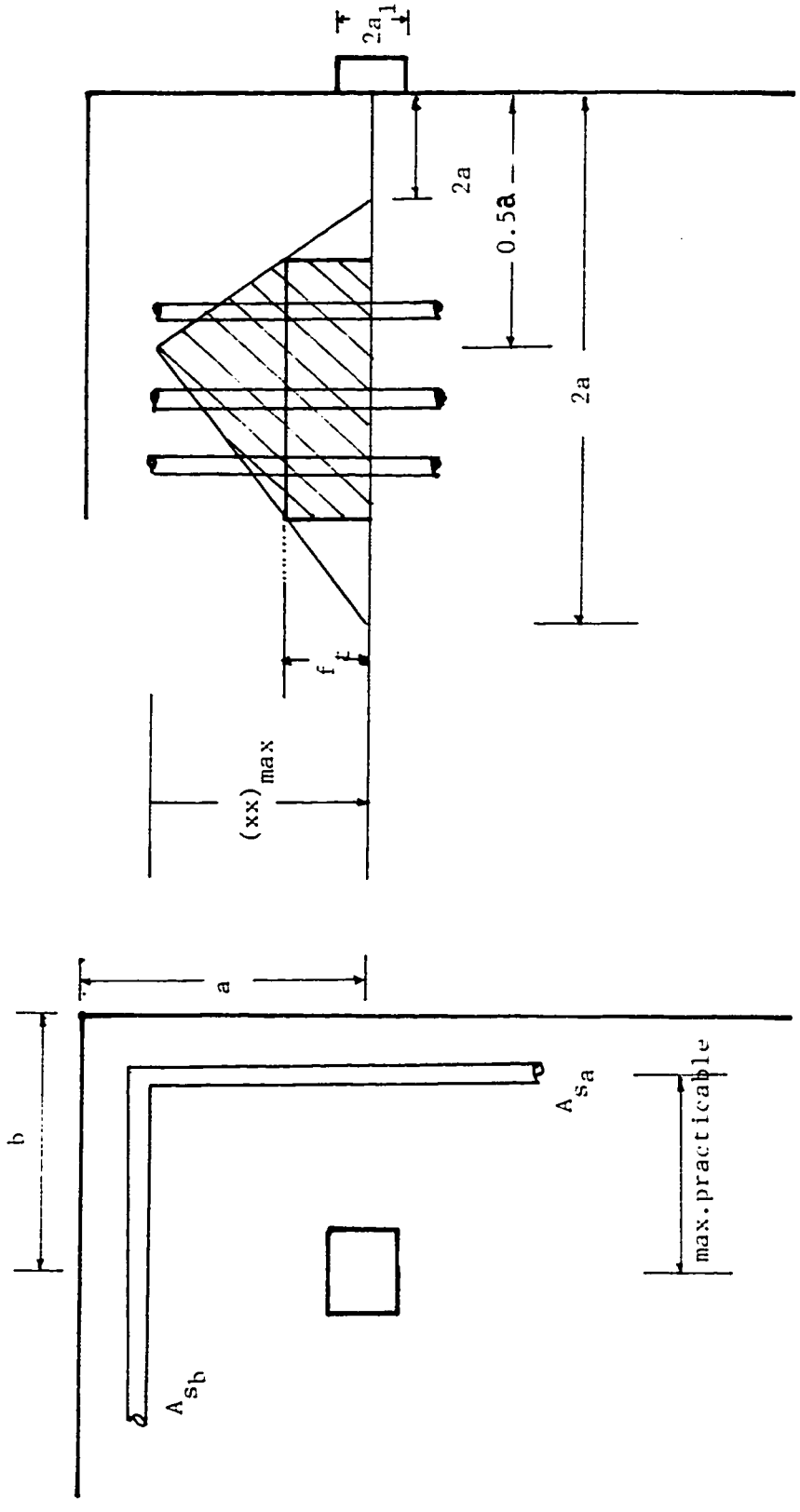

FIGURE 9.7 : The rectangular stirrup reinforcement

FOR EXTERNAL ANCHORAGES

$\frac{a_1}{a}$	0.2	0.3	0.4	0.5	0.6	≥ 0.7
$\frac{T}{F}$	0.32	0.28	0.24	0.20	0.15	0.11

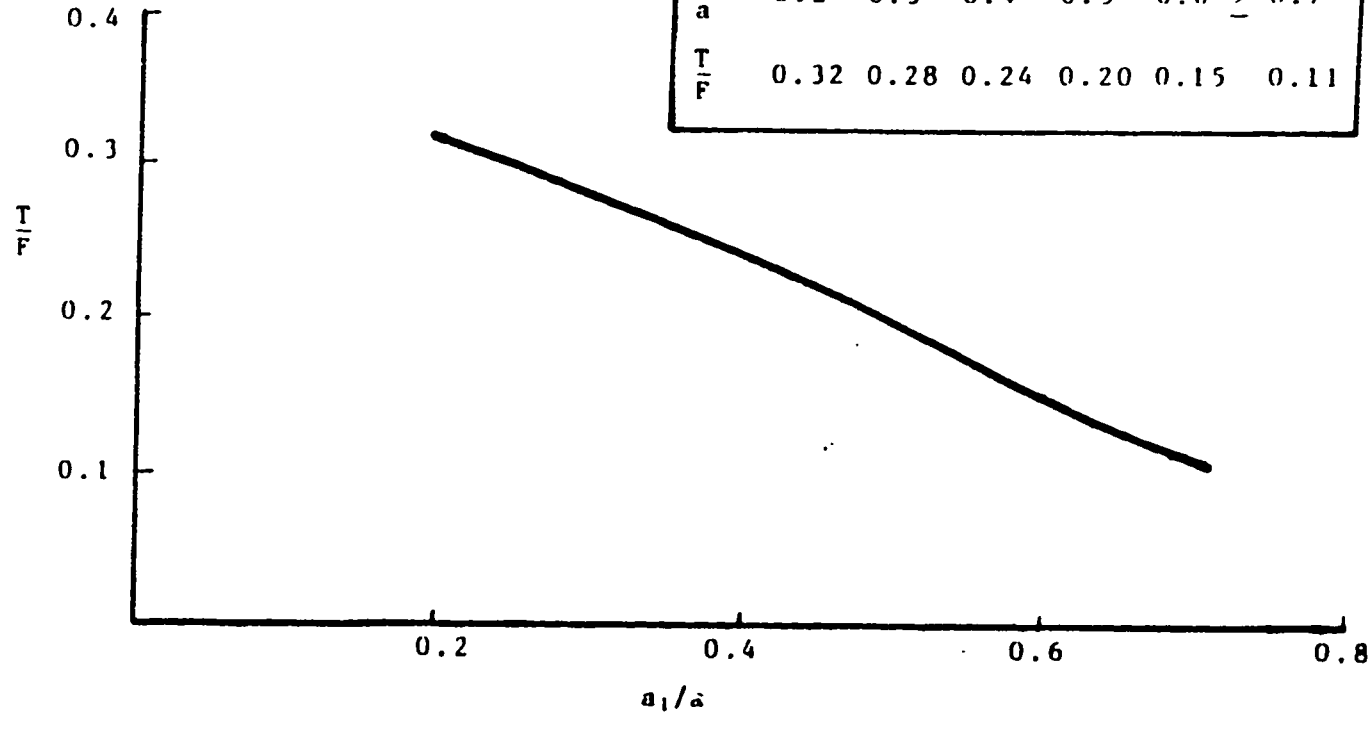

FOR EMBEDDED ANCHORAGES

$\frac{a_1}{a}$	0.2	0.3	0.4	0.5	0.6	≥ 0.7
$\frac{T}{F}$	0.22	0.20	0.17	0.14	0.12	0.10

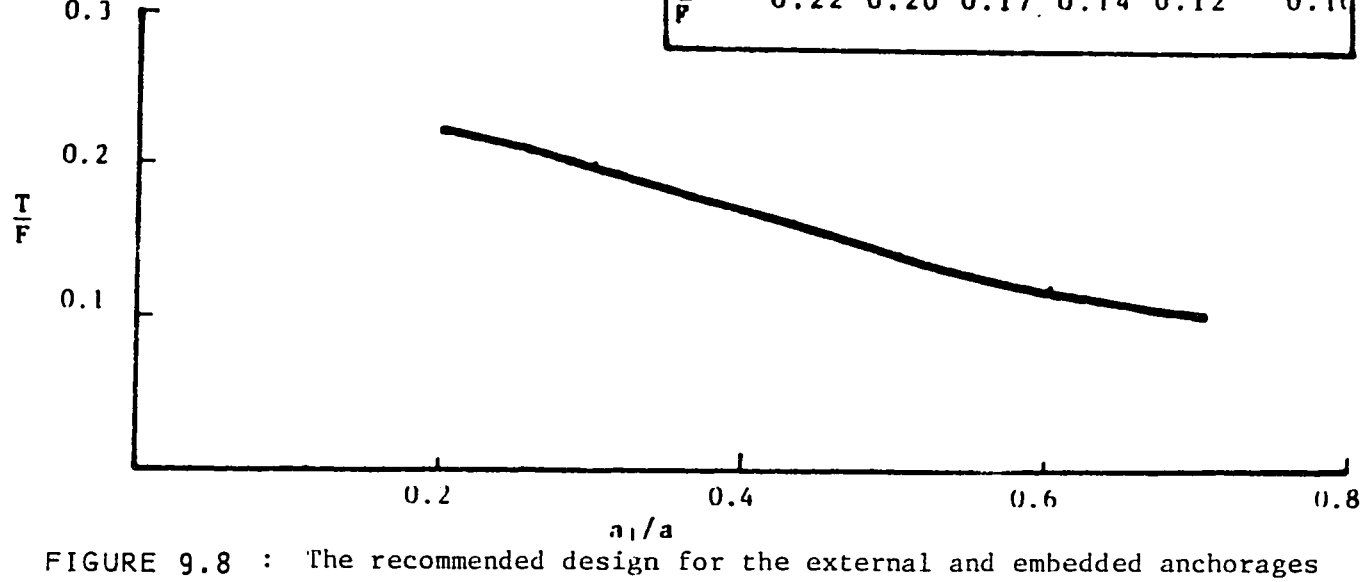

FIGURE 9.8 : The recommended design for the external and embedded anchorages

chapter **10**

CONCLUSIONS

In general the mode of failure of an end block subjected to prestressing forces is determined by high subsurface shears in the vicinity of the anchorage unit and also by regions of transverse tensile stresses which are associated with the diffusion of the prestressing force from the anchorage unit into the structure. As a result of the present investigation a number of features have become apparent which will enable a better understanding of the behaviour and design of anchorage zones.

The major stresses resisting the applied load in the end block are compressive and have much larger magnitudes than the corresponding transverse tensile stresses. In all the models investigated the normal principal compressive stress behind the anchorage unit was of an order of more than five times the uniform compression at the end of the anchor block. Concrete successfully withstands these stresses by virtue of an indicated triaxial state of compression behind the anchorage which bestows to the

concrete therein considerable additional strength due to the resulting confinement.

In the case of external anchorage end block very large sub-surface shear stresses, reaching a maximum value of threetimes the mean compression occur just beneath the edge of the loaded area. Experiments on the failure mechanism of concrete end blocks showed that these sub-surface shears were critical and caused the onset of failure.

It is observed that a zone of tensile stress always exists a short distance below the back of the anchorage unit. It was found that the transverse tensile stress and the total tensile force in this zone varied significantly with the load concentration ratio and a relationship between these parameters has been established from these test results. It was however found that the positions of maximum (0.55a) and zero (0.2a) tensile stress were practically independent of the variations in the load concentration ratios. The results of this investigation also show that the load concentration ratio alone, however, is inadequate to define the maximum value of the transverse tensions. It was found that the

proximity of the anchorage unit to the surface plane also played an important role in conjunction with the load concentration ratio in the prediction of maximum transverse tensile stress levels. It is noteworthy that this parameter has been hitherto overlooked.

Contrary to the suggestions of some theoretical solutions the maximum value of the transverse tensile stress does not necessarily occur on the surface plane. This renders, at least in some cases, the conclusions from surface observations of concrete end block open to criticism.

It was found that almost all two-and three-dimensional theoretical solutions underestimate the critical tensile stresses and forces and completely overlook the real significance of the high sub-surface shears in the immediate vicinity of the anchorage units. It is these critical sub-surface shears which cause a well defined shear wedge under the bearing finally causing the propogation of tensile cracks in a complex compression-tension stress field. The values of maximum transverse tensile stresses and tensile forces obtained in this investigation were found to be in good agreement with the comprehensive test results of Zielinski and Rowe made on

concrete end block models. This indicates as well that the photoelastic methodology provides a realistic picture of the nature of magnitude and stress distribution and that Poisson's ratio differential effect is small.

Zones of tensile stresses are also found in the corners of all the end block models investigated. An analysis of the present tests indicates that the tensile stresses in the spalling zones are parasitic in nature and arise as a result of the mismatching between zones subjected to large compressive stresses and other regions which are not loaded directly.

In the case of multianchorage models in addition to zones of tensile stresses beneath each anchorage unit, tensile zones were also found to exist between the anchorage units. These zones are shallow and the reinforcement for these zones should be detailed as close to the surface as possible. The creation of these zones is akin to the existence of spalling zones in the two corners and could be explained by the mode of load dispersion for each individual prestressing force. These zones exist throughout the width of the end block and

and by virtue of the fairly high stress gradients render this region vulnerable to potential cracking and failure. The existing experimental evidence on concrete end blocks confirms this conclusion.

Test results for the multi-anchorage end block illustrate the advantage of dividing the loaded area into multiple anchorage units. The maximum tensile forces in the tensile regions beneath the anchorage units are reduced and in a practical case this would permit a substantial reduction in the total amount of steel reinforcement. It is also noticed that the length in which complete diffusion of the prestressing force takes place is reduced. This would allow the adoption of a shorter end block thereby resulting in a corresponding reduction of the self weight.

The fundamental difference in the stress distributions between the external and embedded anchorage units arise from the difference in the mode of load transfer. It was found that a little more than one third of the load applied at the embedded anchorage unit was transmitted through shear tractions on the longitidunal surface of the anchorage unit. Only the balance was

transferred by bearing action. This improved diffusion mechanism of load transfer obviously results in a reduction in the level of maximum tensile stresses and forces. The maximum transverse tensile forces for the embedded anchorage were only 65 to 70% of the corresponding values for the external anchorage units. The corner spalling stresses are also considerably reduced. It would therefore appear that the performance of an end block would be improved if the prestressing force were transferred to the anchorage zone through an inserted unit. In the embedded anchorage unit the maximum transverse tensile stress occurs of a distance away from the base of the anchorage unit and not from the loaded face.

Both the foregoing conclusions regarding the embedded anchorage units are contrary to the conclusions of Zielinski and Rowe and in line with Guyon's contentions.

On the basis of tests on single concentrically loaded end blocks two sets of values for embedded and external anchorage units have been proposed to predict the tensile forces for the various $\frac{a_1}{a}$ ratios. Test data from the multi-anchorage model indicates that the symmetrical prism method, when used in conjunction with the author's

values, provides an excellent prediction of the actual tensile force in the multi-anchorage prestressing system.

The results of the single and multi-anchorage end blocks indicate that the maximum hoop stress in the duct is not critical. It was,however, found that the presence of the duct shifts the position of the maximum tensile stress from along the central load line to the anchorage unit edge line.

It is observed that the state of stress in the anchorage zone is of a complex three-dimensional nature. In each tension zone under the anchorage units the state of stress is of a bi-axial tension in transverse directions combined with longitudinal compressions. In the tension zones between the anchorages also the state of stress is of a bi-axial tension. Under the anchorage units, however, the state of stress if of a tri-axial compression resulting in a confinement of concrete leading to a stiffer concrete wedge at the back of the anchorage unit. These conditions profoundly affect the failure mechanism of concrete in the anchorage zone. The simple approach to a failure criterion in terms of a limiting strain or stress is to be ruled out and a

more complex mechanism of failure is observable. It was found that high sub-surface shears in the vicinity of the anchorage unit initiate a punching type of failure and the subsequent propagation of tensile cracks in a complex compression-tension stress field caused by the wedging action of the concrete cone governs the failure of the end block.

REFERENCES

[1] Guyon, Y. Prestressed Concrete. 1st edition, London Contractors Record and Municipal Engineering, 1953, p. 127

[2] Guyon, Y. "Contraintes dans les pieces prismatiques soumises a des forces appliquees sur leurs bases, an voisinage de ces bases", International Association for Bridge and Structural Engineering. Publications, Vol. 11, 1951. pp. 165-226.

[3] Morsch, E. "Uber die Berechnung der Gelenkquader" Beton und Eisen, 1924, No.12, pp. 156-161.

[4] Bortsch, R. "Die spannungen in Walzgelenkquadern" Beton und Eisen, Vol. 35, No. 4, 1935, pp. 61-66.

[5] Magnel, G. "Design of the ends of presterssed concrete beams" Concrete and Constructional Engineering, Vol. 44, No.5, 1949, pp. 141-148.

[6] Chaikes,S. "Calculdes about des poutres en beton precontraint. Congre's International du Beton Precontraint a' Gand, September 1951, pp. B41-1-B41-27.

[7] Bleich, F., "Der gerade stab mit rechtackquerschnitt als ebenes problem" Der Bauingenieur (Berlin), N..9, 1923, pp.255-259 and No.10, 1923, pp. 304-307.

[8] Sievers, H., "Die Berechnung von Auflagerbanken und Auflagerquadern von Bruckenpfeilern" Der Bauingenieur, Vol.27, No.6, 1952, pp. 209-213.

"Uber den spannunqseustand im Bereich der Ankerplatten von Spanngliedern vorgespannter Stahlbeton-konstruktionen" Der Bauingenieur, Vol.31, No.4, 1956, pp. 134-135.

[9] Douglas, D.J. and Trahair, N.S. "An examination of the stresses in the anchorage zone of a post-tensioned prestressed concrete beam" Magazine of concrete research (Lond.), Vol.12, No.34, 1960, pp. 9-18.

[10] Sundara Raja Iyengar, K.T. and Yogananda, C.V., "A three-dimensional stress distribution in the anchorage zone of a post-tensioned concrete beam" Magazine of Concrete Research, Vol. 18, No.55, 1966, pp. 75-84.

[11] Sundara Raja Iyengar, K.T. and Prabhakara, M.K., "A three-dimensional elasticity solution for rectangular prisms under end loads" Zeitschrift Fur Angewandte Mathematik und Mechanik (ZAMM), Vol. 49, N..6, 1969, pp.321-332.

[12] Yettram, A.L. and Robbins, K., "Anchorage zone stresses in axially post-tensioned member of uniform rectangular section" Magazine of Concrete Research (Lond.), Vol.21, No.67, 1969, pp. 103-112.

"Anchorage zone stresses in axially post-tensioned I-section member with end blocks" Magazine of Concrete Research (Lond.), Vol. 23, No.74, 1971, pp.37-42.

[13] Zielinski, J. and Rowe, R.E., "An investigation of the stress distribution in the anchorage zone of post-tensioned concrete members," Research Report N'.9, Cement and Concrete Association (London), Sept. 1960.

"The stress distribution associated with groups of anchorages in post-tensioned concrete members" Research Report No.13, Cement and Concrete Association (london), Oct. 1962.

[14] Taylor, S.J., "Anchorage bearing stresses" Conference on pre-stressed concrete pressure vessels,Institution of Civil Engineers(London),1968,Group H,paper 49, pp. 563-576.

[15] Christodoulides, S.P., "The distribution of stresses around the end anchorages of prestressed concrete beams. Comparison of the results obtained photoelastically with strain gauge measurements and theoretical solutions" Publications International Association for Bridge and Structural Engineering, Vol. 16, 1956, pp. 55-70.

[16] Sampson R.C. "Photoelastic analysis methodology and its application to Nerva structures", NASA-CR-132213, Aerojet - General Corp., Sacramento, CA, June 1972.

[17] Shell C, Brown J.M. and Peatfield A.M. "The three-dimensional photoelastic stress analysis of constant thickness cylindrical dam under hydraulic loading" Civil Engineering Research Association, Technical Report TR/AD/1,April 1964, p.9.

[18] Shell C., Brown J.M. "Photoelastic stress determination in a double curvature arch dam" Civil Engineering Research Association, Technical Report TR/AD/2, May, 1964,p.8.

[19] Ramaswamy, G.S. and Goel, H., "Stresses in end blocks of prestressed beams by lattice analogy" Proceedings of the World Conference on Prestressed Concrete at Sanfrancisco, July 1957, pp. 23.1 - 23.4.

[20] Gilder, H.A. "An analytical investigation of some problems in prestressed concrete", M.Sc. thesis, University of London, 1953.

[21] Gerstner, R.W. and Zienskiewicz, O.C., "A note on anchorage zone stresses" Journal of the American Concrete Institute, Proceedings Vol. 59, No.1962, pp.970-975.

22 Rydzewski, J.R. and Whitbread, F.J., "Short end blocks for prestressed beams" Structural Engineer, Vol. 41, No.2, 1963, pp. 41-53.

23 Schlech, W., "Die spannunqszustande beim Auflager eines spannbetontragers" Beton und Stahlbetonbau, Vol.58, No.7, 1963, pp. 157-171.

24 Som, P.K. and Ghosh, K., "Anchorage zone stresses in pre-stressed concrete beams" Jl. of structures div., Proceedings American Society of Civil Engineers, Vol.90, No.ST-4, 1964, pp. 49-62.

[25] Lenschow, R.J. and Sozen, M.A., "Practical analysis of the anchorage zone problem in prestressed beams" Journal of American Concrete Institute, Proceedings Vol. 62, 1965, pp. 1421-1439.

[26] Gaynor, M. A simplified analysis of the bursting forces due to a single prestressing anchorage, Structural Engineer Aug. 1966, 44 (Nov. 8) 231 to 236.

[27] Ban, S. Nuguruma, H. and Ogaki, Z., "Anchorage zone stress distributions in post-tensioned concrete members" Proceedings of the World Conference on Prestressed Concrete at San Francisco, July 1957, pp. 16.1-16.4.

[28] Christodoulides, S.P., "Two-dimensional investigation of the end anchorages of post-tensioned concrete beams" The Structural Engineer, Vol.33, No.4, 1955, pp.120-133.

[29] Gergely, P. and Sozen, M.A., "Design of anchorage zone reinforcement in prestressed concrete beams" Jl. of Prestressed Concrete Institute, Vol. 12, No.2, 1967, pp. 63-75.

[30] Sargious, M., "Beitrag Zur Ermittlung der Hauptzugspannungen am Endauflager vorgespannter Betonbalken" Ph.D. thesis, Technische Hochsohule, Stuttgart, July 1960.

[31] Rydzewski, J.R. and Whitbread, F.J., "Short end blocks for prestressed beams" Structural Engineer, Vol. 41, No.2, 1963, pp. 41-53.

[32] Ti Huang,"Stresses in end blocks of a post-tensioned prestressed beam" Journal of American Concrete Institute, Proc. Vol.61, 1964, pp. 591-601.

[33] Tassi, G. and Windisch, A. Analysis and model testing of the anchorage zone of post-tensioned beams Proc. FIP Congress (New York), 1974.

[34] Kiyokazu Higashida and Hiroyuki Nkajima, Experimental study on reinforcement of multiple anchorages zone in post-tensioned concrete members. Proc. FIP Congress (New York), 1974.

[35] Band R.V. and Racke' H.H. "Die elastischen und spannungsoptischen Eigenschaften Von Araldit Giessharz B bu 20°C in Abhangigkeit Von der Hartermenge" Schweiz. Arch. angew wiss V. Tech, Vol.21, No.8, 1955.

[36] Spooner. H, and McConnel L.D., "An ethoxylene resin for photoealastic work", British Journal of Appl.Physics, Vol.4, p. 181, 1953.

[37] Dixon, J.R., "Problem of materials for composite models in photoelastic frozen stress work", British Journal Applied Physics, Vol.13, 1962, p.64.

[38] Levew, M.M. Proceedings Soc. Exp. Stress Analysis, 6, No.1, 1948, p.19.

[39] Frocht M.M. and Guernsey, R. (JR) "Studies in three-dimensional photoelasticity", Proceedings of the First US National Congress of Applied Mechanics, Dec. 1952, pp.301-307.

[40] Frocht M.M. and Guernsey, R. (JR). "A special investigation to develop a general method of three-dimensional photoelastic stress analysis", NACA Technical Note No.2822, December 1952.

[41] Frocht M.M. and Guernsey, R. (JR). "Further work on the general three-dimensional photoelastic problem", J. of Applied Mechanics, June 1955, Vol.22, No.2, pp.183-189.

[42] Kammuller K. and Jeske, O."Umtersuchungen uber Federgelenke aus Stahlbeton" Deustcher Ausschuss fur stahlbeton. No. 125, 1957, pp.30.

[43] Dowrick, D.J., "Anchorage zone reinforcement for post-tensioned concrete" Civil Engineering and Public Works Review, Vol.59, 1964, pp. 1101-1107.

[44] Al-Musallam, Abdallah Abdul-Karim, "A Photoelastic Investigation of the Stress Distribution in the Anchorage Zones of Post-Tensioned Concrete Slabs, M.Sc. Thesis, UPM, February, 1980.